

THÈSE

En vue de l'obtention du

DOCTORAT DE L'UNIVERSITÉ DE TOULOUSE

Délivré par :

Institut National Polytechnique de Toulouse (INP Toulouse)

Discipline ou spécialité :

Dynamique des fluides

Présentée et soutenue par :

M. GERARDO DEL GUERCIO

le vendredi 7 novembre 2014

Titre :

OPTIMAL STREAKS AMPLIFICATION IN WAKES AND VORTEX SHEDDING CONTROL

Ecole doctorale :

Mécanique, Energétique, Génie civil, Procédés (MEGeP)

Unité de recherche :

Institut de Mécanique des Fluides de Toulouse (I.M.F.T.)

Directeur(s) de Thèse :

M. CARLO COSSU

Rapporteurs :

M. JEAN-CHRISTOPHE ROBINET, ENSAM - ARTS ET METIERS PARISTECH

M. OLIVIER CADOT, ENSTA PARIS

Membre(s) du jury :

M. PIERRE BRANCHER, UNIVERSITE TOULOUSE 3, Président

M. CARLO COSSU, INP TOULOUSE, Membre

M. GREGORY PUJALS, PSA PEUGEOT CITROEN, Membre

M. PIER BENOIT, ECOLE CENTRALE DE LYON, Membre

Gerardo Del Guercio

Optimal streaks amplification in wakes and vortex shedding control

Acknowledgement

Doing a PhD project is tough by definition but having a good environment around you can both stimulate and make you never feel alone.

The daily meetings with you, Carlo, have always been an inspiration to go deep inside the meaning of the basic knowledge and to understand those small but fundamental details that make science in general so fascinating. Mainly, I have learned from you how investigate science has to be amusing and be inspired by that genuine curiosity. Your always positive attitude made me work in a very comfortable and relaxed environment despite all the difficulties that working on a scientific project can have. On the professional and human side, I make treasure of all the things I learned from you.

Being in a long geographic distance, it has never been a problem with you, Gregory. Discuss with you about the theoretical aspects of the work we have done helped me to see from a direct point view further the relevant aspects to make solid that bridge between the academic investigation and the practical needs. Then, working with you during the relatively short time I spent in Vélizy, it has been on the amount of knowledge gained very dense. Despite the other many responsibilities, you have always been there to help me. I do appreciate this professional, friendly and always kind way to work you have.

As far as I spent most of the time during the Phd in Toulouse there are many people that I want to mention. If I found a very friendly and pleasant environment in the laboratory is mainly credit of Luigi, Tobias and Subhendu. Discussions, coffee breaks and lunches done together will be among the nicest and funny memories I'll bring with me. I am also grateful to all the members of the IMFT who were always collaborative and helpful.

The time I spent in Paris was made very nice also by the professional and warm environment I found in the SFTA group in the Research and Development Department at PSA. I want to thank Vincent and Fabien for all the positive remarks and the continued interest on my work and all the other members of the team who were always nice and ready to help. I can not avoid to mention Cyril and Giacomo and thank them to be friends more than always helpful and available colleagues.

The journey that brought me in France started so long ago. It could have never started or moved forward without my family. A great and important gratitude goes to them. On the other side being far from home was never very tough since I found a piece of family in Toulouse, thank you for all the support Gianluca, Sara, Tiziana, Remi, Luca and Paulo.

Thank you to all of you.

Abstract

Optimal energy amplifications of quasi-streamwise structures are computed in a parallel wake, a synthetic weakly non-parallel wake and in the circular cylinder wake. It is found that very large energy amplifications can be sustained by these wakes. The energy amplifications increase with the spanwise wavelength of the perturbations except in the circular cylinder wake where maximum energy growths are reached for $\lambda_z \approx 5 - 7\,D$. The optimally amplified structures are streamwise streaks. When forced with finite amplitudes these streaks are shown, in parallel wakes, to be able to completely suppress the absolute instability. The global instability of the weakly non-parallel and the circular cylinder wakes can be completely suppressed by streaks of moderate amplitude. The control energy required to stabilize the wake is very small when optimal perturbations are used, and it is shown to be always smaller than the one that would be required by a spanwise unifirm (2D) control. It is also shown that the sensitivity of the global mode growth rate is quadratic and that therefore usual first order sensitivity analyses are unable to predict the high efficiency of the control-by-streaks strategy. The last part of this work offers preliminary results on the experimental investigation of the control by streaks in the case of a turbulent wake past 3D bodies. Streaks artificially forced in the absolute instability region of the flow are shown to be able to modify the wake dynamics.

Résumé

Les amplifications optimales d'énergie de structures quasiment alignées dans le sens de l'écoulement sont calculées dans le cas d'un sillage paralléle, d'un sillage synthètique faiblement non-paralléle et du sillage d'un cylindre. Il a été observé que de très grandes amplifications d'énergie peuvent être supportés par ces sillages. L'amplification d' énergie s'accroît avec la longueur d'onde des perturbations en envergure à l'exception du sillage du cylindre pour lequel l'accroissement d'énergie est maximal pour $\lambda_z \approx 5 - 7\,D$. Les structures amplifiées de manière optimale sont les streaks fluctuant dans le sens de l'ècoulement. Il est montré que ces streaks sont capables de supprimer complètement l'instabilité absolue d'un sillage parallèle lorsqu'ils sont déclenchés avec une amplitude finie. L'instabilité globale d'un sillage faiblement non-parallèle et celle du sillage d'un cylindre peuvent être complètement supprimées par des streaks d'amplitude modeste. L'énergie de contrôle requise pour stabiliser le sillage est trés faible lorsque les perturbations optimales sont utilisées, et il est montré qu'elle est toujours plus faible que celle qui devrait être utilisée pour un contrôle uniforme en envergure (2D). Il est aussi montré que la dépendance du taux de croissance est quadratique et que, par conséquent, les classiques analyses de sensibilité au premier ordre ne permettent pas de prédire la grande efficacité de la technique de contrôle par streaks.

La dernière partie de ce travail livre des résultats préliminaires sur l'étude expérimentale du contrôle par streaks dans le cas du sillage turbulent d'un corps 3D. Il est montré que les streaks forcés artificiellement dans la zone d'instabilité absolue de l'écoulement sont capables de modifier la dynamique du sillage.

Contents

Contents i

1 Introduction 1
1 Industrial context . . . 1
2 Bluff body wakes . . . 3
3 Control of $2D$ wakes . . . 4
4 About this thesis . . . 6

2 Background 9
1 Stability and instabilities of parallel open flows . . . 9
2 Global instabilities in non-parallel flows . . . 10
3 Non-modal energy amplification . . . 11

3 A tale of three 2D wakes: the prologue 15
1 Monkewitz's model parallel wakes . . . 15
2 A weakly non-parallel 'synthetic' wake . . . 16
3 The circular cylinder wake at low Reynolds number . . . 17

4 Optimally amplified streamwise streaks in wakes 19
1 Optimal temporal energy growth in parallel wakes . . . 19
2 Optimal spatial energy growth in weakly non parallel synthetic wakes . . . 20
3 Optimal blowing and suction on the circular cylinder . . . 23

5 Stabilizing effect of streaks 27
1 Non linear streaky basic flows . . . 27
2 Quenching of the absolute instability in parallel wakes . . . 31
3 Suppression of the global instability in non parallel wakes . . . 32
4 Non linear simulations . . . 34

6 A sensitive issue 37
1 The first order sensitivity paradox . . . 37
2 Quadratic sensitivity and 3D control efficiency in parallel wakes . . . 38
3 Quadratic sensitivity and 3D efficiency in non parallel wakes . . . 39

7 Effects of streaks forcing on a turbulent wake past a 3D bluff body 43
1 Motivations . . . 43
2 Experimental set-up . . . 43

3 Natural flow case 45
4 Roughness Elements and streaks 45
5 Analysis of the Controlled case 48
6 Conclusions 52

8 Conclusions **53**

Appendix **59**

A General tools **59**
1 Numerical simulations 59
2 Fundamental and subharmonic, symmetric and antisymmetric modes 61
3 Impulse response analysis in parallel wakes 62
4 Computing the growth rate of global modes 64
5 Computing optimal temporal energy growths in parallel wakes 64

B An adjoint-free subspace reduction algorithm to compute optimal spatial amplifications in non-parallel wakes **67**

Bibliography **69**

Articles **79**

Chapter 1

Introduction

1 Industrial context

On the verge of an environmental and energetical crisis, car manufacturers have to meet with regulations imposed by *CAFE* (Corporate Average Fuel Emission) whose main objective is to reduce their average CO_2 emission from $132.2\,g/km$ in 2012 to $95\,g/km$ in 2020. While huge improvements could be achieved with new engines (e.g. 3 cylinders), a large amount of fuel could be saved by lowering the penalty introduced by drag (the force exerted on a body which opposes to its motion).

The main sources of drag for cars lay in tyres and aerodynamics. Drag due to tyres increases linearly with the speed of the vehicle, while the aerodynamic drag dependence is quadratic. Typically, aerodynamic drag becomes larger than the tyres drag at $70\,km/h$ and it is more than 70% of the total drag above $90\,km/h$ (see figure 1.1).

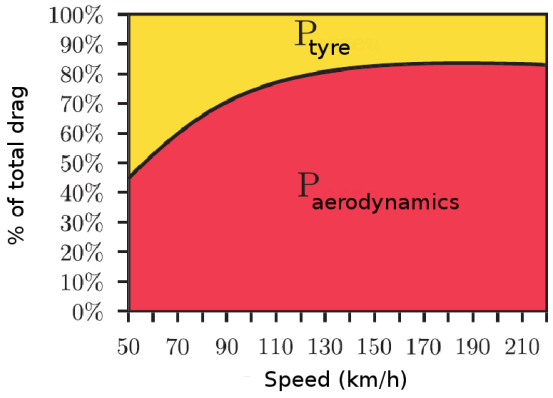

Figure 1.1: Relative percentage of the tyre drag and the aerodynamic drag for increasing speed for a city car. Internal source PSA.

Aerodynamic drag can be decomposed into viscous drag and pressure drag. Viscous drag is due to friction of the flow over the surface of the body while pressure drag is due to momentum losses occurring in separated flow regions which induce a difference between the pressure exerted on the front and the rear of the body.

For streamlined bodies such as e.g. airplanes or submarines at the cruise speed, the separated flow regions, if there are any, are very small so the main source of resistance to motion is viscous drag while the remaining amount is pressure drag and induced drag. Conversely, for bluff (i.e. non streamlined) bodies the opposite is true and the main source of drag is pressure drag.

One way to reduce the drag penalty could be to design highly streamlined cars. Nevertheless, this approach fails to cope with practical constraints such as habitability, ergonomics, safety, cooling not mentioning style. For those reasons car manufacturers let designers and architects draw the main shapes and optimize their aerodynamic properties afterwards.

In this context, in a previous investigation founded by PSA, Pujals *et al.* (2010*b*) obtained a substantial drag reduction (10% on the total drag) using a suitable distribution of small cylindrical elements placed on the roof of a simplified vehicle model (the so-called Ahmed body). The small cylinders, which were immersed in the boundary layer, were used to generate low energy spanwise periodic streamwise vortices which induced the streamwise growth of spanwise periodic (3D) regions of high and low streamwise velocity (the so-called streamwise streaks). The presence of the streaks was instrumental in suppressing the flow separation of the slanted (25°) rear surface of the Ahmed body, as shown in figure 1.2, and therefore reducing the total pressure drag. A fundamental idea used by Pujals *et al.* (2010*b*) and in other previous studies (e.g. Cossu & Brandt, 2002, 2004; Fransson *et al.*, 2004, 2005, 2006) was to force 'optimal' streamwise vortices which lead to the streamwise streaks of maximum energy via the lift-up effect (Landahl, 1980; Schmid & Henningson, 2001).

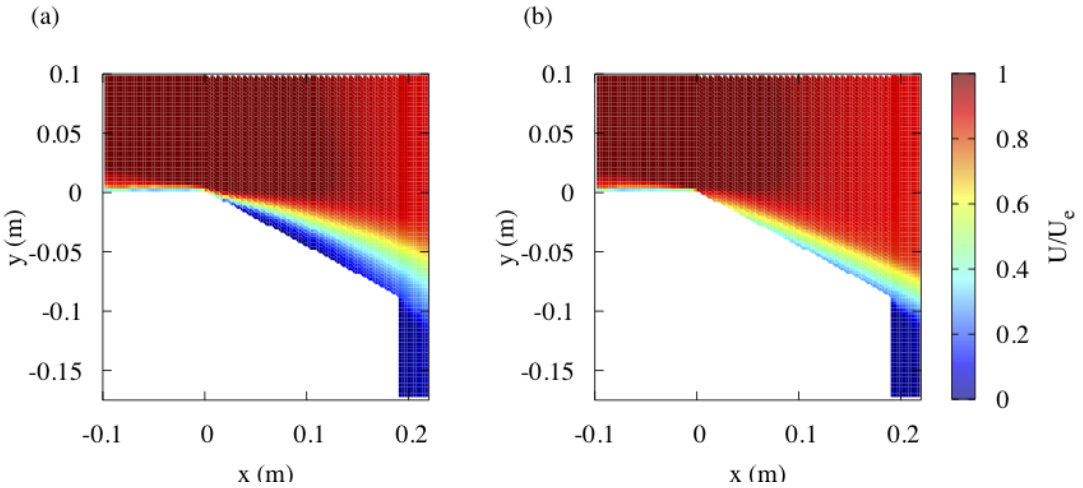

Figure 1.2: Separation control with streaks on an Ahmend body. Time averaged streamwise velocity U/U_e around the rear-end in the symmetry plane using PIV. The flow is from left to right. (a) Uncontrolled case. (b) Optimally controlled case with configuration where the streaks on the roof of the Ahmed body are excited at the optimal position found. Source: Pujals *et al.* (2010*b*).

The control strategy used by Pujals *et al.* (2010*b*), however, was ineffective for high slant angles and therefore for the case of blunt trailing edges, such as those of monospace cars, vans or trucks. The main questions that has motivated the present work were: Can the approach of Pujals *et al.* (2010*b*) be modified to control massive separations around bodies with a blunt

trailing edge? If yes, how?

In the case of blunt trailing edge the large scale vortex shedding developing in the wake is the main source of pressure drag. A digression is therefore necessary to summarize the state of the art on the understandings of the origins of vortex shedding in bluff body wakes as well as the strategies attempted to date in order to control it.

2 Bluff body wakes

Bluff bodies are typically characterized by boundary layer separation leading to wide wakes whose cross-stream size is comparable to that of the body. The massive flow separation of bluff bodies and the complex vortex dynamics which develops in the wake lead to a significant decrease of the pressure recovery on the rear part of the body and therefore to a dramatic increase of the pressure drag as well as undesirable unsteady loads.

The basic physics of bluff body wakes is best understood in two-dimensional flows, the canonical case study being the circular cylinder wake. Assuming the flow to be incompressible and viscous, the relevant control parameter is the Reynolds number $Re = U_\infty D/\nu$ (where U_∞ is the velocity, D is the diameter of the body and ν is the kinematic viscosity of the fluid). For $Re \leq 47$ the flow is steady and symmetric but above above 47 two-dimensional vortices are periodically shed in the wake (von Kármán vortex shedding, see figure 1.3). In correspondence to the onset of vortex shedding the base pressure coefficient (C_{pb}) at the aft of the cylinder, which is strongly correlated with the pressure drag, shows a sharp decrease, as shown in figure 1.4. Further increase of the Reynolds number leads to an increasingly three-dimensional and

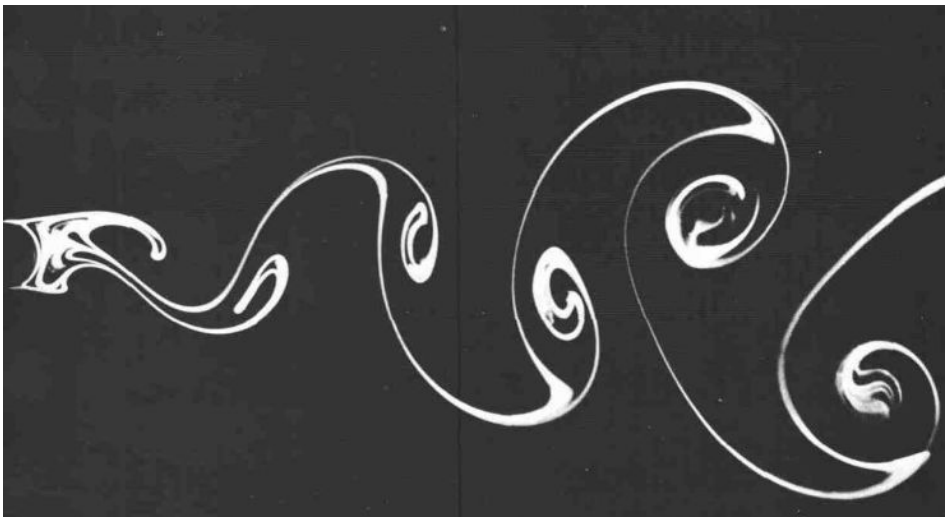

Figure 1.3: The von Kármán vortex shedding in the wake of a circular cylinder, $Re = 140$. Source: Van Dyke (1982).

complex structure of the wake. This feature of bluff-bodies wake flows remains observed for larger Reynolds numbers, even if modulated by turbulence and trying to quantify their impact Cantwell & Coles (1983) reports that for circular cylinder's near wake a percentage around 45% of the velocity fluctuations are due to the coherent structures at $Re \approx 10^5$.

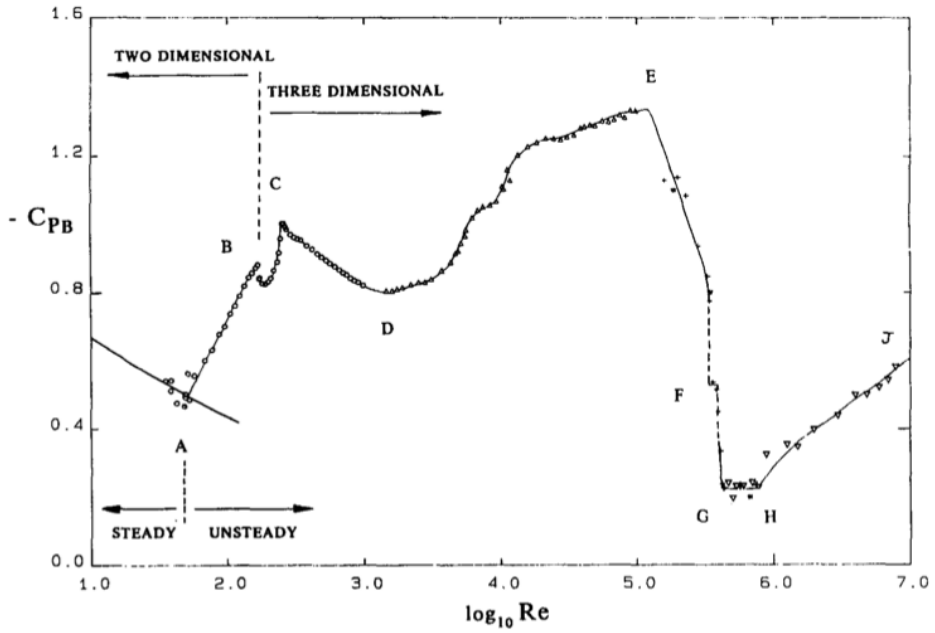

Figure 1.4: Plot of base pressure coefficient C_{pb} over a large range of Reynolds numbers. A plot of base pressure coefficient is particularly useful as a basis for discussion of the various flow regimes. The base pressure coefficient is surprisingly sensitive to the process of vortex formation in the near wake, which itself is affected strongly by the evolution of various $2D$ and $3D$ wake instabilities, as Reynolds numbers are varied. Source: Williamson (1996).

The vortex shedding's origins can be tracked back to the instability of the wake developing donwstream of the bluff body. The wake velocity profiles in the near wake become unstable at very low Reynolds number values ($Re \approx 6$) and for $Re \geq 25$ this instability becomes sufficiently strong to develop against the mean flow (absolute instability). Further increase of the Reynolds number leads then to creation of a finite region of absolute instability that can destabilize the whole wake acting as a 'wave-maker' (Chomaz *et al.*, 1988; Monkewitz, 1988; Huerre & Monkewitz, 1990). The resulting self sustained oscillations are triggered by the wavemaker region, and are then amplified donwnstream in the convectively unstable region (see chapter 2 for more details).

3 Control of $2D$ wakes

The main goal of active (with energy input) and passive (without energy input) bluff body control strategies has been to attenuate or quench vortex shedding. The most investigated framework is, again, that of two-dimensional ($2D$) wakes.

3.1 $2D$ control

Many different strategies have been tested in order to reduce shedding using spanwise uniform ($2D$) control. The main goal of these control strategies is to reduce the absolute instability in

the wave-maker region. This reduction can be e.g. achieved by base bleed as shown by Schumm *et al.* (1994) (see figure 1.5) or base suction as shown by Leu & Ho (2000). However, these active control techniques require large levels of bleeding ($\approx 0.2\,U_\infty$) or suction ($\approx 0.46\,U_\infty$) to stabilize the shedding. We will see in the next section that control based on 3D perturbations requires much less energy to achieve the same goal.

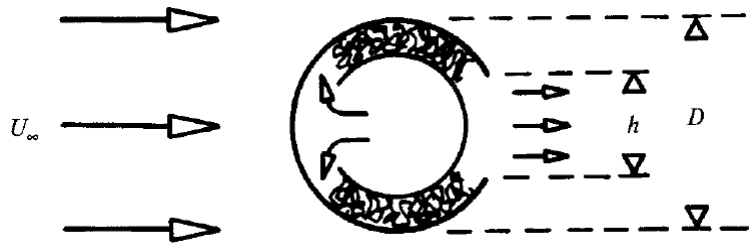

Figure 1.5: 2D control. Schematic cross-section of the cylinder with base bleed with D and h that stands for the diameter of the cylinder and the height of the bleed arch. Source Schumm *et al.* (1994)

A 2D passive control technique which has received a lot of attention is based on the placement of a thin control wire in the near wake of the cylinder which is able to suppress the shedding in the laminar regime ($Re \leq 80$), as shown by Strykowski & Sreenivasan (1990). A convincing theoretical interpretation of the stabilizing mechanism has been recently advanced and is based on the first-order sensitivity analysis of the global instability with respect to basic flow modifications (Chomaz, 2005; Giannetti & Luchini, 2007). In these studies it was shown that the control wire must be placed in the wavemaker region of the wake which roughly corresponds to the region of absolute instability. First-order sensitivity analyses are also useful to compute the wake modifications which optimally reduce the absolute growth rate (Hwang & Choi, 2006) and have been applied to a host of other flows such as the one behind a backward facing step (Barbagallo *et al.*, 2012) or the flow in a wall cavity (Yamouni *et al.*, 2013).

The 2D wire control technique has been recently extended to the turbulent case where large drag reductions have been achieved (see e.g. Sakamoto *et al.*, 1991; Parezanović & Cadot, 2009*a*,*b*, 2012; Cadot *et al.*, 2009).

3.2 3D control

A second class of control techniques (3D control) is based on the spanwise periodic modulation of the wake. In the case of passive control these modifications can be obtained by modulating the bluff body geometry, as shown in figure 1.6. In particular, Zdravkovich (1981) (panel *a*) applied an helical strake to a circular cylinder geometry while Tanner (1975) (panel *b*) studied a segmented trailing edge. Tombazis & Bearman (1997) installed a spanwise wavy modulation of the blunt trailing edge on a cigar shaped body (panel *c*) followed by Bearman & Owen (1998) who tested the wavy modification on the front stagnation face (panel *d*). Both these technique were later combined by Darekar & Sherwin (2001). Tabs placed at the edge of the blunt surface have been used by Park *et al.* (2006) (panel *g*). Vortex shedding suppression can also be achieved using active control in the form of blowing and suction through slots placed on the bluff body surface, as shown by Kim & Choi (2005).

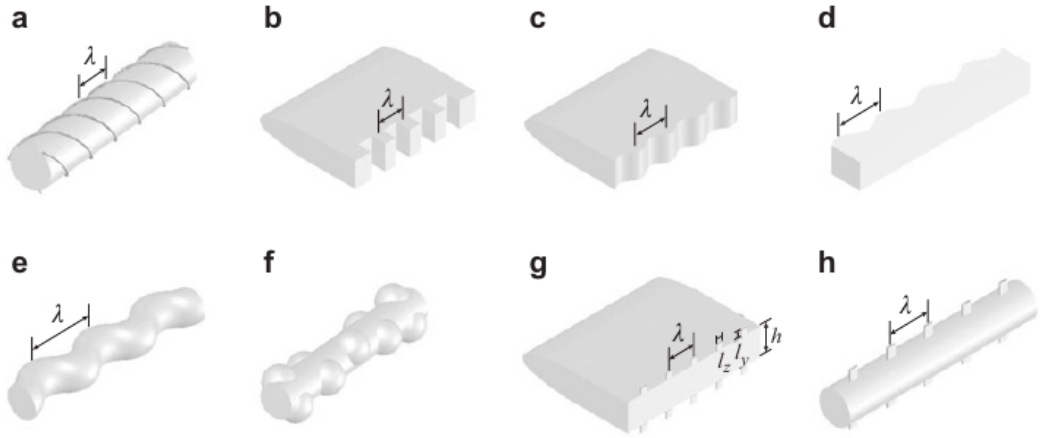

Figure 1.6: $3D$ forcing by passive means: (a) helical strake, (b) segmented trailing edge, (c) wavy trailing edge, (d) wavy stagnation face, (e) sinusoidal axis, (f) hemispherical bump, and (g,h) small-size tab. Source Choi *et al.* (2008)

All the techniques above mentioned can be characterized by the amplitudes and the spanwise wavelength of the control. The amplitude can be the blowing suction coefficient used by Kim & Choi (2005), the height of the tabs of Park *et al.* (2006) or the amplitude of the leading and trailing edge modulations used by Darekar & Sherwin (2001). Minimal amplitudes to either suppress vortex shedding or achieve a determined base pressure reduction typically correspond to y-symmetric (varicose) forcing with well defined optimal spanwise wavelengths. In the case of the circular cylinder, for example, the optimal spanwise wavelength is $5-7\,D$ at least up to $Re = 3900$. $3D$ control techniques have proven to be highly efficient and to be effective in a very large range of Reynolds numbers. Kim & Choi (2005) obtained a 20% reduction of the total drag at $Re = 100$ with a bleeding coefficient of $C_\nu = 0.0012$, much smaller than the $C_\nu = 0.04$ required by $2D$ forcing. Park *et al.* (2006) obtained, with the optimal tabs configuration, a $\approx 30\%$ increase of the base pressure in a high Reynolds numbers regime ($Re = 20\,000 - 80\,000$).

The theoretical understanding of the mechanisms underlying $3D$ control is much less developed than for $2D$ control. Most of the explanations have been advanced in terms of vortex dynamics in the wake. Very recently, however, important progress has been made from a stability theory perspective. In particular, Hwang *et al.* (2013) have shown that spanwise periodic modulations of the 2D wake profile (that we interpret as streamwise streaks) have a stabilizing action on the absolute instability. They, however, did also show that the first order sensitivity of 3D perturbations is zero and that 2D perturbations are predicted to be more efficient than 3D ones in the framework of their analysis. The apparent contradiction of these results with the experimental observations prompts for further investigation of this issue.

4 About this thesis

Nowadays, most cars are of hatchback or squareback type (Hucho, 1987), meaning their rear-end can be considered as blunt. Many studies being either theoretical or experimental have proven the ability of $3D$ actuation (albeit not being necessarily streaks) to perform flow

control on various geometries (most of them still being $2D$ ones). Consequently, the main question motivating the present work is: can streaks be used to efficiently manipulate massive separations past bluff bodies? If that is so, how do they act on the dynamics of such wakes?

The first part of our investigation has focused on the computation of optimal perturbations sustained by different types of $2D$ wakes. Are those optimal perturbations streamwise vortices evolving into streamwise streaks? If that is so, are they highly amplified? Could they be used for control purpose? Do they have some stabilizing effect on the unstable mode responsible for vortex shedding just like the spanwise modulations studied by Hwang *et al.* (2013)?

Keeping in mind some possible application of this strategy to automotive geometries, we then have to investigate how could such perturbations be forced on a $3D$ bluff body with a blunt rear-end at high Reynolds number. Can roughness elements be used in the spirit of Fransson *et al.* (2005) or Pujals *et al.* (2010*b*)? Can they really (i.e. in a wind tunnel experiment) act on the shedding mode? What are the relevant parameters of actuation?

The present manuscript is organized as follow: in chapter 2 we briefly recall the main concepts related to stability analyses that we will use throughout the thesis. In chapter 3, we describe the three base-flows we will consider as prototypes of wake flows with increasing complexity. Chapter 4 and 5 are devoted to respectively optimal perturbations sustained by those base-flows and their stabilizing effect on the unstable shedding mode when they are enforced. Chapter 6 gives some new insight on the sensitivity analysis while chapter 7 eventually presents the results of an experimental validation on a simplified $3D$ bluff body geometry. Chapter 8 gives a summary of all our conclusions on this study and discuss them.

Chapter 2

Background

In this chapter the main instability concepts that will we used in the following are briefly recalled.

1 Stability and instabilities of parallel open flows

We closely follow Huerre & Monkewitz (1990) in introducing the concepts of absolute and convective instability in parallel flows. Consider the evolution of small perturbations of a parallel steady basic flow $\mathbf{U} = [U(y), 0, 0]$, a Fourier-Laplace transform of the linearized equations leads to examine normal mode solutions of the type $\mathbf{u}(x, y, t) = \widehat{\mathbf{u}}(\alpha, y)\, e^{i\,(\alpha\, x - \omega\, t)}$, where α is the wavenumber for the streamwise direction x, ω is the complex frequency and variations in the spanwise direction z are, at this stage, neglected. The normal modes satisfy a dispersion relation $\mathcal{D}(\omega, \alpha) = 0$ which can be associated to a spatio-temporal linear operator $\mathcal{L}(x, t)$ through an inverse Laplace-Fourier transform. The stability properties of the basic flow are revealed by the analysis of the Green function $\mathcal{G}(x, t)$ (linear impulse response) of $\mathcal{L}$ which satisfies:

$$\mathcal{L}\,\mathcal{G}(x, t) = \delta(x)\,\delta(t), \tag{2.1}$$

where δ denotes the Dirac delta function.The flow is *linearly stable* if:

$$\lim_{t\to\infty} \mathcal{G}(x, t) = 0 \quad \forall\ x/t = constant, \tag{2.2}$$

while it is *linearly unstable* if:

$$\lim_{t\to\infty} \mathcal{G}(x, t) = \infty \ along\ at\ least\ one\ ray\ x/t = constant. \tag{2.3}$$

Following standard definitions initially used in plasma physics (Landau & Lifshitz, 1959; Briggs, 1964; Bers, 1975), an unstable basic flow is said to be *convectively unstable* if:

$$\lim_{t\to\infty} \mathcal{G}(x, t) = 0 \ along\ the\ ray\ x/t = 0, \tag{2.4}$$

while it is *absolutely unstable* if:

$$\lim_{t\to\infty} \mathcal{G}(x, t) = \infty \ along\ the\ ray\ x/t = 0. \tag{2.5}$$

For convectively unstable flows, therefore, the perturbations are not unstable enough to overcome the downstream advection and grow against the flow, while the opposite is true for

absolutely unstable flows (see figure 2.1 for a sketch). However, convectively unstable flows can largely amplify, in the downstream direction, periodic perturbations that would be applied at a fixed spatial station. Indeed, the spatial stability problem is well defined in convectively unstable flows while it is not in absolutely unstable flows.

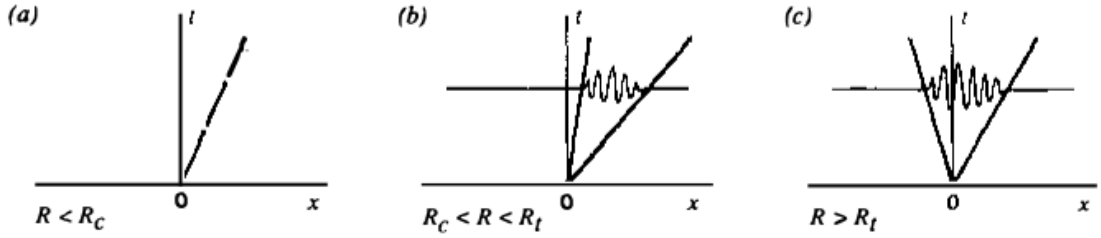

Figure 2.1: Sketches of typical impulse responses developing in basic flows which are respectively: (a) stable, (b) convectively unstable, (c) absolutely unstable. Source Huerre & Monkewitz (1990).

2 Global instabilities in non-parallel flows

Global stability analysis deals with steady non-parallel basic flows $\mathbf{U} = [U(x,y), V(x,y), 0]$. Small perturbations to non-parallel basic flows satisfy the linearized Navier-Stokes equations that we formally write as $\partial\boldsymbol{\phi}/dt = \mathbf{L}_{NS}\,\boldsymbol{\phi}$, where $\boldsymbol{\phi}$ is the perturbation state vector and $\mathbf{L}_{NS}$ is the linearized Navier-Stokes operator. The streamwise inhomogeneity of the basic flow precludes the use of the Fourier transform in the streamwise direction x. The global eigenvalues s and associated global modes $\widehat{\boldsymbol{\phi}}(x,y)$ satisfy the global eigenvalue problem $s\,\widehat{\boldsymbol{\phi}} = \mathbf{L}_{NS}\,\widehat{\boldsymbol{\phi}}$. The flow is globally stable if the real part of all eigenvalues is negative $s_r < 0$ while it is globally unstable if at least one eigenvalue has positive real part $s_r > 0$.

In the case where the basic flow is only weakly non-parallel, it makes sense to try to relate the global stability properties of the basic flow to the local stability properties of the parallel basic flows obtained by extending to infinity the local profile $U(X,y)$, where the slow variable X is considered as a parameter and no more an eigenfunction direction.

An important relation has been established between local and global instabilities at the end of the 80ies. Chomaz *et al.* (1988) have shown that "the existence of a pocket of absolute instability is a necessary but not sufficient condition to the onset of amplified global oscillation. The region of absolute instability must reach a critical size in order for resonances to occur". These conclusions, found on the generalized linear Ginzburg-Landau model, have been confirmed by the local stability analyses of wakes (Monkewitz, 1988) and in many other flows (Huerre & Monkewitz, 1990), and by a rigorous asymptotic analysis of the linearized Navier-Stokes equations (Monkewitz *et al.*, 1993). For instance, for the circular cylinder wake, Monkewitz (1988) finds a transition from local stability to local convective instability at $Re \approx 6$, a region of local absolute instability appears at $Re \approx 25$ before the onset of the global instability at $Re_1 = 47$ as an Hopf bifurcation (Provansal *et al.*, 1987; Sreenivasan *et al.*, 1987). At the onset of the global instability the region of absolute instability coincides approximately with the recirculation region, which extends to $\approx 4\,D$ downstream the cylinder.

These findings relate the appearance of a global instability, e.g. inducing the vortex shedding in the circular cylinder wake, to the existence of a 'wave-maker', the absolute instability region, where unstable waves can travel upstream and downstream and are therefore allowed to resonate. The wave-maker action is spatially amplified downstream in the convectively unstable region and finally damped in the further downstream stable region leading to the characteristic shapes of linear global modes.

The relation between local and global instability is also essential for flow control applications. In order to stabilize the global instability, and therefore the vortex shedding, it is sufficient to reduce enough, the region of local absolute instability in the near wake.

3 Non-modal energy amplification

The amplification of streamwise streaks in shear flows is physically explained by the lift-up effect (see e.g. Schmid & Henningson, 2001). Their amplification is, however, not explained by the classical modal stability analysis as it is not associated to an unstable mode. Indeed, in the small amplitudes approximation, streamwise streaks decay when $t \to \infty$ (or $x \to \infty$ in the spatial framework) and are therefore only transiently amplified. The mathematical explanation of the streaks transient energy growth is related to the non normality of the linear operator $\mathbf{L}$ in initial value problems of the type $d\boldsymbol{\phi}/dt = \mathbf{L}\,\boldsymbol{\phi}$. The question is: can some structures be transiently amplified in an asymptotically linearly stable system? Assuming that the eigenvalues s of $\mathbf{L}$ are all simple and using the modal decomposition $\boldsymbol{\phi} = \sum_m \boldsymbol{\psi}^{(m)} q_m$ the kinetic energy of the perturbations $K = \| \boldsymbol{\phi} \|^2 /2$ can be expressed as:

$$\| \boldsymbol{\phi} \|^2 = \sum_m \sum_n \langle \boldsymbol{\psi}^{(m)}, \boldsymbol{\psi}^{(n)} \rangle q_m^* q_n = \sum_m \sum_n \langle \boldsymbol{\psi}^{(m)}, \boldsymbol{\psi}^{(n)} \rangle q_m^*(0) q_n(0) e^{(s^{(m)*} + s^{(n)})t},$$

where $\langle ., . \rangle$ is the inner product of the considered state space. If $\mathbf{L}$ is a normal operator the eigenfunctions are orthogonal and all the modes are uncoupled. The last relation reduces to $\| \boldsymbol{\phi} \|^2 = \| \boldsymbol{\psi}^{(m)} \|^2 \; |q_m(0)|^2 e^{2 s_r^{(m)} t}$ and if the whole spectrum is stable, energy can only decreases for all times. So a necessary condition for the existence of transient growth is the operator $\mathbf{L}$ is *non-normal*.

The transient energy growth is easily understood by geometric construction on a simple system with state vector $\boldsymbol{\phi} = (\phi_1, \phi_2)$ and non-orthogonal eigenfunctions $\boldsymbol{\psi}^{(1)}$ and $\boldsymbol{\psi}^{(2)}$ both corresponding to stable eigenvalues. As shown in figure 2.2, for this system, consider a unit length initial condition $\mathbf{f}$ defined as the difference between two non orthogonal eigenfunctions, $\boldsymbol{\psi}^{(1)}$ and $\boldsymbol{\psi}^{(2)}$. As time progresses the eigenfunction components decrease. The vector $\mathbf{f}$ transiently increases in length and aligns itself with the least stable eigenfunction direction. Of course in the limit of large times $\mathbf{f}$ will decrease to zero.

Depending on the 'shape' of the initial condition, therefore, non-normal linear systems can sustain transient energy growths. An important question is that of finding the 'most dangerous' initial condition leading to the maximum energy growth. The *optimal energy amplification* $G(t)$, defined as:

$$G(t) = \max_{\boldsymbol{\phi}_0 \neq 0} \frac{\| \boldsymbol{\phi}(t) \|^2}{\| \boldsymbol{\phi}_0 \|^2}, \tag{2.6}$$

is the envelope of all the possible growth curves that can be realized by the system. At each specific target time corresponds a different initial condition. But it is labeled like *optimal initial condition* $\boldsymbol{\phi}_0^{(opt)}$ the one that leads to the *maximum transient energy growth* $G_{max} = \max_t G(t)$,

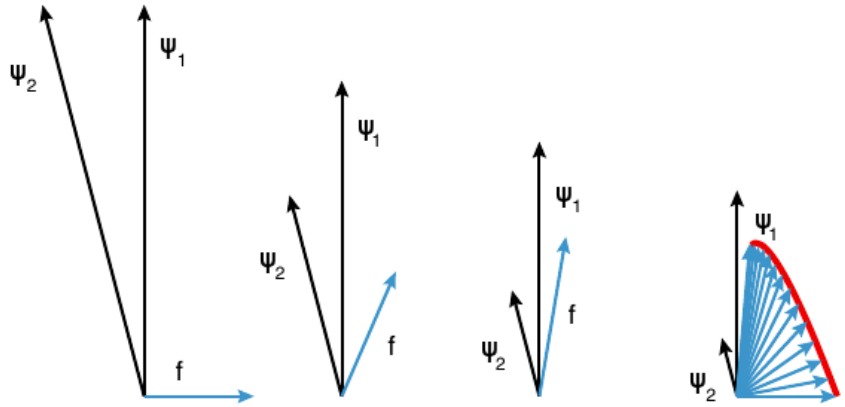

Figure 2.2: Vector example of transient growth. Starting on the left, the vector f is defined as the difference between the nearly collinear vectors ψ_1 and ψ_2. During iteration (proceeding to the right of the figure) the vector $\mathbf{f}$ gradually turns into the direction of ψ_1 (sketch on the right), but increases substantially in length, before decaying to zero. Thus, the superposition of decaying non orthogonal eigenfunctions can produce, in the short term, growth in the norm of a perturbation. Source: Schmid (2007).

which is obtained at $t = t_{max}$. The optimally amplified structures are then those computed for the response of the system at t_{max}.

Let us illustrate the computation of optimal energy growths on the following simple linear initial value problem mimicking the dynamics of streaks (ϕ_1) and vortices (ϕ_2) in parallel shear flows (see e.g. Farrell & Ioannou, 1996; Schmid & Henningson, 2001):

$$\frac{d}{dt}\begin{pmatrix}\phi_1\\ \phi_2\end{pmatrix} = \begin{bmatrix}-\frac{2}{3Re} & 1\\ 0 & -\frac{1}{5Re}\end{bmatrix}\begin{pmatrix}\phi_1\\ \phi_2\end{pmatrix}. \tag{2.7}$$

The system is completed by the initial conditions $\phi_1(0) = \phi_{10}$ and $\phi_2(0) = \phi_{20}$. The eigenvalues $s_1 = -2/(3\,Re)$ and $s_2 = -1/(5\,Re)$ of $\mathbf{L}$ have negative real part indicating linear stability of the system. The eigenvectors are $\psi_1 = [1\ 0]^T$ and $\psi_2 = [1\ 7/(15Re)]^T$. The optimal transient growths $G(t)$ [1] sustained by the system (2.7) are computed for $Re = 25$, 50 and 100 and reported in figure 2.3. From figure 2.3(a) it is seen that $G(t)$ increases when the Reynolds number increases. In particular G_{max} grows like Re^2 and the time t_{max} like Re (see how they overlap in one curve in figure 2.3(b) when rescaled). Another interesting test is the follow one. From the already mentioned literature about the lift-up effect we know that the optimal initial structures are streamwise elongated spanwise periodic vortices while the optimally amplified structures are streaks. Those two structures, the initial and the optimal response, can be seen as "orthogonal" between them, since the former have the normal and the spanwise components of the velocity non zero and the latter has as only non zero components the downstream one. The same behavior can be found if the vector $\phi_0 = [0\ 1]$ is given like initial condition of the system (2.7). At $t = t_{max}$ and $Re = 25$ the optimal response will be $\phi = [0.9998\ \ 0.0187]$ which can be easily proved to be orthogonal to the initial condition.

[1] $G(t)$ is easily computed as the norm $\|e^{\mathbf{L}\,t}\|$ with standard MATLAB or Scilab routine.

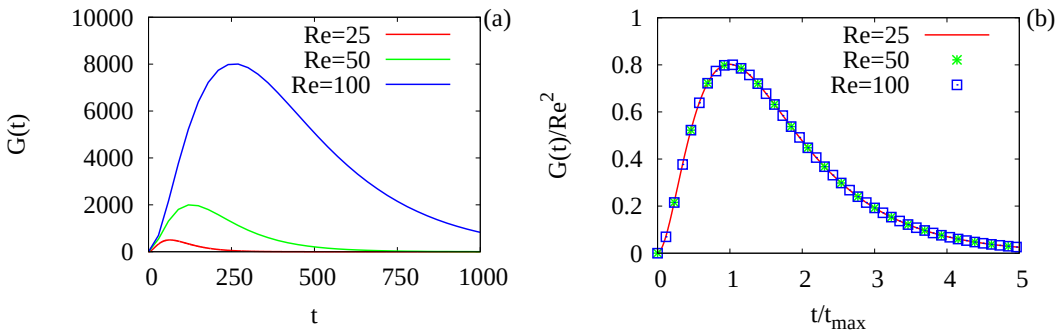

Figure 2.3: Optimal transient energy growth of a toy system. Panel *a*: optimal transient energy growth $G(t)$ of the linear operator of the system (2.7). Panel *b*: rescaled optimal energy growth.

Chapter 3

A tale of three 2D wakes: the prologue

In this chapter we introduce three wakes used in our study by order of increasing complexity: a parallel model wake, a weakly non-parallel 'synthetic' wake and the circular cylinder wake. Below, we describe in more details the stability properties of such flows as well as their uncontrolled dynamics. Their optimal perturbations and the stabilization of these basic flows will be discussed in chapters 4 and 5 respectively.

1 Monkewitz's model parallel wakes

The parallel wake basic flows we consider are defined by $\mathbf{U}_{2D} = [U_M(y), 0, 0]$, where U_M is the velocity profile proposed by Monkewitz & Nguyen (1987) and Monkewitz (1988) and used in a number of successive studies including e.g. those of Delbende & Chomaz (1998) and Hwang *et al.* (2013):

$$U_M(y) = 1 + \Lambda \left[\frac{2}{1 + \sinh^{2N}(y \sinh^{-1} 1)} - 1 \right], \tag{3.1}$$

where $\Lambda = (U_c^* - U_\infty^*)/(U_c^* + U_\infty^*)$, and U_c^* and U_∞^* are the centerline and the free stream velocity, respectively. The streamwise velocity profile $U(y)$ is made dimensionless with respect to the reference velocity $U_{ref}^* = (U_c^* + U_\infty^*)/2$. The spatial coordinates are made dimensionless with respect to the reference length δ^* which is the distance from the centreline to the point where the velocity is equal to U_{ref}^*. The Reynolds number used in the study of these parallel wakes is defined as $Re = U_{ref}^* \delta^* / \nu$. In addition to the Reynolds number, the parameters defining the basic flow and its stability are Λ and N. The velocity ratio Λ controls the depth of the wake: $\Lambda = -1$ e.g. corresponds to zero centerline velocity. The shape factor N prescribes the ratio of the mixing layer thickness to the wake width: $N = \infty$ defines a top-hat wake bounded by two vortex sheets and $N = 1$ which leads to the standard $sech^2 y$ wake (see figure 3.1).

Monkewitz (1988) studied the linear stability of this model of wakes as a function of Re, Λ and N. One of the most salient results, reported in the right panel of figure 3.1, is the boundary of the absolute instability region in parameter space. For $N^{-1} = 0$ (i.e. $N = \infty$) the profiles are mainly convectively unstable for the considered range of Λ at a given Reynolds number. Then when N^{-1} increases around the value 0.5 (i.e. $N = 2$) the range of Λ where the profile are absolutely unstable increases. Then for larger values around $N^{-1} \approx 1$, the region of absolutely instability for lower Reynolds number decreases with a rate higher than those

for larger Reynolds number. Monkewitz (1988) confirms the existence of a region of absolute instability in the near wake at the onset of the global instability by associating the streamwise evolution of the nonparallel wake to a path in the Re, Λ, N parameter space.

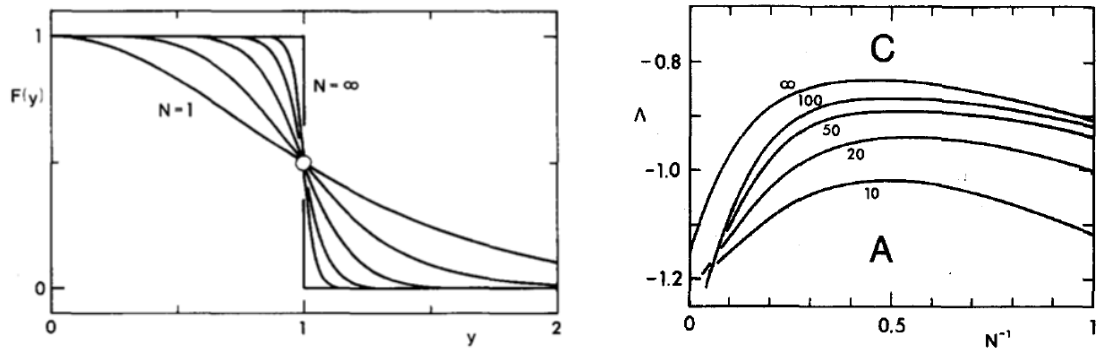

Figure 3.1: Monkewitz's parallel wake profiles. Left panel: $F(y) = (1+\sinh^{2N}[y\sinh^{-1}(1)])^{-1}$. When N and Λ changes the velocity profile can be easily adapted to the particular downstream position of the wake's development. Right panel, absolute instability boundary in the $\Lambda - N^{-1}$ plane for different Reynolds number indicated close to the curves (A stands for absolutely unstable while C stands for convectively unstable). Source: Monkewitz (1988).

In the following we will use as a case-study the velocity profile corresponding to the values $Re = 50$, $\Lambda = -1$ and $N = 1$ corresponding to a strong absolute instability.

We have analyzed the stability properties of the considered wake by post processing the linear impulse response obtained by DNS (see appendix A). The temporal analysis shows that the maximum growth rate $\omega_{i,max}$ is equal to 0.256, the parallel wake is then clearly strongly unstable. The 2D parallel wake (case A for the parallel analysis in the followings chapters) shows to be absolutely unstable with an absolute growth rate $\sigma(v = 0) = 0.073$ and a wavepacket trailing edge velocity $v^- = 0.089$. These values are in good agreement with Monkewitz (1988).

2 A weakly non-parallel 'synthetic' wake

Triantafyllou *et al.* (1987) have shown that non-parallel wakes can sustain vortex shedding even in the absence of the bluff-body generating the wake. 'Synthetic' wakes have therefore been used to investigate theoretical concepts in a simplified setting (see e.g. Pier & Huerre, 2001). The synthetic wake is generated by enforcing a Monkewitz's profile at the inflow boundary in a DNS. The numerical integration domain is chosen wide and long enough to avoid numerical artifacts (see appendix A). The parameters of the inflow profile are $N = 1$ and $\Lambda = -1.35$, which ensures a small upstream recirculation region. The Reynolds number is based on the inflow wake profile $Re = U^*_{ref}(x = 0)\,\delta(x = 0)/\nu$. The basic flow is found as a steady solution of the Navier-Stokes equations with enforced cross-stream-symmetry. It corresponds to a weakly non-parallel wake which slowly diffuses while evolving downstream (see figure 3.2(a)).

If the cross-stream-symmetry condition is removed, the synthetic wake sustains a global instability and periodic vortex shedding for $Re \gtrsim 39$. In the following we will consider the globally unstable case at $Re = 50$ where shedding is observed (see figure 3.2(b)). The global stability properties of this basic flow are retrieved from the integration of the linearized Navier-Stokes equations, as explained in appendix A. At $Re = 50$, the most unstable linear global mode has a growth rate of $s_r = 0.0325$.

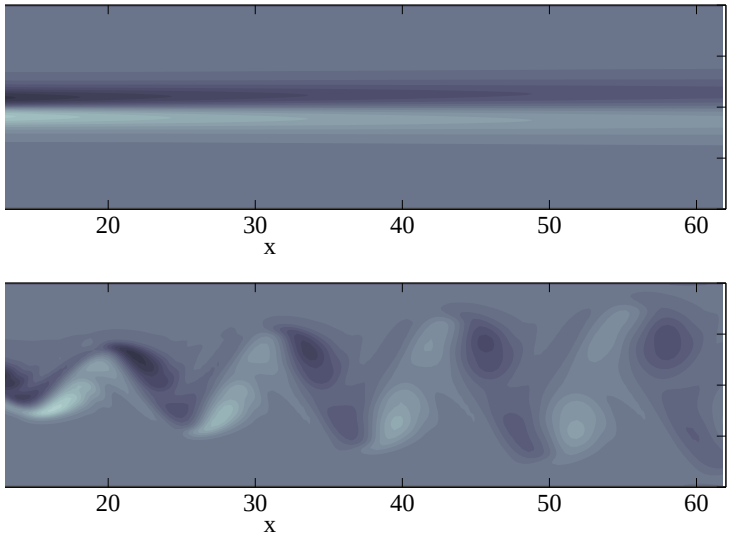

Figure 3.2: Synthetic non parallel wake: spanwise vorticity fields $\omega_z(x, y)$ associated to the reference 2D non-parallel wake at $Re = 50$. Top panel: (unstable) basic 2D flow profile obtained by enforcing the y-symmetry of the solution. Bottom panel: Snapshot of the periodic self-sustained state obtained without enforcing the y-symmetry of the solution.

3 The circular cylinder wake at low Reynolds number

The third case considered is the widely studied circular cylinder wake in the unstable regime at low values of the Reynolds number. As for the synthetic wake, the basic flow is a steady solution of the Navier-Stokes equations obtained upon enforcement of the y-symmetry condition. The basic solution corresponds to the symmetric steady flow with a recirculation region behind the circular cylinder. We have verified that the main characteristics of the computed basic flow, such as the drag coefficient or the length of the separation bubble, are in agreement with those found by e.g. Fornberg (1980), Dennis & Chang (1970) and Giannetti & Luchini (2007).

If the y symmetry constraint is removed, the flow displays the well known periodic vortex shedding (see figure 3.3). We have checked that, in the unstable regime, the values of the drag coefficient and the Strouhal number are in good agreement with previous results (in particular with Kim & Choi (2005) at $Re = 100$).

Like for the synthetic wake case, the global instability of the basic flow is studied by integrating in time the linearized Navier-Stokes equation. The computed linear growth rates

of the uncontrolled $2D$ cylinder wake are reported in table 3.1 with all the Reynolds number considered.

Re	L_R	s_r
50	3.1 D	0.010
75	4.6 D	0.095
100	6.2 D	0.123

Table 3.1: Considered cases for the circular cylinder's wake. L_R is the value of the recirculation region of the steady unstable basic flow, while s_r is the global growth rate.

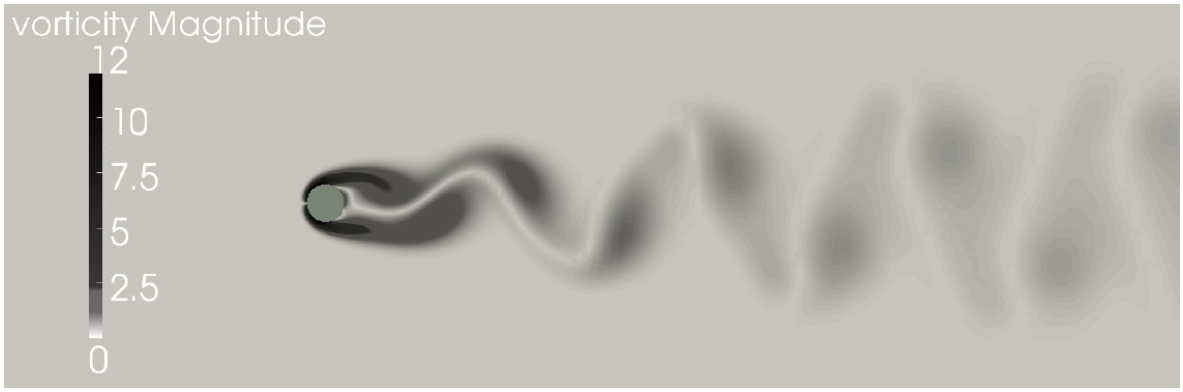

Figure 3.3: Spanwise vorticity ω_z for the flow around a circular cylinder at $Re = 75$.

Chapter 4

Optimally amplified streamwise streaks in wakes

1 Optimal temporal energy growth in parallel wakes

We begin with optimal temporal energy growths of streamwise perturbations sustained by the parallel wake $\mathbf{U}_{2D} = [U_M(y), 0, 0]$, with $U_M(y)$ given in eq. (3.1) and the parameters specified in the chapter 3. The considered Reynolds numbers range from 25 to 100.

As it is well known (see e.g. Schmid & Henningson, 2001), in parallel flows, because of the translational invariance, optimal growths can be computed separately for each Fourier mode of the perturbation velocity field $\widehat{\mathbf{u}}(\alpha, y, \beta, t)\, \mathrm{e}^{i(\alpha x + \beta z)}$. The optimal energy growths, defined in (2.6), are based on the usual energy density norm [1] $\|\widehat{\mathbf{u}}\|^2 = (1/\mathcal{V}_{ref}) \int_{\mathcal{V}} |\widehat{\mathbf{u}}|^2 \, d\mathcal{V}$. For the considered values of Re the wake is unstable. For e.g. $Re \gtrsim 25$ an unstable region exists in the plane $(\alpha - \beta)$ centered on the two dimensional perturbations ($\beta = 0$) and with $0 < \alpha \lesssim 1.75$. Optimal transient growths will be computed for streamwise uniform perturbations which are linearly stable. Streamwise uniform perturbations are considered both because they are the most transiently amplified in stable wall-bounded shear flows and because they well mimic the perturbations that would be spatially forced by steady passive devices.

Since the basic flow is symmetric with respect to the plane $y = 0$, the perturbations are separated in two separate classes: *varicose* [for which $\widehat{u}(-y) = \widehat{u}(y)$, $\widehat{v}(-y) = -\widehat{v}(y)$, $\widehat{w}(-y) = \widehat{w}(y)$], and *sinuous* (whit the opposite symmetries). Standard numerical algorithms, validated in previous investigations (see appendix A) are used to compute the optimal growths and the associated optimal perturbations for $\alpha = 0$ and wavenumbers β in the range $0.1 - 2$.

From the analysis of Gustavsson (1991) it is expected that for streamwise uniform perturbations G_{max} and t_{max} are proportional respectively to Re^2 and Re (see also figure 2.3). This is indeed verified by the present computed growths of varicose and sinuous perturbations as shown in figure 4.1. The maximum growths G_{max} and the associated t_{max} are also seen to increase with the perturbation spanwise wavelength $\lambda_z = 2\pi/\beta$ apparently without bound, similarly to what is observed e.g. in vortex columns in unbounded domains by Pradeep & Hussain (2006) and Antkowiak & Brancher (2004). From figure 4.1 it is also seen that varicose perturbations are slightly less amplified than the sinuous ones.

Similarly to what was found in wall-bounded shear flows, optimal initial conditions corre-

[1] $\mathcal{V}_{ref} = 2\delta L_x L_z$, δ as defined for the Monkewitz's profile and L_x and L_z the non dimensional size in the downstream and spanwise directions respectively.

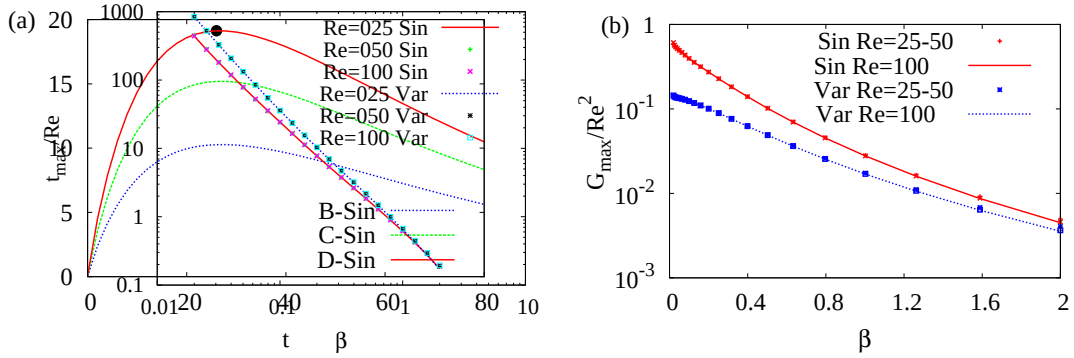

Figure 4.1: Rescaled maximum energy amplifications in parallel wakes: rescaled maximum time t_{max}/Re (panel a) and rescaled maximum growth G_{max}/Re^2 (panel b) dependence on β for sinuous and varicose perturbations.

spond to spanwise periodic streamwise vortices while the most amplified perturbations correspond to spanwise periodic streamwise streaks. Optimal perturbations computed for $Re = 50$ and $\beta = 1$, are reported in Figure 4.2. In the case of varicose perturbations (Figure 4.2a) there are two antisymmetric rows of vortices on each side of the wake symmetry axis inducing symmetric streaks, while in the case of sinuous perturbations (Figure 4.2b) a single row of vortices centred on the wake symmetry axis induces antisymmetric streaks.

When the spanwise wavenumber β is decreased (the spanwise wavelength $\lambda_z = 2\pi/\beta$ is increased), the size of optimal perturbations increases both in the spanwise and in the normal direction y. The velocity of optimal varicose initial vortices is e.g. non negligible up to $y \approx \lambda_z$, which highlights the difficulty of forcing optimal perturbations with low values of β in practical applications.

We conclude that high energy streaks can be efficiently amplified by parallel wakes at moderate Re.

2 Optimal spatial energy growth in weakly non parallel synthetic wakes

The analysis developed for parallel wakes based on temporal optimal perturbations has provided essential informations on the physics of streaks amplification in wakes. Some important questions are however left unanswered by this preliminary analysis. For instance, it is not a priori clear that large energy amplifications can be obtained in non-parallel wakes at low Reynolds numbers; indeed, the downstream wake diffusion not only reduces the basic flow shear fuelling the transient growth but also increases the local spanwise wavenumber which has a further stabilizing influence.

A second problem is that in practical applications, *spatial* energy growths must be considered and that the algorithm used to compute them ideally should be extendible to real applications where the body is present. This has led us to design an algorithm which, to our knowledge, has never been used before in this context and which is also highly efficient and scalable and can be extended to real wakes configurations (we will show results for the circular cylinder's wake in section 3). This algorithm, described in appendix B, is based on

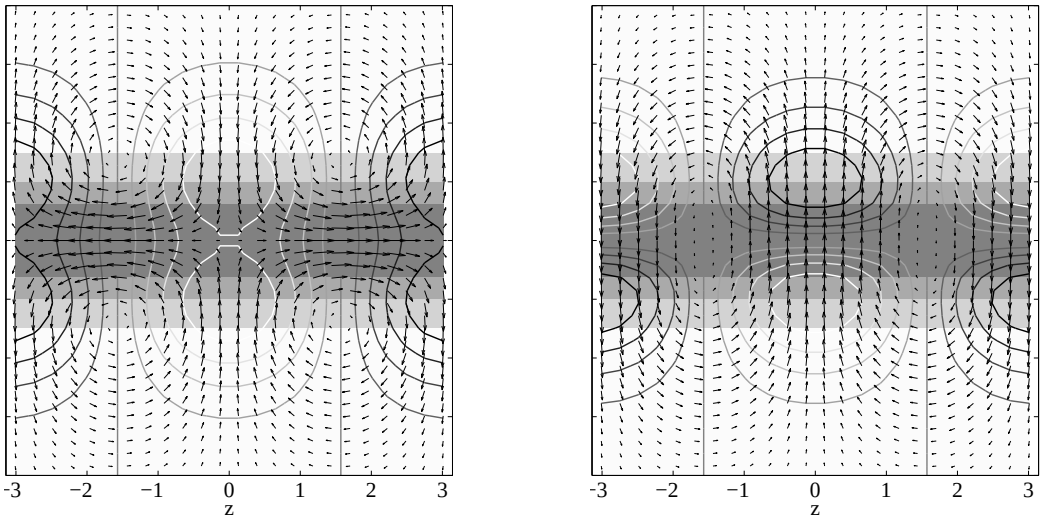

Figure 4.2: Optimal perturbations of the parallel wake: Cross-stream view of the v_0^{opt}-w_0^{opt} components of optimal initial vortices (arrows) and of the u component of the corresponding maximally amplified streak (contour-lines: high speed streaks in whiter lines and low speed streaks in darker lines) for $Re = 50$ and $\beta = 1, \alpha = 0$. Optimal varicose perturbations are reported in the left panel (a), while sinuous ones are reported in the right panel (b). The 2D basic flow wake streamwise velocity is reported in grey-scale with white corresponding to the freestream velocity and dark gray to zero (wake centreline).

a set of independent DNS of the linearized equations whose output is used to compute the energy growths in a subspace. The number of DNS is increased until convergence is achieved.

The spatial optimal growth is computed as follows. Instead of considering the temporal energy growth of streamwise uniform initial perturbations (given at $t = 0$) as in the parallel case, we consider the downstream energy growth of steady perturbations injected at $x = 0$ (inflow boundary). As in the temporal analysis it was found that the most amplified perturbations consist in streamwise vortices, the following inlet conditions are considered: $\mathbf{u}_0 = (u_0, v_0, w_0) = (0, \partial\psi/\partial z, -\partial\psi/\partial y)$. Single-harmonic spanwise periodic perturbations can be considered without loss of generality: $\psi' = f(y)\sin(\beta z)$. As we will see in chapter 5, varicose perturbations (mirror-symmetric with respect to the $y = 0$ plane) are the most efficient for control purposes (Choi *et al.*, 2008; Hwang *et al.*, 2013) even if they are slightly less amplified than sinuous ones. Therefore we enforce $f(-y) = -f(y)$ which induces varicose streaks. For this case, the spatial optimal energy growth is defined as:

$$G(x) = \max_{\mathbf{u}_0} \frac{e(x)}{e_0}, \tag{4.1}$$

where $e(x) = \frac{1}{2\delta\lambda_z}\int_{-\infty}^{\infty}\int_0^{\lambda_z} \mathbf{u}\cdot\mathbf{u}\, dy\, dz$, is the energy associated to a streamwise position x and $e_0 = e(x = 0)$.

To compute $G(x)$ we use an increasing set of inflow conditions (see appendix B) chosen as: $\mathbf{b}_0^{(m)}(y, z) = (0, \partial\psi^{(m)}/\partial z, -\partial\psi^{(m)}/\partial y)$ with $\psi^{(m)} = f_m(y)\sin(\beta z)$ and $f_m(y) = -f_m(y)$ for

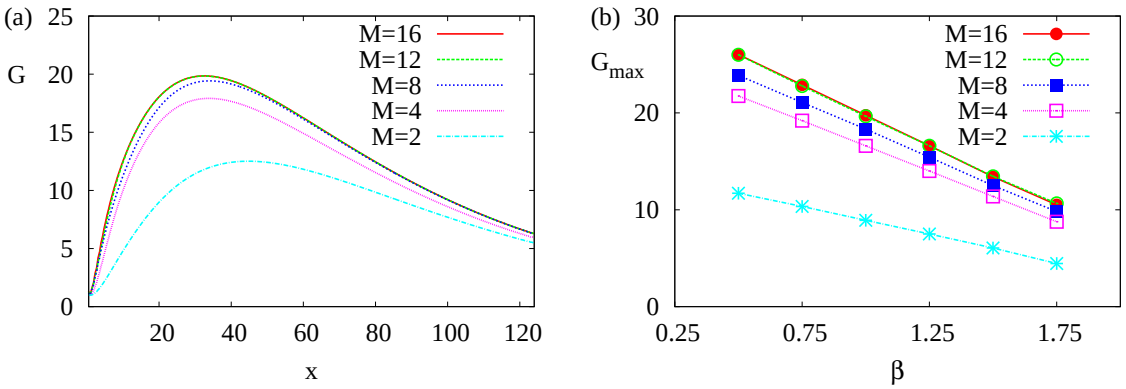

Figure 4.3: Optimal energy growth in the non parallel synthetic wake: convergence of $G(x)$ for $\beta = 1$ (panel a) and of the maximum energy growth $G_{max}(\beta)$ when the number M of linearly independent inflow conditions is increased at $Re = 50$. Well converged results are obtained for $M = 16$.

$m = 1, \ldots, M$. We have found well suited the set $f_m = \sin(2m\pi y/L_y)$, where the numerical box extends from $-L_y/2$ to $L_y/2$ in the y direction.

Optimal energy growths have been computed for a set of spanwise wavenumbers β increasing M until a precision of 1% or higher on G_{max} was achieved. The convergence of the optimal growth curves with increasing M is quite fast, and this holds for all the considered values of β, as can be seen in figure 4.3. Well converged results, with relative variations below 1% are obtained with only $M = 16$ terms. It is also seen how, consistently with results form the local analysis above, the maximum growth $G_{max} = \max_x G(x)$ increases with increasing spanwise wavelength $\lambda_z = 2\pi/\beta$, i.e. with decreasing β, figure 4.3(b).

The optimal inflow perturbations ($x = 0$) and the maximum response ($x = x_{max}$) associated to the maximum growth G_{max} obtained for $\beta = 1$ are reported in figure 4.4. The optimal inflow perturbations consist in two rows of vortices on each side of the $y = 0$ plane, with opposite rotation on each side. These vortices induce the growth of y-symmetric (varicose) streaks.

The observed trends are in agreement with those found in our previous local analysis (see section 1). However, the maximum spatial growth rates obtained in the non-parallel case are smaller than the temporal ones obtained at the same β under the frozen and parallel flow approximation. This is not surprising because the nominal values of β and Re of the non-parallel results are based on the properties of the wake profile at the inflow ($x = 0$). These values would be different downstream, e.g at x_{max}, if based on properties of the wake computed at the local x value. As the dimensional reference length $\delta^*(x)$ (the y^* value where $U^*_{2D}(y^*) = U^*_{ref}$), increases with x, a dimensionless wavenumber $\beta = \beta^*\delta^*$ based on the local scale, would increase going downstream. As the maximum growth rate is a decreasing function of β (see figure 4.1), it is not surprising that the maximum growth rates are smaller than the ones that would be obtained if the wake was parallel. Therefore the results of the present analysis should be compared to the ones of the local analysis obtained at larger values of β.

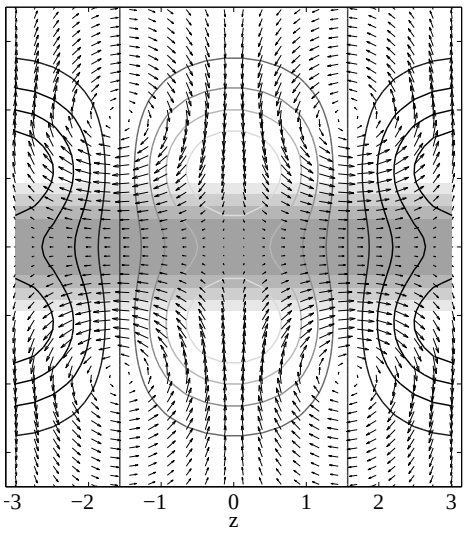

Figure 4.4: Optimal perturbations of the non parallel synthetic wake: view of the cross-stream v_0^{opt}-w_0^{opt} components of optimal vortices (arrows forced at the inflow ($x = 0$) and of the streamwise u component of the corresponding optimal streaks (contour-lines) at $x = x_{max}$ for $Re = 50$, $\beta = 1$. The streamwise velocity at the inflow $U_0(y)$ is also reported in grey-scale with white corresponding to the freestream velocity and dark grey to zero (wake centreline).

3 Optimal blowing and suction on the circular cylinder

The analysis developed on the weakly non parallel synthetic wake has shown its potential for sustaining large spatial energy growths where upstream vortices lead to the spatial transient amplification of high energy streamwise streaks. This mechanism is of general nature because it has been obtained in the absence of the body. However, an important issue unaddressed is how optimal steady vortices can be forced, in practical applications, on the body surface. We addressed this questions for the canonical case of the circular cylinder's wake. For this flow, we want to understand if large spatial energy amplifications can be obtained by using control on the cylinder surface at low Reynolds numbers. Many questions arise in this case. How do these optimal amplifications relate to those obtained for the idealized non-parallel wake? Does an optimally amplified finite spanwise wavelength exist in this case? If so, what is its value and how does this value compare to spanwise wavelengths that minimize the control energy? What is the minimum energy required to stabilize the global instability?

The theoretical setting considered in the previous section for the case of the non parallel synthetic wake can be easily applied, with the proper corrections, to the present case. The perturbations are always assumed to be varicose and they are introduced via radial blowing and suction $u_w(\theta, z)$ modulated along the span of the cylinder [2].

The optimal spatial energy amplification $G(x)$ is the one defined in eq. (4.1) with:

$$e(x) = \frac{1}{\pi\,\lambda_z}\int_{-\infty}^{\infty}\int_{0}^{\lambda_z} \mathbf{u}\cdot\mathbf{u}\,dy\,dz \qquad e_w = \frac{1}{2\,\pi\,\lambda_z}\int_{0}^{2\pi}\int_{0}^{\lambda_z} u_w^2\,d\theta\,dz, \tag{4.2}$$

[2] θ is the azimuthal coordinate.

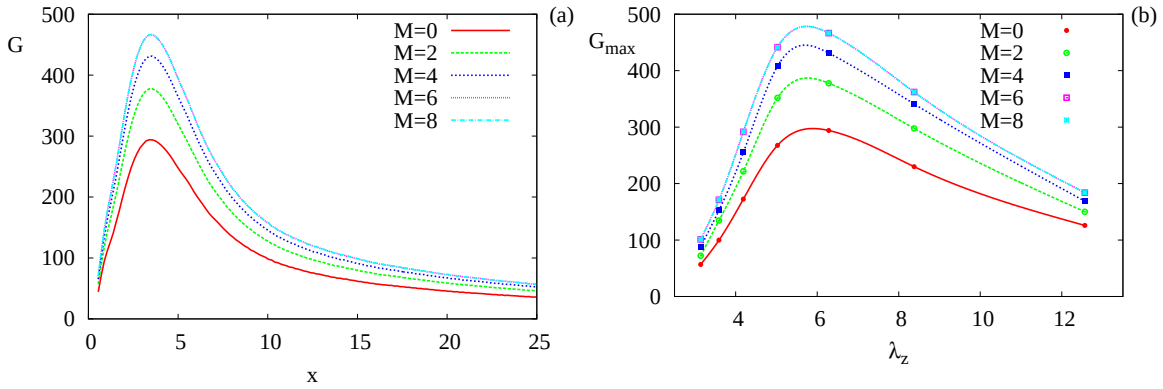

Figure 4.5: Optimal energy growth in the circular cylinder's wake: convergence of the optimal energy growth $G(x)$ for $\lambda_z = 2\pi$ (panel a) and of $G_{max}(\lambda_z)$ (panel b) at $Re = 75$ when the number M of linearly independent distributions of wall blowing and suction is increased. Well converged results are obtained for $M = 6$.

where $e(x)$ is the energy at a given x-position and e_w is the input energy injected at body's surface. The computation of the optimal distribution $u_w^{opt}(\theta, z)$ is based on the same algorithm used for the synthetic wake (see appendix B).

As the basic flow $\mathbf{U}_{2D}$ is spanwise invariant and the equations linear, single-harmonic spanwise periodic perturbations can be considered without loss of generality: $u_w(\theta, z) = f(\theta)\sin(2\pi z/\lambda_z)$ with $f(-\theta) = f(\theta)$ which leads to varicose streaks. A standard cosine series expansion in θ is used leading to the choice $b_w^{(m)}(\theta, z) = \cos(m\,\theta)\sin(2\pi z/\lambda_z)$ (where $m = 0, \ldots, M$) for the set of linearly independent input conditions used in the algorithm described in appendix B. Also here, optimal energy growths have been computed by increasing M until a precision of 1% or higher on G_{max} was achieved for a set of spanwise wavelengths λ_z.

Typical $G(x)$ and $G_{max}(\lambda)$, as well as their convergence history, obtained for $Re = 75$ are reported in figure 4.5. From the figure it is seen that the optimal growths are converged with more than 1% precision with only $M = 6$ terms.

The computations have been repeated at $Re = 50$ and $Re = 100$. The convergence of the results with M is similar to the $Re = 75$ case. As shown in Figure 4.6, the main effect of an increase of Re is to increase the optimal amplifications G_{max} and then to slightly increase the position x_{max} where this maximum is attained. The large amplifications found are consistent with those found in the previous investigations mentioned in this chapter but also with those of Abdessemed *et al.* (2009) who found optimal *temporal* energy amplifications of the order of $10 - 10^2$ for initial perturbations with $4 \lesssim \lambda_z \lesssim 8$ at $Re = 45$. From figure 4.6(b) is it also seen that x_{max} is an increasing function of λ_z. The most amplified wavelengths are reported in table 4.1.

The radial distributions $\widetilde{u}_w^{opt}(\theta)$ of the blowing and suction $\widetilde{u}_w^{opt}(\theta)\sin(2\pi z/\lambda_z)$ are shown in Figure 4.7. They correspond to spanwise periodic blowing and suction with a maximum near $\theta \approx \pm 90^o$ and minima at the bow and the stern of the cylinder. The variations of $\widetilde{u}_w^{opt}(\theta)$ with λ_z and Re are small and may be neglected in a first approximation. As shown in Figure 4.8, the spanwise periodic blowing and suction induce counter-rotating streamwise vortices which decay downstream while forcing the growth of varicose streamwise streaks. Also in this relatively complicated flow, therefore, the main mechanism at play seems to be

Re	λ_z	x_{max}
50	6.5	3.4
75	5.7	3.5
100	6.1	3.6

Table 4.1: Circular cylinder's wake: most amplified wavelength λ_z and the position x_{max} for the considered Reynolds numbers.

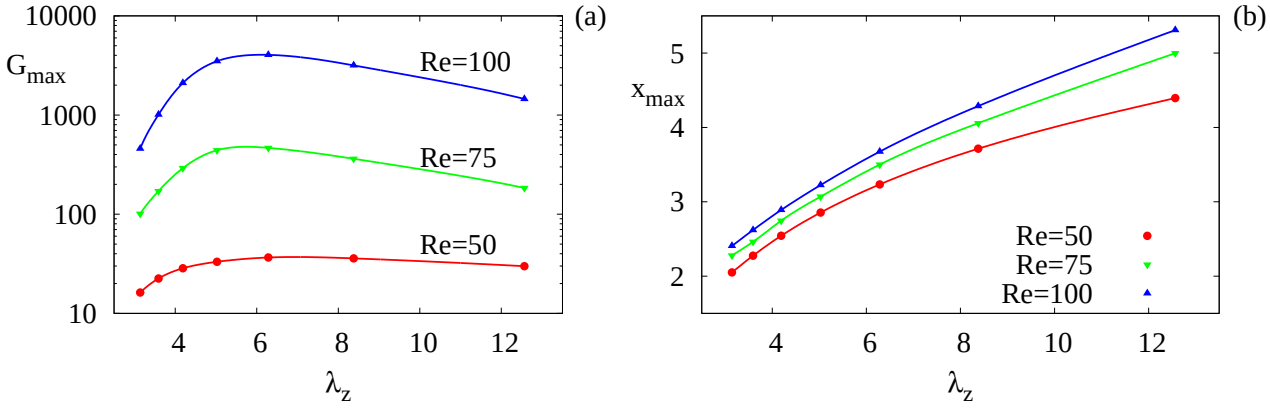

Figure 4.6: Maximum amplification in the cylinder's wake: dependence on the spanwise wavelength λ_z of the maximum transient energy growth G_{max} (panel a) and of the streamwise station x_{max} (panel b) where the maximum is attained for the selected Reynolds numbers $Re = 50$, $Re = 75$ and $Re = 100$.

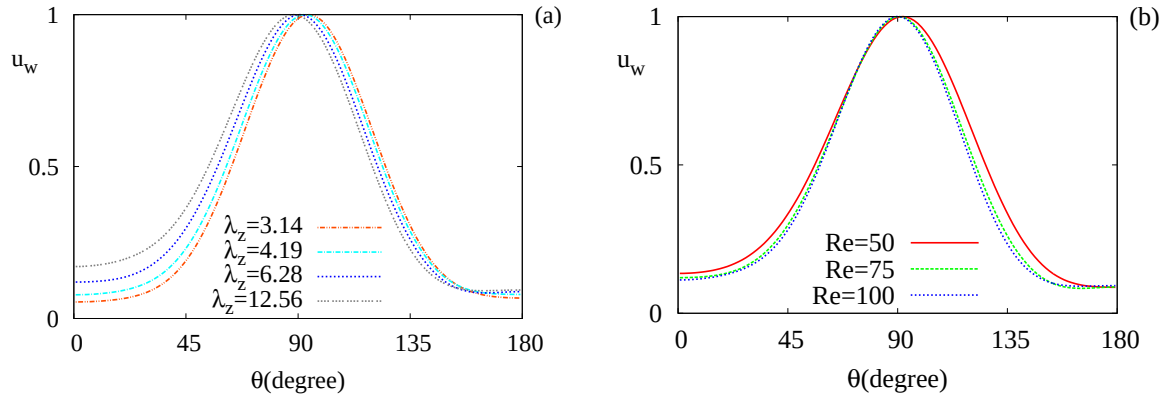

Figure 4.7: Circular cylinder wake: Azimuthal distributions $\widetilde{u}_w^{opt}(\theta)$ of the blowing and suction normalized by their maximum value. Panel a: results obtained for a set of spanwise wavelengths λ_z at $Re = 75$. Panel b: distributions pertaining to the most amplified λ_z at each considered Reynolds number.

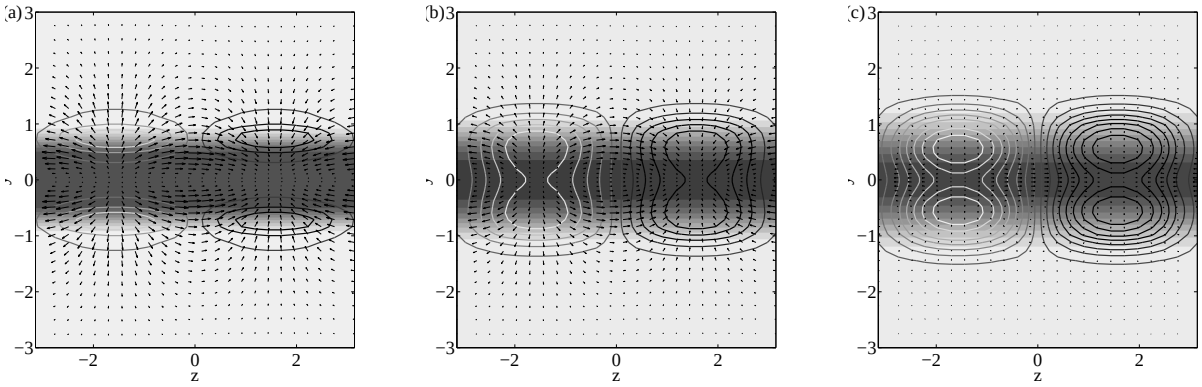

Figure 4.8: Optimal perturbations in the cylinder wake: Cross-stream ($y-z$) view of the velocity perturbations forced by the blowing and suction at $Re = 75$, $\lambda_z = 2\pi$ at the three selected streamwise stations: $x = 1/2$ (cylinder stern, panel a), $x = x_{max}/2$ (midway to the position of maximum streak amplitude, panel b) and $x = x_{max}$ (position of maximum streak amplitude, panel c). The scales with which are plotted the streamwise u (streamwise streaks, contour-lines) and the cross-stream v-w components (streamwise vortices, arrows) are the same in all panels. The reference 2D basic flow streamwise velocity $U_{2D}(y)$ is also reported in grey-scale with light grey corresponding to the freestream velocity and dark grey the minimum velocity (wake centreline).

the lift-up effect.

The fact that optimal values of the wavelength λ_z exist is a remarkable difference with the case of the weakly non parallel wake. Since the weakly non parallel wake is an unbounded flow no limitation on the size of the structure in the normal direction was given and so G_{max} was a monotonic function of λ_z. In the present case a strong limitation, which afflicts (positively) also the number of components of the base for the calculus of the optimal perturbations, is that the control is localized on the body's surface. So finite effective extension in y direction can be attained, and therefore a maximum value of G_{max} is reached in correspondence of a particular λ_z.

Chapter 5

Stabilizing effect of streaks

The influence of finite amplitude streaks on the wake's stability is developed in two separate steps following the approach used in a number of previous studies (Reddy *et al.*, 1998; Andersson *et al.*, 2001; Brandt *et al.*, 2003; Cossu & Brandt, 2004; Park *et al.*, 2011). First, nonlinear 'streaky wakes' are computed by enforcing linear optimal perturbations with finite amplitude and integrating the nonlinear Navier-Stokes equations. We will address in the future to 'streaky' basic flow $\mathbf{U}_{3D}$ to indicate the superimposition of the effects of the *primary perturbations*, those which give birth to streaks, on the $2D$ wake, $\mathbf{U}_{2D}$. $\mathbf{U}_{3D}$ is a spanwise modulated basic flow which presents alternating regions of high speed donwstream velocity and region of low speed donwstream velocity. Then, the linear stability analysis of the computed basic flows is assessed by considering the evolution of the small *secondary perturbations* superposed to those streaky basic flows. Finally, non-linear simulations, where secondary perturbations are no more required to be small, are used to confirm the results of the linear analysis in the nonlinear regime.

1 Non linear streaky basic flows

Streaky parallel wakes. The optimal linear perturbations (streamwise vortices) described in chapter 4, are now considered with finite initial amplitude[1] A_0 and are used as initial condition $\mathbf{U}_{3D0}(y,z) = \mathbf{U}_M(y) + A_0\mathbf{u}_0^{(opt)}(y,z)$. The nonlinear Navier-Stokes equations are then numerically integrated for the selected initial conditions (see appendix A for details on the numerical simulations) providing a family of basic flows $\mathbf{U}_{3D}(y,z,t,A_0)$, parametrized by A_0 for the considered Reynolds number $Re = 50$. The streaks are characterized by their amplitude which is measured extending the standard definition of Andersson *et al.* (2001):

$$A_s(t,A_0) = \frac{\max_{y,z}\left[U_{3D}(y,z,t) - U_{2D}(y)\right] - \min_{y,z}\left[U_{3D}(y,z,t) - U_{2D}(y)\right]}{2\left(\max_y U_{2D}(y) - \min_y U_{2D}(y)\right)} \tag{5.1}$$

In this definition the streak amplitude is defined as half the maximum deviation of the streaky $3D$ profile from the reference $2D$ profile divided by the maximum velocity variation of the

[1] Finite amplitude A_0 have to be associated to the optimal initial perturbations to allow an increasing amplitude in the considered wake. The optimal initial conditions (see chapter 4.1) are normalized such as $\|\mathbf{u}_0^{(opt)}\| = 1$. Given this assumption, if e_0 is the level of energy associated to the initial condition for the parallel wake, $A_0 = \sqrt{e_0}$. For more details about the explicit expression we remind to the section with papers attached to the manuscript.

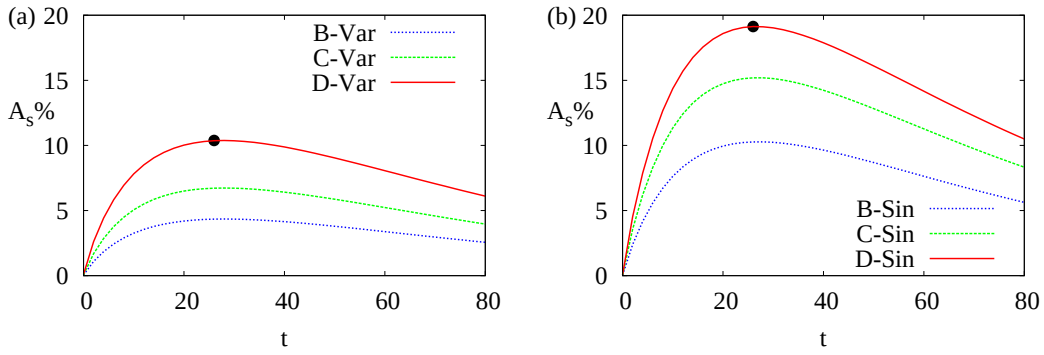

Figure 5.1: Streaky parallel wakes: Temporal evolution of nonlinear streaks amplitude $A_s(t)$ for selected initial amplitudes A_0 of the initial optimal perturbations and for varicose (left panel a) and sinuous (right panel b) perturbations. For all cases $Re = 50$ and $\beta = 1$. See table 5.1 for the legend of cases and the associated initial amplitudes A_0.

inflow $2D$ reference profile.

In figure 5.1 are reported the nonlinear streaks amplitude temporal evolutions for $Re = 50$ and $\beta = 1$ for varicose and sinuous perturbations of selected amplitudes. Case A corresponds to the reference two-dimensional wake profile $U_M(y)$ (no streaks) while cases B, C and D are obtained by increasing the initial optimal perturbation amplitude A_0. The plots show the temporal transient growth and the increasing level of amplitude when higher amplitude A_0 are considered (see table 5.1).

In figure 5.2 are shown the cross-stream section of the streaky varicose and sinuous case D basic flows. and sinuous case. Varicose perturbations are symmetric to respect the normal direction and, since they are modulated in the spanwise direction, regions where the wake thickness is thicker are followed by regions where it is thinner. Sinuous perturbations are instead antisymmetric to respect the normal direction and high and low speed streaks show the same wake thickness.

Streaky non parallel synthetic and cylinder's wakes. Non-parallel synthetic streaky ($3D$) wake basic flows[2] $\mathbf{U}_{3D}(x, y, z; A_0)$ are computed by enforcing at $x = 0$ the inflow condition $\mathbf{U} = U_0(y)\mathbf{e}_x + A_0\mathbf{u}_0^{(opt)}$ and by then computing the corresponding steady solution of the (nonlinear) Navier-Stokes equations. The specific values $Re = 50$ and $\lambda_z = 2\pi$ are considered.

In the case of the circular cylinder the streaky basic flows are computed by enforcing at the wall the boundary condition [3] $U_w(\theta, z) = A_w u_w^{(opt)}(\theta, z)$ and by then computing the corresponding steady solution of the nonlinear Navier-Stokes equations.

In both cases, as the streaky solution may be unstable, the symmetry with respect $y = 0$ plane is enforced, exactly as done to compute the spatial developing natural basic flow $\mathbf{U}_{2D}$.

[2]Similarly as for the case of parallel wake, the optimal perturbations can be normalized such as $\|\mathbf{u}_0^{(opt)}\| = 1$. If e_0 is the level of energy associated to the boundary inlet for the weakly non parallel wake, $A_0 = \sqrt{e_0}$.

[3]Finite amplitude A_w associated to the optimal blowing and suction (see chapter 4.3) can be normalized such as $\|\mathbf{u}_w^{(opt)}\| = 1$. Then $A_w = \sqrt{e_w}$ with e_w as previously defined.

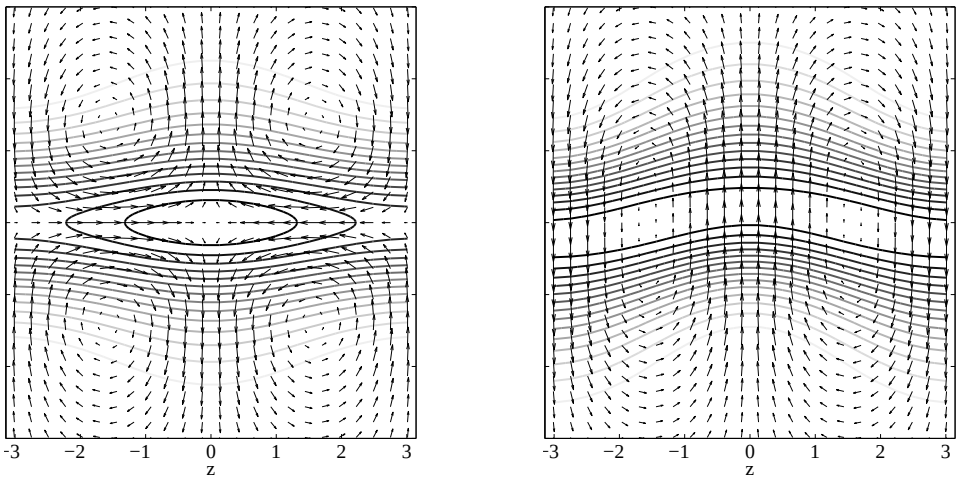

Figure 5.2: Streaky parallel wakes: Cross-stream view of case D varicose (left panel a) and sinuous (right panel b). Contour lines: iso-levels of the total streamwise velocity $U_I(y,z)$ extracted at the time of maximum amplitude.

Case:	A	B-Var	C-Var	D-Var	B-Sin	C-Sin	D-Sin
A_0	0	$1.25\,10^{-2}$	$1.94\,10^{-2}$	$3.00\,10^{-2}$	$2.00\,10^{-2}$	$2.93\,10^{-2}$	$3.66\,10^{-2}$
$A_{s,max}$	0	4.35%	6.73%	10.38%	10.27%	15.02%	18.80%

Table 5.1: Streaky parallel wakes: A_0 is the finite initial amplitude given to the linear optimal perturbations. $A_{s,max}$ is the maximum streak amplitude reached in the nonlinear numerical simulation. Case A corresponds to the reference two-dimensional wake profile $U_M(y)$. Cases B, C and D are obtained by increasing A_0.

The spatial evolution of the streaks is monitored using the amplitude definition:

$$A_s(x) = \frac{\max_{y,z}\left[U_{3D}(x,y) - U_{2D}(x,y)\right] - \min_{y,z}\left[U_{3D}(x,y) - U_{2D}(x,y)\right]}{2U_{ref}}, \tag{5.2}$$

where $U_{ref} = 2\Lambda$ for the synthetic wake and $U_{ref} = U_\infty$ for the circular cylinder wake. The nonlinear streaks amplitude evolution $A_s(x)$ associated to the velocity fields $\mathbf{U}_{3D}$ are reported in figure 5.3 for selected increasing perturbation amplitudes of the boundary optimal input. The parameters of the selected cases are reported in tables 5.2 for the synthetic and the cylinder wake respectively.

In the cylinder case we consider the intermediate Reynolds number $Re = 75$ and the spanwise wavelength $\lambda_z = 2\pi$. For the considered Reynolds numbers the maximum streaks amplitudes are reached inside the region of absolute instability of the reference $2D$ wake ($x \lesssim 5$ at $Re = 75$). The basic flows consist in increasingly streaky wakes (see figure 5.4).

Case:	A_0	$A_s(x=2.7)\%$	$A_{s,max}\%$
A	0	0	0
B	0.057	2.47	10.35
C	0.086	3.71	15.15
D	0.120	5.20	20.44
E	0.171	7.39	27.27

Case:	A_w	$u_{w,max}\%$	$A_{s,max}\%$
A	0	0	0
B	0.0031	0.75	10.45
C	0.0048	1.2	16.16
D	0.0080	2.1	25.44

Table 5.2: Streaky non parallel wakes: on the left the considered streaky basic flows for the weakly non parallel wake. A_0 is the finite amplitude given, at the inflow, to the linear optimal boundary perturbations (vortices) while $A_{s,max}$ is the maximum streak amplitude reached. $A_s(x=2.7)$ is the amplitude of the streaks in the middle of the absolute instability region. On the right panel the streaky basic flows for the circular cylinder's wake. A_w is the finite amplitude of the optimal blowing and suction corresponding to the rms value of the blowing-suction velocity and $u_{w,max}$ is the maximum absolute value of the blowing or suction velocity. $A_{s,max}$ is the maximum streak amplitude reached in the wake.

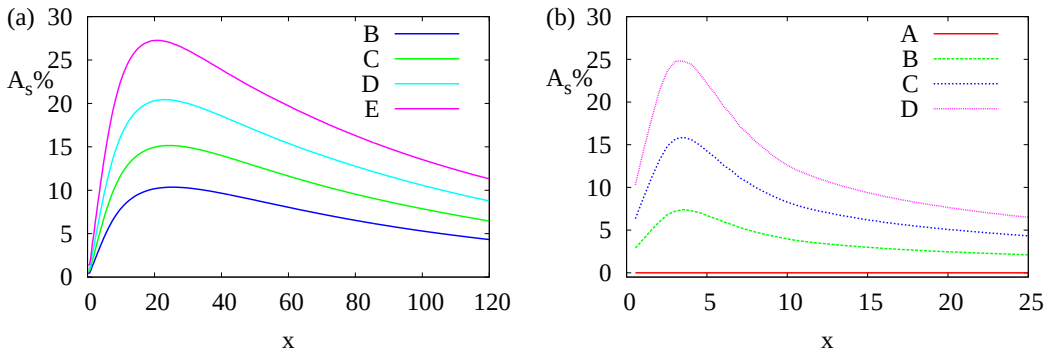

Figure 5.3: Streaky non parallel wakes: Spatial evolution of the streaks amplitudes $A_s(x)$ for increasing amplitudes A_0 of the inflow optimal perturbations for the non parallel synthetic wake (panel a) and for the circular cylinder streaky wakes (panel b) for increasing amplitudes A_w of the blowing and suction.

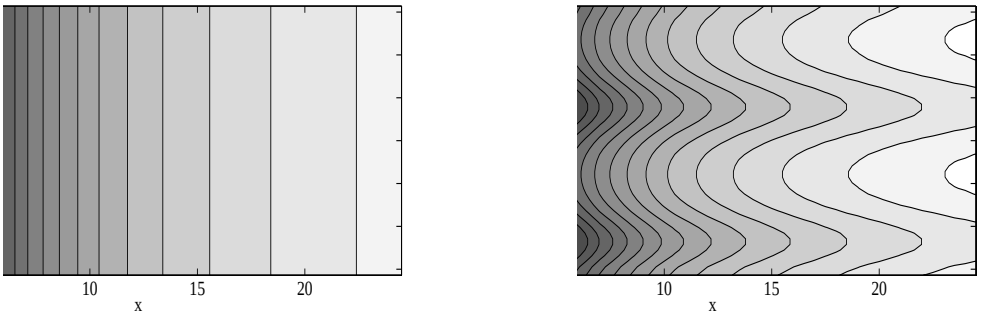

Figure 5.4: Circular cylinder's wake. Distribution of the streamwise velocity $u(x, y = 0, z)$ at the $y = 0$ symmetry plane for two selected basic flows. The reference 2D case A is reported in panel a, and the streaky wake C in panel b. Contour levels are spaced by $U_\infty/20$ while the body extend from $x = [0; 0.5]$

2 Quenching of the absolute instability in parallel wakes

Nonlinear streaks of moderate amplitude evolve on a viscous time scale, as can be seen from figure 5.1. As the wake inflectional instabilities are of inviscid nature, they evolve on the shorter convective time scales. It is therefore appropriate to analyze the *local* spatio-temporal instability properties of the streaky wake profiles 'frozen' at the time of maximum streak amplitude. The streaky basic flows $\mathbf{U}_{3D}(y, z, t_{max}, A_0)$ are those described in section 1.

The temporal and spatio-temporal properties of the streaky wakes are retrieved from the impulse response computed by direct numerical simulation of the linearized Navier-Stokes equations, similarly to Brandt *et al.* (2003) (this technique is an extension of the one used by Delbende *et al.*, 1998; Delbende & Chomaz, 1998, as detailed in appendix A).

The stability of both fundamental modes, having same spanwise periodicity λ_z as the basic flow and subharmonic modes, having instead a periodicity of $2\,\lambda_z$ is analyzed at once by performing the numerical simulations in a spanwise-periodic domain of length $L_z = 2\lambda_z$; this domain contains two low-high speed streak pairs. Only one initial pulse is therefore enforced at $t = 0$ in the 'doubled' domain. The growth rates of fundamental and subharmonic, symmetric and antisymmetric modes can be separated using spanwise Fourier transforms (see appendix A).

The temporal growth rate curves $\omega_i(\alpha)$ are reported in panels a and c of figure 5.5. The $2D$ reference wake, case A is linearly unstable with a maximum growth rate $\omega_{i,max} = 0.256$. When streaks of increasing amplitude are forced the maximum growth rate is reduced. The leading modes have same symmetries as basic flow profiles (fundamental-symmetric) and varicose streaks are found to be more effective in stabilizing the temporal instability. For instance, $\omega_{i,max}$ is reduced by $\approx 12\%$ using varicose streaks with $A_s \approx 10\%$ (case $D-Var$) and by 10% for sinuous streaks with $A_s \approx 18\%$ (case $D - Sin$).

The spatio-temporal growth rate $\sigma(v)$ curves are reported in panels b and d of figure 5.5. The 2D reference wake (case A) is absolutely unstable with an absolute growth rate $\sigma(v = 0) = 0.073$ and the wave-packet trailing-edge traveling upstream with velocity $v^- = -0.089$. The absolute growth-rate is reduced when streaks of increasing amplitude are forced and can become negative for sufficiently large streaks amplitudes transforming the absolute instability into a convective instability. Varicose streaks are found more effective in stabilizing

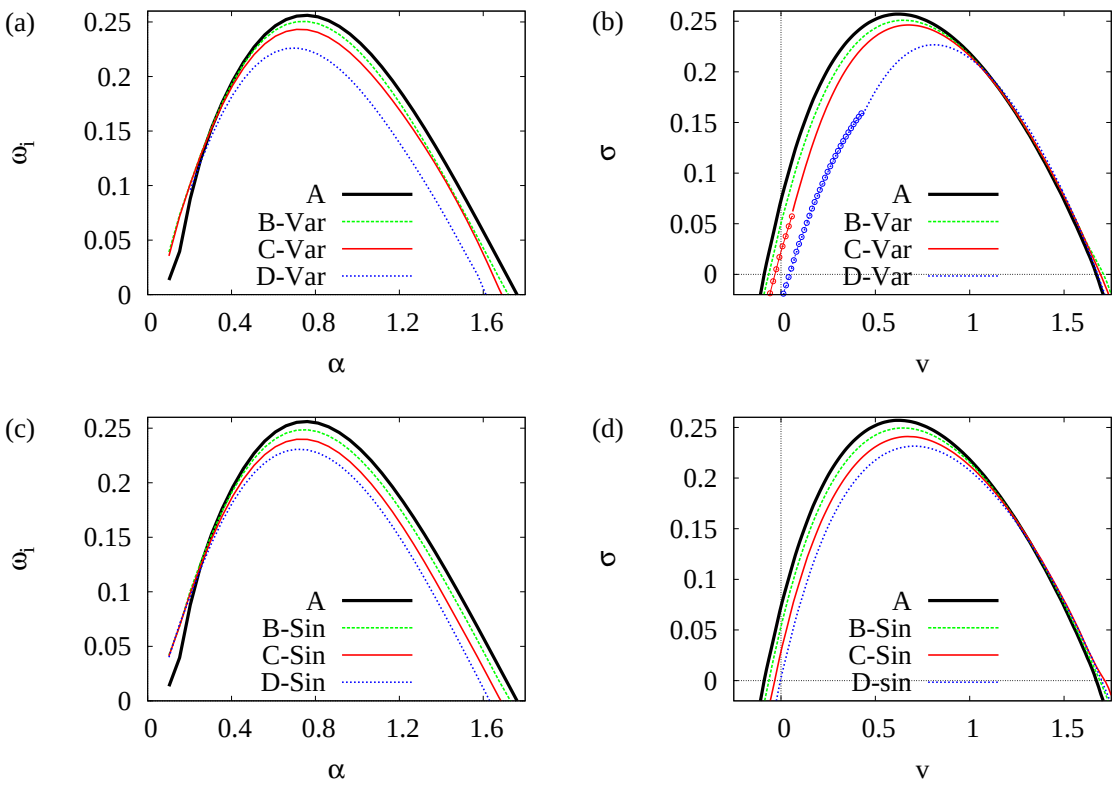

Figure 5.5: Stabilization of parallel wakes: Stabilizing effect of varicose (panels a and b) and sinuous (panels c and d) streaks on temporal (panels a and c) and spatio-temporal (panels b and d) growth rates. Case A corresponds to the 2D reference wake while cases B, C and D correspond to increasing streaks amplitudes. The basic flow is absolutely unstable if $\sigma(v = 0) > 0$. The presence of symbols on parts of the stability curves denotes the range where subharmonic modes are dominating.

the absolute instability than sinuous streaks. The varicose streak $D - Var$ with $A_s \approx 10\%$ is already convectively unstable while amplitudes above $A_s \approx 18\%$ (case $D - Sin$) are necessary for sinuous streaks to drive the instability from absolute to convective. For sinuous streaks, the leading modes in the $\sigma(v)$ curves are fundamental-symmetric (same symmetries as the basic flow streaks in the spanwise direction). For varicose streaks fundamental symmetric modes are the leading ones except for large amplitude streaks at sufficiently small values of v where subharmonic-antisymmetric modes are dominating and therefore rule the quenching of the absolute instability.

3 Suppression of the global instability in non parallel wakes

The linear global stability analysis for the spatially developing wakes (synthetic and circular cylinder's wake) is performed via a direct numerical simulation of the Navier-Stokes equations linearized upon the $3D$ streaky basic flows $\mathbf{U}_{3D}$. In section 2, for the local stability analysis, it was shown that for large streaks amplitudes, the dominant absolute mode is subharmonic,

i.e. its spanwise wavelength is twice that of the basic flow streaks. We therefore integrate the linearized equations in a domain including two basic flow streaks wavelengths ($L_z = 2\lambda_z$). For the reference $2D$ wake (case A for both the non parallel wake), a random solenoidal perturbation velocity field is chosen as initial condition on the secondary perturbations and the integration is continued in time until the emergence of the unstable global mode. This perturbation field is then re-normalized to a small amplitude and used as initial condition for all the considered cases. The global eigenvalue is then computed, as explained in appendix A, checking the temporal growth of the global perturbation kinetic energy.

Non parallel synthetic wake. The linear global stability of the streaky synthetic wake is studied at a Reynolds number $Re = 50$ and $\lambda_z = 2\pi$ (corresponding to $\beta = 1$). The temporal evolution of the global perturbation kinetic energy is reported in figure 5.6(a). After an initial transient extending to $t \approx 70$, the dependence of E' on time is exponential (a straight line in the lin-log scales used in the figure), where the rate of growth or of decay is twice the growth rate of the global mode. As anticipated in chapter 3, the reference $2D$ wake (case A) is strongly linearly unstable at $Re = 50$. The forcing of $3D$ linearly optimal perturbations of increasing amplitude has a stabilizing effect on the global instability. The growth rate is first reduced for low amplitude streaks (cases B and C), is then rendered quasi-neutral (case D) and finally completely stable for sufficiently large streak amplitudes (case E). In the neutral and stable case the streaks amplitudes $A_s(x = 2.7)$, measured in the middle of the absolute instability region of the reference $2D$ wake, are respectively of $\approx 5\%$ and $\approx 7\%$ (see table 5.2). These values are not far from the $\approx 8\%$ value at which the absolute instability was completely quenched in our previous local stability analysis. Also remark that, in the present non-parallel case A_s is given in terms of the entrance reference maximum $\Delta U_{2D}(x = 0)$, but if it was based on the local value of $\Delta U_{2D}(x)$ which is decreased with x, this would result in even larger downstream values of A_s. The stabilization of the global mode therefore appears to be associated to a strong reduction of the pocket of absolute instability that drives the global mode oscillations in the 2D reference case. These results confirm, for the fist time, to our knowledge, that the vortex shedding suppression obtained by forcing streamwise streaks is associated to the suppression of the *linear* global instability.

Circular cylinder's wake The global linear stability of the streaky cylinder's wake is examined by integrating in time the Navier-Stokes equations linearized with respect to the considered $\mathbf{U}_{3D}(x, y, z; A_0)$ (see table 5.2 for the considered cases). As shown in figure 5.6(b), $E'(t)$ grows exponentially in time, after the extinction of the initial transient. For $Re = 75$, the reference $2D$ wake (case A) is linearly unstable. In the presence of increasing amplitudes of blowing and suction and therefore of increasing amplitudes of the streaks, the growth rate of the global mode is initially reduced (cases B and C) to become negative for case D as shown in figure 5.6(b) for $\lambda_z = 2\,\pi$.

The dependence on the spanwise wavelength λ_z of the critical amplitudes A_c for which the global instability is suppressed is reported in Figure 5.7 in terms of both A_w and $A_{s,max}$. For $Re = 75$, the spanwise wavelength minimizing the control amplitudes necessary for the stabilization of the global instability is $\lambda_z \approx 6$. While when the Reynolds number is increased to $Re = 100$, the spanwise wavelength minimizing the control amplitudes is reduced to $\lambda_z \approx 5.3$. These results are in very good agreement with those of Kim & Choi (2005) who finds that the minimum drag is achieved for $\lambda_z = 5 - 6$ (but at the fastest rate for $\lambda_z = 6$) at

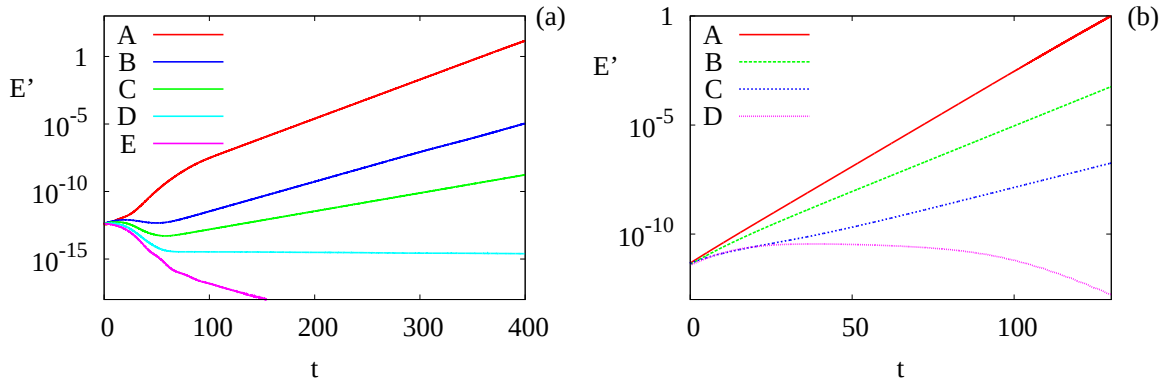

Figure 5.6: Stabilization of the linear global instability in non-parallel wakes: Temporal evolution of the (global) kinetic energy density of secondary perturbations $E'(t)$. Panel a: synthetic wake at $Re = 50$ and $\lambda_z = 2\pi$. Panel b: circular cylinder's wake at $Re = 75$ and $\lambda_z = 2\pi$.

$Re = 80$ and for $\lambda_z = 4 - 5$ (but at the fastest rate for $\lambda_z = 5$) at $Re = 100$. Smaller energy is required to suppress the global instability when using blowing and suction instead of localized blowing and suction (0.62% instead of 8% of U_∞ in terms of maximum blowing/suction velocity and $5.6\,10^{-5}$ instead of $1.2\,10^{-3}$ in terms of momentum coefficient of forcing $C_\mu = 2\pi A_w^2$ at $Re = 100$). This is not surprising given the observed large differences in energy gains obtained using these different distributions of blowing and suction.

For all the considered spanwise wavenumbers, largest streaks amplitudes are required to stabilize the global instability at $Re = 100$ than at $Re = 75$. This is expected, because at $Re = 100$ the global mode is more unstable than at $Re = 50$ and it can be expected that largest streaks amplitudes are required to quench it. However, the amplitudes of the blowing and suction, required to stabilize the global instability are *smaller* at $Re = 100$ than at $Re = 75$, for all the considered λ_z. The increase of energy amplification of the control due to the lift-up associated to an increase in Reynolds number (see figure 4.6a) therefore overcomes the increase of control action necessary to quench the more unstable global mode. In other words, the results reported in figure 5.7(a) confirm the essential role played by the non-normal amplification of streaks in the stabilization of the global instability.

4 Non linear simulations

The effect of the forcing of $3D$ linear optimal perturbations for the non parallel wakes are here presented in the nonlinear regime. The same grids used in linear simulations for the stability analysis have been used in the nonlinear ones. Let us first consider the case of the non parallel synthetic wake. The permanent harmonic self-sustained state supported by the reference $2D$ wake is allowed to develop. For the case of the synthetic wake, this $2D$ (spanwise uniform) self-sustained state is then given as an initial condition in the presence of the optimally amplified streaks of increasing amplitude. As expected from the linear analysis, the global level of oscillations in the wake is reduced when the amplitude of the enforced optimal perturbations is increased (see figure 5.8(a)). A stable steady streaky wake is found for case E, where the oscillations are completely suppressed. Snapshots of the streamwise velocity in the $y = 0$ plane are reported in figure 5.9 for all the considered cases. For the

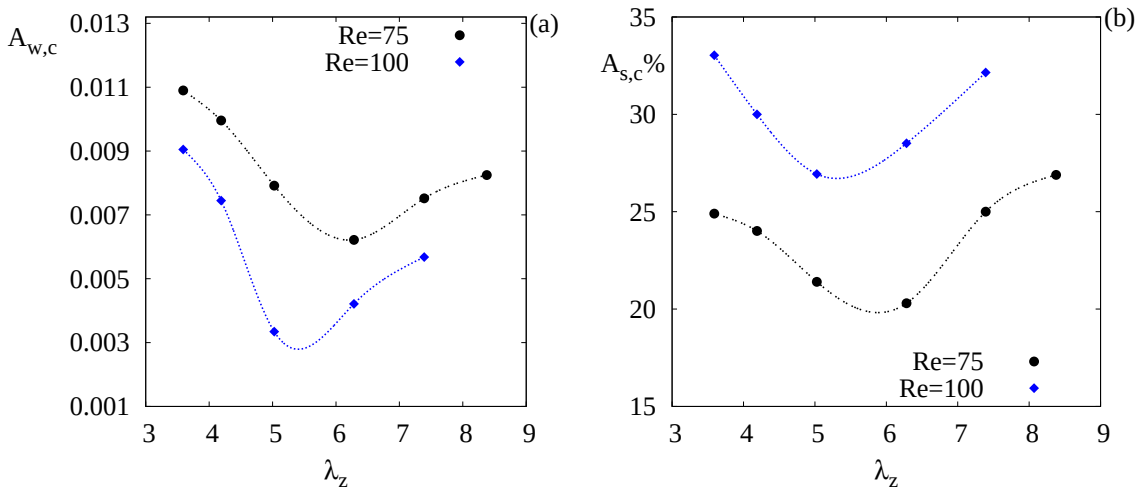

Figure 5.7: Stabilization of the linear global instability in the circular cylinder wake: Dependence on the spanwise wavelength of the critical amplitude of the forcing $A_{w,c}$ (panel a) and of the streaks $A_{s,c}$ (panel b), for which the global instability is suppressed. Data pertaining to $Re = 75$ and $Re = 100$.

reference 2D wake (case A), the self-sustained state is spanwise uniform (2D) with structures corresponding to standard von Kármán vortices. These vortical structures become increasingly modulated in the spanwise direction for increasing amplitudes A_0 of the forcing. Unsteady structures are completely suppressed for case E, where the basic flow streamwise streaks remain the only visible structures in the wake.

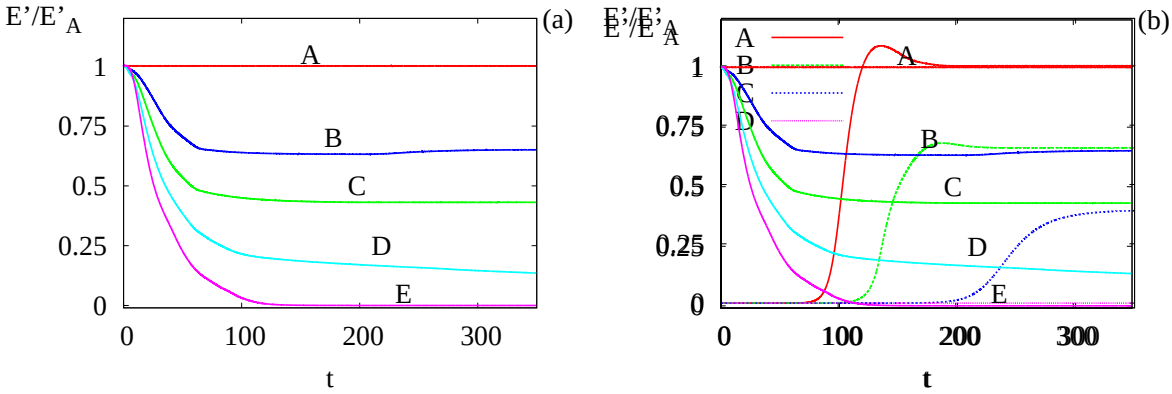

Figure 5.8: Non linear simulations of the stabilization of non-parallel wakes: Temporal evolution $E'(t)$ of the total perturbation kinetic energy, integrated over the whole computational box in the non linear simulations. Panel a, synthetic wake. Panel b, circular cylinder's wake.

Something similar is demonstrated also for the non linear simulations of the optimally amplified streaky basic flows in the circular cylinder's wake, figure 5.8(b). In that case the solenoidal initial distrurbance was left to develop in a non linear regime. The results confirm in the case linearly global stable (case E) also the norm of the non linear perturbations goes

to zero.

These results confirm that the suppression of the linear global instability by the streaks does indeed explain the suppression of the shedding.

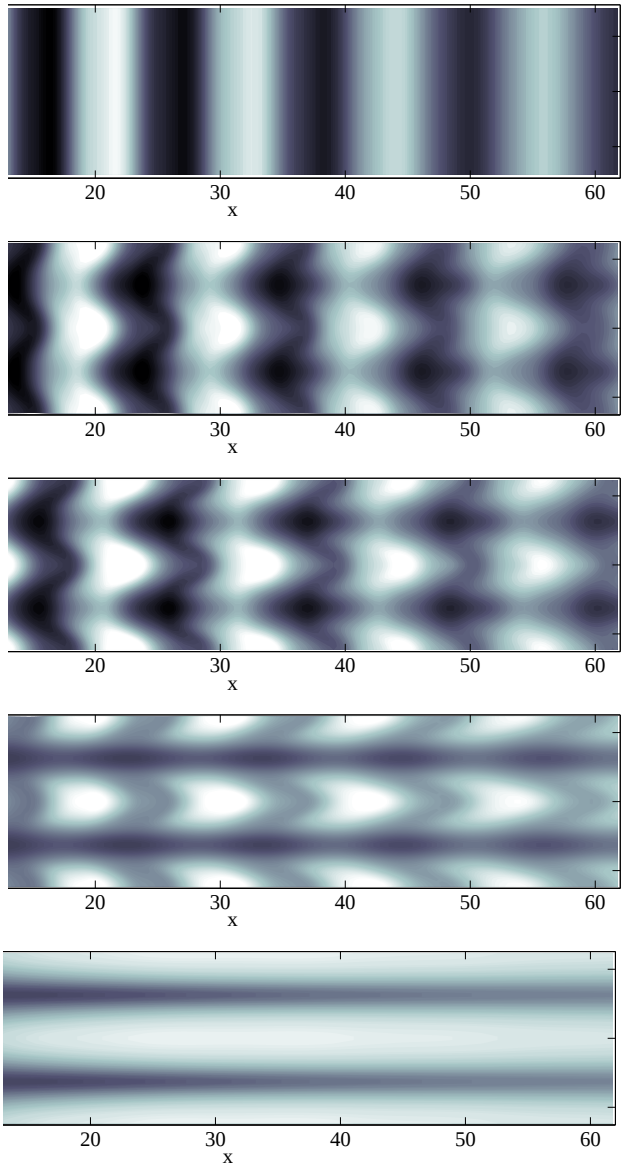

Figure 5.9: Snapshots from fully nonlinear simulations of the weakly non parallel wake. Streamwise perturbation velocity $u(x, y = 0, z)$ in the $y = 0$ symmetry plane in the permanent regime ($t = 250$). The reference $2D$ case A is reported in panel a, while cases B, C, D and E, obtained by increasing the amplitude A_0 of the inflow optimal perturbations, are reported in panels b to e (top to bottom). Case A displays self-sustained periodic oscillations of $2D$ structures in the wake. These structures become increasingly 3D and of smaller rms value for increasing values of the enforced A_0 (cases B to D). The oscillations are completely suppressed in case E where the stable streaky basic flow is observed after transients are extinguished.

Chapter 6

A sensitive issue

1 The first order sensitivity paradox

The stabilization induced by some control action, such as e.g. basic flow modifications, is usually characterized by the the first-order sensitivity of the considered growth rate γ with respect to the amplitude of the control A defined in the limit of small control amplitudes as $\mu_1 = d\gamma/dA|_{A=0}$ (see e.g. Alizard *et al.*, 2010).

So far, first-order sensitivity analyses have mainly dealt with $2D$ control. Hwang *et al.* (2013) have shown that the first order sensitivity of the absolute growth rate to $3D$ spanwise periodic modifications of the basic flow is zero. This represents a paradox. Indeed, according to this analysis $2D$ perturbations are expected to be more efficient than $3D$ ones while exactly the opposite is observed (see e.g. Kim & Choi, 2005).

This apparent paradox is not explained by possible shortcomings of the local stability analysis because it is easy to show that the sensitivity of the *global* growth rate to $3D$ spanwise periodic modifications of the basic flow is also zero. Indeed, following e.g. Bottaro *et al.* (2003) and Chomaz (2005), let us denote by $\mathbf{L}_{2D}$ the Navier-Stokes operator linearized near the basic flow $\mathbf{U}_{2D}$ and by $\mathbf{w}$, s, $\mathbf{w}^+$ respectively its leading global mode, eigenvalue and adjoint global mode. For very small values of the amplitude of optimal perturbations, the basic flow is modified by a small amount $\delta\mathbf{U} = \mathbf{U}_{3D} - \mathbf{U}_{2D}$ that induces a small change $\delta\mathbf{L}$ in the linear operator. The first order change of the leading eigenvalue induced by this small variation is $\delta s =< \mathbf{w}^+, \delta\mathbf{L}\mathbf{w} > / < \mathbf{w}^+, \mathbf{w} >$ where the inner product is defined as follow: $< \mathbf{a}, \mathbf{b} >= \int_0^{L_x} \int_{-L_y/2}^{L_y/2} \int_0^{L_z} \mathbf{a} \cdot \mathbf{b}\, dx\, dy\, dz$. The variation in $\delta\mathbf{L}$ induced by $\delta\mathbf{U}$ consists only in spanwise periodic terms as $\delta\mathbf{U}$ is itself spanwise periodic. As the global and adjoint modes of the unperturbed operators are spanwise uniform, it follows that $< \mathbf{w}^+, \delta\mathbf{L}\mathbf{w} >= 0$ and therefore that δs=0. This is not the case for $2D$ (spanwise uniform) perturbations of $\mathbf{U}$ for which the first-order variation of the leading eigenvalue is, in general, non-zero.

We therefore remain with some unanswered questions. Is it really true that $3D$ control is more efficient than $2D$ control? If yes, why is $3D$ control more efficient than $2D$ control? If yes, is this only due to the more efficient forcing of $3D$ perturbations which partially exploits the lift-up effect? What is the leading order dependence of growth rates on the $3D$ control amplitude? Is it quadratic, as found by Hwang *et al.* (2013) for small values of A, also at large values of A where stabilization is achieved? Is it quadratic also in the non-parallel case? Is there a range where $2D$ perturbations are more efficient than $3D$ ones?

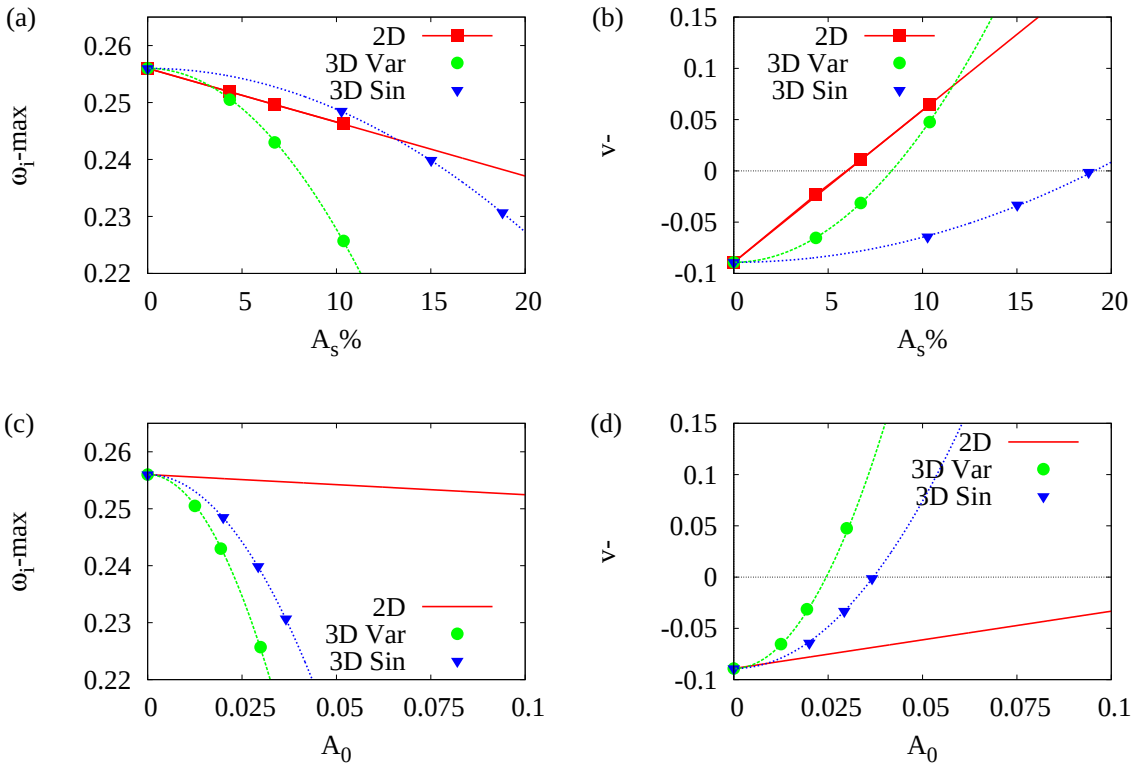

Figure 6.1: Sensitivity of parallel wakes: dependence of the maximum growth rate $\omega_{i,max}$ (panels a and c) and of the wave-packet trailing edge velocity v^- (panels b and d) on the streak amplitude A_s (panels a and b) and on the initial disturbance amplitude A_0 (panels c and d). Zero amplitudes correspond to the $2D$ wake reference case A ($2D$) spanwise uniform perturbation has been also considered for comparison. Symbols denote data points while lines are linear and quadratic best fits to the data points.

2 Quadratic sensitivity and 3D control efficiency in parallel wakes

Hwang *et al.* (2013) show that for small streaks amplitude the sensitivity to spanwise-sinusoidal ($3D$) basic flow perturbations depends quadratically on their amplitudes. To ascertain if these predictions extend to the considered nonlinear streaks and to the maximum temporal growth rate sensitivity, we report in figure 6.1 the dependence of the maximum growth rate $\omega_{i,max}$ and of the wave-packet trailing edge velocity v^- on the streak amplitude [1] A_s. We also consider the effect on stability of a $2D$ (spanwise uniform) perturbation with a profile $u_{2D}(y)$ equal to the high-speed varicose streak profile $\hat{u}(y)$ (see Del Guercio *et al.*, 2014*c*, for details).[2]

[1] We consider v^- and not $\sigma(v = 0)$ as a measure of the absolute or convective nature of the instability because the used numerical method (impulse response analysis) does not provide well converged results for negative growth rates.

[2] The amplitude A_s of this 2D basic flow modification is defined by eq. (5.2) but removing the 1/2 factor that accounted for the presence of high and low speed streaks.

From figure 6.1 it is seen that indeed $\omega_{i,max}$ and v^- depend quadratically on A_s when considering streaky basic flow modifications but linearly when considering a 2D basic flow modification. The conclusions of Hwang *et al.* (2013) are therefore confirmed by the present results and extended to much higher amplitudes where the absolute instability is completely suppressed.

Considering the stabilization of the maximum temporal growth rate, the quadratic sensitivity of the streaks to A_s even if it gives a weaker effect than 2D basic flow modifications at very small streaks amplitudes, can provide a larger effect at larger A_s. This is not the case for the quenching of absolute instability, where 2D basic flow modifications are able to drive v^- to positive values for lower A_s values than 3D basic flow modifications, as already remarked by Hwang *et al.* (2013).

As the streaks have been forced using linearly optimal initial conditions, it is interesting to analyze the dependence of the stabilizing actions not in terms of the basic flow distortion amplitude A_s but on the amplitude A_0 of the initial perturbation. This dependence is also reported in figure 6.1, where, again quadratic and linear sensitivities of $\omega_{i,max}$ and v^- on A_0 are observed for 3D and 2D basic flow perturbations respectively. In term of A_0, the optimal 3D perturbations are much more effective than 2D perturbations in stabilizing the flow. This is not surprising because, in first approximation, a factor of $\sqrt{2G_{max}}$ is gained trough the lift-up effect when forcing optimal $3D$ control using optimal initial vortices instead of enforcing the $2D$ profile with the same streak shape. For the considered case for instance the absolute-convective instability transition is enforced with optimal 3D streaks with values of A_0 roughly ten times smaller than those necessary when using 2D basic flow modifications (one hundred times smaller in terms of the control kinetic energy).

3 Quadratic sensitivity and 3D efficiency in non parallel wakes

In the case of non-parallel wakes one has to investigate the variations of the global growth rate with respect to the control amplitude. Let us first consider the case of the synthetic wake. The dependence of the global growth rate s_r on the inflow optimal perturbation amplitude A_0 is plotted in figure 6.2(a). The dependence of s_r on the amplitude of the streaks is reported as a function of $A_s(x = 2.7)$ in the middle of the absolute instability region, figure 6.2 (panels (b) and (c) for a zoom). In the same figures the variation of s_r induced by a $2D$ perturbation of the basic flow is also reported for comparison. [3]

From these figures it is clearly seen how the first order sensitivities ds_r/dA_0 and ds_r/dA_s computed for $A_0 = A_s = 0$ are zero for the $3D$ perturbations and non-zero for the $2D$ perturbations as predicted by the first order sensitivity analysis. According to a first-order sensitivity analysis one would expect $2D$ perturbations to be more effective than $3D$ ones in quenching the global instability, but the opposite is observed. $3D$ perturbations stabilize the global mode at a value of $A_s(x = 2.7)$ more than five times smaller than for $2D$ perturbations, and more than ten times smaller in terms of A_0.

Similar results are found in the case of the circular cylinder's wake at $Re = 75$ for various λ_z and are reported in figure 6.3. In this case, in addition to the amplitude of the blowing and

[3] The $2D$ perturbation has the same y shape as the optimal streak shape in the middle of the absolute instability region ($x = 2.7$) but is uniform instead of periodic in the spanwise direction. For this $2D$ perturbation, A_0 is unambiguously defined and A_s is defined as the maximum associated ΔU taken at $x = 2.7$.

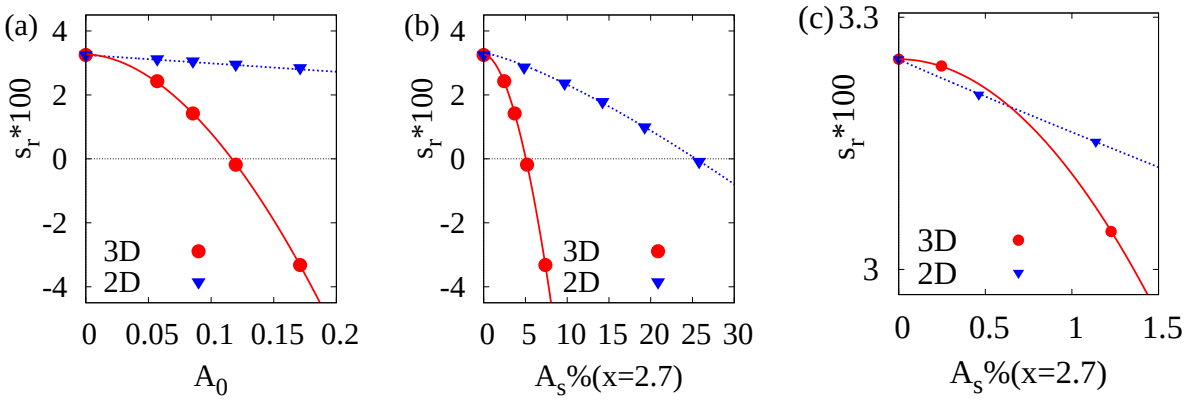

Figure 6.2: Sensitivity of the non-parallel synthetic wake for $\lambda_z = 2\,\pi$ and $Re = 50$: dependence of the maximum growth rate of the global eigenvalue s_r on the inflow optimal perturbation amplitude A_0 (panel a) and on the streak amplitude $A_s(x = 2.7)$ measured in the centre of the absolute region of the reference 2D wake (panel b and c for a zoomed plot). A spanwise uniform perturbation (2D) has been also considered for comparison. Symbols denote data points while lines are best fits to the data points.

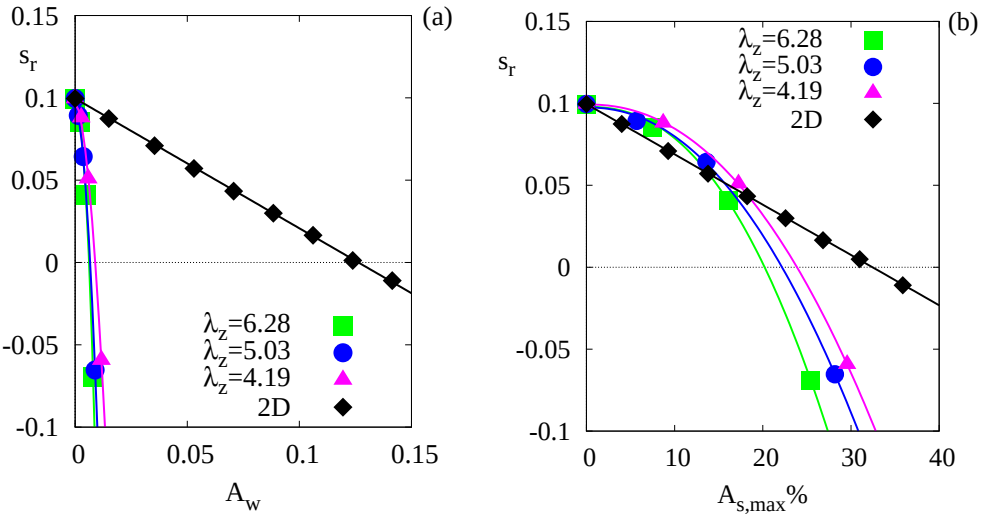

Figure 6.3: Sensitivity of the circular cylinder's wake $\lambda_z = 2\,\pi$ and $Re = 75$: dependence of the global mode growth rate s_r on the blowing and suction amplitude A_0 (panel a) and on the maximum streak amplitude $A_{s,max}$ (panel b). A spanwise uniform perturbation ($2D$) has been also considered for comparison. Symbols denote data points while lines are best fits to the data points using a quadratic interpolation for the 3D data and a linear interpolation for $2D$ data.

suction A_w, the results are expressed also in terms of the maximum streaks amplitude $A_{s,max}$ which is reached inside the absolute region.

In order to compare $3D$ and $2D$ controls, we have computed the growth rate variations induced by spanwise uniform ($2D$) wall blowing and suction [4] with $m = 1$ azimuthal dependence $U_w = A_{2D}\cos(\theta)$. This $2D$ control has zero net mass flux and is associated to bleeding in the wake, which is known to efficiently reduce the absolute growth rate Monkewitz (1988). Figure 6.3 presents the comparison with the two kinds of control.

The quadratic relation of the global growth rate s_r is here again found both for the amplitude of the blowing and suction A_w and the amplitude of the streaks $A_{s,max}$ while the curve for the $2D$ control is well approximated by a straight line. Therefore, the considered $2D$ perturbations are more stabilizing than the optimal $3D$ ones only for $A_{s,max} \lesssim 14\%$, corresponding to the negligible $A_w \approx 0.005$. As already observed in the previous sections, a higher efficiency of $3D$ perturbations is expected in terms of A_w, because they can exploit the energy gain associated to the lift-up effect, which is a $3D$ mechanism. We have also verified that qualitatively similar results are obtained for a few other shapes of the $2D$ forcing. These results are in accordance with the finding of Kim & Choi (2005) that $3D$ perturbations are more effective than $2D$ ones in suppressing vortex shedding.

The last remark regards a difference between the sensitivity analysis for the parallel case and those for the non parallel wakes. Even if both the analyses confirm a quadratic sensitivity of the stability properties, the stabilization of the global instability by $3D$ perturbations is more efficient than the $2D$ perturbations not only in term of A_w, which could be expected from the lift-up effect implication, but also in term of the streaks amplitude contrary to what is observed in the parallel case.

[4] The analogous of the streak amplitude is defined, for the $2D$ perturbation as the maximum of the basic flow streamwise velocity variation induced by the $2D$ suction.

Chapter 7

Effects of streaks forcing on a turbulent wake past a 3D bluff body

In this section we present an extension of the control by streaks approach. In order to fit to automotive motivations, this experimental study is conducted on a $3D$ bluff body for a Reynolds number lying in the turbulent regime. Anyway these results are preliminary and therefore need further confirmations.

1 Motivations

The squareback body proposed by Ahmed *et al.* (1984), see figure 7.1, is a generic car model aimed at studying the wake of squareback car geometries. The dynamics of such wake flow have recently proved to be even richer than what we thought since, depending on the ground clearance, it can feature a global oscillation of the wake due to the interaction of the opposed shear layers as well as a bistable behaviour, see e.g. Grandemange (2013).

Flow control past such $3D$ bodies usually involves active blowing and suction (Rouméas *et al.*, 2009; Wassen *et al.*, 2010; Bruneau *et al.*, 2011), the use of vortex generators (Aider *et al.*, 2010) or flaps (Khalighi *et al.*, 2001; Beaudoin & Aider, 2008; Fourrié *et al.*, 2011) used to change the orientation of the flow close to the separation point, this latter being the approach used for real cars optimization with spoilers or diffusers. Another control strategy based on reducing the activity of the oscillating global mode of $3D$ axisymmetric body has proved to be efficient in the laminar régime (Weickgenannt & Monkewitz, 2000; Sevilla & Martinez-Bazan, 2004).

2 Experimental set-up

The experiments have been conducted in the PSA Peugeot Citroën in-house facility in the Aerodynamics Department in Vélizy. The wind-tunnel is of closed-return type with a $0.8\,m$ long test section and a $0.3\,m \times 0.3\,m$ cross-sectional area. The temperature can be kept constant and uniform within $\pm 0.5^o C$. The contraction ratio is 8 and the velocity can be controlled from $7m\,s^{-1}$ up to $45m\,s^{-1}$. In the following, we denote by x, y and z the streamwise, wall-normal and spanwise directions respectively and by U, V and W the associated velocity components.

The model used here is a squareback Ahmed body. It is $L = 150\,mm$ long, $W = 68\,mm$ wide and its height is $H = 50\,mm$ hence respecting the proportions of a full scale Ahmed

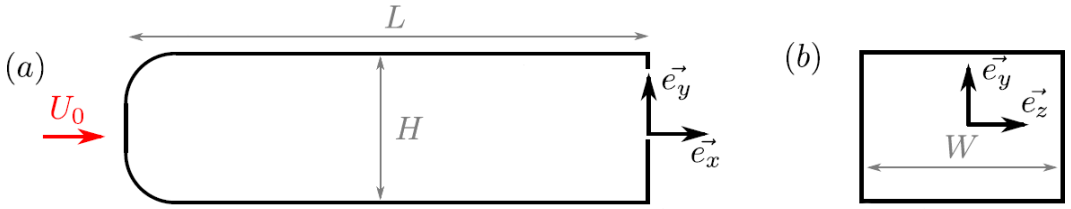

Figure 7.1: Squareback Ahmed body. Panel (a): lateral view, H indicates the height and L the length. Panel (b): rear back side, W stands for the span.

body (see e.g. Ahmed *et al.*, 1984). In order to get rid of ground effects and to focus mainly on the shedding activity, the body is hung in the middle of the test section with 8 wires whose diameter is $0.7\,mm$ (see figure 7.2). The free stream velocity is set to $U_0 = 9\,m\,s^{-1}$ leading to a Reynolds number based on the height of the body of $Re_H = U_0 H/\nu = 30000$. The origin of the axis is taken at mid-width and mid-height of the blunt rear-end of the model.

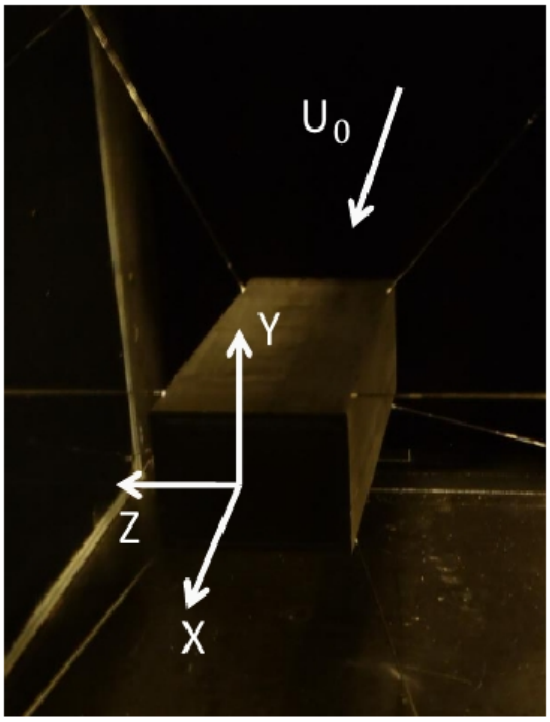

Figure 7.2: Photo of the set up. The flow investing the $3D$ bluff body exits from the vein with uniform velocity U_0. The reference frame with origin in the center of the back rear surface of the body is also shown.

Velocity measurements are performed with Particle Image Velocimetry (PIV) and hot-wire anemometry (HW). The PIV system is Dantec's Dynamic Studio associated with a $120mJ$ Nd:Yag double cavity laser and a $4Mpx$ FlowSense CCD camera, both being placed on tra-

verse systems in order to enable quick changes of the measurement plane. For each plane or configuration, a collection of 2000 pairs of images was acquired at a frequency of $7Hz$ and then post-processed using 32×32 interogation window with 50% overlap leading to fields of view of $300mm \times 300mm$ with a spatial resolution of $2.4\,mm \times 2.4\,mm$. Time-resolved velocities are obtained with a hot-wire probe oriented to get the streamwise component U. The probe is a Dantec $55R01$ type fixed on a $55H22$ support, the whole system being placed on a $3D$ traverse system and connected to Dantec's StreamWare device. Data are acquired at a sampling frequency of $2.5kHz$ over a 10 minutes period of time.

3 Natural flow case

The time averaged streamwise velocity component U/U_0 is depicted in the panel (a) of figure 7.3 for the plane symmetry $z = 0$. The flow is from left to right, the model being depicted as the white rectangle on the left part of the figure, and the streamwise component of the velocity has been scaled with the free stream velocity. A large recirculation region (shown as the black dashed line) is present up to $x_R/H = 1.45$. The boundary layer thickness at the trailing edge of the model is around $\delta_{99}/H \approx 0.32$ (i.e. $\delta_{99} \approx 16mm$). Panels (b), (c) and (d) of figure 7.3 respectively display the $< u'^2 >$, $< v'^2 >$ and $< u'v' >$ components of the Reynolds stresses. As expected, the near wake experiences high levels of fluctuations due to the shear layers developing from the separation edge; the maximum value being $< u'^2 >_{max} /U_0^2 = 0.045$, $< v'^2 >_{max} /U_0^2 = 0.031$ and $< u'v' >_{max} /U_0^2 = 0.02$.

In order to confirm that these fluctuations can be ascribed to some coherent wake motion, we conducted hot-wire measurements in the shear layers and some other locations on the wake as displayed in figure 7.4 for two downstream positions: $x_1 = 3\,H$ and $x_2 = 5\,H$ (measurements inside the recirculation bubble have been conducted but did not show any evidence of a global mode, according to Kiya & Abe (1999), they are not shown here for sake of conciseness).

The autopower spectra for each measurement location are displayed on figure 7.5, the left panel standing for x_1 while the right one stands for x_2. As one can see, different behavior can be observed depending on the location of the probe in the cross-flow plane. Placing the probe on each of two shear layer originating from the top and bottom faces of the model (respectively locations A and B), power spectral densities (PSD) clearly show a peak around $St_{H1} = f_1 * H/U_0 = 0.17$ (corresponding to a frequency $f_1 = 30\,Hz$). Looking at the spectral behavior on the lateral shear layers (points C and D), PSD show a peak around $St_{H2} = 0.12$ (corresponding to $f_2 = 21\,Hz$).

Similar behavior as already been observed by Kiya & Abe (1999) in the wake of elliptical or rectangular plates or Grandemange *et al.* (2013) in the case of a squareback Ahmed body with ground effect. According to these authors, those peaks are due a global mode responsible for some large scale hairpin vortex shedding in the wake.

4 Roughness Elements and streaks

Like in previous studies, cylindrical roughness elements have been used to force coherent streaks, see figure 7.6. The main parameters defining the actuation are: the height k of the roughness elements, their diameter d, the spanwise spacing λ and their position respective to the separation edge X_0. Contrary to Pujals *et al.* (2010*b*); where only one array of roughness elements was used on the roof of the model; one array is placed on each side of the model.

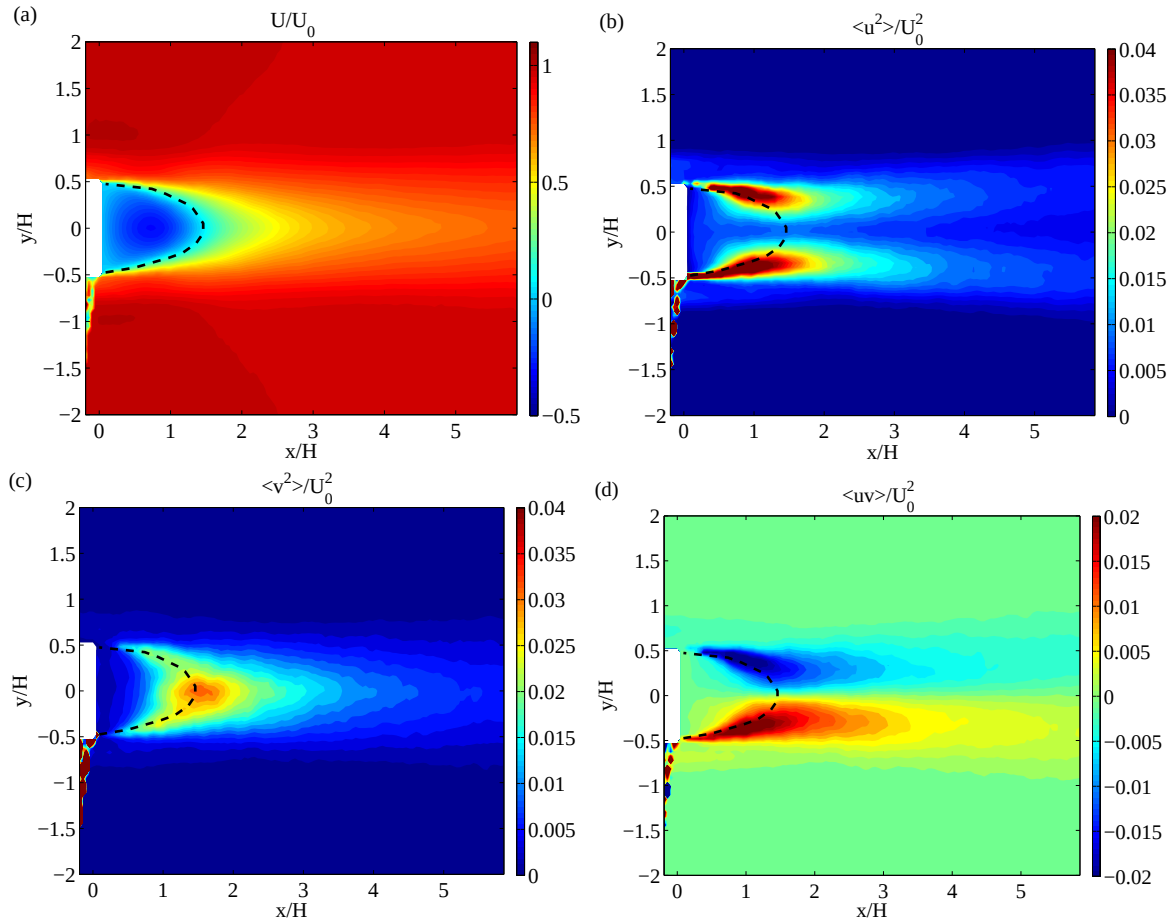

Figure 7.3: Time averaged statistics of the natural flow in the symmetry plane $z = 0$, (a) U/U_0, (b) $< u'^2 > /U_0^2$, (c) $< v'^2 > /U_0^2$ and (d) $< u'v' > /U_0^2$. On each panel the $U = 0$ line is displayed as the black dashed line.

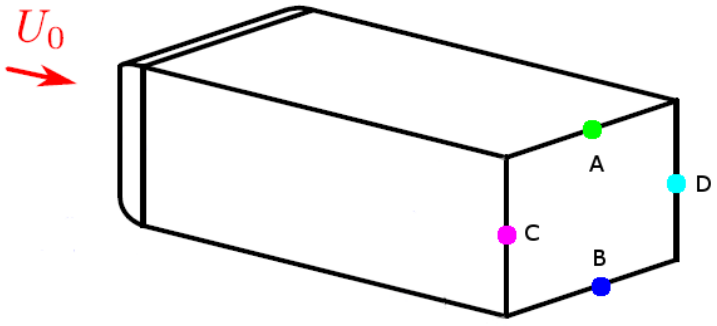

Figure 7.4: Locations of the hot-wire probe in a cross-flow plane in the wake of the model.

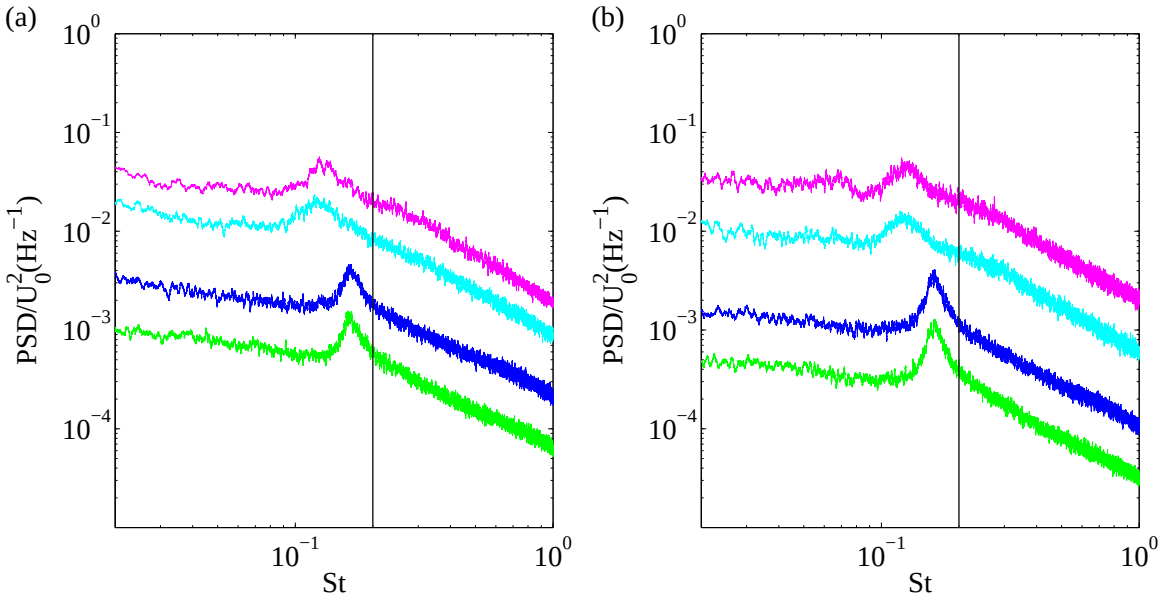

Figure 7.5: Power Spectral Densities (PSD) measured at the positions exposed in figure 7.4 for the natural case. Panel (a), $x_1 = 3\,H$. Panel (b), $x_1 = 5\,H$. Vertical line indicates the Stroual number $St = 0.2$.

Due to the relatively thick boundary layer the height is fixed at $k = 9\,mm = 0.56\,\delta_{99}$ while the diameter of the cylinders is $d = 4\,mm$. Based on previous observations (White, 2002; Fransson *et al.*, 2005; Hollands & Cossu, 2009), we set the ratio $\lambda/d = 4$ leading to a spanwise wavelength of $16mm$.

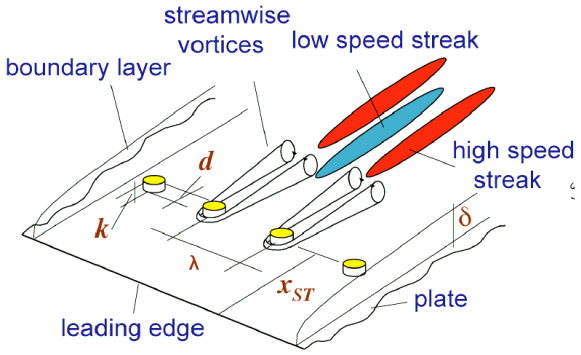

Figure 7.6: Schematic exposition of the spatially streaks development on a flat plate when cylindrical roughness element of diameter d and height k are positioned in a cross direction with a spacing λ.

Figure 7.7 shows a visualization of the time averaged flow measured downstream of one roughness array (the roughness elements are depicted as white disks) at a distance $k/2$ of the model. The flow is from left to right and the streamwise velocity is scaled with U_0 while both streamwise and wall-normal directions are scaled with the wavelength λ. The black dashed line

represents the recirculation bubble in the symmetry plane $z = 0$. The mean flow is modulated in the y direction and looking at the contours values, we can see how streaks experience a spatial transient growth thanks to the lift-up effect, their amplitude as defined by

$$A_s = \frac{U_{HSS}(x, Y/k = 0.5) - U_{LSS}(x, Y/k = 0.5)}{2U_0},$$

where U_{HSS} (resp. U_{LSS}) is the streamwise velocity in a high (resp. low) speed streaks, being maximum in the recirculation region and of value $\approx 10\%$.

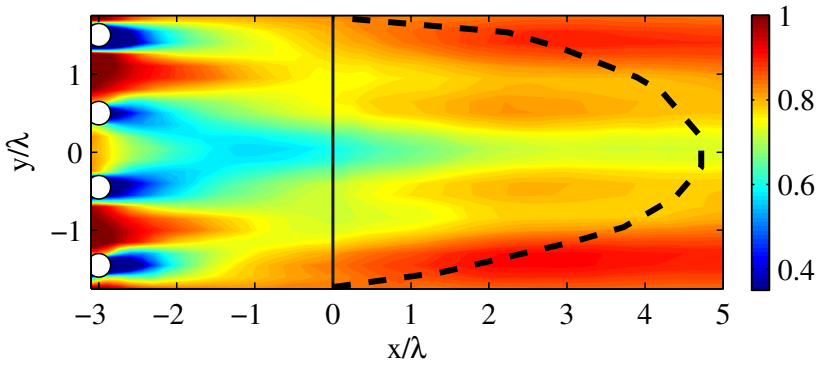

Figure 7.7: Time averaged streamwise velocity component U/U_0 shown at a distance from the body $Y = 0.5\,k$.

5 Analysis of the Controlled case

Looking for some effect on the global shedding, we investigate how those streaks act on the quantities we looked at in the section dedicated to the natural flow. Hence, giving a look at the time averaged streamwise velocity displayed on panel (a) of figure 7.8, we can observe a large increase of the recirculation bubble, its length changing from $x_r = 1.45H$ in the natural case to $1.9H$ in the controlled case. In addition, the use of streaks tends to drasticaly lower the intensity of fluctuations in the whole wake (see panels (b), (c) and (d)), their maximum value dropping to $< u'^2 >_{max} /U_0^2 = 0.027$, $< v'^2 >_{max} /U_0^2 = 0.017$ and $< u'v' >_{max} /U_0^2 = 0.007$. All these observations indicate a strong weakening of the shear layers dynamics in presence of streaks.

Autopower spectra for the controlled wake are displayed on figure 7.9. The PSD show a decrease of the amplitude of both peaks, indicating that streaks seem to alter the global shedding process.

Dealing with drag reduction, Pujals *et al.* (2010*b*) emphasize the relevance of the parameter X_0. According to their study and to our conclusions, the major effect of streaks on the base-flow is expected when their amplitude reaches its maximum value close to the flow feature we want to control (i.e. separation point in the case of a marginal separation, absolute instability region in the case of large scale shedding), the prescribed value being 4λ according to Pujals *et al.* (2010*a*,*b*). Indeed, changing the location of the four arrays over the model would have a strong impact on the results. In figure 7.10 we have reported maps of $< u'v' > /U_0^2$ as well as the $U = 0$ line for X_0 locations ranging from $X_0 = 4\,\lambda$ (panel (a)) to $X_0 = \lambda$ (panel (d)).

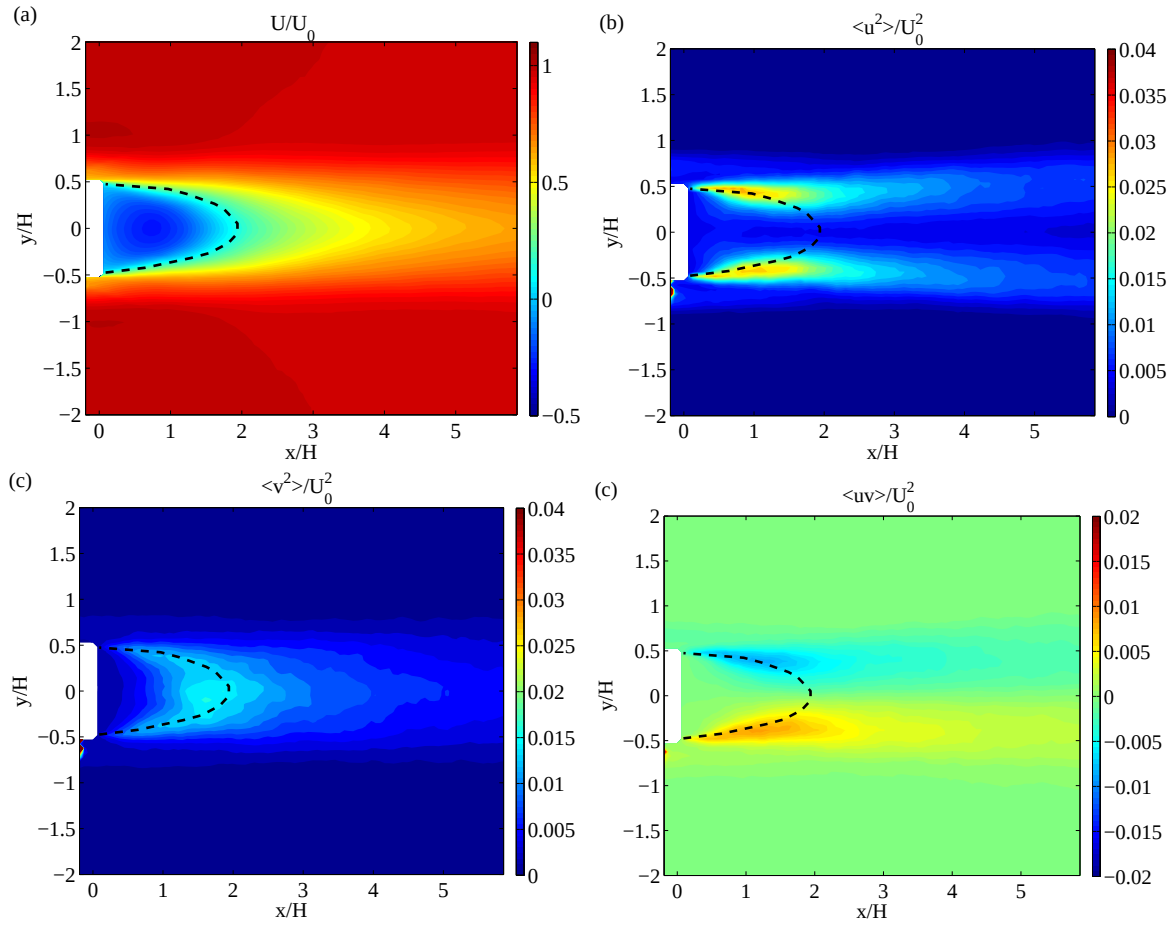

Figure 7.8: Time averaged statistics of the controlled flow in the symmetry plane $z = 0$, (a) U/U_0, $(b) < u'^2 > /U_0^2$, $(c) < v'^2 > /U_0^2$ and $(d) < u'v' > /U_0^2$. On each panel the $U = 0$ line is displayed as the black dashed line. The controlled parameters are $k = 9mm$, $d = 4mm$ and $X_0 = 3\lambda$.

Hence, moving arrays closer to the near wake region ($X_0 = 4\lambda$ to 3λ i.e. the maximum amplitude of streaks moving towards the absolute instability region), the effect of streaks on the dynamics becomes more obvious : the intensity of fluctuations sharply decreases. Moving arrays even closer to the rear-end, streaks still reduce fluctuations but in smaller proportion. The same conclusions can be drawn concerning the recirculation length which increases until $X_0 = 3\lambda$ and then starts to decrease. The evolution of the most relevant quantities are summarized in table 7.1 confirming there is an optimal position X_0.

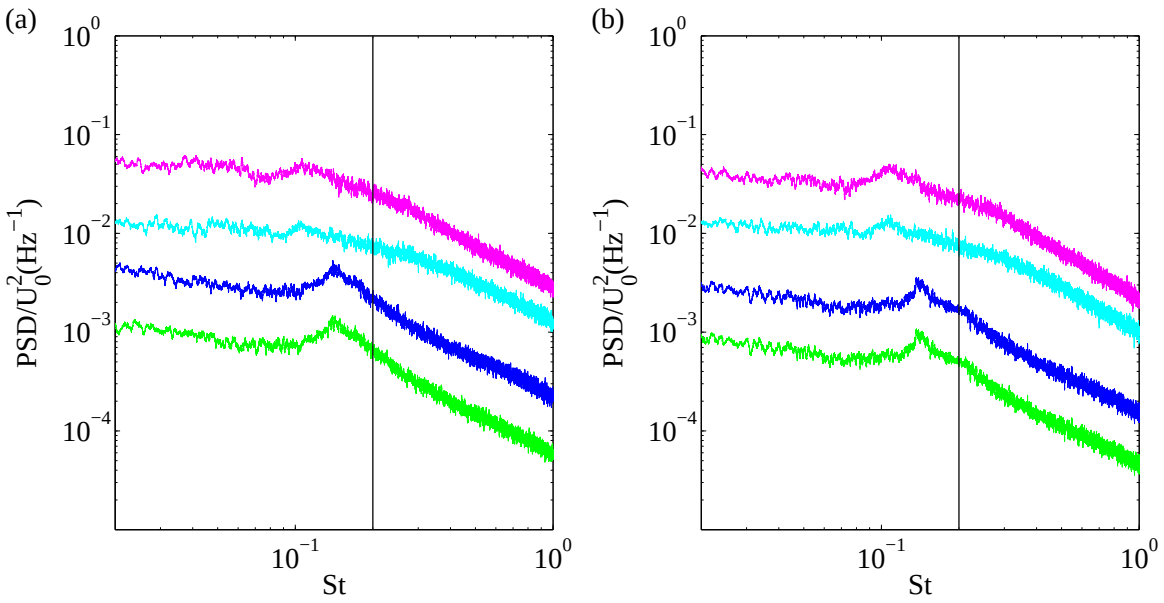

Figure 7.9: Power Spectral Densities (PSD) measured at the positions exposed in figure 7.4 when the control with roughness elements is considered. Panel (a), $x_1 = 3\,H$. Panel (b), $x_1 = 5\,H$

Table 7.1: Properties of the flow varying the location of the roughness arrays on the model.

X_0	$A_{s,max}(x = 0.75H)$	x_r/H	$< u'^2 >_{max} /U_0^2$	$< v'^2 >_{max} /U_0^2$	$< u'v' >_{max} /U_0^2$
natural case	0.0	1.45	0.045	0.031	0.02
4λ	6%	1.6	0.040	0.027	0.016
3λ	10%	1.9	0.027	0.017	0.007
2λ	8.2%	1.8	0.032	0.022	0.011
1λ	7.3%	1.7	0.038	0.026	0.014

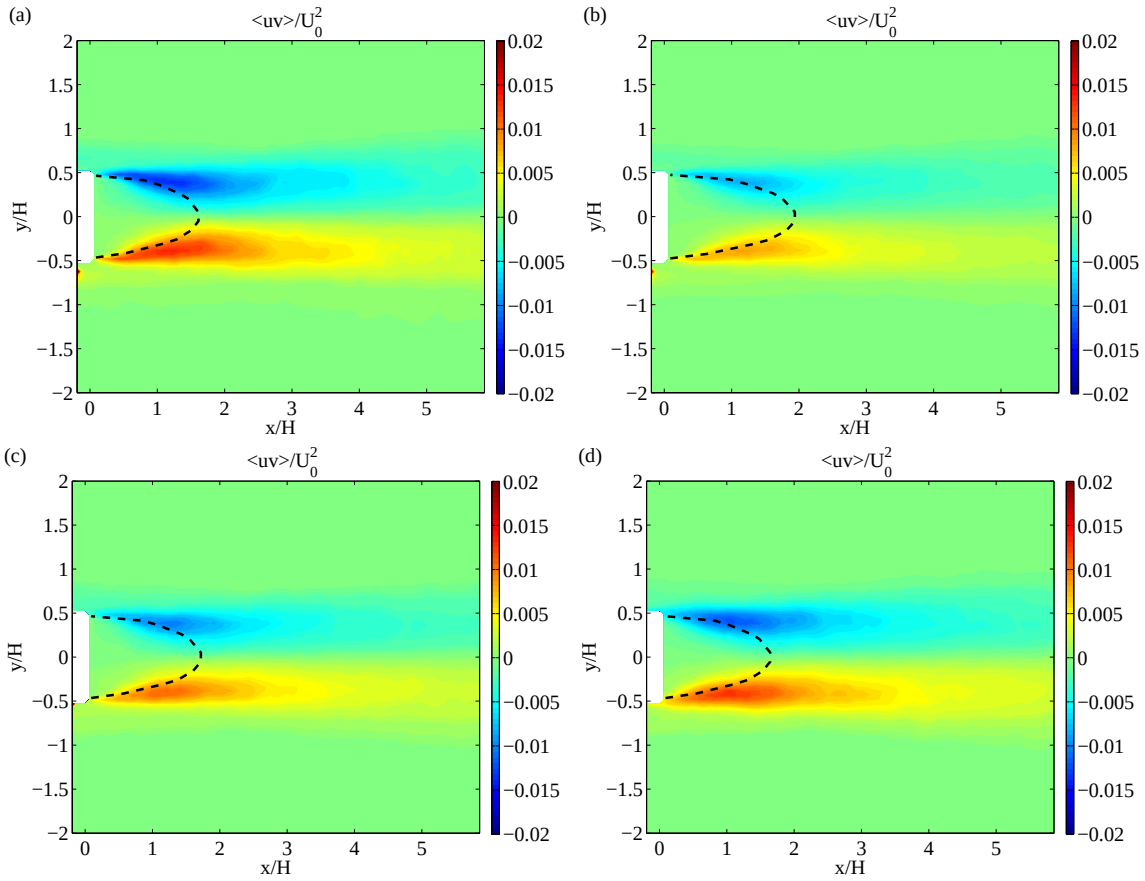

Figure 7.10: $< u'v' > /U_0^2$ distributions in the wake of the model equipped with roughness elements located $4\,\lambda$ (a), $3\,\lambda$ (b), $2\,\lambda$ (c) and λ (d) from the rear-end.

6 Conclusions

In this chapter, we study the flow past a squareback Ahmed body wihtout ground effect for a Reynolds number $Re_H = 30000$. The natural flow case shows a mean recirculation region extending up to $x_R/H = 1.45$ as well as some large scale unsteady activity in the wake. HW measurements in the shear layers show two peaks of energy around $St_{H1} = 0.17$ (upper and bottom shear layers) and $St_{H2} = 0.12$ (two lateral shear layers).

When streaks are artificially forced on the model surface using suitably designed roughness elements arrays, the dynamics of the wake can be altered. Hence, time averaged flow for the controlled case show a increased recirculation bubble (see figure 7.11(a)) while fluctuations are strongly weakened.

The spectral activity shows a reduction of the peak amplitudes and a weak backward shift of the frequencies where the main activities are registered, as shown in right panel of figure 7.11.

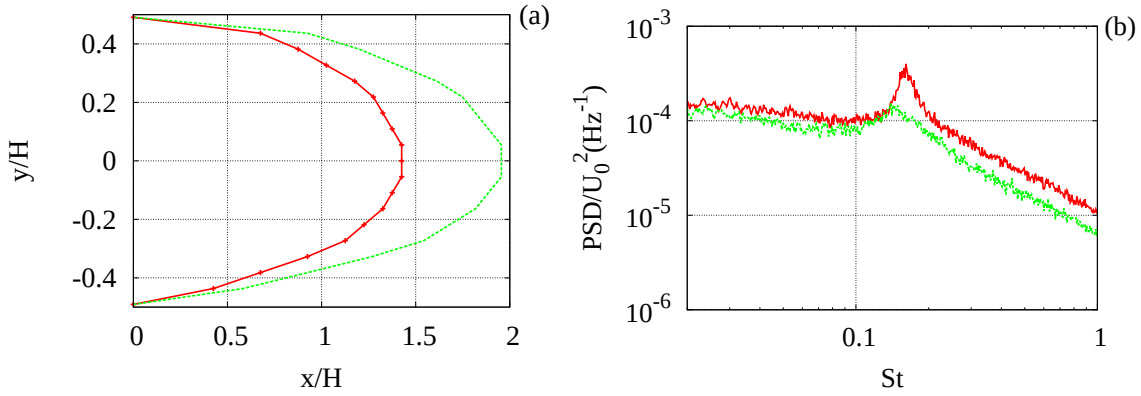

Figure 7.11: Panel (a), recirculation region at $z = 0$ for the natural flow case and the controlled case. Panel (b), power spectral density measured at $x_1 = 3\,H$ in the lower shear layer. Natural flow case is displayed in continuous red line and the controlled case is the green dashed line.

These results are, however, preliminary. Further investigations are required in order to draw general conclusions.

Chapter 8

Conclusions

It is useful to summarize here the main motivations and the main results of this thesis.

Summary of the motivations of this study. One of the main motivations of this study is the industrial need to reduce the pressure drag of cars of prescribed shape. Reducing pressure drag, and therefore fuel consumption and gas emissions is particularly important in the actual delicate moment for the automotive market which is aiming at performance increase. The previous work of Pujals *et al.* (2010*b*) did show that $\approx 10\%$ reductions of the total drag can be achieved by forcing the transient growth of streaks in the turbulent boundary layer on the roof of an Ahmed body. The energy of the actuators was amplified by the flow itself through the lift-up effect. It was shown that in that case the streaks suppressed the separation of the slanted (25°) rear surface of the Ahmed body. The main questions motivating the present work is: can the approach of Pujals *et al.* (2010*b*) be modified to control massive separations around bodies with a blunt trailing edge? If yes, how?

There is an rich literature on the control of vortex shedding in the wake of bluff bodies. Most of the theoretically based investigations on vortex shedding control have considered the $2D$ control of $2D$ wakes. In this case, the suppression of the shedding has been related to the stabilization of the absolute instability. However, $2D$ control, even if well understood, is usually less efficient than $3D$ control which, on the contrary, is less understood and mainly in terms of vortex dynamics. The recent study of Hwang *et al.* (2013), however, led to a breakthrough by proving that low amplitude streaks induce a decrease of the absolute growth rate in parallel wakes. It was however not clear if the streaks considered by Hwang *et al.* (2013) could completely stabilize the absolute instability and if they could stabilize the global instability in a non-parallel wake. As the lift-up effect is inherently $3D$, in this study, we had not only to qualify and quantify the optimal amplification of streaks in wakes, but also to push forward the theoretical interpretation of $3D$ control.

Parallel wakes. In the first part of the study, published in the *Journal of Fluid Mechanics* (Del Guercio *et al.*, 2014*c*), we have computed the optimal temporal transient energy growths sustained by a parallel Monkewitz's wake at $Re = 50$. We have shown that the optimal initial conditions consist of streamwise vortices and the most amplified perturbations are streamwise streaks. The optimal energy growths have been shown to scale on Re^2 and increase with the spanwise wavelength λ_z of the perturbations. We have then investigated the stabilizing action on the temporal and absolute instabilities of *nonlinear* streaks forced by finite amplitude

optimal perturbations. We have shown that the absolute instability can be completely stabilized with relatively small amplitudes of the streaks, therefore extending the initial findings of Hwang *et al.* (2013). We have also shown that, because of the large energy amplification associated with the lift-up effect, it is much more efficient to force the initial vortices than to directly force the streaks in order to implement the control. These results have been very encouraging because they give, at least in this simplified case, affirmative answers to the initial questions motivating this study: Yes, optimal streaks can be very efficiently forced in wakes. Yes, the absolute instability at the origin of vortex shedding can be stabilized by the optimal streaks. Yes, the use of optimal initial vortices leads to a very efficient control.

An additional question was that of the compared efficiencies of $2D$ and $3D$ perturbations. Hwang *et al.* (2013) had shown that the first order sensitivity of the absolute growth rate to $3D$ spanwise periodic modifications of the basic flow is zero, while it is not for $2D$ perturbations. For the small streaks amplitudes they considered they indeed found that $2D$ perturbations were more effective, in terms of streak amplitude, than $3D$ ones in the stabilization of the absolute instability. This finding was in apparent contradiction with the results of Kim & Choi (2005) who found that $3D$ blowing and suction is more efficient than $2D$ blowing and suction in suppressing the shedding in a circular cylinder wake. Our initial guess was that an important stabilizing role could be played by the $2D$ nonlinear mean flow distortion induced by the $3D$ streaks, as in boundary layers (Cossu & Brandt, 2002). This guess was proved wrong by an analysis of the energy production terms who showed that the nonlinear mean flow distortion is not the main mechanism responsible for the stabilization. The explanation must be therefore already present in the linearized context. A key result that we found using optimal perturbations is that when growth rates reductions induced by $2D$ and $3D$ control are expressed in terms of the initial perturbation amplitude (instead that in terms of final streaks amplitudes) $3D$ perturbations appear to be much more efficient that $2D$ one in reducing temporal and absolute growth rates.

The non-parallel synthetic wake. Encouraged by the positive results found on parallel wakes we have considered optimal spatial amplifications in non-parallel wakes. An important preliminary step has been the design and the validation of an adjoint-free, subspace-based algorithm for the computation of the optimal *spatial* energy growths of perturbations forced by inflow or wall boundary conditions. This algorithm, described in appendix B, is based on a set of independent simulations of the linearized Navier-Stokes equations. The algorithm is scalable because additional simulations can be added to the set of the already computed ones in order to increase the accuracy of the results. The convergence of the algorithm has proven quite fast in the considered cases, with converged results obtained with O(10) independent simulations. Another advantage of the algorithm is that it is implemented as a post-processing of DNS-based results and does not require the modification of the DNS codes to e.g. implement the solution of adjoint equations.

In the second part of the study published in *Physics of Fluids* (Del Guercio *et al.*, 2014*a*) we have therefore introduced the use of this new algorithm to compute optimal spatial transient energy growths of steady inflow varicose perturbations sustained by a weakly non-parallel wake. The considered wake is 'synthetic' because it is generated by an inflow condition and not directly by a bluff body, therefore removing the complications related to the boundary conditions on the body and to the strong non-parallelism of real wakes. We find that the considered non-parallel wake sustains significant optimal spatial transient growths. The maximum

growths and the downstream positions where these are achieved increase with the spanwise wavelength of the perturbations, in agreement with what found in parallel wakes. The optimal inlet and most amplified perturbations are similar to the ones found in the parallel case. The non-parallelism leads to a downstream increase of the local wavenumber of the perturbations and therefore induces a stabilizing effect on the energy growth.

We have found that the strong *linear global instability* of the uncontrolled basic flow can be completely suppressed by forcing optimal perturbations with finite amplitudes. Nonlinear simulations validate this finding in the nonlinear regime. To our knowledge this is the first direct proof that the suppression of vortex shedding by $3D$ control is due to the stabilization of the linear global instability. We have then shown that the first order sensitivity of the *global* growth rate on the control amplitude is zero and that the growth rate reductions are proportional to the square of the control amplitude up to the stabilizing amplitudes. We also show that in this non-parallel case $2D$ perturbations are less efficient than $3D$ ones to stabilize the wake not only in terms of inflow perturbation (control) amplitude but also in terms of streaks amplitudes and this despite the respective linear and quadratic sensitivity on the control amplitude.

The circular cylinder's wake. In the third part of the thesis, published in a second paper in the *Journal of Fluid Mechanics* (Del Guercio *et al.*, 2014*b*) we have considered the circular cylinder's wake. The forcing of optimal perturbations is realized through spanwise periodic blowing and suction at the wall. In this case the big questions are: is this forcing efficient to generate the streamwise vortices that will induce the streamwise streaks? Are the optimal streaks efficient in stabilizing the global instability? The answers are more positive than initially expected. First, we find that very large spatial transient energy growths are achieved in this configuration. Maximum growths and the position where they are achieved increase with the Reynolds number. Maximum optimal amplification of blowing and suction is achieved for spanwise wavelengths λ_z in the range $5D-7D$ at the considered Reynolds numbers ranging from 50 to 100. Furthermore, for these spanwise wavelengths, the maximum growth is reached inside the absolute instability (wave-maker) region of the wake. The fact that G_{max} is not an always increasing function of λ_z is related to the fact that optimal perturbations corresponding to large spanwise wavelengths are very 'tall' and therefore expensive to force from the wall. The finite most amplified λ_z therefore represent the optimal compromise between two antagonist behaviors of the higher amplification and of the higher cost of optimal perturbations at large λ_z.

We have then investigated the influence on the linear global instability of the finite amplitude optimal blowing and suction. A key result is that the critical control amplitude A_w required to suppress the global instability *is reduced* by an increase of Re (from 75 to 100). This was not expected because the global instability is stronger at $Re = 100$ than at $Re = 75$. However, this result can be explained by recalling that as the maximum energy growths increase with the Reynolds number the cost of the control decreases with Re. The decreasing cost of the optimal energy amplification, related to the lift-up effect physics, is therefore able to overcome the increase of the growth rate of the global instability. Finally, also in this case, $3D$ optimal perturbations are much more efficient than $2D$ blowing and suction in achieving the complete stabilization of the global mode. The sensitivity of the global mode growth rate to the 3D control is, also in this case, quadratic.

Effectiveness of the 'optimal growth to control' approach. A key result of these three first parts of the thesis is to show that forcing optimal vortices instead of directly forcing the streaks in parallel and non-parallel wakes is much more efficient and that the energy amplification associated to this process plays a key role in the stabilization. Our results therefore extend to $2D$ wakes the approach already tested in boundary layers where linearly optimal streamwise vortices were forced to induce streaks and stabilize $2D$ unstable Tollmien-Schlichting waves and delay transition to turbulence (Cossu & Brandt, 2002, 2004; Fransson *et al.*, 2005, 2006). Of course, it remains to be shown that this technique is also as effective in the case of 3D and/or turbulent wakes. This is the object of current intensive investigation.

Experimental study of a 3D wake. In the given time it has not been possible to theoretically and numerically investigate the case of 3D wakes or to extend our results to the turbulent regime similarly to what e.g. done in turbulent boundary layers and channel flows. It has been, however, possible to begin to test some of our ideas in some experiments on the control of a turbulent 3D bluff body wake. Since no optimal perturbations for these wakes are available at this time, the design of the perturbations has been semi-empirical and driven by the knowledge acquired through studying $2D$ wakes. A crown of roughness elements placed around the sides of the body allowed us to stimulate the creation of streaks on the shear layer of the turbulent mean wake profile. This turned out to influence the properties of the wake: (a) the length of the recirculation bubble is increased, (b) velocity fluctuations in the shear layers are reduced, (c) the amplitude of the peaks associated with the shedding mode is also reduced. These results are, however, preliminary and require further investigations. For instance, we should better verify the reduction of the fluctuations and check that the coherent mode's spectral peak is global and not simply related to a downstream shift of the coherent structures. Also, many questions remain unanswered at this stage. What happens when the ground is taken into account? Is the streaks influence relevant also at larger Reynolds numbers? These are a few points that would be interesting to investigate.

Appendix

Appendix A

General tools

1 Numerical simulations

Numerical simulations of the Navier-Stokes equations have been performed using the OpenFoam open-source code (see http://www.openfoam.org).

The code is based on a finite volume discretization of the Navier-Stokes equation which are solved using the PISO (Pressure Implicit with Splitting of Operator) algorithm (see e.g. Issa, 1986). The second order accurate Crank-Nicolson scheme with automatic time stepping and CFL adaptation is used to advance the solutions in time. Several maximum temporal steps have been tested during the validation to guarantee the agreement with the reference cases.

The original code is programmed to solve the Navier-Stokes equation for the total velocity field, no decomposition are a priori implemented. An important part of my work has consisted in developing and validating a code reformulated in perturbation form and, in particular, the linearized version. These new solvers have been validated e.g. by reproducing the optimal transient growths sustained by laminar channel flows computed by Reddy & Henningson (1993), or finding the correct value of the growth rate of the most unstable mode of the Bickley jet (see e.g. Drazin & Reid, 1981).

1.1 Simulations of parallel wakes

In the case of the parallel wakes, simulation have been used to compute non linear streaky basic flows (non linear solver) and the impulse response (linear solver).

The flow is solved inside the domain $[0, L_x] \times [-L_y/2, L_y/2] \times [0, L_z]$ that is discretized using a grid with N_x and N_z equally spaced points in the streamwise and spanwise directions respectively. N_y points are used in the y direction using a stretching which allows to density points in the region where the basic flow shear is not negligible. Typically, results have been obtained using $L_x = 124, L_y/2 = 10, L_z = 2\pi$ and $N_x = 300, N_y = 160, N_z = 24$ with $\Delta x = 0.4$, $\Delta z = 0.26$ and a minimum $\Delta y = 0.01$ on the symmetry axis and a maximum $\Delta y = 0.1$ near the free-stream boundary. Periodic boundary conditions have been enforced in the streamwise and spanwise directions and zero normal gradients of velocity and pressure have been enforced at the free stream boundaries ($|y| = L_y/2$). An increase of $L_y/2$ from 10 to 15 or an increase of the number of points from $N_y = 160$ to $N_y = 320$ did not affect the energy density more than 2%.

1.2 Simulations of non parallel synthetic wakes

Numerical simulations of the Navier-Stokes equations have been used to compute the $2D$ weakly non-parallel basic flow (non-linear equations with y-symmetry enforced), the optimal perturbations of the $2D$ wake (linearized equations), the nonlinear streaky basic flows (non-linear equations with y-symmetry enforced) and the global linear stability of these basic flows (with the linearized equations).

The flow is solved inside the domain $[0, L_x] \times [-L_y/2, L_y/2] \times [0, L_z]$ that is discretized using a grid with N_x and N_z equally spaced points in the streamwise and spanwise directions respectively. N_y points are used in the y direction using stretching to density points in the region where the basic flow shear is not negligible.

β	$L_z = \lambda_z$	Nz	$Ly/2$	Ny	Lx	Nx
0.5	12.57	48	20	240	124	300
0.75	8.38	48	20	240	124	300
1	6.28	24	10	160	124	300
1.25	5.03	24	10	160	124	300
1.5	4.20	12	10	160	124	300
1.75	3.60	12	10	160	124	300

Table A.1: Numerical grids used for the computation of optimal perturbations of the weakly non parallel synthetic wake.

Different grids have been used to compute optimal linear perturbations of different spanwise wavenumbers, as reported in table A.1. Nonlinear streaky basic flows for $\beta = 1$ have been computed using the same grid used for the computation of the linear optimals at the same β. For the linear and nonlinear simulations of the perturbations to the $3D$ streaky basic flows, however, the domain is doubled in the y direction ($[-L_y/2, L_y/2]$ instead of $[0, L_y/2]$) as the y symmetry is no more enforced. The box is also doubled in the spanwise direction ($L_z = 2\lambda_z$) in order to include subharmonic perturbations. The corresponding N_y and N_z are also doubled leading to a grid with $L_x = 124$, $L_y/2 = 10$, $L_z = 4\pi$, $N_x = 300$, $N_y = 160$,$Nz = 48$ with $\Delta x = 0.4$, $\Delta z = 0.26$ and a minimum $\Delta y = 0.01$ on the symmetry axis and a maximum $\Delta y = 0.1$ near the freestream boundary.

1.3 Simulations of the circular cylinder's wake

The flow is solved in a C-type domain centred on the cylinder with L_x, L_y and L_z streamwise, transverse and spanwise extensions respectively (see figure A.1). Several preliminary tests guided us to the choice $L_x = 70$ and $L_y = 80$, with, $L_z = \lambda_z$ for the optimization studies and $L_z = 2\lambda_z$ for the global stability analysis and the nonlinear simulations; this has allowed us to take in account the influence of the subharmonic modes, as detailed following in the text. The grid density is increased in the $x - y$ plane in the regions of high shear. $N_x = 300$ and $N_y = 200$ points were used in the streamwise and transverse directions respectively, with $\Delta x_{min} = 0.01$, $\Delta x_{max} = 0.2$, $\Delta y_{min} = 0.01$ and $\Delta y_{max} = 0.2$ inside the internal sub-blocks. A uniform grid spacing is used in the spanwise direction always with $\Delta z \approx 0.25$ and a number of points summarized in table A.2. We have verified that with the chosen mesh the length of the recirculation region of steady symmetric solutions, and the drag coefficient do match

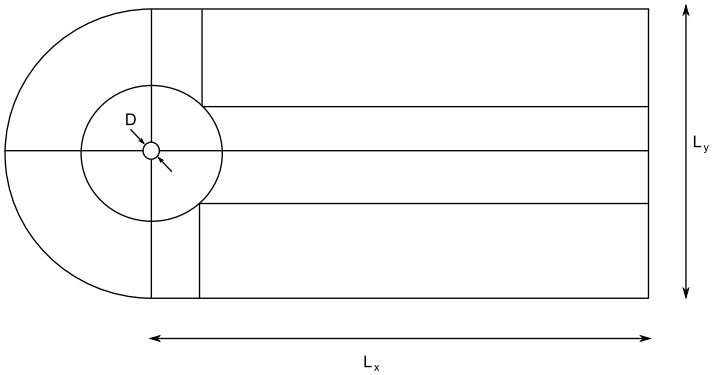

Figure A.1: Numerical solution domain for the simulations of the flow around a circular cylinder. Only the boundaries of the grid sub-blocks are reported to keep the figure readable.

λ_z	12.57	8.37	6.28	5.03	4.20	3.60	3.14
N_z	48	34	24	20	16	14	12

Table A.2: Simulations of the circular cylinder wake. Spanwise extension L_z of the solution domain and number of points N_z used in that direction for the computation of the basic flows and of the optimal perturbations. L_z and N_z are doubled for the global stability analysis and for the nonlinear simulations.

within 1% accuracy those found by Kim & Choi (2005) and Giannetti & Luchini (2007) in the 2D case and in the range of considered Reynolds numbers. Extending the domain size in the streamwise direction to $L_x = 100$ or in the transverse direction to $L_y = 100$ does not improve much these results. For 3D simulations we have verified in a few selected cases (in particular the $M = 1$ direct numerical simulations in the optimization studies) that the perturbation energy (used to compute global growth rates) does not change by more than 1% when the number of grid points is doubled in the spanwise direction.

2 Fundamental and subharmonic, symmetric and antisymmetric modes

All the numerical simulations of the evolutions of the perturbations to the given basic flows are performed in a spanwise-periodic domain of length twice that of the basic flow streaks $L_z = 2\lambda_z$ where $\lambda_z = 2\pi/\beta$. The perturbations can be decomposed into the contributions of fundamental and subharmonic modes, and be can further be decomposed into symmetric and antisymmetric with respect to the $y = 0$ plane. The fundamental modes with an even symmetry (same as that of the basic flow streaks) are of the form with $\beta_k^F = k\beta$, where β is the wavenumber of the basic flow streaks.

$$\widehat{u}(y,z) = \sum_{k=1}^{\infty} \tilde{u}_k(y) \cos \beta_k^F z; \quad \widehat{v}(y,z) = \sum_{k=1}^{\infty} \tilde{v}_k(y) \cos \beta_k^F z; \quad \widehat{w}(y,z) = \sum_{k=1}^{\infty} \tilde{w}_k(y) \sin \beta_k^F z.$$

Fundamental modes with opposite symmetry admit the expansion:

$$\widehat{u}(y,z)=\sum_{k=1}^{\infty}\tilde{u}_k(y)\sin\beta_k^F z;\quad \widehat{v}(y,z)=\sum_{k=1}^{\infty}\tilde{v}_k(y)\sin\beta_k^F z;\quad \widehat{w}(y,z)=\sum_{k=1}^{\infty}\tilde{w}_k(y)\cos\beta_k^F z.$$

For subharmonic modes the spanwise periodicity of the disturbances is twice that of the basic flow and therefore we define $\beta_k^S=[(k+1)/2]\beta$. Subharmonic symmetric modes are expanded as

$$\widehat{u}(y,z)=\sum_{k=1}^{\infty}\tilde{u}_k(y)\cos\beta_k^S z;\quad \widehat{v}(y,z)=\sum_{k=1}^{\infty}\tilde{v}_k(y)\cos\beta_k^S z;\quad \widehat{w}(y,z)=\sum_{k=1}^{\infty}\tilde{w}_k(y)\sin\beta_k^S z.$$

while subharmonic antisymmetric modes admit the expansion:

$$\widehat{u}(y,z)=\sum_{k=1}^{\infty}\tilde{u}_k(y)\sin\beta_k^S z;\quad \widehat{v}(y,z)=\sum_{k=1}^{\infty}\tilde{v}_k(y)\sin\beta_k^S z;\quad \widehat{w}(y,z)=\sum_{k=1}^{\infty}\tilde{w}_k(y)\cos\beta_k^S z.$$

Given a perturbation velocity field, e.g obtained from linearized DNS, the respective contributions of the fundamental and subharmonic, symmetric/antisymmetric modes to the total field can be retrieved by a straightforward partitioning of the spanwise discrete Fourier transform of the velocity field into odd-even harmonic real-imaginary parts.

3 Impulse response analysis in parallel wakes

The techniques used to retrieve the temporal and spatio-temporal stability properties of parallel basic flow from the numerically computed impulse response closely follow the ones used by Brandt *et al.* (2003), which are the three-dimensional extension of the ones developed by Delbende *et al.* (1998) and Delbende & Chomaz (1998) for two-dimensional wakes.

Consider the generic perturbation variable $q(x,y,z,t)$. Concerning the temporal stability analysis, in order to determine the dependence of the temporal growth rate ω_i on the (real) streamwise wavenumber α, the amplitude spectrum of $q(x,y,z,t)$ is defined as

$$\widetilde{Q}(\alpha,t)=\Big(\int_{-L_y/2}^{L_y/2}\int_0^{L_z}|\tilde{q}(\alpha,y,z,t)|^2dy\,dz\Big)^{1/2},\tag{A.1}$$

where $\tilde{q}(\alpha,y,z,t)$ is the Fourier transform of the variable q in the streamwise direction. The asymptotic exponential regime is attained for large times where the leading temporal mode emerges with growth rate ω_i well approximated by:

$$\omega_i(\alpha)\sim\frac{\partial}{\partial t}\ln\widetilde{Q}(\alpha,t),\qquad t\to\infty,\tag{A.2}$$

which can be numerically computed by the finite difference approximation

$$\omega_i(\alpha)\approx\frac{\ln[\widetilde{Q}(\alpha,t_2)/\widetilde{Q}(\alpha,t1)]}{t_2-t_1}.\tag{A.3}$$

The selected times t_1 and t_2 in the above approximation need to be sufficiently large to ensure the extinction of transients. Hence the temporal stability of the basic flow is determined by

the maximum growth rate $\omega_{i,max}$, which establishes that the basic flow is temporally stable if $\omega_{i,max} < 0$ while unstable if $\omega_{i,max} > 0$.

The spatio-temporal stability analysis considers the development of the impulse response wave packet along $x/t = v$ rays, which is equivalent to the investigation of modes of real group velocity v. The initial impulse is numerically approximated, in terms of stream function, as:

$$\psi'(x,y,z) = A_{II}\, e^{-\frac{(x-x_0)^2}{2\sigma_x^2} - \frac{(y-y_0)^2}{2\sigma_y^2} - \frac{(z-z_0)^2}{2\sigma_z^2}}, \tag{A.4}$$

which is the three-dimensional extension of the initial condition used by Delbende & Chomaz (1998) for the same type of analysis of 2D wakes. We computed the linear impulse response by direct numerical simulation of the Navier-Stokes equations linearized near the given frozen basic flow.
The corresponding perturbation velocity components are given by $(u', v', w') = (\partial\psi/\partial y, -\partial\psi/\partial x, 0)$ and the amplitude A_{II} is set sufficiently small to avoid overflows during the linear simulation. The parameters $\sigma_x = 0.83$, $\sigma_y = 0.83$ and $\sigma_z = 0.30$ have been chosen small enough to reproduce a localized impulse within the limits of a good resolution. The impulse is centered in x_0, y_0, z_0, chosen to ensure that no particular symmetry is preserved by the initial condition.

The use of the Hilbert transform allows to demodulate the wave packet and define its amplitude unambiguously with respect to spatial phase oscillations. To this end, the analytical complex field variable $q_H(x,y,z,t)$ associated with $q(x,y,z,t)$ through the x-convolution $*$ is defined as

$$\bar{q}(x,y,z,t) = \left[\delta(x) + \frac{i}{\pi x}\right] * q(x,y,z,t). \tag{A.5}$$

where the symbol designates the convolution operator with respect to x. The complex field $\bar{q}(x,y,z,t)$ generalizes the complex exponential representation of a sine wave to an arbitrary real function $q(x,y,z,t)$. In wavenumber space, equation (A.5) reduces to

$$q_H(\alpha,y,z,t) = 2H(\alpha)\tilde{q}(\alpha,y,z,t), \tag{A.6}$$

where $H(\alpha)$ is the Heavyside unit-step function. In other words, the Fourier transform of the analytical field is obtained by setting to zero all the Fourier modes of negative streamwise wavenumber. The integration of the analytical field q_H in the cross-stream (y,z) plane then yields the amplitude Q defined by

$$Q(x,t) = \Big(\int_{-L_y/2}^{L_y/2} \int_0^{L_z} |q_H(x,y,z,t)|^2 dy\, dz \Big)^{1/2}. \tag{A.7}$$

According to steepest-descent arguments Bers (1983), the long-time behaviour of the wave packet along each spatio-temporal ray $x/t = v$ is

$$Q(x,t) \propto t^{-1/2}\, e^{i[\alpha(v)x - \omega(v)t]}, \qquad t \to \infty, \tag{A.8}$$

where $\alpha(v)$ and $\omega(v)$ represent the complex wavenumber and frequency travelling at the group velocity v. In (A.8), the real part of the exponential

$$\sigma(v) = \omega_i(v) - k_{x,i}(v)v \tag{A.9}$$

denotes the spatio-temporal growth rate observed while traveling at the velocity v and it can be evaluated for large t directly from the amplitude Q in (A.8) as

$$\sigma(v) \sim \frac{\partial}{\partial t} \ln[t^{1/2}\, Q(vt,t)] \tag{A.10}$$

that can be approximated with

$$\sigma(v) \approx \frac{\ln[Q(vt_2,t_2)/Q(vt_1,t_1)]}{t_2-t_1} + \frac{\ln(t_2/t_1)}{2\,(t_2-t_1)}, \tag{A.11}$$

to which apply the same considerations discussed about.
For unstable basic flow $\sigma(v) > 0$ in the range $[v^-, v^+]$, where v^- and v^+ are respectively the trailing edge and leading edge velocity of a downsteam traveling wavepacket. The absolute growth rate $\sigma(v=0)$ defines the nature convective or absolute of the unstable wavepacket, indeed for $\sigma(v=0) < 0$, i.e.: $v^- > 0$, the basic flow is *convectively unstable*, while for $\sigma(v=0) > 0$, i.e.: $v^- < 0$, it is *absolutely unstable*.

4 Computing the growth rate of global modes

In the present work the most unstabe (or least stable) global mode $\widehat{\boldsymbol{\phi}}(x,y,z)$ and the corresponding eigenvalue s are retrieved by monitoring the temporal evolution of the global perturbation kinetic energy around the given basic flow ($\mathbf{U}_{2D}$ for the natural case and $\mathbf{U}_{3D}$ for the controlled case):

$$E' = \frac{1}{\mathcal{V}_{ref}} \int_0^{L_x} \int_{-L_y/2}^{L_y/2} \int_0^{L_z} \boldsymbol{\phi}' \cdot \boldsymbol{\phi}' \; dx\, dy\, dz, \tag{A.12}$$

where $\mathcal{V}_{ref}$ is the reference volume of the computational domain and L_x, L_y and L_z are the size in the downstream, normal and spanwise direction respectively.

In a linear framework, after an initial transient, the most unstable global mode will emerge:

$$E' \approx \langle \widehat{\boldsymbol{\phi}}^1, \widehat{\boldsymbol{\phi}}^1 \rangle \, e^{2\, s_r^1 \, t}.$$

5 Computing optimal temporal energy growths in parallel wakes

Optimal growths $G(t,\alpha,\beta)$ are computed along quite standard lines, described e.g. in Schmid & Henningson (2001). The linearized Navier-Stokes equations are recast in terms of the cross-stream velocity and vorticity $v-\eta$. The system satisfied by Fourier modes $\widehat{v}(y,t;\alpha,\beta)e^{i(\alpha x+\beta z)}$, $\widehat{\eta}(y,t;\alpha,\beta)e^{i(\alpha x+\beta z)}$ is the standard Orr-Sommerfeld-Squire system (see e.g. Schmid & Henningson, 2001):

$$\nabla^2 \frac{\partial \widehat{v}}{\partial t} = \mathcal{L}_{\mathcal{OS}} \widehat{v}; \qquad \frac{\partial \widehat{\eta}}{\partial t} = -i\beta \frac{dU}{dy} \widehat{v} + \mathcal{L}_{\mathcal{SQ}} \widehat{\eta} \tag{A.13}$$

where the Orr-Sommerfeld and Squire operators are:

$$\mathcal{L}_{\mathcal{OS}} = -i\alpha \left[U(\mathcal{D}^2 - k^2) - \frac{d^2U}{dy^2} \right] + \frac{1}{Re}(\mathcal{D}^2 - k^2)^2, \tag{A.14}$$

$$\mathcal{L}_{\mathcal{SQ}} = -i\alpha U + \frac{1}{Re}(\mathcal{D}^2 - k^2), \tag{A.15}$$

and where $\mathcal{D}$ denotes d/dy and $k^2 = \alpha^2 + \beta^2$. The system is discretized on grid of N_y points uniformly distributed in $[-L_y/2, L_y/2]$. Differentiation matrices based on second-order

accurate finite differences have been used to discretize the Orr-Sommefeld-Squire system. Most of the results have been obtained with $N_y = 201$ and L_y ranging from 20 to 120 for the perturbations with the smallest spanwise wavenumbers (largest spanwise wavelengths). The results do not change if N_y is doubled to 401 and L_y is increased by half. We have also verified that the results do not change if differentiation matrices based on Fourier series instead of finite differences discretization provided that L_y is large enough. The distretization has also been validated against temporal growth rates of Bickley jets available in the literature. Once the linear operator is discretized, standard methods and codes already used in previous investigations (e.g. Lauga & Cossu, 2005; Pujals *et al.*, 2009; Cossu *et al.*, 2009) are used to compute the optimal growth and the associated optimal perturbations.

Appendix B

An adjoint-free subspace reduction algorithm to compute optimal spatial amplifications in non-parallel wakes

As discussed in chapter 4 we have not found in the literature any algorithm suitable to compute the optimal *spatial* growths in bluff body wakes that could be used to compute e.g. the optimal blowing and suction on the body skin. Previous computations of optimal spatial growths such as those of Andersson *et al.* (1999) or Luchini (2000) were based on direct-adjoint methods developed under the assumption of the streamwise parabolicity of the equations. In those computations the variable t was essentially replaced by the variable x. This has led us to design a new algorithm. The main idea is to approximate the linear response of the system to inflow or wall forcing in a subspace, compute optimal growths in this subspace, and achieved convergence by increasing the subspace dimension. The set of states with which the subspace is built consists in the set of steady perturbation velocity fields corresponding to a set of linearly independent inflow boundary conditions or wall forcings (e.g. blowing and suctions).

Let us introduce the algorithm for the case of the weakly non-parallel synthetic wake. We denote by $\mathbf{U}_{2D}$ the $2D$ basic flow obtained using $U_0(y)$ as inlet velocity profile. Consider then the steady perturbations $\mathbf{u}$ of $\mathbf{U}_{2D}$ obtained by perturbing the inlet profile $U_0(y)$ with steady inflow perturbations $\mathbf{u}_0(y,z)$. In particular, spanwise periodic perturbations of wavelength λ_z are considered.

Let us now decompose the inlet perturbation on a set of linearly independent functions $\mathbf{b}_0^{(m)}$, in practice limited to M terms, as:

$$\mathbf{u}_0(y,z) = \sum_{m=1}^{M} q_m \mathbf{b}_0^{(m)}(y,z). \tag{B.1}$$

Under the assumption of small perturbations, the steady response to the inflow perturbations satisfies the steady linearized Navier-Stokes equations. Denoting by $\mathbf{b}^{(m)}(x,y,z)$ the perturbation velocity field obtained using $\mathbf{b}_0^{(m)}(y,z)$ as inlet perturbation, from the linearity of the operator follows that:

$$\mathbf{u}(x,y,z) = \sum_{m=1}^{M} q_m \mathbf{b}^{(m)}(x,y,z), \tag{B.2}$$

where the coefficients q_m are the same used in (B.1). The spatial optimization problem defined by equation (4.1) can therefore be approximated in terms of the M-dimensional control vector

$\mathbf{q}$ as:

$$G(x) = \max_{\mathbf{q}} \frac{\mathbf{q}^T \mathbf{H}(x) \mathbf{q}}{\mathbf{q}^T \mathbf{H}_0 \mathbf{q}}, \tag{B.3}$$

where the components of the symmetric matrices $\mathbf{H}(x)$ and $\mathbf{H}_0$ are:

$$H_{mn}(x) = \frac{1}{2\delta\lambda_z} \int_{-\infty}^{\infty} \int_0^{\lambda_z} \mathbf{b}^{(m)}(x,y,z) \cdot \mathbf{b}^{(n)}(x,y,z)\, dy\, dz, \tag{B.4}$$

$$H_{0,mn} = \frac{1}{2\delta\lambda_z} \int_{-\infty}^{\infty} \int_0^{\lambda_z} \mathbf{b}_0^{(m)}(y,z) \cdot \mathbf{b}_0^{(n)}(y,z)\, dy\, dz. \tag{B.5}$$

Within this formulation $G(x)$ is easily found as the largest (real) eigenvalue μ_{max} of the generalized $M \times M$ eigenvalue problem $\mu \mathbf{H}_0 \mathbf{w} = \mathbf{H}\mathbf{w}$. The corresponding eigenvector is the optimal set of coefficients $\mathbf{q}^{(opt)}$ maximizing the kinetic energy amplification at the selected streamwise station x. The corresponding inlet perturbation is $\mathbf{u}_0^{(opt)}(y,z) = \sum_{m=1}^{M} q_m^{(opt)} \mathbf{b}_0^{(m)}(y,z)$. In the limit $M \to \infty$ the approximated solution converges to the exact solution. The computational cost to reach convergence are, in practical cases, are limited to a finite dimension of the subspace M.

The algorithms is easily extended to the computation of the optimal blowing and suction on the circular cylinder. The control radial velocity enforced at the cylinder surface $u_w(\theta, z)$ is decomposed on a set of linearly independent functions $b_w^{(m)}$, in practice limited to M terms, as:

$$u_w(\theta, z) = \sum_{m=1}^{M} q_m b_w^{(m)}(\theta, z). \tag{B.6}$$

If the perturbation velocity field obtained using $b_w^{(m)}(\theta, z)$ as inlet perturbation is denoted by $\mathbf{b}^{(m)}(x,y,z)$, from linearity it follows that

$$\mathbf{u}(x,y,z) = \sum_{m=1}^{M} q_m \mathbf{b}^{(m)}(x,y,z). \tag{B.7}$$

In this case the matrices $\mathbf{H}(x)$ and $\mathbf{H}_w$ become:

$$H_{mn}(x) = \frac{1}{\pi\lambda_z} \int_{-\infty}^{\infty} \int_0^{\lambda_z} \mathbf{b}^{(m)}(x,y,z) \cdot \mathbf{b}^{(n)}(x,y,z)\, dy\, dz; \tag{B.8}$$

$$H_{w,mn} = \frac{1}{2\pi\lambda_z} \int_0^{\lambda_z} \int_0^{2\pi} b_w^{(m)}(\theta, z)\, b_w^{(n)}(\theta, z)\, d\theta\, dz. \tag{B.9}$$

Then the procedure to compute $G(x)$ follows the same steps discussed above and the corresponding eigenvector $\mathbf{q}^{(opt)}$ is the set of optimal coefficients maximizing the kinetic energy amplification at the selected streamwise station x and the corresponding optimal blowing and suction is given by $u_w^{(opt)}(\theta, z) = \sum_{m=1}^{M} q_m^{(opt)} b_w^{(m)}(\theta, z)$.

Bibliography

Abdessemed, N., Sharma, A. S., Sherwin, S. & Theofilis, V. 2009 Transient growth analysis of the flow past a circular cylinder. *Physics of Fluids (1994-present)* **21** (4), 044103.

Achenbach, E. 1974 Vortex shedding from spheres. *Journal of Fluid Mechanics* **62** (02), 209–221.

Ahmed, S., Ramm, G. & Faltin, G. 1984 Some salient features of the time-averaged ground vehicle wake. *Tech. Rep.*. SAE Technical Paper.

Aider, J.-L., Beaudoin, J.-F. & Wesfreid, J. E. 2010 Drag and lift reduction of a 3d bluff-body using active vortex generators. *Experiments in Fluids* **48** (5), 771–789.

Alizard, F., Cherubini, S. & Robinet, J.-C. 2009 Sensitivity and optimal forcing response in separated boundary layer flows. *Physics of Fluids (1994-present)* **21** (6), 064108.

Alizard, F., Robinet, J.-C. & Rist, U. 2010 Sensitivity analysis of a streamwise corner flow. *Physics of Fluids (1994-present)* **22** (1), 014103.

Andersson, P., Berggren, M. & Henningson, D. S. 1999 Optimal disturbances and bypass transition in boundary layers. *Physics of Fluids (1994-present)* **11** (1), 134–150.

Andersson, P., Brandt, L., Bottaro, A. & Henningson, D. S. 2001 On the breakdown of boundary layer streaks. *Journal of Fluid Mechanics* **428**, 29–60.

Antkowiak, A. & Brancher, P. 2004 Transient energy growth for the Lamb–Oseen vortex. *Physics of Fluids (1994-present)* **16** (1), L1–L4.

Bagheri, S. & Hanifi, A. 2007 The stabilizing effect of streaks on Tollmien-Schlichting and oblique waves: A parametric study. *Physics of Fluids (1994-present)* **19** (7), 078103.

Balachandar, S., Mittal, R. & Najjar, F. 1997 Properties of the mean recirculation region in the wakes of two-dimensional bluff bodies. *Journal of Fluid Mechanics* **351**, 167–199.

Barbagallo, A., Dergham, G., Sipp, D., Schmid, P. J. & Robinet, J.-C. 2012 Closed-loop control of unsteadiness over a rounded backward-facing step. *Journal of Fluid Mechanics* **703**, 326–362.

Barkley, D. & Henderson, R. D. 1996 Three-dimensional Floquet stability analysis of the wake of a circular cylinder. *Journal of Fluid Mechanics* **322**, 215–241.

Bearman, P. 1967 The effect of base bleed on the flow behind a two-dimensional model with a blunt trailing edge (base bleed effects on flow behind two-dimensional model with blunt trailing edge, measuring base pressure, shedding frequency and vortex formation). *Aeronautical Quarterly* **18**, 207–224.

Bearman, P. W. & Owen, J. C. 1998 Reduction of bluff-body drag and suppression of vortex shedding by the introduction of wavy separation lines. *Journal of Fluids and Structures* **12** (1), 123–130.

Beaudoin, J.-F. & Aider, J.-L. 2008 Drag and lift reduction of a 3d bluff body using flaps. *Experiments in Fluids* **44** (4), 491–501.

Berger, E. 1967 Suppression of vortex shedding and turbulence behind oscillating cylinders. *Physics of Fluids (1958-1988)* **10** (9), S191–S193.

Bers, A. 1975 Linear waves and instabilities. In *Plasma physics–les houches 1972*.

Bers, A. 1983 Space-time evolution of plasma instabilities-absolute and convective. In *Basic plasma physics. 1*.

Bottaro, A., Corbett, P. & Luchini, P. 2003 The effect of base flow variation on flow stability. *Journal of Fluid Mechanics* **476**, 293–302.

Brandt, L., Cossu, C., Chomaz, J., Huerre, P. & Henningson, D. S. 2003 On the convectively unstable nature of optimal streaks in boundary layers. *Journal of Fluid Mechanics* **485**, 221–242.

Briggs, R. J. 1964 Electron-stream interaction with plasmas .

Bruneau, C.-H., Creusé, E., Depeyras, D. & Gillieron, P. 2011 Active procedures to control the flow past the ahmed body with a 25 degree rear window. *International Journal of Aerodynamics* **1** (3), 299–317.

Bruneau, C.-H., Creusé, E., Depeyras, D., Gilliéron, P. & Mortazavi, I. 2010 Coupling active and passive techniques to control the flow past the square back Ahmed body. *Computers & Fluids* **39** (10), 1875–1892.

Butler, K. M. & Farrell, B. F. 1992 Three-dimensional optimal perturbations in viscous shear flow. *Physics of Fluids A: Fluid Dynamics (1989-1993)* **4** (8), 1637–1650.

Cadot, O., Thiria, B. & Beaudoin, J.-F. 2009 Passive drag control of a turbulent wake by local disturbances. In *IUTAM Symposium on Unsteady Separated Flows and their Control*, pp. 529–537. Springer.

Cantwell, B. & Coles, D. 1983 An experimental study of entrainment and transport in the turbulent near wake of a circular cylinder. *Journal of Fluid Mechanics* **136**, 321–374.

Choi, H., Jeon, W.-P. & Kim, J. 2008 Control of flow over a bluff body. *Annual Review of Fluid Mechanics* **40**, 113–139.

Choi, H., Lee, J. & Park, H. 2014 Aerodynamics of heavy vehicles. *Annual Review of Fluid Mechanics* **46**, 441–468.

Chomaz, J., Huerre, P. & Redekopp, L. 1988 Bifurcations to local and global modes in spatially developing flows. *Physical Review Letters* **60** (1), 25.

Chomaz, J.-M. 2005 Global instabilities in spatially developing flows: non-normality and nonlinearity. *Annual Review of Fluid Mechanics* **37**, 357–392.

Cossu, C. 1997 Analisi di stabilitá lineare e nonlineare del flusso viscoso intorno ad un cilindro circolare. Tesi di Dottorato in Ingegneria Aerospaziale, Universitá *La Sapienza*, Roma, Italia.

Cossu, C. 2014 On the stabilizing mechanism of 2d absolute and global instabilities by 3d streaks. *arXiv preprint arXiv:1404.3191* .

Cossu, C. & Brandt, L. 2002 Stabilization of Tollmien–Schlichting waves by finite amplitude optimal streaks in the blasius boundary layer. *Physics of Fluids (1994-present)* **14** (8), L57–L60.

Cossu, C. & Brandt, L. 2004 On Tollmien-Schlichting-like waves in streaky boundary layers. *European Journal of Mechanics-B/Fluids* **23** (6), 815–833.

Cossu, C., Chevalier, M. & Henningson, D. 2007 Optimal secondary energy growth in a plane channel flow. *Physics of Fluids (1994-present)* **19**, 058107.

Cossu, C. & Chomaz, J. 1997 Global measures of local convective instabilities. *Physical Review Letters* **78** (23), 4387.

Cossu, C., Pujals, G. & Depardon, S. 2009 Optimal transient growth and very large–scale structures in turbulent boundary layers. *Journal of Fluid Mechanics* **619**, 79–94.

Darekar, R. M. & Sherwin, S. J. 2001 Flow past a square-section cylinder with a wavy stagnation face. *Journal of Fluid Mechanics* **426**, 263–295.

Del Guercio, G., Cossu, C. & Pujals, G. 2014*a* Optimal perturbations of non-parallel wakes and their stabilizing effect on the global instability. *Physics of Fluids (1994-present)* **26** (2), 024110.

Del Guercio, G., Cossu, C. & Pujals, G. 2014*b* Optimal streaks in the circular cylinder wake and suppression of the global instability. *Journal of Fluid Mechanics* **752**, 572–588.

Del Guercio, G., Cossu, C. & Pujals, G. 2014*c* Stabilizing effect of optimally amplified streaks in parallel wakes. *Journal of Fluid Mechanics* **739**, 37–56.

Delbende, I., Chomaz, J. & Huerre, P. 1998 Absolute/convective instabilities in the Batchelor vortex: a numerical study of the linear impulse response. *Journal of Fluid Mechanics* **355**, 229–254.

Delbende, I. & Chomaz, J.-M. 1998 Nonlinear convective/absolute instabilities in parallel two-dimensional wakes. *Physics of Fluids (1994-present)* **10** (11), 2724–2736.

Dennis, S. & Chang, G.-Z. 1970 Numerical solutions for steady flow past a circular cylinder at Reynolds numbers up to 100. *Journal of Fluid Mechanics* **42** (03), 471–489.

Drazin, P. & Reid, W. 1981 Hydrodynamic stability. *Cambridge U. Press, Cambridge* .

Duell, E. G. & George, A. 1993 Measurements in the unsteady near wakes of ground vehicle bodies. *Tech. Rep.*. SAE Technical Paper.

Duell, E. G. & George, A. 1999 Experimental study of a ground vehicle body unsteady near wake. *Tech. Rep.*. SAE Technical Paper.

Fabre, D., Auguste, F. & Magnaudet, J. 2008 Bifurcations and symmetry breaking in the wake of axisymmetric bodies. *Physics of Fluids (1994-present)* **20** (5), 051702.

Farrell, B. F. & Ioannou, P. J. 1996 Generalized stability theory. part I: Autonomous operators. *Journal of the atmospheric sciences* **53** (14), 2025–2040.

Fornberg, B. 1980 A numerical study of steady viscous flow past a circular cylinder. *Journal of Fluid Mechanics* **98** (04), 819–855.

Fourrié, G., Keirsbulck, L., Labraga, L. & Gilliéron, P. 2011 Bluff-body drag reduction using a deflector. *Experiments in Fluids* **50** (2), 385–395.

Fransson, J., Brandt, L., Talamelli, A. & Cossu, C. 2004 Experimental and theoretical investigation of the non-modal growth of steady streaks in a flat plate boundary layer. *Physics of Fluids (1994-present)* **16**, 3627–3638.

Fransson, J., Talamelli, A., Brandt, L. & Cossu, C. 2006 Delaying transition to turbulence by a passive mechanism. *Physical Review Letters* **96**, 064501.

Fransson, J. H., Brandt, L., Talamelli, A. & Cossu, C. 2005 Experimental study of the stabilization of Tollmien–Schlichting waves by finite amplitude streaks. *Physics of Fluids (1994-present)* **17** (5), 054110.

Giannetti, F. & Luchini, P. 2007 Structural sensitivity of the first instability of the cylinder wake. *Journal of Fluid Mechanics* **581**, 167–197.

Grandemange, M. 2013 Analysis and control of three-dimensional turbulent wakes. Phd thesis, ENSTA Paris, Paris, France.

Grandemange, M., Gohlke, M. & Cadot, O. 2013 Turbulent wake past a three-dimensional blunt body. Part 1: Global modes and bi-stability. *Journal of Fluid Mechanics* **722**, 51–84.

Gustavsson, L. H. 1991 Energy growth of three-dimensional disturbances in plane Poiseuille flow. *Journal of Fluid Mechanics* **224**, 241–260.

Hamilton, J. M., Kim, J. & Waleffe, F. 1995 Regeneration mechanisms of near-wall turbulence structures. *Journal of Fluid Mechanics* **287**, 317–348.

Hœpffner, J., Brandt, L. & Henningson, D. S. 2005 Transient growth on boundary layer streaks. *J. Fluid Mech.* **537**, 91–100.

Hollands, M. & Cossu, C. 2009 Adding streamwise streaks in the plane Poiseuille flow. *Comptes Rendus Mécanique* **337** (3), 179–183.

Hucho, W.-H. 1987 Aerodynamics of road vehicles .

Huerre, P. & Monkewitz, P. A. 1990 Local and global instabilities in spatially developing flows. *Annual Review of Fluid Mechanics* **22** (1), 473–537.

Hwang, Y. & Choi, H. 2006 Control of absolute instability by basic-flow modification in a parallel wake at low Reynolds number. *Journal of Fluid Mechanics* **560**, 465–475.

Hwang, Y., Kim, J. & Choi, H. 2013 Stabilization of absolute instability in spanwise wavy two-dimensional wakes. *Journal of Fluid Mechanics* **727**, 346–378.

Issa, R. I. 1986 Solution of the implicitly discretised fluid flow equations by operator-splitting. *Journal of computational physics* **62** (1), 40–65.

Khalighi, B., Chen, K.-H. & Iaccarino, G. 2012 Unsteady aerodynamic flow investigation around a simplified square-back road vehicle with drag reduction devices. *Journal of Fluids Engineering* **134** (6), 061101.

Khalighi, B., Zhang, S., Koromilas, C., Balkanyi, S., Bernal, L. P., Iaccarino, G. & Moin, P. 2001 Experimental and computational study of unsteady wake flow behind a bluff body with a drag reduction device. *Tech. Rep.*. SAE Technical Paper.

Kim, J. & Choi, H. 2005 Distributed forcing of flow over a circular cylinder. *Physics of Fluids (1994-present)* **17** (3), 033103.

Kiya, M. & Abe, Y. 1999 Turbulent elliptic wakes. *Journal of fluids and structures* **13** (7), 1041–1067.

Landahl, M. T. 1980 A note on an algebraic instability of inviscid parallel shear flows. *J. Fluid Mech.* **98**, 243–251.

Landau, L. & Lifshitz, E. 1959 Fluid mechanicspergamon. *New York* **61**.

Lauga, E. & Cossu, C. 2005 A note on the stability of slip channel flows. *Physics of Fluids (1994-present)* **17** (8), 088106.

Leu, T.-S. & Ho, C.-M. 2000 Control of global instability in a non-parallel near wake. *Journal of Fluid Mechanics* **404**, 345–378.

Lifshitz, E. M. & Pitaevskii, L. P. 1981 *Physical kinetics*. Butterworth Heinemann.

Luchini, P. 2000 Reynolds-number-independent instability of the boundary layer over a flat surface: optimal perturbations. *Journal of Fluid Mechanics* **404**, 289–309.

Matsubara, M. & Alfredsson, P. H. 2001 Disturbance growth in boundary layers subjected to free-stream turbulence. *Journal of fluid mechanics* **430**, 149–168.

Monkewitz, P. & Nguyen, L. 1987 Absolute instability in the near-wake of two-dimensional bluff bodies. *Journal of fluids and structures* **1** (2), 165–184.

Monkewitz, P. A. 1988 The absolute and convective nature of instability in two-dimensional wakes at low Reynolds numbers. *Physics of Fluids (1958-1988)* **31** (5), 999–1006.

Monkewitz, P. A., Huerre, P. & Chomaz, J.-M. 1993 Global linear stability analysis of weakly non-parallel shear flows. *Journal of Fluid Mechanics* **251**, 1–20.

Noto, K., Ishida, H. & Matsumoto, R. 1985 A breakdown of the karman vortex street due to the natural convection. *Flow Visualization* **3**, 348.

Owen, J. C., Bearman, P. W. & Szewczyk, A. A. 2001 Passive control of viv with drag reduction. *Journal of Fluids and Structures* **15** (3), 597–605.

Parezanović, V. & Cadot, O. 2009*a* The impact of a local perturbation on global properties of a turbulent wake. *Physics of Fluids (1994-present)* **21** (7), 071701.

Parezanović, V. & Cadot, O. 2009*b* Modulated global mode of a controlled wake. In *Advances in Turbulence XII*, pp. 217–220. Springer.

Parezanović, V. & Cadot, O. 2012 Experimental sensitivity analysis of the global properties of a two-dimensional turbulent wake. *Journal of Fluid Mechanics* **693**, 115–149.

Park, H., Jeon, W.-P., Choi, H. & Yoo, J. Y. 2007 Mixing enhancement behind a backward-facing step using tabs. *Physics of Fluids (1994-present)* **19** (10), 105103.

Park, H., Lee, D., Jeon, W.-P., Hahn, S., Kim, J., Kim, J., Choi, J. & Choi, H. 2006 Drag reduction in flow over a two-dimensional bluff body with a blunt trailing edge using a new passive device. *Journal of Fluid Mechanics* **563**, 389–414.

Park, J., Hwang, Y. & Cossu, C. 2011 On the stability of large-scale streaks in turbulent Couette and Poiseuille flows. *Comptes Rendus Mécanique* **339** (1), 1–5.

Pier, B. 2008 Local and global instabilities in the wake of a sphere. *Journal of Fluid Mechanics* **603**, 39–61.

Pier, B. & Huerre, P. 2001 Nonlinear self-sustained structures and fronts in spatially developing wake flows. *Journal of Fluid Mechanics* **435**, 145–174.

Pradeep, D. & Hussain, F. 2006 Transient growth of perturbations in a vortex column. *Journal of Fluid Mechanics* **550**, 251–288.

Provansal, M., Mathis, C. & Boyer, L. 1987 Bénard-von Kármán instability: transient and forced regimes. *Journal of Fluid Mechanics* **182**, 1–22.

Pujals, G. 2010 Perturbations optimales dans les écoulements de paroi turbulents et application au controle de décollement. Phd thesis, Ecole Polytechnique, Paris, France.

Pujals, G., Cossu, C. & Depardon, S. 2010*a* Forcing large-scale coherent streaks in a zero-pressure-gradient turbulent boundary layer. *Journal of Turbulence* (11).

Pujals, G., Depardon, S. & Cossu, C. 2010*b* Drag reduction of a 3d bluff body using coherent streamwise streaks. *Experiments in Fluids* **49** (5), 1085–1094.

Pujals, G., García-Villalba, M., Cossu, C. & Depardon, S. 2009 A note on optimal transient growth in turbulent channel flows. *Physics of Fluids (1994-present)* **21** (1), 015109.

Reddy, S. C. & Henningson, D. S. 1993 Energy growth in viscous channel flows. *Journal of Fluid Mechanics* **252**, 209–238.

Reddy, S. C., Schmid, P. J., Baggett, J. S. & Henningson, D. S. 1998 On stability of streamwise streaks and transition thresholds in plane channel flows. *Journal of Fluid Mechanics* **365**, 269–303.

Rouméas, M., Gilliéron, P. & Kourta, A. 2009 Analysis and control of the near-wake flow over a square-back geometry. *Computers & Fluids* **38** (1), 60–70.

Ruiz, T., Sicot, C., Brizzi, L. E., Laumonier, J., Borée, J. & Gervais, Y. 2009 Unsteady near wake of a flat disk normal to a wall. *Experiments in Fluids* **47** (4-5), 637–653.

Ryan, K., Thompson, M., Hourigan, K. *et al.* 2005 Three-dimensional transition in the wake of bluff elongated cylinders. *Journal of Fluid Mechanics* **538**, 1–29.

Sakamoto, H. & Haniu, H. 1990 A study on vortex shedding from spheres in a uniform flow. *Journal of Fluids Engineering* **112** (4), 386–392.

Sakamoto, H., Tan, K. & Haniu, H. 1991 An optimum suppression of fluid forces by controlling a shear layer separated from a square prism. *Journal of fluids engineering* **113** (2), 183–189.

Schmid, P. J. 2007 Nonmodal stability theory. *Annual Review of Fluid Mechanics* **39**, 129–162.

Schmid, P. J. & Henningson, D. S. 2001 *Stability and transition in shear flows*, , vol. 142. Springer.

Schoppa, W. & Hussain, F. 2002 Coherent structure generation in near-wall turbulence. *Journal of Fluid Mechanics* **453**, 57–108.

Schumm, M., Berger, E. & Monkewitz, P. A. 1994 Self-excited oscillations in the wake of two-dimensional bluff bodies and their control. *Journal of Fluid Mechanics* **271**, 17–53.

Sevilla, A. & Martinez-Bazan, C. 2004 Vortex shedding in high Reynolds number axisymmetric bluff-body wakes: local linear instability and global bleed control. *Physics of Fluids (1994-present)* **16** (9), 3460–3469.

Sreenivasan, K., Strykowski, P. & Olinger, D. 1987 Hopf bifurcation, Landau equation, and vortex shedding behind circular cylinders. In *Forum on unsteady flow separation*, , vol. 1, pp. 1–13.

Strykowski, P. & Sreenivasan, K. 1990 On the formation and suppression of vortex shedding at low Reynolds numbers. *Journal of Fluid Mechanics* **218**, 71–107.

Taneda, S. 1978 Visual observations of the flow past a sphere at Reynolds numbers between 104 and 106. *Journal of Fluid Mechanics* **85** (01), 187–192.

Tanner, M. 1975 Reduction of base drag. *Progress in Aerospace Sciences* **16** (4), 369–384.

Theofilis, V. 2011 Global linear instability. *Annual Review of Fluid Mechanics* **43**, 319–352.

Tombazis, N. & Bearman, P. 1997 A study of three-dimensional aspects of vortex shedding from a bluff body with a mild geometric disturbance. *Journal of Fluid Mechanics* **330**, 85–112.

Trefethen, L., Trefethen, A., Reddy, S., Driscoll, T. *et al.* 1993 Hydrodynamic stability without eigenvalues. *Science* **261** (5121), 578–584.

Triantafyllou, G. S., Kupfer, K. & Bers, A. 1987 Absolute instabilities and self-sustained oscillations in the wake of circular cylinders. *Physical Review Letters* **59** (17), 1914.

Van Dyke, M. 1982 An album of fluid motion .

Verzicco, R., Fatica, M., Iaccarino, G., Moin, P. & Khalighi, B. 2002 Large eddy simulation of a road vehicle with drag-reduction devices. *AIAA journal* **40** (12), 2447–2455.

Waleffe, F. 1995 Hydrodynamic stability and turbulence: beyond transients to a self-sustaining process. *Studies in Applied Mathematics* **95** (3), 319–343.

Wassen, E., Eichinger, S. & Thiele, F. 2010 Simulation of active drag reduction for a square-back vehicle. In *Active Flow Control II*, pp. 241–255. Springer.

Weickgenannt, A. & Monkewitz, P. A. 2000 Control of vortex shedding in an axisymmetric bluff body wake. *European Journal of Mechanics-B/Fluids* **19** (5), 789–812.

White, E. B. 2002 Transient growth of stationary disturbances in a flat plate boundary layer. *Physics of Fluids (1994-present)* **14** (12), 4429–4439.

Williamson, C. H. 1996 Vortex dynamics in the cylinder wake. *Annual review of fluid mechanics* **28** (1), 477–539.

Willis, A. P., Hwang, Y. & Cossu, C. 2010 Optimally amplified large-scale streaks and drag reduction in turbulent pipe flow. *Physical Review E* **82** (3), 036321.

Wood, C. 1967 Visualization of an incompressible wake with base bleed. *Journal of Fluid Mechanics* **29** (02), 259–272.

Yamouni, S., Sipp, D. & Jacquin, L. 2013 Interaction between feedback aeroacoustic and acoustic resonance mechanisms in a cavity flow: a global stability analysis. *Journal of Fluid Mechanics* **717**, 134–165.

Yasuo, M., Kunio, H. & Takayoshi, N. 1986 A fundamental study of symmetrical vortex generation behind a cylinder by wake heating or by splitter plate or mesh. *International Journal of Heat and Mass Transfer* **29** (8), 1193–1201.

Zdravkovich, M. 1981 Review and classification of various aerodynamic and hydrodynamic means for suppressing vortex shedding. *Journal of Wind Engineering and Industrial Aerodynamics* **7** (2), 145–189.

Articles

1

Article 1

Published in Journal of Fluid Mechanics ***739*** *pp37-56, 2014*

J. Fluid Mech. (2014), *vol.* 739, *pp.* 37–56. © Cambridge University Press 2013
doi:10.1017/jfm.2013.619

Stabilizing effect of optimally amplified streaks in parallel wakes

Gerardo Del Guercio[1,2], Carlo Cossu[1,†] and Gregory Pujals[2]

[1]CNRS – Institut de Mécanique des Fluides de Toulouse (IMFT), Allée du Professeur Camille Soula, F-31400 Toulouse, France

[2]PSA Peugeot Citroën, Centre Technique de Velizy, 2 Route de Gisy, 78943 Vélizy-Villacoublay CEDEX, France

(Received 9 July 2013; revised 9 October 2013; accepted 14 November 2013; first published online 13 December 2013)

We show that optimal perturbations artificially forced in parallel wakes can be used to completely suppress the absolute instability and to reduce the maximum temporal growth rate of the inflectional instability. To this end we compute optimal transient energy growths of stable streamwise uniform perturbations supported by a parallel wake for a set of Reynolds numbers and spanwise wavenumbers. The maximum growth rates are shown to be proportional to the square of the Reynolds number and to increase with spanwise wavelengths with sinuous perturbations slightly more amplified than varicose ones. Optimal initial conditions consist of streamwise vortices and the optimally amplified perturbations are streamwise streaks. Families of nonlinear streaky wakes are then computed by direct numerical simulation using optimal initial vortices of increasing amplitude as initial conditions. The stabilizing effect of nonlinear streaks on temporal and spatiotemporal growth rates is then determined by analysing the linear impulse response supported by the maximum amplitude streaky wakes profiles. This analysis reveals that at $Re = 50$, streaks of spanwise amplitude $A_s \approx 8\,\%U_\infty$ can completely suppress the absolute instability, converting it into a convective instability. The sensitivity of the absolute and maximum temporal growth rates to streak amplitudes is found to be quadratic, as has been recently predicted. As the sensitivity to two-dimensional (2D, spanwise uniform) perturbations is linear, three-dimensional (3D) perturbations become more effective than the 2D ones only at finite amplitudes. Concerning the investigated cases, 3D perturbations become more effective than the 2D ones for streak amplitudes $A_s \gtrsim 3\,\%U_\infty$ in reducing the maximum temporal amplification and $A_s \gtrsim 12\,\%U_\infty$ in reducing the absolute growth rate. However, due to the large optimal energy growths they experience, 3D optimal perturbations are found to be much more efficient than 2D perturbations in terms of initial perturbation amplitudes. Despite their lower maximum transient amplification, varicose streaks are found to be always more effective than sinuous ones in stabilizing the wakes, in accordance with previous findings.

Key words: absolute/convective instability, flow control, wakes/jets

† Email address for correspondence: carlo.cossu@imft.fr

1. Introduction

Vortex shedding in the wake of bluff bodies is a robust feature associated with undesirable unsteady loads and mean drag increase on the body. An important, enduring research effort aims at understanding the mechanisms by which the shedding self-sustains and how it could be attenuated or even suppressed. In the circular cylinder wake, the canonical flow used to test theories and control concepts, the shedding sets in at a critical Reynolds number ($\approx$47) via a global instability. Self-sustained oscillations associated with global instability are supported by a finite region of local absolute instability near the body (see e.g. Chomaz, Huerre & Redekopp 1988; Huerre & Monkewitz 1990).

Different techniques have been proposed to suppress vortex shedding in two-dimensional wakes, among which an effective one is based on three-dimensional (3D) wake perturbations. Indeed, it has long been known that wrapping a helical cable around a cylinder (e.g. Zdravkovich 1981) or designing spanwise periodic trailing or leading edges of blunt bodies (starting with Tanner 1972, and followed by many others) can attenuate two-dimensional (2D) vortex shedding with a beneficial effect on mean drag and unsteady force peak fluctuations. We refer the reader to the review by Choi, Jeon & Kim (2008) for a clear discussion of these previous results and the associated references.

At low Reynolds numbers, 3D forcing can lead to the complete suppression of vortex shedding when spanwise wavelengths of the 3D perturbations are in the range of $\approx$1–6 diameters. In addition, 3D perturbations are found to require smaller perturbation amplitudes than spanwise uniform (2D) perturbations (Kim & Choi 2005). The nature and characteristics of the observed stabilizing effects have been mainly interpreted in terms of vorticity dynamics. Hwang, Kim & Choi (2013) (but see also Choi *et al.* 2008) have put forward an appealing explanation based on linear stability analysis. These authors convincingly show that spanwise modulations of parallel wake profiles lead to an attenuation of the absolute instability growth rate in a range of perturbation wavelengths than is in accordance with experimental and direct numerical simulation (DNS) findings. They also show that varicose perturbations are more effective than sinuous ones, in accordance with previous results of Kim *et al.* (2004), Kim & Choi (2005) and Park *et al.* (2006), and that for the amplitudes they consider, the absolute instability is far more sensitive to 2D than to 3D perturbations. However, from their study, it is not clear whether absolute instability can be completely suppressed and what is the effect of wake modulations on the maximum temporal growth rate of the instability, which affects the mode amplification in the convective region. Furthermore, in this previous analysis, a shape assumption is made on the 3D basic flow modification that neglects the nonlinear deformations appearing at moderate perturbation amplitudes.

A related problem, with a similar mathematical structure but quite different physical mechanisms involved, is that of stabilization of 2D boundary layers. In particular, Cossu & Brandt (2002, 2004) found that optimal 3D spanwise modulations (streamwise streaks) of the 2D Blasius boundary layer developing on a flat plate have a stabilizing effect on the 2D Tollmien–Schlichting instability, which develops above the critical Reynolds number. The optimal 3D perturbations used to control the boundary layer are those leading to the maximum energy growth in the linear approximation. Optimal spanwise periodic counter-rotating streamwise vortices are used to induce the transient growth of spanwise periodic streamwise streaks associated with spanwise modulations of the streamwise velocity profile. The optimal energy growth in this process is of $O(Re^2)$ (see e.g. Gustavsson 1991). The linearly

optimal vortices were then used, with finite amplitude, as input in fully nonlinear Navier–Stokes simulations to compute nonlinearly saturated streaks. The 2D (spanwise averaged) modification of the boundary layer profile induced by the 3D streaks plays a crucial role in the stabilization (Cossu & Brandt 2002). This 2D modification is not captured by simply adding linear streaks to the boundary layer profile. It was also found that a key stabilizing role is played by the work of Reynolds shear stresses against the spanwise basic flow shear Cossu & Brandt (2004). The stabilizing action of streaks on TS waves and the effective delay of transition to turbulence using this technique was later confirmed experimentally (Fransson *et al.* 2005, 2006).

Inspired by the type of analysis developed for boundary layers, one may therefore wonder if similar conclusions can be reached in plane 2D wakes. Some natural questions that arise are as follows. Can large transient energy growths of spanwise periodic perturbations be supported by 2D wakes? If yes, how does the maximum energy growth scale with the Reynolds number? Do nonlinearly saturated streamwise streaks have a stabilizing effect on the wake inflectional instability? If yes, what level of growth rate reductions can be attained? Do nonlinearly saturated optimal streamwise streaks have a stabilizing effect on the wake absolute instability? How would these effects relate to those described by Hwang *et al.* (2013)? Is it possible to completely suppress the absolute instability? Does the nonlinear spanwise mean (2D) flow distortion play an important role in the stabilizing mechanism? How is the stabilizing effect related to the work of Reynolds stresses? The scope of the present investigation is to try to answer these questions.

The analysis will be developed on parallel wake profiles proposed by Monkewitz (1988), which have been used as a laboratory for stability analyses of plane wakes in a number of previous studies, such as those of Delbende & Chomaz (1998), Hwang & Choi (2006) and Hwang *et al.* (2013). The advantage of this approach is that the results are genuinely related to the wake structure, and not to the specific generating body's surface shape and physics.

After a brief description of the problem setup, given in § 2, the optimal energy growths, inputs and outputs supported by the considered wake profiles are computed and discussed in § 3. The temporal and spatiotemporal stability of nonlinear streak profiles issued by linear optimal initial conditions is analysed in § 4. A summary and discussion of the main results are reported in § 5. Details of the method used in the computation of optimal energy growths, in the direct numerical simulations and in the extraction of the temporal and spatiotemporal stability results from the numerical simulation of the impulse response are given in the Appendix.

2. Mathematical model

In the following, essentially two kinds of basic flows will be considered. The first type is the usual (spanwise uniform i.e. 2D) parallel wake $\boldsymbol{U}_M = \{U_M(y), 0, 0\}$, where the streamwise velocity profile $U_M(y)$ is the one proposed by Monkewitz (1988):

$$U_M(y) = 1 + \Lambda \left[\frac{2}{1 + \sinh^{2N}(y \sinh^{-1} 1)} - 1 \right], \tag{2.1}$$

with $\Lambda = (U_c^* - U_\infty^*)/(U_\infty^* + U_c^*)$, U_c^* the centreline and U_∞^* the free stream velocity (dimensional variables are starred). The velocity profile U_M is made dimensionless with respect to the reference velocity $U_{ref}^* = (U_c^* + U_\infty^*)/2$. The spatial coordinates are made dimensionless with respect to the reference length δ^*, which is the distance from the centreline to the point where the 2D wake velocity is equal to U_{ref}^*. In the

following we consider the value $\Lambda = -1$, corresponding to a zero centreline velocity, which has been used by Delbende & Chomaz (1998) and Hwang *et al.* (2013), for example, and the shear concentration parameter value $N = 1$, which corresponds to the same shear profile as the Bickley jet. The $U_M(y)$ profile obtained with these parameters is shown in figure 3(*a*).

In addition to the standard 2D wakes, the stability of spanwise modulated 3D 'streaky wakes' $\boldsymbol{U} = \{U(y, z), 0, 0\}$ will be considered in the following (where we let x denote the streamwise direction, y the transverse and z the spanwise one). For both types of wake profiles, the evolution of perturbations $\boldsymbol{u}', p'$ to the basic flow wake $\boldsymbol{U}, P$ is ruled by the Navier–Stokes equations, written in perturbation form as

$$\boldsymbol{\nabla} \cdot \boldsymbol{u}' = 0, \tag{2.2}$$

$$\frac{\partial \boldsymbol{u}'}{\partial t} + (\boldsymbol{\nabla U})\boldsymbol{u}' + (\boldsymbol{\nabla u}')\boldsymbol{U} + (\boldsymbol{\nabla u}')\boldsymbol{u}' = -\boldsymbol{\nabla} p' + \frac{1}{Re}\nabla^2 \boldsymbol{u}'. \tag{2.3}$$

The flow is assumed incompressible and the fluid viscous with kinematic viscosity ν. The Reynolds number $Re = U^*_{ref}\delta^*/\nu$ is based on the characteristic velocity and length scale of the basic flow which are used to make dimensionless velocities and lengths. In the linearized stability framework the term $(\boldsymbol{\nabla u}')\boldsymbol{u}'$ is neglected.

3. Optimal perturbations of 2D wakes

The first step of our analysis consists in finding the optimal initial perturbations leading to the maximum amplification of the kinetic energy of the response at time t. For parallel basic flows the optimal growths of Fourier modes $\widehat{\boldsymbol{u}}(\alpha, y, \beta, t)\mathrm{e}^{\mathrm{i}(\alpha x+\beta z)}$ of streamwise and spanwise wavenumbers α and β can be considered separately. The optimal temporal energy amplification G is defined, in the usual way, as the ratio of the kinetic energy density associated with $\widehat{\boldsymbol{u}}$ at time t to the kinetic energy of the initial condition $\widehat{\boldsymbol{u}}_0$ optimized over non-zero $\widehat{\boldsymbol{u}}_0$, $G(\alpha, \beta, t) = \sup_{\widehat{\boldsymbol{u}}_0} \|\widehat{\boldsymbol{u}}\|^2/\|\widehat{\boldsymbol{u}}_0\|^2$, where $\|\widehat{\boldsymbol{u}}\|^2 = (1/\mathscr{V}_{ref}) \int_{\mathscr{V}} |\widehat{\boldsymbol{u}}|^2 \, d\mathscr{V}$ and $\mathscr{V}_{ref} = 2\delta L_x L_z$ in the present case. Two-dimensional parallel wakes, like the one defined in (2.1), are unstable to inflectional instabilities if Re is not too small. For the values $Re \gtrsim 25$ considered in this study, an unstable region exists in the (α, β) plane centred around the 2D ($\beta = 0$) unstable waveband $0 < \alpha \lesssim 1.75$. In this study we are not interested in the optimal amplification of unstable perturbations but in their stabilization by optimally amplified stable disturbances. We will therefore consider the optimal growth of streamwise uniform ($\alpha = 0$) perturbations, both because they mimic the perturbations that would be spatially forced by steady passive devices and because they are linearly stable.

As the U_M profile is symmetric with respect to $y = 0$, perturbations to this profile are separated into varicose perturbations, for which $\widehat{u}(-y) = \widehat{u}(y)$, $\widehat{v}(-y) = -\widehat{v}(y)$, $\widehat{w}(-y) = \widehat{w}(y)$, and sinuous perturbations that have opposite symmetry properties. Standard methods, described in § A.1, have been used to compute $G(t)$ for both varicose and sinuous perturbations for $Re = 25, 50$ and 100 and for spanwise wavenumbers β ranging from 0.1 to 2 with $\alpha = 0$. For all these parameters the computed $G(t)$ curves typically have a single maximum $G_{max}(\alpha = 0, \beta, Re) = \sup_t G(t, \alpha = 0, \beta, Re)$, attained at t_{max}, and tend to zero for large times. The maximum optimal growths G_{max} computed for sinuous perturbations are reported in figure 1(*a*) as a function of β for the selected Reynolds numbers. From this figure it is seen how G_{max} increases with Re. From the analysis of Gustavsson (1991) it is expected that for streamwise uniform perturbations G_{max} and t_{max} are proportional to Re^2 and Re respectively. This is indeed verified for both G_{max} (see figure 1*b*) and t_{max} (not shown).

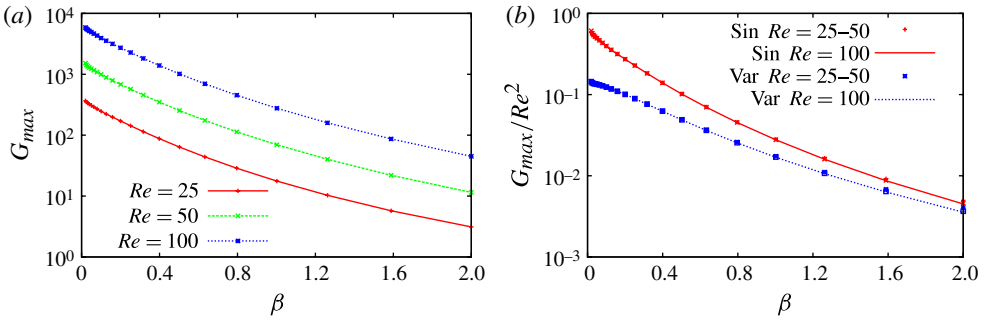

FIGURE 1. (Colour online) (*a*) Dependence of the maximum growth rate G_{max} of streamwise uniform ($\alpha = 0$) sinuous perturbations on the spanwise wavenumber β for three selected Reynolds numbers Re. (*b*) Rescaled maximum growth rate G_{max}/Re^2 dependence on β for sinuous (solid line, red) and varicose (dashed line, blue) perturbations. The lines correspond to the rescaled $Re = 100$ data, while the $Re = 25$ and $Re = 50$ rescaled data are shown as points. It can be seen how, when rescaled, data obtained at different Re collapse onto the same curve.

The maximum growths G_{max} and the associated t_{max} are also seen to increase with the perturbation spanwise wavelength $\lambda_z = 2\pi/\beta$, at least in the λ_z range examined. Varicose perturbations follow the same trend as sinuous ones, with the same Re scaling and a similar increase with λ_z of G_{max}, but are slightly less amplified than sinuous perturbations, as shown in figure 1(*b*).

Similar to what has been found in wall-bounded shear flows, optimal initial conditions correspond to spanwise periodic streamwise vortices while the most amplified perturbations correspond to spanwise periodic streamwise streaks. Optimal perturbations computed for $Re = 50$ and $\beta = 1$ are reported in figure 2. In the case of varicose perturbations (figure 2*a*), there are two antisymmetric rows of vortices on each side of the wake symmetry axis inducing symmetric streaks, while in the case of sinuous perturbations (figure 2*b*), a single row of vortices centred on the wake symmetry axis induces antisymmetric streaks. When the spanwise wavenumber β is decreased (the spanwise wavelength $\lambda_z = 2\pi/\beta$ is increased), the size of optimal perturbations increases in both the spanwise and the normal direction y, as shown in figure 3. The velocity of optimal varicose initial vortices is, non-negligible up to $y \approx \lambda_z$, which highlights the difficulty of forcing optimal perturbations with low values of β in practical applications such as those based on the body's leading and trailing edge deformation (Bearman & Owen 1998; Darekar & Sherwin 2001, e.g.) or on blowing and suction (Kim & Choi 2005).

4. Influence of streaks on wake stability

4.1. *Basic flow streaky wakes*

Nonlinear streaky wakes are computed following the same rationale used in previous studies of the stability of streaks in wall-bounded flows, such as those of Reddy *et al.* (1998), Andersson *et al.* (2001), Brandt *et al.* (2003), Cossu & Brandt (2004) and Park, Hwang & Cossu (2011). Optimal linear perturbations (streamwise vortices) with finite initial amplitude A_0 are used as initial condition $\boldsymbol{U}_{I0}(y, z) = \boldsymbol{U}_M(y) + A_0\boldsymbol{u}_I^{(opt)}(y, z)$, where $\|\boldsymbol{u}_I^{(opt)}\| = 1$. The nonlinear Navier–Stokes equations are then numerically integrated for the selected initial conditions (see § A.2 for numerical details), providing

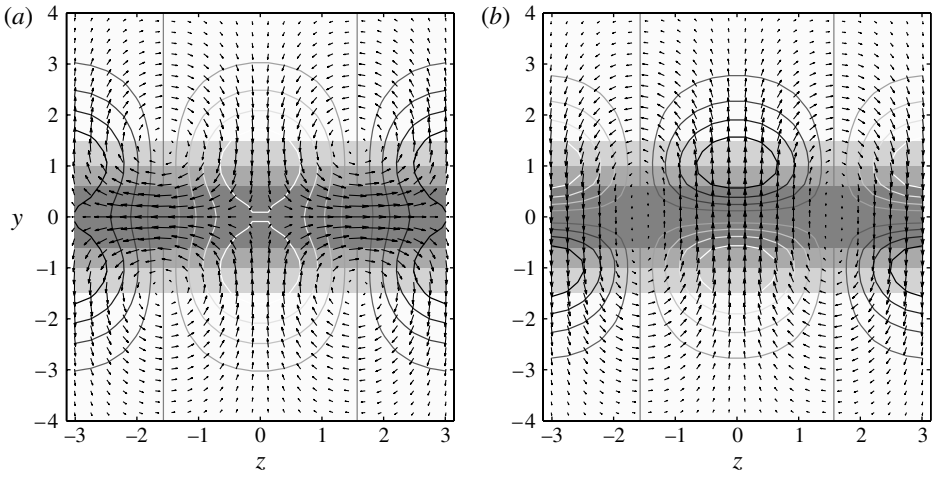

FIGURE 2. Cross-stream view of the v'–w' components of optimal initial vortices (arrows) and of the u' component of the corresponding maximally amplified streak (contour lines) for $Re = 50$ and $\beta = 1, \alpha = 0$. Optimal varicose perturbations are reported in (a), while sinuous ones are reported in (b). The 2D basic flow wake streamwise velocity is shown in grey-scale, with white corresponding to the free stream velocity and dark grey to zero (wake centreline).

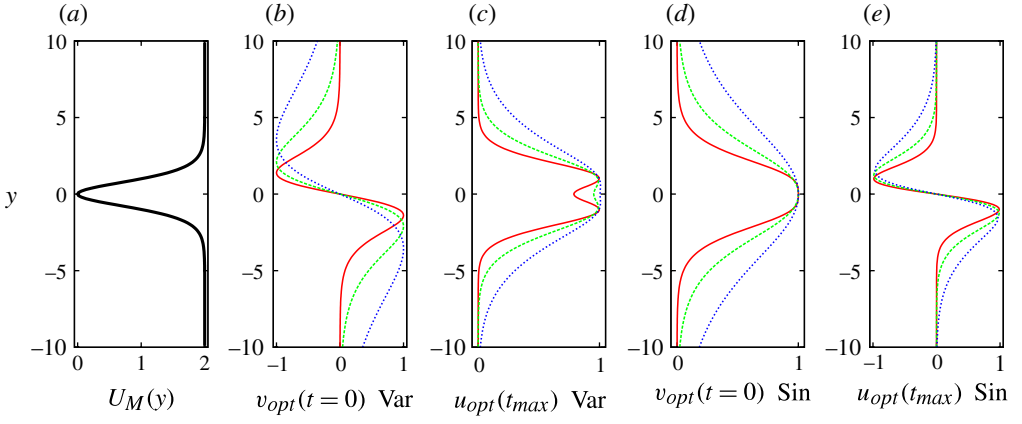

FIGURE 3. (Colour online) Normalized amplitude of the $\widehat{v}(y)$ component of the optimal initial ($t = 0$) vortices (b,d) and the $\widehat{u}(y)$ component of the corresponding optimally amplified ($t = t_{max}$) streaks (c,e), corresponding to the varicose (b,c) and sinuous (d,e) perturbations, for $\beta = 1$. i.e. $\lambda_z = 6.28$ (solid, red). $\beta = 0.5$. i.e. $\lambda_z = 12.56$ (dashed, green). and $\beta = 0.25$. i.e. $\lambda_z = 25.13$ (dotted, blue). The 2D wake basic flow profile $U_M(y)$ is also reported in (a) for comparison.

a family of basic flows $\boldsymbol{U}_I(y, z, t, A_0)$, parametrized by A_0 for the Reynolds number considered. The amplitude of the streaks is measured, extending the definition proposed by Andersson *et al.* (2001):

$$A_s(t, A_0) = \frac{1}{2} \frac{\max_{y,z}(U_I(y, z, t, A_0) - U_M(y)) - \min_{y,z}(U_I(y, z, t, A_0) - U_M(y))}{\max_y U_M(y) - \min_y U_M(y)}. \quad (4.1)$$

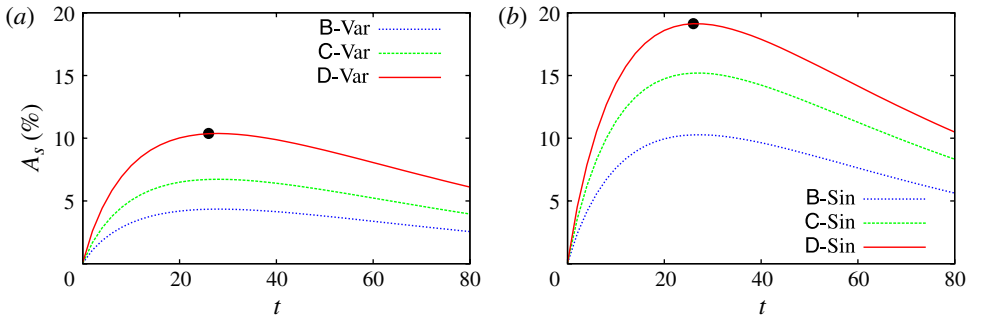

FIGURE 4. (Colour online) Temporal evolution of nonlinear streak amplitude $A_s(t)$ for selected initial amplitudes A_0 of the initial optimal perturbations and for varicose (a) and sinuous (b) perturbations. For all cases, $Re = 50$ and $\beta = 1$. See table 1 for the legend of cases and the associated initial amplitudes A_0.

Case	A	B-Var	C-Var	D-Var	B-Sin	C-Sin	D-Sin
A_0	0	1.25×10^{-2}	1.94×10^{-2}	3.00×10^{-2}	2.00×10^{-2}	2.93×10^{-2}	3.66×10^{-2}
$A_{s,max}$	0	4.35 %	6.73 %	10.38 %	10.27 %	15.02 %	18.80 %

TABLE 1. The nonlinear streaky wakes considered. A_0 is the finite initial amplitude given to the linear optimal perturbations. $A_{s,max}$ is the maximum streak amplitude reached in the nonlinear numerical simulation. Case A corresponds to the reference two-dimensional wake profile $U_M(y)$. Cases B, C and D are obtained by increasing A_0.

In figure 4 we display the temporal evolution of the amplitudes of nonlinear streaks for $Re = 50$ and $\beta = 1$, for varicose and sinuous perturbations of selected amplitudes. As reported in table 1, case A corresponds to the reference two-dimensional wake profile $U_M(y)$ (no streaks), while cases B, C and D are obtained by increasing the initial optimal perturbation amplitude A_0.

In the following we will analyse the local spatiotemporal instability properties of the streaky wake profiles 'frozen' at the time of maximum streak amplitude, following the approach used by Reddy *et al.* (1998), Andersson *et al.* (2001), Brandt *et al.* (2003), Cossu & Brandt (2004) and Park *et al.* (2011), among others. The local analysis is justified by the fact that streaks decay slowly (for example, the varicose D streak changes its amplitude by $\approx 4\,\%$ in $\Delta t \approx 50$) when compared to the fast growth of unstable perturbations (typical maximum growth rates are of the order of $1/4$, and therefore during $\Delta t \approx 50$ they would have been amplified by a factor of $e^{50/4} \approx 270\,000$). The streaky basic flows corresponding to the varicose and sinuous case D are reported in figure 5.

4.2. *Stability analysis based on linear impulse response*

The linear stability properties of streaky wake profiles, including the convective or absolute nature of any instability, are revealed by the analysis of the linear impulse response (Green's function) that they support. The basic flow is linearly stable if the amplitude of impulse response tends to zero as $t \to \infty$ and unstable otherwise. In the unstable case, the instability is absolute if the impulse response amplitude grows in the position of the initial pulse, while it is convective if it grows while being advected

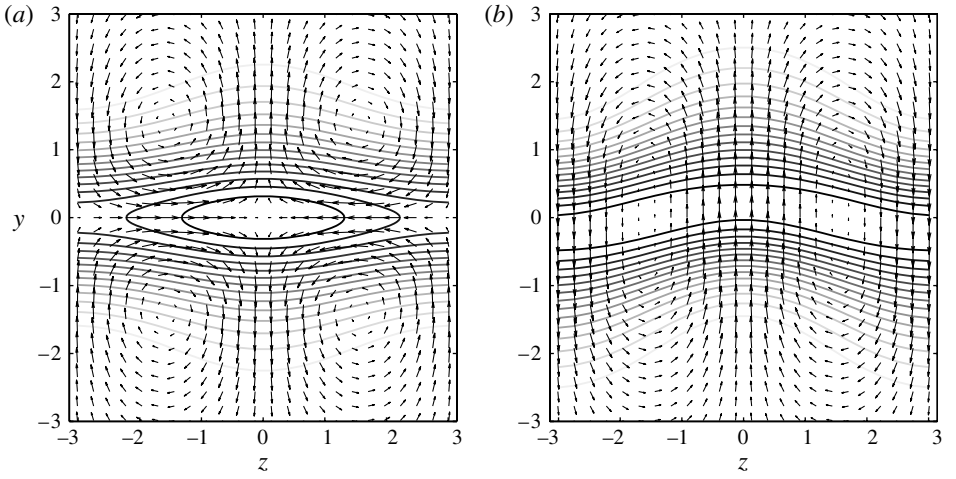

FIGURE 5. Cross-stream view of case D varicose (a) and sinuous (b) nonlinear streaky wake basic flows. Contour lines, iso-levels of the total streamwise velocity $U_I(y, z)$ extracted at the time of maximum amplitude (black circles in figure 4); arrows, v–w components of optimal initial vortices given as initial condition at $t = 0$.

by the flow but eventually tends to zero in the position of the initial pulse (Huerre & Monkewitz 1990).

The linear impulse response is computed by direct numerical simulation of the Navier–Stokes equations linearized near the frozen streaky basic flow profiles $U_I(y, z, t, A_0)$ described in § 4.1. To mimic forcing by a delta function in time and space, the initial condition is defined in terms of a 2D stream function as

$$\psi'(x, y, z) = A_{II} \mathrm{e}^{-((x-x_0)^2/2\sigma_x^2)-((y-y_0)^2/2\sigma_y^2)-((z-z_0)^2/2\sigma_z^2)}, \tag{4.2}$$

which is the three-dimensional extension of the initial condition used by Delbende & Chomaz (1998) for the same type of analysis of 2D wakes. The corresponding perturbation velocity components are given by $(u', v', w') = (\partial\psi/\partial y, -\partial\psi/\partial x, 0)$ and the amplitude A_{II} is set sufficiently small to avoid overflows during the linear simulation. The parameters $\sigma_x = 0.83$, $\sigma_y = 0.83$ and $\sigma_z = 0.30$ have been chosen small enough to reproduce a localized impulse within the limits of a good resolution. The impulse is centred at $x_0 = 62$, $y_0 = 1$, $z_0 = \pi/4$, ensuring that no particular symmetry is preserved by the initial condition.

According to standard Floquet theory (see e.g. Nayfeh & Mook 1979), normal modes of the spanwise periodic basic flow of spanwise wavelength λ_z may be sought in the form

$$q(x, y, z, t) = \tilde{q}(y, z) \mathrm{e}^{\mathrm{i}(\alpha x + \gamma\beta z - \omega t)}, \tag{4.3}$$

where q is the generic flow variable. $\gamma \in [0, 1/2]$ is the detuning parameter and ω is the complex frequency. Hwang *et al.* (2013) found absolute instabilities in spanwise modulated wakes only for fundamental ($\gamma = 0$) and subharmonic ($\gamma = 1/2$) modes. Fundamental modes have the same spanwise periodicity λ_z as the basic flow, while subharmonic modes have periodicity $2\lambda_z$. Both types of mode will be considered together by performing numerical simulations in a spanwise periodic domain of length $L_z = 2\lambda_z$. In this framework, the spanwise z-variable is an eigenfunction direction just

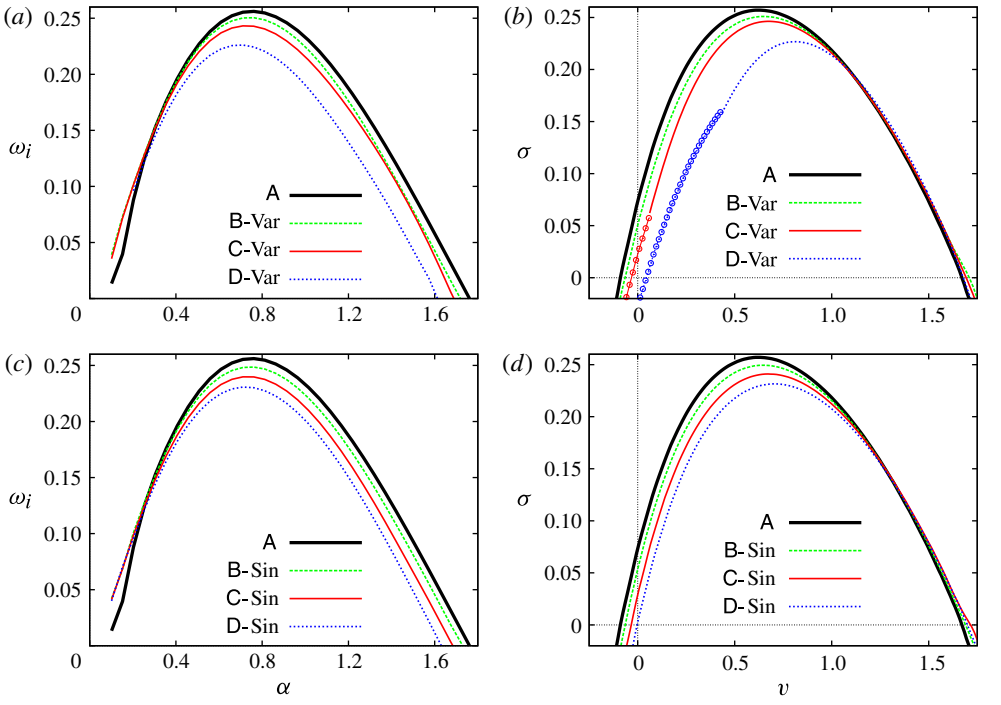

FIGURE 6. (Colour online) Stabilizing effect of varicose (*a*,*b*) and sinuous (*c*,*d*) streaks on temporal (*a*,*c*) and spatiotemporal (*b*,*d*) growth rates of linear perturbations. Case A corresponds to the 2D reference wake while cases B, C and D correspond to increasing streak amplitudes. The basic flow is absolutely unstable if $\sigma(v=0)>0$. The presence of symbols on parts of the stability curves denotes the range where subharmonic modes are dominating.

as the transverse y variable. Note that only one initial pulse is enforced at $t=0$ in the given 'doubled' domain. The growth rates of fundamental and subharmonic, symmetric and antisymmetric modes can be separated using spanwise Fourier transforms. In particular, fundamental modes have harmonics with wavenumbers $\beta_n^{(F)}=n\beta$, while for subharmonic modes $\beta_n^{(S)}=(n+1/2)\beta$ with $n=1,2,\ldots$ and where β is the spanwise wavenumber of the basic flow streaks (fundamental wavenumber). Further details are given in § A.3.

The temporal growth rate curves $\omega_i(\alpha)$ are extracted from the numerically computed impulse response as described in § A.4 and are reported in figure 6. The 2D reference wake, case A, as is well known, is linearly unstable with a maximum growth rate $\omega_{i,max}=0.256$. When streaks of increasing amplitude are forced, the maximum growth rate is reduced. The leading modes have the same symmetries in z as basic flow profiles (fundamental–symmetric in the terminology of § A.3), and varicose streaks are found to be more effective at stabilizing the temporal instability. For instance, $\omega_{i,max}$ is reduced by $\approx$12 % using varicose streaks with $A_s\approx 10\,\%$ (case D-Var) and by 10 % for sinuous streaks with $A_s\approx 18\,\%$ (case D-Sin).

The absolute or convective nature of the instability can be determined from the spatiotemporal growth rate $\sigma(v)$, which is the temporal growth rate observed by an observer travelling along the spatiotemporal ray $x/t=v$. For the considered wake profiles, which are unstable, $\sigma>0$ in the range $v\in[v^-,v^+]$, where v^- and v^+

are respectively the trailing and leading edge velocities of the wave packet. In the present situation, therefore, the instability is absolute for $\sigma(v=0)>0$, i.e. if $v^-<0$. The maximum value of σ corresponds to the maximum temporal growth rate $\omega_{i,max}$. The $\sigma(v)$ curves have been extracted from the numerically computed impulse responses following the standard procedure explained in § A.4, which has already been used by Delbende & Chomaz (1998) and Brandt *et al.* (2003) and Lombardi *et al.* (2011), among others; these are shown in figure 6. The 2D reference wake (case A) is absolutely unstable with an absolute growth rate $\sigma(v=0)=0.073$ and the wave-packet trailing-edge travelling upstream with velocity $v^-=-0.089$. The absolute growth rate is reduced when streaks of increasing amplitude are forced, and can become negative for sufficiently large streak amplitudes transforming the absolute instability into a convective instability. Varicose streaks are found to be more effective at stabilizing the absolute instability than sinuous streaks. The varicose streak D-Var with $A_s\approx 10\,\%$ is already convectively unstable, while amplitudes above $A_s\approx 18\,\%$ (case D-Sin) are necessary for sinuous streaks to drive the instability from absolute to convective. For sinuous streaks, the leading modes in the $\sigma(v)$ curves are fundamental–symmetric (the same symmetries as the basic flow streaks in the spanwise direction). For varicose streaks, fundamental–symmetric modes are the leading ones, except for large-amplitude streaks at sufficiently small values of v, where subharmonic–antisymmetric modes are dominant and therefore control the quenching of the absolute instability.

4.3. *Sensitivity to basic flow modifications and cost of the stabilization*

By an asymptotic (small-amplitude) sensitivity analysis, Hwang & Choi (2006) have shown that the absolute growth rate variation depends linearly on the amplitude of spanwise uniform (2D) perturbations of the basic flow. Hwang *et al.* (2013) show that the sensitivity to spanwise sinusoidal (3D) basic flow perturbations depends quadratically on their amplitudes. To verify whether these predictions extend to the nonlinear streaks considered and to maximum temporal growth rate sensitivity, we report in figure 7 the dependence of the maximum growth rate $\omega_{i,max}$ and of the wave-packet trailing edge velocity v^- on the streak amplitude A_s. We consider v^- and not $\sigma(v=0)$ as a measure of the absolute or convective nature of the instability because the numerical method used (impulse response analysis) does not provide well-converged results for negative growth rates. We also consider the effect on the stability of a 2D (spanwise uniform) perturbation with a profile $u_{2D}(y)$ equal to the high-speed varicose streak profile $\widehat{u}(y)$. The amplitude A_s of this 2D basic flow modification is defined by (4.1), but removing the $1/2$ factor that accounted for the presence of high- and low-speed streaks. From figure 7 it is seen that $\omega_{i,max}$ and v^- do indeed depend quadratically on A_s for streaky basic flow modifications, but linearly for a 2D basic flow modification. The conclusions of the sensitivity analysis of Hwang *et al.* (2013) are therefore confirmed by the present results, despite the fact that in our computations, for increasing A_s nonlinear streaks change not only their amplitude but also, slightly, their shape. Considering the stabilization of the maximum temporal growth rate, the quadratic sensitivity of the streaks to A_s, even if it gives a weaker effect than 2D basic flow modifications at very small streak amplitudes, can provide a larger effect at larger A_s. This is not the case for the quenching of absolute instability, where 2D basic flow modifications are able to drive v^- to positive values for lower A_s values than 3D basic flow modifications, as already remarked by Hwang *et al.* (2013). However, as the streaks have been forced using linearly optimal initial conditions, it is interesting to analyse the dependence of the stabilizing actions not only on the basic flow distortion

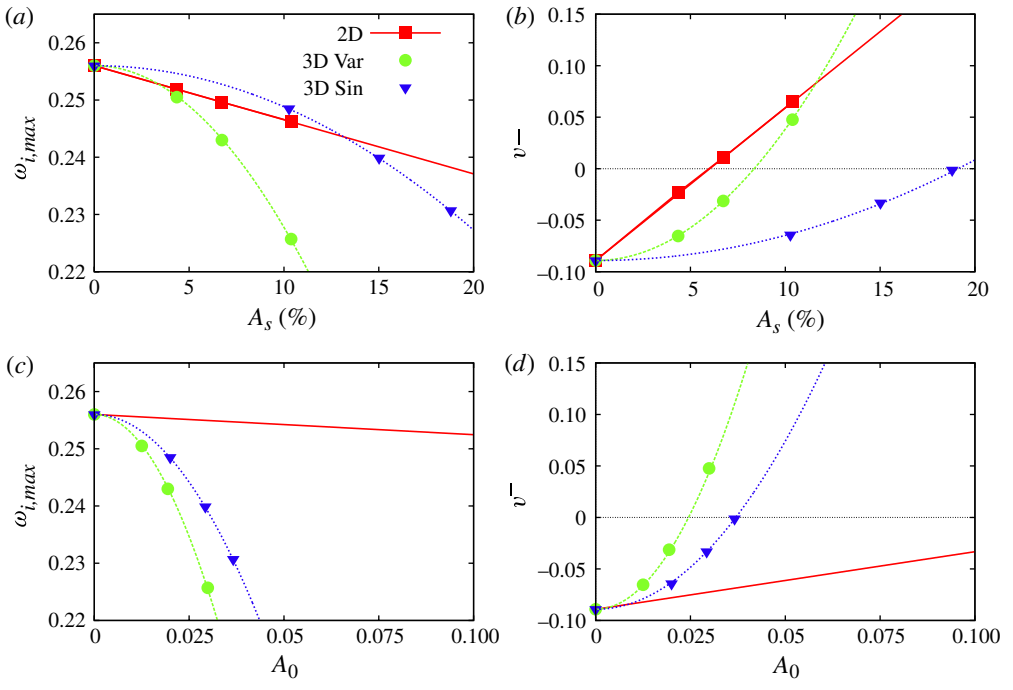

FIGURE 7. (Colour online) Dependence of the maximum growth rate $\omega_{i,max}$ (*a*,*c*) and the wave-packet trailing edge velocity v^- (*b*,*d*) on the streak amplitude A_s (*a*,*b*) and the initial disturbance amplitude A_0 (*c*,*d*). Zero amplitudes correspond to the 2D wake reference case. A (2D) spanwise uniform perturbation has been also considered for comparison. Symbols denote data points, while lines are linear and quadratic best fits to the data points.

amplitude A_s but on the amplitude A_0 of the initial perturbation based on energy density:

$$A_0^2 = \frac{1}{2\delta L_x L_z} \int_0^{L_x} \int_{-\infty}^{\infty} \int_0^{L_z} \boldsymbol{u}'_0 \cdot \boldsymbol{u}'_0 \, \mathrm{d}x \, \mathrm{d}y \, \mathrm{d}z. \tag{4.4}$$

This dependence is also reported in figure 7, where, again quadratic and linear sensitivities of $\omega_{i,max}$ and v^- on A_0 are found for 3D and 2D basic flow perturbations respectively. When the amplitude of initial conditions is considered, however, optimal 3D perturbations are shown to be more effective than 2D perturbations at stabilizing the flow. This is not surprising because, in a first approximation, a factor of $\sqrt{2G_{max}}$ is gained through the lift-up effect when forcing optimal 3D streaks using optimal initial vortices instead of enforcing the 2D profile with the same streak shape. For the presently considered case, for instance, the absolute–convective instability transition is enforced with optimal 3D streaks with values of A_0 more than six times smaller than those necessary when using 2D basic flow modifications (one hundred times smaller in terms of kinetic energy). Note also that the lift-up amplitude gain increases like Re (like Re^2 in terms of energy), and therefore the cost of forcing 3D perturbations of given amplitude decreases when the Reynolds number is increased. These results suggest that the key ingredient of the success of wake control strategies based on 3D flow modifications mainly relies on the large energy gains associated with the lift-up effect.

Case	A	D-Var	$\overline{\text{D}}$-Var	$\widetilde{\text{D}}$-Var	$\widetilde{\text{D}}_{lin}$-Var
$\omega_{i,max}$	0.2560	0.2257	0.2495	0.2305	0.2262
v^-	−0.089 050	0.047 561	−0.0052	0.022 891	0.017 337

TABLE 2. Comparison of maximum growth rate $\omega_{i,max}$ and of the wave-packet trailing edge velocity v^- computed for the unperturbed wake (case A, profile $U_M(y)$), the genuine varicose streak D (profile $U_M(y) + \Delta U(y,z)$) and the 'synthetic' streaks $\overline{\text{D}}$-Var (with profile $U_M(y) + \overline{\Delta U}(y)$), $\widetilde{\text{D}}$-Var (with profile $U_M(y) + \widetilde{\Delta U}(y,z)$) and $\widetilde{\text{D}}_{lin}$-Var (with profile $U_M(y) + \widetilde{\Delta U}_{lin}(y,z)$).

5. Analysis of the stabilizing mechanism

5.1. *Role of streaks' 2D mean flow distortion in the stabilizing mechanism*

In § 4.2 it has been shown that the forcing of streaks has a stabilizing effect on $\omega_{i,max}$ and v^-. One important question concerns the stabilizing mechanism. In the case of the stabilization of boundary layer instability it was found that a crucial role was played by the (nonlinear) spanwise mean flow distortion. Following Cossu & Brandt (2002), we therefore separate the wake distortion $\Delta U(y,z) = U(y,z) - U_M(y)$ induced by the streaks into the spanwise averaged part $\overline{\Delta U}(y)$ and the spanwise varying part $\widetilde{\Delta U}(y,z) = \Delta U(y,z) - \overline{\Delta U}(y)$. Nonlinear effects are necessary to generate $\overline{\Delta U}(y)$. To evaluate the respective effects of the spanwise periodic streak component $\widetilde{\Delta U}$ and of the basic flow spanwise mean distortion $\overline{\Delta U}$, we have repeated the impulse response analysis on the artificial basic flows $\widetilde{\text{D}}$-Var and $\overline{\text{D}}$-Var obtained by taking into account only the spanwise varying or the spanwise uniform part of the basic flow distortion, i.e. $U_{\widetilde{D}} = U_M + \widetilde{\Delta U}$ and $U_{\overline{D}} = U_M + \overline{\Delta U}$. The values of $\omega_{i,max}$ and of v^- pertaining to these artificial basic flows are compared to those obtained for the genuine streaky wake D-Var in table 2. From this table it is seen that, in contrast to what is found in boundary layers, the streaks' stabilizing action is not to be attributed to the 2D mean flow distortion $\overline{\Delta U}(y)$ but to its 3D spanwise varying part $\widetilde{\Delta U}$, which is, for example, able to quench the absolute instability on its own. To understand whether streak deformations due to nonlinearities are relevant in the stabilization mechanism, the additional synthetic streaky wake $\widetilde{\text{D}}_{lin}$-Var has been considered. Its velocity profile $U_M(y) + \widetilde{\Delta U}_{lin}(y,z)$ is obtained by adding the linear optimal streak profile to the reference 2D wake with the same amplitude as streak D. The results show that the stabilization induced by this linear streak is comparable to that induced by both $\widetilde{\Delta U}$ and the full streak ΔU, which are all able to quench the absolute instability.

5.2. *Analysis of kinetic energy production and dissipation terms*

Further insight into the mechanism by which the streaks stabilize the wake inflectional instability can be gained by the analysis of the different terms contributing to temporal growth of total perturbation kinetic energy, which is the well-known Reynolds–Orr equation (see e.g. Schmid & Henningson 2001):

$$\frac{1}{2}\frac{\mathrm{d}}{\mathrm{d}t}\int_{\mathscr{V}} \boldsymbol{u}'\cdot\boldsymbol{u}'\,\mathrm{d}\mathscr{V} = -\int_{\mathscr{V}} \boldsymbol{u}'\otimes\boldsymbol{u}' : \boldsymbol{\nabla U}\,\mathrm{d}\mathscr{V} - \frac{1}{Re}\int_{\mathscr{V}} \boldsymbol{\nabla u}' : \boldsymbol{\nabla u}'\,\mathrm{d}\mathscr{V}. \tag{5.1}$$

This equation states that the rate of change of perturbation kinetic energy is given by the sum of a production term, given by the work of Reynolds stresses against the

Case	$\omega_{i,max}$	$\widehat{P}_y/2\widehat{K}$	$\widehat{P}_z/2\widehat{K}$	$-\widehat{D}/2\widehat{K}$
A	0.256 00	0.298 20	0.000 00	−0.043 20
B-Var	0.249 26	0.295 58	−0.001 31	−0.045 01
C-Var	0.243 07	0.293 34	−0.004 26	−0.046 01
D-Var	0.225 34	0.292 84	−0.008 62	−0.058 88

TABLE 3. Maximum temporal growth rates and normalized kinetic energy production and dissipation components pertaining to the varicose streaky wakes.

basic flow shear, and a dissipation term, which is always negative. Cossu & Brandt (2004) have shown that for perturbations in the form of normal modes $\widehat{\boldsymbol{u}}(y,z)\mathrm{e}^{\mathrm{i}(\alpha x-\omega t)}$, the Reynolds–Orr equation reduces to the following decomposition for the temporal growth rate:

$$\omega_i = \frac{\widehat{P}_y}{2\widehat{K}} + \frac{\widehat{P}_z}{2\widehat{K}} - \frac{\widehat{D}}{2\widehat{K}}, \tag{5.2}$$

with the definitions

$$\widehat{K} = \frac{1}{\lambda_z}\int_0^{\lambda_z}\int_{-\infty}^{\infty}(\widehat{u}\,\widehat{u}^* + \widehat{v}\,\widehat{v}^* + \widehat{w}\widehat{w}^*)\,\mathrm{d}y\,\mathrm{d}z, \tag{5.3}$$

$$\widehat{P}_y = \frac{1}{\lambda_z}\int_0^{\lambda_z}\int_{-\infty}^{\infty} -(\widehat{u}\,\widehat{v}^* + \widehat{u}^*\widehat{v})\frac{\partial U}{\partial y}\,\mathrm{d}y\,\mathrm{d}z, \tag{5.4}$$

$$\widehat{P}_z = \frac{1}{\lambda_z}\int_0^{\lambda_z}\int_{-\infty}^{\infty} -(\widehat{u}\,\widehat{w}^* + \widehat{u}^*\widehat{w})\frac{\partial U}{\partial z}\,\mathrm{d}y\,\mathrm{d}z, \tag{5.5}$$

$$\widehat{D} = \frac{1}{\lambda_z}\int_0^{\lambda_z}\int_{0}^{\infty} 2(\widehat{\xi}\,\widehat{\xi}^* + \widehat{\eta}\,\widehat{\eta}^* + \widehat{\zeta}\,\widehat{\zeta}^*)\,\mathrm{d}y\,\mathrm{d}z, \tag{5.6}$$

where $\widehat{\boldsymbol{u}} = (\widehat{u},\widehat{v},\widehat{w})$ are the three velocity components of the normal mode and $(\widehat{\xi},\widehat{\eta},\widehat{\zeta})$ the corresponding vorticity components. The different terms of (5.2) have been computed for the varicose streaky wakes considered in § 4 and are reported in table 3 in correspondence to the most amplified streamwise wavenumber α_{max} for which the maximum growth rate $\omega_{i,max}$ is obtained. As it is well known, the instability of the 2D reference wake is explained by the large production term $\widehat{P}_y$, which exceeds the dissipation term $\widehat{D}$ when the Reynolds number is not exceedingly low. The forcing of streaks induces a stabilizing effect on all the components contributing to the growth rate. Not only is the $\widehat{P}_y$ production term reduced and the dissipation term increased, but the additional production term $\widehat{P}_z$ comes into play with a stabilizing effect. The stabilizing action on all the terms increases when the streak amplitude is increased and is of the same order of magnitude for all terms.

6. Summary of the main results and discussion

6.1. *Summary of main results*

Concerning optimal energy growth of stable perturbations supported by 2D parallel wakes, in the first part of the study we have shown the following.

(i) Parallel 2D wakes can sustain large transient growths of 3D streamwise uniform perturbations that are linearly stable. For instance, the maximum growth supported by perturbations of spanwise wavelength $\lambda_z = 2\pi$ ($\beta = 1$) is $G_{max} = 70$ at $Re = 50$.

(ii) The maximum energy growth is proportional to Re^2 in accordance with what is observed in other shear flows. Therefore, for instance, at $Re = 100$ the maximum energy growth of $\lambda_z = 2\pi$ perturbations is four times larger ($G_{max} = 280$) than at $Re = 50$.

(iii) Maximum energy growth also increases with spanwise perturbation wavelengths (i.e. for decreasing β), but in this case optimal perturbations correspond to structures of ever larger cross-stream extension that would probably be difficult to enforce in practical applications. This result is similar to what is observed, for example, in vortex columns in unbounded domains (Pradeep & Hussain 2006).

(iv) The most amplified perturbations are sinuous. Varicose perturbations are slightly less amplified (but by less than a factor of two). Optimal initial perturbations consist of streamwise vortices that induce the growth of streamwise streaks that modulate the wake's streamwise velocity in the spanwise direction. The cross-stream shape of the width of the wake is sinuous or varicose depending on the enforced perturbations.

In the second part of the study, we analysed the influence on stability of nonlinear streak modulations of the wake enforced by optimal initial streamwise vortices of increasing amplitude. The specific values $\beta = 1$, $Re = 50$ were considered. We have shown the following.

(i) Nonlinear streamwise streaks induced by optimal initial vortices reduce both the maximum temporal growth rate and the absolute growth rate of the inflectional instability.

(ii) Varicose streaks are more stabilizing than sinuous streaks of the same amplitude.

(iii) It is possible to suppress the absolute instability with small streak amplitudes ($A_s \approx 8\,\%U_\infty$).

(iv) The decrease of the maximum growth rate and of the absolute instability depends quadratically on the amplitude of streaks and on the amplitude of initial perturbations used to force them.

(v) When compared to 2D basic flow perturbations, whose stabilizing effect is linearly proportional to their amplitude, 3D varicose streak perturbations are more efficient in terms of amplitude A_s, when $A_s \gtrsim 3\,\%U_\infty$ with respect to maximum temporal amplification and $A_s \gtrsim 12\,\%U_\infty$ when absolute growth rates are considered. However, when the comparison is made in terms of the required initial perturbation amplitude A_0, optimal 3D perturbations are much more efficient than 2D perturbations (more than six times). This is due to the efficiency of the lift-up effect leading to large energy growths, with the efficiency increasing with Reynolds number. Varicose perturbations remain more efficient than sinuous ones even when their initial amplitude A_0 is considered, despite the fact that their optimal linear growth is lower.

(vi) Contrary to what is observed in the stabilization of boundary layers by streaks, the spanwise averaged nonlinear mean-flow distortion induced by nonlinear streaks does not play a crucial role in the stabilization. The spanwise oscillating part of the streaks plays the most important role, with optimal linear streak shapes as effective as nonlinear streak shape in the stabilization.

(vii) The decomposition of the maximum temporal growth rate into the different components due to energy production and dissipation shows that the streaks' stabilizing action acts on all these components by increasing the energy dissipation, reducing the 2D-type energy production and inducing a stabilizing (negative) energy production term related to the work of Reynolds stress against basic flow spanwise shear.

6.2. *Discussion*

As discussed in § 1, the second part of the study is strongly related to a set of previous investigations on vortex shedding, quenching or weakening enforced via 3D basic flow modulations. The stabilizing effect we find is indeed in agreement with numerous previous studies showing that spanwise modulations of the bluff body shape or spanwise modulated blowing and suction can have a stabilizing effect on vortex shedding (see Choi *et al.* 2008). In particular, in a very recent investigation, Hwang *et al.* (2013) have shown that 3D spanwise modulations of the 2D wake streamwise velocity reduce the absolute growth rate of unstable perturbations supported by Monkewitz (1988) wake profiles. Our results confirm the findings of Hwang *et al.* (2013), and in particular the stabilizing effect on absolute instability, the fact that varicose perturbations are more effective than sinuous ones, and the quadratic sensitivity of the absolute growth rate to the amplitude of 3D basic flow modifications. However, we extend their investigation by showing that by using streaks of moderate but still not excessive amplitudes, absolute instability can be completely suppressed, and not only reduced. Also, more insight into the stabilizing mechanism has been given by its analysis in terms of spanwise mean and oscillating contributions to the stabilization and in terms of respective contributions of the work of Reynolds stresses and of the dissipation to the stabilizing mechanism. The main conclusion here is that the success of vortex shedding 3D basic flow modifications can be attributed both to the very efficient amplification of streamwise streaks that ultimately stabilize the flow and to the quadratic dependence of the stabilization on their amplitude. This quadratic dependence, which is a weak point at very low amplitudes, allows high sensitivity to 3D basic flow modifications at larger amplitudes, where practically relevant effects are attained.

Another relevant result that extends what was previously known is that not only absolute growth rates but also maximum temporal growth rates are reduced by enforcing optimal streaks. The growth rate reductions we have documented are moderate, but probably much larger reductions can be achieved by forcing streaks of only slightly larger amplitude, thanks to the quadratic sensitivity of the growth rate reductions on streak amplitudes (see figure 7). As both optimal perturbations, maximum energy growth supported by parallel 2D wakes and modal growth rates of parallel 3D wakes are unchanged by the addition of a uniform velocity, our results, except for the absolute instability analysis, directly extend to, say, jets with the same shear profile.

Only parallel wakes have been considered in the present investigation, both because the main interest is on local stability properties, and also for the sake of conciseness and clarity. It will nonetheless be important to complete the study by computing optimal perturbations in a non-parallel spatial stability setting, similar to what has been done for boundary layers by Andersson, Berggren & Henningson (1999), for example, and to assess the influence of those optimal perturbations on global stability. As unstable global modes in non-parallel wakes are sustained by a pocket of local absolute instability, it is expected that forcing streaks of sufficiently large amplitude

could stabilize the global instability. Such a stabilizing action is, however, not expected to apply to situations where the basic flow non-parallelism alters the nature of the global instability, such as in wakes developing behind rotating cylinders (Pralits, Giannetti & Brandt 2013). These issues are currently under close scrutiny. The present analysis is also currently being extended to the turbulent case where 3D mean flow modifications are also effective at attenuating von Kármán vortex shedding (e.g. Kim & Choi 2005), proceeding along the same lines as in wall-bounded shear flows (Cossu, Pujals & Depardon 2009; Pujals *et al.* 2009; Hwang & Cossu 2010; Pujals, Depardon & Cossu 2010).

Acknowledgements

G.D.G. acknowledges the support of ANRT via the convention CIFRE 742/2011.

Appendix. Methods

A.1. *Computation of optimal perturbations*

Optimal growths $G(t, \alpha, \beta)$ are computed along quite standard lines, described in Schmid & Henningson (2001), for example. The linearized Navier–Stokes equations are recast in terms of the cross-stream velocity and vorticity v–η. The system satisfied by Fourier modes, $\widehat{v}(y, t; \alpha, \beta)\mathrm{e}^{\mathrm{i}(\alpha x+\beta z)}$, $\widehat{\eta}(y, t; \alpha, \beta)\mathrm{e}^{\mathrm{i}(\alpha x+\beta z)}$, is the standard Orr–Sommerfeld–Squire system,

$$\nabla^2 \frac{\partial \widehat{v}}{\partial t} = \mathscr{L}_{\mathscr{OS}}\widehat{v}; \quad \frac{\partial \widehat{\eta}}{\partial t} = -\mathrm{i}\beta \frac{\mathrm{d}U}{\mathrm{d}y}\widehat{v} + \mathscr{L}_{\mathscr{SQ}}\widehat{\eta}, \tag{A 1}$$

where the Orr–Sommerfeld and Squire operators are

$$\mathscr{L}_{\mathscr{OS}} = -\mathrm{i}\alpha \left[U(\mathscr{D}^2 - k^2) - \frac{\mathrm{d}^2 U}{\mathrm{d}y^2} \right] + \frac{1}{Re}(\mathscr{D}^2 - k^2)^2, \tag{A 2}$$

$$\mathscr{L}_{\mathscr{SQ}} = -\mathrm{i}\alpha U + \frac{1}{Re}(\mathscr{D}^2 - k^2), \tag{A 3}$$

and where $\mathscr{D}$ denotes $\mathrm{d}/\mathrm{d}y$ and $k^2 = \alpha^2 + \beta^2$. The system is discretized on a grid of N_y points uniformly distributed in $[-L_y/2, L_y/2]$. Differentiation matrices based on second-order accurate finite differences have been used to discretize the Orr–Sommerfeld–Squire system. Most of the results have been obtained with $N_y = 201$ and L_y, ranging from 20 to 120 for the perturbations with the smallest spanwise wavenumbers (largest spanwise wavelengths). The results do not change when N_y is doubled to 401 and when L_y is increased by half. We have also verified that the results do not change if differentiation matrices are based on Fourier series instead of finite differences, provided that L_y is large enough. The discretization has also been validated against temporal growth rates of Bickley jets available in the literature. Once the linear operator is discretized, standard methods and codes already used in previous investigations (e.g. Lauga & Cossu 2005; Cossu *et al.* 2009; Pujals *et al.* 2009) are used to compute the optimal growth and the associated optimal perturbations.

A.2. *Direct numerical simulations*

Numerical simulations of nonlinear and linearized Navier–Stokes equations have been performed using the *OpenFOAM* open-source DNS code (see http://www.openfoam.org). We have modified the code to allow for the solution of the Navier–Stokes equation in perturbation form and in order to add a set of additional output data.

The flow is solved inside the domain $[0, L_x] \times [-L_y/2, L_y/2] \times [0, L_z]$, which is discretized using a grid with N_x and N_z equally spaced points in the streamwise and spanwise directions respectively. N_y points are used in the y direction using a stretching that allows us to increase point density in the region where the basic flow shear is not negligible. Typically, results have been obtained using $L_x = 124, L_y/2 = 10, L_z = 2\pi$ and $N_x = 300, N_y = 160, N_z = 24$ with $\Delta x = 0.4$, $\Delta z = 0.26$ and a minimum of $\Delta y = 0.01$ on the symmetry axis and a maximum of $\Delta y = 0.1$ near the free stream boundary. Periodic boundary conditions have been used in the streamwise and spanwise directions and zero normal gradients of velocity and pressure have been enforced at the free stream boundaries ($|y| = L_y/2$). An increase of $L_y/2$ from 10 to 15 or an increase of the number of points from $N_y = 160$ to $N_y = 320$ did not affect the energy density more than 2 %. Also, the combined results of the DNS and the stability analysis algorithms described below have been checked against existing results both for the temporal stability analysis (temporal growth rates of the Bickley jet) and the temporal and spatiotemporal growth rates of Monkewitz profiles.

A.3. *Fundamental and subharmonic, symmetric and antisymmetric modes*

As mentioned in § 4.2, the numerical simulations of the linear impulse response are performed in a spanwise periodic domain of length twice that of the basic flow streaks $L_z = 2\lambda_z$ where $\lambda_z = 2\pi/\beta$. The impulse response can be decomposed into the contributions of fundamental and subharmonic modes, which can be further decomposed into symmetric and antisymmetric. The fundamental modes with an even symmetry (the same as that of the basic flow streaks) are of the form with $\beta_k^F = k\beta$, where β is the wavenumber of the basic flow streaks:

$$\widehat{u}(y,z) = \sum_{k=1}^{\infty} \tilde{u}_k(y) \cos \beta_k^F z, \quad \widehat{v}(y,z) = \sum_{k=1}^{\infty} \tilde{v}_k(y) \cos \beta_k^F z, \quad \widehat{w}(y,z) = \sum_{k=1}^{\infty} \tilde{w}_k(y) \sin \beta_k^F z. \tag{A 4}$$

Fundamental modes with the opposite symmetry admit the expansions

$$\widehat{u}(y,z) = \sum_{k=1}^{\infty} \tilde{u}_k(y) \sin \beta_k^F z, \quad \widehat{v}(y,z) = \sum_{k=1}^{\infty} \tilde{v}_k(y) \sin \beta_k^F z, \quad \widehat{w}(y,z) = \sum_{k=1}^{\infty} \tilde{w}_k(y) \cos \beta_k^F z. \tag{A 5}$$

For subharmonic modes the spanwise periodicity of the disturbances is twice that of the basic flow, and therefore we define $\beta_k^S = [(k+1)/2]\beta$. Subharmonic–symmetric modes are expanded as

$$\widehat{u}(y,z) = \sum_{k=1}^{\infty} \tilde{u}_k(y) \cos \beta_k^S z, \quad \widehat{v}(y,z) = \sum_{k=1}^{\infty} \tilde{v}_k(y) \cos \beta_k^S z, \quad \widehat{w}(y,z) = \sum_{k=1}^{\infty} \tilde{w}_k(y) \sin \beta_k^S z, \tag{A 6}$$

while subharmonic–antisymmetric modes admit the expansions

$$\widehat{u}(y,z) = \sum_{k=1}^{\infty} \tilde{u}_k(y) \sin \beta_k^S z, \quad \widehat{v}(y,z) = \sum_{k=1}^{\infty} \tilde{v}_k(y) \sin \beta_k^S z, \quad \widehat{w}(y,z) = \sum_{k=1}^{\infty} \tilde{w}_k(y) \cos \beta_k^S z. \tag{A 7}$$

Given a perturbation velocity field, obtained from linearized DNS, for example, the respective contributions of the fundamental and subharmonic, symmetric and

antisymmetric modes to the total field can be retrieved by a straightforward partitioning of the spanwise discrete Fourier transform of the velocity field into odd/even harmonic real/imaginary parts.

A.4. *Temporal and spatiotemporal stability analysis from the impulse response*

The techniques used to retrieve the temporal and spatiotemporal stability properties of parallel basic flow profile $U(y, z)$ from the numerically computed impulse response closely follow those used by Brandt *et al.* (2003), which are the three-dimensional extension of those developed by Delbende & Chomaz (1998) and Delbende, Chomaz & Huerre (1998) for two-dimensional wakes.

Consider the generic perturbation variable $q(x, y, z, t)$, already separated into its fundamental and subharmonic, symmetric and antisymmetric parts as described in § A.3. Concerning the temporal stability analysis, in order to determine the dependence of the temporal growth rate ω_i on the (real) streamwise wavenumber α, the amplitude spectrum of $q(x, y, z, t)$ is defined as

$$\widetilde{Q}(\alpha, t) = \left(\int_{-L_y/2}^{L_y/2} \int_0^{L_z} |\tilde{q}(\alpha, y, z, t)|^2 \, \mathrm{d}y \, \mathrm{d}z \right)^{1/2}, \tag{A 8}$$

where $\tilde{q}(\alpha, y, z, t)$ is the Fourier transform of the variable q in the streamwise direction. The asymptotic exponential regime is attained for large times, where the leading temporal mode emerges with growth rate (imaginary part of ω) well approximated by

$$\omega_i(\alpha) \sim \frac{\partial}{\partial t} \ln \widetilde{Q}(\alpha, t), \quad t \to \infty, \tag{A 9}$$

which can be numerically computed by the finite difference approximation

$$\omega_i(\alpha) \approx \frac{\ln[\widetilde{Q}(\alpha, t_2)/\widetilde{Q}(\alpha, t1)]}{t_2 - t_1}. \tag{A 10}$$

The selected times t_1 and t_2 in the above approximation need to be sufficiently large to ensure the extinction of transients. The values used for the presented results have been selected by exploring different pairs t_1, t_2 until results have satisfactorily converged to less than 1 % relative error.

The spatiotemporal stability analysis considers the development of the impulse response wave packet along $x/t = v$ rays, which is equivalent to the investigation of modes of real group velocity v (see e.g. Huerre & Rossi 1998). The use of the Hilbert transform allows us to demodulate the wave packet and define its amplitude unambiguously with respect to spatial phase oscillations. To this end, the analytical complex field variable $q_H(x, y, z, t)$ associated with $q(x, y, z, t)$ through the x-convolution $*$ is defined as

$$\bar{q}(x, y, z, t) = \left[\delta(x) + \frac{\mathrm{i}}{\pi x} \right] * q(x, y, z, t). \tag{A 11}$$

In wavenumber space, (A 11) reduces to

$$q_H(\alpha, y, z, t) = 2H(\alpha)\tilde{q}(\alpha, y, z, t), \tag{A 12}$$

where $H(\alpha)$ is the Heaviside unit-step function. The integration of the analytical field q_H in the cross-stream (y, z) plane then yields the amplitude Q defined by

$$Q(x,t) = \left(\int_{-L_y/2}^{L_y/2} \int_0^{L_z} |q_H(x,y,z,t)|^2 \, \mathrm{d}y \, \mathrm{d}z \right)^{1/2}. \tag{A 13}$$

According to steepest-descent arguments (e.g. Bers 1983), the long-time behaviour of the wave packet along each spatiotemporal ray $x/t = v$ is

$$Q(x,t) \propto t^{-1/2} \mathrm{e}^{\mathrm{i}[\alpha(v)x - \omega(v)t]}, \quad t \to \infty, \tag{A 14}$$

where $\alpha(v)$ and $\omega(v)$ represent the complex wavenumber and frequency travelling at the group velocity v. In (A 14), the real part of the exponential

$$\sigma(v) = \omega_i(v) - k_{x,i}(v)v \tag{A 15}$$

denotes the temporal growth rate observed while travelling at the velocity v, and it can be evaluated for large t directly from the amplitude Q in (A 14) as

$$\sigma(v) \sim \frac{\partial}{\partial t} \ln[t^{1/2} Q(vt, t)], \tag{A 16}$$

which can be approximated with

$$\sigma(v) \approx \frac{\ln[Q(vt_2, t_2)/Q(vt_1, t_1)]}{t_2 - t_1} + \frac{\ln(t_2/t_1)}{2(t_2 - t_1)}, \tag{A 17}$$

to which apply the same considerations discussed for (A 10).

REFERENCES

Andersson, P., Berggren, M. & Henningson, D. 1999 Optimal disturbances and bypass transition in boundary layers. *Phys. Fluids* **11** (1), 134–150.

Andersson, P., Brandt, L., Bottaro, A. & Henningson, D. 2001 On the breakdown of boundary layer streaks. *J. Fluid Mech.* **428**, 29–60.

Bearman, P. W. & Owen, J. C. 1998 Reduction of bluff-body drag and suppression of vortex shedding by the introduction of wavy separation lines. *J. Fluids Struct.* **12** (1), 123–130.

Bers, A. 1983 Space–time evolution of plasma instabilities: absolute and convective. In *Handbook of Plasma Physics,* vol. 1 (ed. M. N. Rosenbluth & R. Z. Sagdeev), pp. 451–517. North-Holland.

Brandt, L., Cossu, C., Chomaz, J.-M., Huerre, P. & Henningson, D. S. 2003 On the convectively unstable nature of optimal streaks in boundary layers. *J. Fluid Mech.* **485**, 221–242.

Choi, H., Jeon, W. P. & Kim, J. 2008 Control of flow over a bluff body. *Annu. Rev. Fluid Mech.* **37**, 357–392.

Chomaz, J. M., Huerre, P. & Redekopp, L. G. 1988 Bifurcations to local and global modes in spatially developing flows. *Phys. Rev. Lett.* **60**, 25–28.

Cossu, C. & Brandt, L. 2002 Stabilization of Tollmien–Schlichting waves by finite amplitude optimal streaks in the Blasius boundary layer. *Phys. Fluids* **14**, L57–L60.

Cossu, C. & Brandt, L. 2004 On Tollmien–Schlichting waves in streaky boundary layers. *Eur. J. Mech.* B **23**, 815–833.

Cossu, C., Pujals, G. & Depardon, S. 2009 Optimal transient growth and very large-scale structures in turbulent boundary layers. *J. Fluid Mech.* **619**, 79–94.

Darekar, R. M. & Sherwin, S. J. 2001 Flow past a square-section cylinder with a wavy stagnation face. *J. Fluid Mech.* **426** (1), 263–295.

Delbende, I. & Chomaz, J.-M. 1998 Nonlinear convective/absolute instabilities of parallel two-dimensional wakes. *Phys. Fluids* **10**, 2724–2736.

DELBENDE, I., CHOMAZ, J.-M. & HUERRE, P. 1998 Absolute and convective instabilities in the Batchelor vortex: a numerical study of the linear impulse response. *J. Fluid Mech.* **355**, 229–254.

FRANSSON, J., BRANDT, L., TALAMELLI, A. & COSSU, C. 2005 Experimental study of the stabilization of Tollmien–Schlichting waves by finite amplitude streaks. *Phys. Fluids* **17**, 054110.

FRANSSON, J., TALAMELLI, A., BRANDT, L. & COSSU, C. 2006 Delaying transition to turbulence by a passive mechanism. *Phys. Rev. Lett.* **96**, 064501.

GUSTAVSSON, L. H. 1991 Energy growth of three-dimensional disturbances in plane Poiseuille flow. *J. Fluid Mech.* **224**, 241–260.

HUERRE, P. & MONKEWITZ, P. A. 1990 Local and global instabilities in spatially developing flows. *Annu. Rev. Fluid Mech.* **22**, 473–537.

HUERRE, P. & ROSSI, M. 1998 Hydrodynamic instabilities in open flows. In *Hydrodynamic and Nonlinear Instabilities* (ed. C. Godrèche & P. Manneville), pp. 81–294. Cambridge University Press.

HWANG, Y. & CHOI, H. 2006 Control of absolute instability by basic-flow modification in a parallel wake at low Reynolds number. *J. Fluid Mech.* **560**, 465–475.

HWANG, Y. & COSSU, C. 2010 Amplification of coherent streaks in the turbulent Couette flow: an input–output analysis at low Reynolds number. *J. Fluid Mech.* **643**, 333–348.

HWANG, Y., KIM, J. & CHOI, H. 2013 Stabilization of absolute instability in spanwise wavy two-dimensional wakes. *J. Fluid Mech.* **727**, 346–378.

KIM, J. & CHOI, H. 2005 Distributed forcing of flow over a circular cylinder. *Phys. Fluids* **39**, 033103.

KIM, J., HAHN, S., KIM, J., LEE, D., CHOI, J., JEON, W. & CHOI, H. 2004 Active control of turbulent flow over a model vehicle for drag reduction. *J. Turbul.* **5** (19).

LAUGA, E. & COSSU, C. 2005 A note on the stability of slip channel flows. *Phys. Fluids* **17**, 088106.

LOMBARDI, M., CAULFIELD, C. P., COSSU, C., PESCI, A. I. & GOLDSTEIN, R. E. 2011 Growth and instability of a laminar plume in a strongly stratified environment. *J. Fluid Mech.* **671**, 184–206.

MONKEWITZ, P. A. 1988 The absolute and convective nature of instability in two-dimensional wakes at low Reynolds numbers. *Phys. Fluids* **31**, 999–1006.

NAYFEH, A. H. & MOOK, D. T. 1979 *Nonlinear Oscillations*. Wiley-Interscience.

PARK, J., HWANG, Y. & COSSU, C. 2011 On the stability of large-scale streaks in turbulent Couette and Poiseuille flows. *C. R. Méc.* **339**, 1–5.

PARK, H., LEE, D., JEON, W. P., HAHN, S., KIM, J. & CHOI, H. 2006 Drag reduction in flow over a two-dimensional bluff body with a blunt trailing edge using a new passive device. *J. Fluid Mech.* **563**, 389–414.

PRADEEP, D. S. & HUSSAIN, F. 2006 Transient growth of perturbations in a vortex column. *J. Fluid Mech.* **550**, 251–288.

PRALITS, J. O., GIANNETTI, F. & BRANDT, L. 2013 Three-dimensional instability of the flow around a rotating circular cylinder. *J. Fluid Mech.* **730**, 5–18.

PUJALS, G., DEPARDON, S. & COSSU, C. 2010 Drag reduction of a 3D bluff body using coherent streamwise streaks. *Exp. Fluids* **49** (5), 1085–1094.

PUJALS, G., GARCÍA-VILLALBA, M., COSSU, C. & DEPARDON, S. 2009 A note on optimal transient growth in turbulent channel flows. *Phys. Fluids* **21**, 015109.

REDDY, S. C., SCHMID, P. J., BAGGETT, J. S. & HENNINGSON, D. S. 1998 On the stability of streamwise streaks and transition thresholds in plane channel flows. *J. Fluid Mech.* **365**, 269–303.

SCHMID, P. J. & HENNINGSON, D. S. 2001 *Stability and Transition in Shear Flows*. Springer.

TANNER, M. 1972 A method for reducing the base drag of wings with blunt trailing edges. *Aeronaut. Q.* **23**, 15–23.

ZDRAVKOVICH, M. M. 1981 Review and classification of various aerodynamic and hydrodynamic means for suppressing vortex shedding. *J. Wind Engng Ind. Aerodyn.* **7**, 145–189.

2

Article 2

Published in Physics of Fluids ***26*** *pp.024110-{1,14}, 2014*

PHYSICS OF FLUIDS **26**, 024110 (2014)

Optimal perturbations of non-parallel wakes and their stabilizing effect on the global instability

Gerardo Del Guercio,[1,2] Carlo Cossu,[1] and Gregory Pujals[2]
[1]*Institut de Mécanique des Fluides de Toulouse, CNRS and Université de Toulouse, Allée du Professeur Camille Soula, 31400 Toulouse, France*
[2]*PSA Peugeot Citroën, Centre Technique de Velizy, 2 Route de Gisy, 78943 Vélizy-Villacoublay Cedex, France*

(Received 11 November 2013; accepted 5 February 2014; published online 24 February 2014)

We compute the spatial optimal energy amplification of steady inflow perturbations in a non-parallel wake and analyse their stabilizing action on the global mode instability. The optimal inflow perturbations, which are assumed spanwise periodic and varicose, consist in streamwise vortices that induce the downstream spatial transient growth of streamwise streaks. The maximum energy amplification of the streaks increases with the spanwise wavelength of the perturbations, in accordance with previous results obtained for the temporal energy growth supported by parallel wakes. A family of increasingly streaky wakes is obtained by forcing optimal inflow perturbations of increasing amplitude and then solving the nonlinear Navier-Stokes equations. We show that the linear global instability of the wake can be completely suppressed by forcing optimal perturbations of sufficiently large amplitude. The attenuation and suppression of self-sustained oscillations in the wake by optimal 3D perturbations is confirmed by fully nonlinear numerical simulations. We also show that the amplitude of optimal spanwise periodic (3D) perturbations of the basic flow required to stabilize the global instability is much smaller than the one required by spanwise uniform (2D) perturbations despite the fact that the first order sensitivity of the global eigenvalue to basic flow modifications is zero for 3D spanwise periodic modifications and non-zero for 2D modifications. We therefore conclude that first-order sensitivity analyses can be misleading if used far from the instability threshold, where higher order terms are the most relevant. © *2014 AIP Publishing LLC*. [http://dx.doi.org/10.1063/1.4866043]

I. INTRODUCTION

Two-dimensional wakes behind bluff bodies support robust self-sustained vortex shedding for sufficiently large Reynolds numbers. The onset of self-sustained oscillations is associated to a global instability supported by a finite region of local absolute instability in the near wake.[1–3] There is a continued interest in controlling vortex shedding because, in addition to inducing unsteady loads on the body, it also leads to an increase of the mean drag.

Spanwise periodic (3D) perturbations of spanwise uniform (2D) wakes, e.g., obtained with periodic modulations of the trailing and/or leading edge of the bluff body[4–7] or spanwise periodic blowing and suction[8] can attenuate and even suppress vortex shedding and reduce the associated undesired drag and unsteady loads (see, e.g., Ref. 9 for a review). Recently, important progress has been made in the understanding of this stabilizing action from a linear stability perspective: Hwang *et al.*[10] show that appropriate 3D spanwise periodic perturbations of 2D absolutely unstable wake profiles lead to a reduction of the absolute growth rate. This reduction is observed for a range of spanwise wavelengths that is in accordance with experimental results, just as the fact that varicose perturbations are more stabilizing than sinuous ones. However, the question of the higher efficiency of 3D perturbations when compared to 2D ones in reducing the absolute growth rate was left partially open by this study. It is indeed known that lower rates of 3D blowing and suction, compared to 2D one, are required to suppress shedding in a cylinder wake.[8] This seems to contrast the fact that the

 © 2014 AIP Publishing LLC

This article is copyrighted as indicated in the article. Reuse of AIP content is subject to the terms at: http://scitation.aip.org/termsconditions. Downloaded to IP: 195.83.231.74 On: Thu, 03 Jul 2014 08:13:51

first-order sensitivity of the absolute instability growth rate with respect to 3D spanwise periodic modifications of the basic flow is zero,[10,11] therefore predicting that, at first order, 2D perturbations are more effective than 3D ones in reducing the absolute growth rate.

A partial explanation of the higher efficiency of 3D perturbations when compared to 2D ones has been given in another recent study[12] where we show that parallel "frozen" 2D wakes can support the large temporal amplification of streamwise streaks from stable spanwise periodic and streamwise uniform streamwise vortices via the lift-up effect.[13,14] The optimal perturbations leading to the optimal amplification of the streaks were computed and it was shown that varicose streaks of relatively small amplitude are able to completely quench the absolute instability.[12] It was also shown that the initial amplitude of optimal 3D perturbations necessary to quench the absolute instability is much smaller than the initial amplitude required by 2D perturbations.

Many questions were however left unanswered by the local temporal analysis developed in our previous investigation.[12] For instance, can optimal spatial amplifications be large in spatially diffusing wakes? The answer is not *a priori* clear because the wake diffusion not only reduces the basic flow shear fuelling the transient growth but also increases the local spanwise wavenumber of the perturbation, which is known from local analysis to reduce the growth. Another question is: are 3D optimal perturbations more efficient than 2D ones in stabilizing a *global* instability? The answer to this question is not obvious because finite downstream distances are needed to attain the maximum energy growth, while the pocket of absolute instability that needs to be controlled is located upstream, and therefore it is not clear how efficient optimal perturbations can be in quenching the absolute instability. The scope of the present study is to answer these questions by considering the *spatial* optimal perturbations and their influence on the *global* stability of *non-parallel* wakes.

An "artificial" wake, left free to spatially develop downstream the enforced inflow wake profile, is introduced as reference 2D basic flow in Sec. III. The use of such a basic flow allows us to find results which are independent of the specific body shape generating the wake and of the particular devices used to generate the optimal perturbations. The optimal spatial perturbations of this non-parallel wake are computed in Sec. IV following the procedure described in Sec. II. These optimal perturbations are defined as the perturbation profiles enforced at the inflow station that lead to the optimal energy amplification $G(x)$ at the downstream station x. This definition is quite different from that of optimal initial or inflow conditions leading to the optimal temporal energy amplification[15,16] $G(t)$. Optimal spatial energy amplifications have already been computed in non-parallel boundary layers by using direct-adjoint methods exploiting the parabolic nature of the boundary layer equations.[17,18] Here we choose to specifically design an alternative scalable optimization method (see Sec. II) that does not rely on the parabolic nature of the equations and that does not require the explicit computation of adjoint operators. The influence of forcing optimal perturbations on the global linear stability is investigated in Sec. V. The results of fully nonlinear simulations that validate these results in the nonlinear regime are reported in Sec. V D, while the used numerical methods are summarized in the Appendix.

II. PROBLEM FORMULATION

In this section the mathematical formulation of the analysis performed in the paper is briefly introduced. The formulation is general and can be applied to other non-parallel shear flows. Specific details about the particular wake profile and perturbations used in this study are mentioned in Secs. III–V.

A reference two-dimensional (2D) non-parallel plane basic flow $\mathbf{U}_{2D}(x, y)$ is obtained as a steady solution of the Navier-Stokes equations with inflow boundary condition $\mathbf{U} = U_0(y)\mathbf{e}_x$ given at $x = 0$ and free-stream conditions $\mathbf{U} \to U_\infty \mathbf{e}_x$ given as $y \to \pm\infty$. We denote by x, y, and z the streamwise, cross-stream, and spanwise coordinates and by $\mathbf{e}_x$, $\mathbf{e}_y$, $\mathbf{e}_z$ the associated unit vectors. The Reynolds number $Re = U^*_{ref}\delta^*/\nu$ is based on the characteristic velocity and length associated to $U_0(y)$ and on the kinematic viscosity ν of the fluid. The non-parallel basic flow $\mathbf{U}_{2D} = U(x, y)\mathbf{e}_x + V(x, y)\mathbf{e}_y$ is invariant to translations and reflections in the spanwise coordinate z (it is therefore two-dimensional or 2D).

This article is copyrighted as indicated in the article. Reuse of AIP content is subject to the terms at: http://scitation.aip.org/termsconditions. Downloaded to IP: 195.83.231.74 On: Thu, 03 Jul 2014 08:13:51

Perturbations $\mathbf{u}'$ to the reference 2D basic flow are ruled by the Navier-Stokes equations in perturbation form:

$$\nabla \cdot \mathbf{u}' = 0, \tag{1}$$

$$\frac{\partial \mathbf{u}'}{\partial t} + (\nabla \mathbf{U})\,\mathbf{u}' + \left(\nabla \mathbf{u}'\right)\mathbf{U} + \left(\nabla \mathbf{u}'\right)\mathbf{u}' = -\nabla p' + \frac{1}{Re}\nabla^2 \mathbf{u}', \tag{2}$$

using $\mathbf{U} = \mathbf{U}_{2D}$ as basic flow.

In the first part of the study, dealing with optimal spatial perturbations of $\mathbf{U}_{2D}$, we consider steady perturbations $\mathbf{u}'$ of $\mathbf{U}_{2D}$ obtained by perturbing the inlet profile $U_0(y)$ with steady inflow perturbations $\mathbf{u}'_0(y, z)$. We are interested in steady perturbations both because they are spatially stable and because they are of interest in passive control applications. In particular, spanwise periodic perturbations of wavelength λ_z will be considered in the following. Considering small perturbations, the nonlinear term $(\nabla \mathbf{u}')\mathbf{u}'$ can be neglected, which makes the perturbation equations linear. Defining the local perturbation kinetic energy density as

$$e'(x) = \frac{1}{2\delta\lambda_z}\int_{-\infty}^{\infty}\int_{0}^{\lambda_z} \mathbf{u}' \cdot \mathbf{u}'\, dy\, dz, \tag{3}$$

the optimal spatial energy amplification of inflow perturbations is defined as

$$G(x) = \max_{\mathbf{u}'_0} \frac{e'(x)}{e'_0}. \tag{4}$$

Different approaches can be used to compute $G(x)$ and the associated optimal inflow perturbation. We choose here to decompose the inlet perturbation on a set of linearly independent functions $\mathbf{b}_0^{(m)}$, in practice limited to M terms, as

$$\mathbf{u}'_0(y, z) = \sum_{m=1}^{M} q_m \mathbf{b}_0^{(m)}(y, z). \tag{5}$$

Denoting by $\mathbf{b}^{(m)}(x, y, z)$ the perturbation velocity field obtained using $\mathbf{b}_0^{(m)}(y, z)$ as inlet perturbation, from the linearity of the operator follows that

$$\mathbf{u}'(x, y, z) = \sum_{m=1}^{M} q_m \mathbf{b}^{(m)}(x, y, z), \tag{6}$$

where the coefficients q_m are the same used in Eq. (5). The optimization problem in Eq. (4) can therefore be recast in terms of the M-dimensional control vector $\mathbf{q}$ as

$$G(x) = \max_{\mathbf{q}} \frac{\mathbf{q}^T \mathbf{H}(x)\mathbf{q}}{\mathbf{q}^T \mathbf{H}_0 \mathbf{q}}, \tag{7}$$

where the components of the symmetric matrices $\mathbf{H}(x)$ and $\mathbf{H}_0$ are

$$H_{mn}(x) = \frac{1}{2\delta\lambda_z}\int_{-\infty}^{\infty}\int_{0}^{\lambda_z} \mathbf{b}^{(m)}(x, y, z) \cdot \mathbf{b}^{(n)}(x, y, z)\, dy\, dz, \tag{8}$$

$$H_{0,mn} = \frac{1}{2\delta\lambda_z}\int_{-\infty}^{\infty}\int_{0}^{\lambda_z} \mathbf{b}_0^{(m)}(y, z) \cdot \mathbf{b}_0^{(n)}(y, z)\, dy\, dz. \tag{9}$$

Within this formulation $G(x)$ is easily found as the largest eigenvalue μ_{max} of the generalized $M \times M$ eigenvalue problem $\mu \mathbf{H}_0 \mathbf{w} = \mathbf{H}\mathbf{w}$. The corresponding eigenvector is the optimal set of coefficients $\mathbf{q}^{(opt)}$ maximizing the kinetic energy amplification at the selected streamwise station x. The corresponding inlet perturbation is $\mathbf{u}'^{(opt)}_0(y, z) = \sum_{m=1}^{M} q_m^{(opt)} \mathbf{b}_0^{(m)}(y, z)$. In the limit $M \to \infty$ the approximated solution converges to the exact solution.

In the second part of the study, the influence of forcing finite amplitude optimal perturbations on linear global stability is investigated. A family of 3D streaky nonlinear non-parallel basic flows

This article is copyrighted as indicated in the article. Reuse of AIP content is subject to the terms at: http://scitation.aip.org/termsconditions. Downloaded to IP: 195.83.231.74 On: Thu, 03 Jul 2014 08:13:51

$\mathbf{U}_{3D}(x, y, z; A_0)$ is obtained by looking for steady solutions of the (nonlinear) Navier-Stokes equations with inflow boundary condition $\mathbf{U}_0(y, z) = U_0(y)\mathbf{e}_x + A_0\mathbf{u}'^{(opt)}_0(y, z)$ given at $x = 0$. $\mathbf{u}'^{(opt)}_0$ is normalized to unit x-local energy so that $e'(0) = A_0^2$ for $\mathbf{u}' = \mathbf{U}_{3D} - \mathbf{U}_{2D}$ (see the definition of e' in Eq. (3)). In general, it is not guaranteed that the linear optimal perturbations are also (nonlinearly) optimal at finite amplitude. However, for the present purpose of open-loop control, this is not a problem as long as they are still largely amplified. Using strictly optimal perturbations is also not critical because it is not likely that strictly optimal perturbations can be forced in a real flow and there is no guarantee that they would be also the optimal ones in reducing the global mode growth rate. The global linear stability of the $\mathbf{U}_{3D}$ basic flows is then analysed by integrating in time the linearized form of the Navier-Stokes equations (1) and (2) in perturbation form with $\mathbf{U} = \mathbf{U}_{3D}$. After the extinction of transients, the leading global mode emerges inducing an exponential growth or decay of the solution. The global growth rate is then deduced from the slope of the global energy amplification curve.

III. NON PARALLEL 2D REFERENCE WAKE

The 2D reference wake is computed by enforcing as inflow boundary condition the following well studied[2] wake profile:

$$U_0(y) = 1 + \Lambda\left[\frac{2}{1 + \sinh^{2N}(y \sinh^{-1} 1)} - 1\right], \tag{10}$$

with $\Lambda = (U_c^* - U_\infty^*)/(U_\infty^* + U_c^*)$, where U_c^* is the centreline and $U_\infty{}^*$ the freestream velocity (dimensional variables are starred). The velocity U_0 is made dimensionless with respect to the reference velocity $U_{ref}^* = (U_c^* + U_\infty^*)/2$. The spatial coordinates are made dimensionless with respect to the reference length δ_0^* that is the distance from the centreline to the point where the 2D wake velocity is equal to U_{ref}^*, computed at the inflow. We set $\Lambda = -1.35$ to ensure a small recirculation in the upstream region of the wake. For $\Lambda = -1.35$, the wake is globally unstable when $Re \gtrsim 39$ (not shown). In the following we will consider the value $Re = 50$ for which numerical simulation (see the Appendix for the numerical details) shows strong self-sustained oscillations in the wake (see Fig. 1(b)). As at $Re = 50$ the only unstable global mode is sinuous (antisymmetric with respect to the $y = 0$ axis), the unstable basic flow $\mathbf{U}_{2D}$ is computed by direct temporal integration by enforcing the y-symmetry of the solutions (otherwise a Newton-based continuation method would have been required). The reference basic flow is shown in Fig. 1(a). It can be seen how the basic flow vorticity, which is maximum at $x = 0$ with peaks at $y \approx \pm 1$, slowly diffuses downstream.

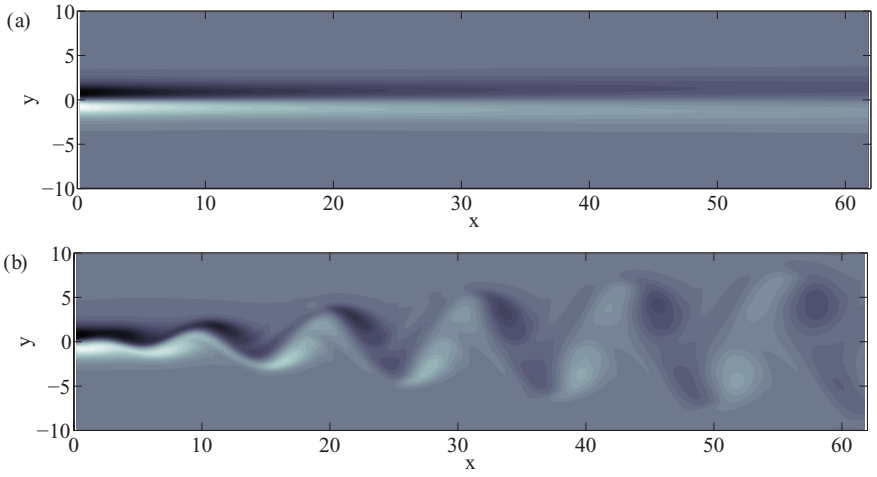

FIG. 1. Spanwise vorticity fields $\omega_z(x, y)$ associated to the reference 2D non-parallel wake at $Re = 50$. (a) (unstable) Basic 2D flow profile obtained by enforcing the y-symmetry of the solution. (b) Snapshot of the periodic self-sustained state obtained without enforcing the y-symmetry of the solution.

This article is copyrighted as indicated in the article. Reuse of AIP content is subject to the terms at: http://scitation.aip.org/termsconditions. Downloaded to IP: 195.83.231.74 On: Thu, 03 Jul 2014 08:13:51

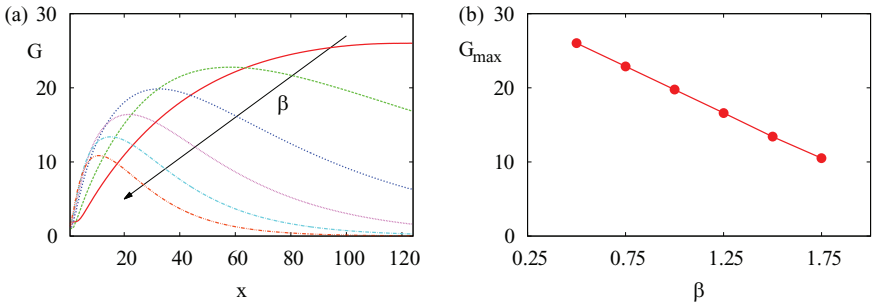

FIG. 2. Optimal spatial energy growths $G(x)$ (panel (a)) computed for the spanwise wavenumbers $\beta = 0.5, 0.75, \ldots, 1.50, 1.75$ at $Re = 50$ (outer to inner). The dependence $G_{max}(\beta)$ of the maximum energy growths on the spanwise wavenumber is reported in panel (b).

IV. OPTIMAL SPATIAL ENERGY GROWTH

Optimal steady inlet perturbations of $\mathbf{U}_{2D}$ maximizing the spatial energy amplification $G(x)$ are computed following the procedure described in Sec. II. Our previous investigation of the optimal temporal energy growth in parallel wakes[12] has shown that the most amplified spanwise periodic and streamwise uniform (corresponding to steady in our spatial framework) perturbations consist in streamwise vortices inducing the growth of streamwise streaks. We therefore consider inlet conditions of the type: $\mathbf{u'}_0 = (u'_0, v'_0, w'_0) = (0, \partial\psi/\partial z, -\partial\psi/\partial y)$. Single-harmonic spanwise periodic perturbations can be considered without loss of generality: $\psi' = f(y)\sin(\beta z)$. As varicose perturbations (mirror-symmetric with respect to the $y = 0$ plane) are the most efficient for control,[9,10,12] even if they are slightly less amplified than sinuous ones,[12] we enforce $f(-y) = -f(y)$ which leads to varicose streaks. The set of linearly independent inflow conditions used in Eq. (5) is chosen as $\mathbf{b}_0^{(m)}(y, z) = (0, \partial\psi^{(m)}/\partial z, -\partial\psi^{(m)}/\partial y)$ with $\psi^{(m)} = f_m(y)\sin(\beta z)$ and $f_m(y) = -f_m(y)$ for $m = 1, \ldots, M$. We have found well suited the set $f_m(y) = \sin(2m\pi y/L_y)$, where the numerical box extends from $-L_y/2$ to $L_y/2$ in the y direction.

Optimal energy growths have been computed for a set of spanwise wavenumbers β increasing M until a precision of 1% or higher on G_{max} was achieved (see also the Appendix for the numerical details of the computations). The computed optimal energy growth curves $G(x, \beta)$ are reported in Fig. 2(a). It is seen how, consistently with results form the local analysis,[12] both the maximum growth $G_{max} = \max_x G(x)$ and the position x_{max} where it is attained increase with increasing spanwise wavelength $\lambda_z = 2\pi/\beta$, i.e. with decreasing β (see also panel (b) of the same figure). The convergence of the optimal growth curves with increasing M is quite fast, and this for all the considered values of β, as can be seen in Fig. 3. Well converged results, with relative variations below 1% are obtained with only $M = 16$ terms.

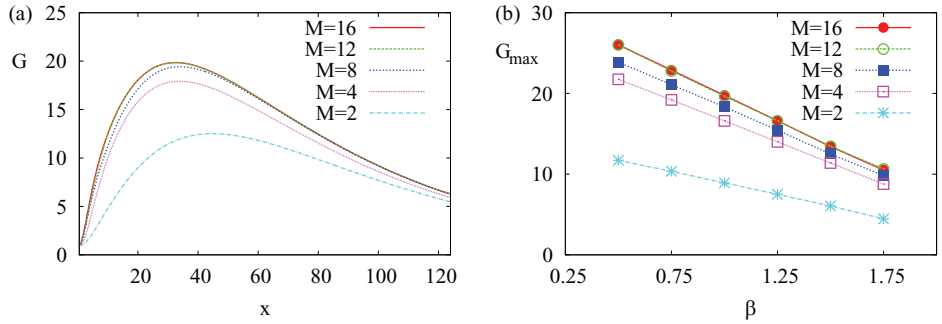

FIG. 3. Convergence of the optimal energy growth $G(x)$ for $\beta = 1$ (panel (a)) and of the maximum energy growth $G_{max}(\beta)$ (panel (b)) when the number M of linearly independent inflow conditions is increased at $Re = 50$. Well converged results are obtained for $M = 16$.

This article is copyrighted as indicated in the article. Reuse of AIP content is subject to the terms at: http://scitation.aip.org/termsconditions. Downloaded to IP: 195.83.231.74 On: Thu, 03 Jul 2014 08:13:51

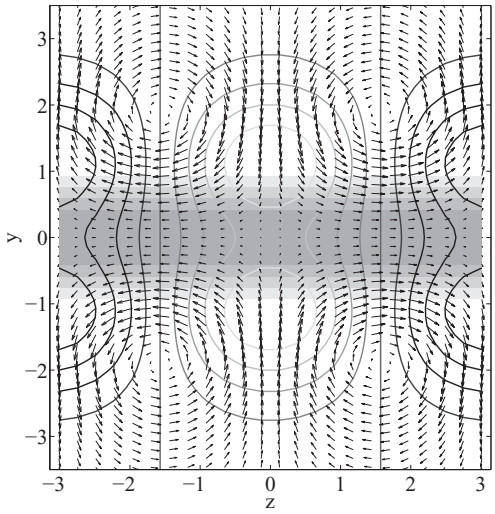

FIG. 4. Cross-stream (y-z) view of the cross-stream v_0'-w_0' components of optimal vortices (arrows) forced at the inflow ($x = 0$) and of the streamwise u' component of the corresponding optimal streaks (contour-lines) at $x = x_{max}$ for $Re = 50$, $\beta = 1$. The 2D basic flow wake streamwise velocity at the inflow $U_0(y)$ is also reported in grey-scale with white corresponding to the freestream velocity and dark grey the minimum velocity (wake centreline).

The optimal inflow perturbations ($x = 0$) and the maximum response ($x = x_{max}$) associated to the maximum growth G_{max} obtained for $\beta = 1$ are reported in Fig. 4. The corresponding velocity profiles are reported in Fig. 5, where additional values of β are also considered. The optimal inflow perturbations consist in two rows of counter-rotating vortices on each side of the $y = 0$ plane, with opposite rotation on each side. These vortices induce the growth of y-symmetric (varicose) streaks. From Fig. 5 it can be seen how, for increasing spanwise wavelengths λ_z (decreasing β), the size of optimal perturbations increases in the normal (y) direction (and of course also in the spanwise z direction).

The observed trends are in agreement with those found in our previous local analysis.[12] However, the maximum spatial growth rates obtained in the non-parallel case are smaller than the temporal ones obtained at the same nominal β under the frozen and parallel flow approximation. This is not surprising because the nominal values of β and Re of the non-parallel results are based on the properties of the wake profile at the inflow ($x = 0$). As the dimensional reference length $\delta^*(x)$ (the y^*

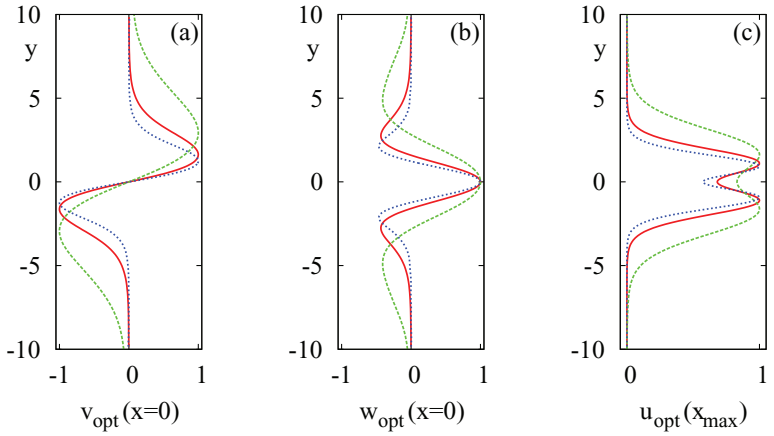

FIG. 5. Normalized amplitude of the $v(x = 0, y, z = 0)$ component (panel (a)) and $w(x = 0, y, z = \lambda_z/4)$ components (panel (b)) of the optimal inflow boundary vortices. The normalized amplitude of the $u(x = x_{max}, y, z = 0)$ streamwise component of the corresponding optimally amplified streaks is plotted in panel (c). Three selected spanwise wavenumbers are considered: $\beta = 0.5$ (dashed line, green), $\beta = 1$ (solid line, red), and $\beta = 1.5$ (dotted line, blue).

This article is copyrighted as indicated in the article. Reuse of AIP content is subject to the terms at: http://scitation.aip.org/termsconditions. Downloaded to IP: 195.83.231.74 On: Thu, 03 Jul 2014 08:13:51

value where $U^*_{2D}(y^*) = U^*_{ref}$) increases with x, a dimensionless wavenumber $\beta = \beta^*\delta^*$ based on the local scale would increase going downstream. As the maximum growth rate is a decreasing function of β, it is not surprising that the maximum growth rates are smaller than the ones that would be obtained if the wake was parallel. Therefore, the results of the present analysis should be compared to the ones of the local analysis obtained at larger values of β.

V. STABILIZING EFFECT OF OPTIMALLY FORCED STREAKS ON GLOBAL MODES

In this second part of the study, we investigate the influence of the forcing of optimal perturbations on the linear global stability of the wake. The input parameter of this analysis is the amplitude A_0 of the forcing at the inflow boundary and the output is the linear growth rate s_r of the global mode supported by the streaky wake. All the results are obtained for $Re = 50$ and $\beta = 1$. The choice of $\beta = 1$ is not completely arbitrary. On the one hand, in order to obtain large energy amplifications, one should choose low values of β. For low β, however, not only would the cross-stream size of the inlet optimal vortices be probably too large to be implemented in practical applications but, even more importantly, large amplitudes of the streaks would be obtained only far downstream (e.g., $x_{max} \approx 120$ for $\beta = 0.5$). This is a problem because the main scope of the control is to reduce the absolute growth rate in the absolute region which extends up to $x \approx 5$. On the other hand, selecting large values of β, in order to have x_{max} in the absolute region, would lead to poor energy amplifications and would exclude any damping in the convective region. The value $\beta = 1$ is a good compromise between these two extrema. In particular, as can be seen from Fig. 2(a), the obtained $G(x)$ for $\beta = 1$ in the region $x \lesssim 10$ are sensibly the same of those obtained for higher β.

A. Streaky wakes basic flows

Non-parallel streaky (3D) wake basic flows $\mathbf{U}_{3D}(x, y, z; A_0)$ are computed by enforcing at $x = 0$ the inflow condition $\mathbf{U} = U_0(y)\mathbf{e}_x + A_0\mathbf{u}'^{(opt)}_0$ and by then computing the corresponding steady solution of the (nonlinear) Navier-Stokes equations, as explained in Sec. II. The solution, which may be unstable, is obtained by enforcing symmetry with respect to the $y = 0$ plane, exactly as done to compute $\mathbf{U}_{2D}$. The local amplitude of the streaks is measured extending the standard definition used in previous studies:[12,19]

$$A_s(x) = \frac{1}{2}\frac{\max_{y,z}\left(U_{3D} - U_{2D}\right) - \min_{y,z}\left(U_{3D} - U_{2D}\right)}{\max_y U_0 - \min_y U_0}. \tag{11}$$

In this definition the streak amplitude at the station x is defined as half the maximum deviation of the streaky 3D profile from the reference 2D profile, at the same x station, normalized by the maximum velocity variation of the inflow 2D reference profile.

The considered values of A_0 and the obtained values of A_s at x_{max} (maximum value of A_s) and in the middle of the absolute instability region ($x = 2.7$) are reported in Table I, where each considered case is given a literal label. Case A corresponds to the reference two-dimensional wake profile $\mathbf{U}_{2D}$ (no streaks) while cases B, C, D, and E are obtained by increasing the inlet amplitude A_0 of the forced optimal perturbations. The nonlinear streaks amplitude evolution $A_s(x)$ associated to the velocity fields $\mathbf{U}_{3D}$ are reported in Fig. 6(a) for the considered cases. From Fig. 7, where streaky basic flows are shown in the symmetry plane $y = 0$, it is seen how, indeed for increasing A_0, the wake is increasingly 3D. The effect of nonlinearity is to slightly reduce the maximum energy growth (from ≈20 in the linear small amplitude limit to ≈17–15 for streaks D and E, not shown) and to induce a mean flow distortion that slightly counteracts the effect of the streaks.

B. Linear global stability analysis

The linear global stability analysis is performed via a direct numerical simulation of the Navier-Stokes equations (1) and (2) linearized upon the 3D streaky basic flows $\mathbf{U}_{3D}$ defined above (Sec. V A). In previous local stability analyses[10,12] it was shown that for large streaks amplitudes,

This article is copyrighted as indicated in the article. Reuse of AIP content is subject to the terms at: http://scitation.aip.org/termsconditions. Downloaded to IP: 195.83.231.74 On: Thu, 03 Jul 2014 08:13:51

TABLE I. Considered nonlinear streaky wake basic flows. A_0 is the finite amplitude given, at the inflow, to the linear optimal boundary perturbations (vortices). $A_{s,max}$ is the maximum streak amplitude reached in the nonlinear numerical simulation. Case A corresponds to the reference two-dimensional wake. Cases B, C, D, and E are obtained by increasing A_0.

Case	A_0	$A_{s,max}$ (%)	$A_s(x = 2.7)$ (%)
A	0.000	0	0
B	0.057	10.3	2.5
C	0.085	15.1	3.7
D	0.120	20.4	5.2
E	0.171	27.3	7.4

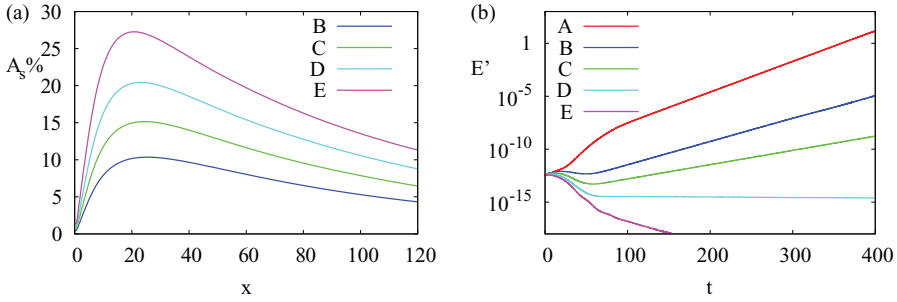

FIG. 6. Spatial evolution of the streaks amplitudes $A_s(x)$ for increasing amplitudes A_0 of the inflow optimal perturbations (panel (a)) and temporal evolution of the global kinetic energy of secondary perturbations $E'(t)$ to the considered reference and streaky basic flows (panel (b)). All the results have been obtained for $Re = 50$ and $\beta = 1$.

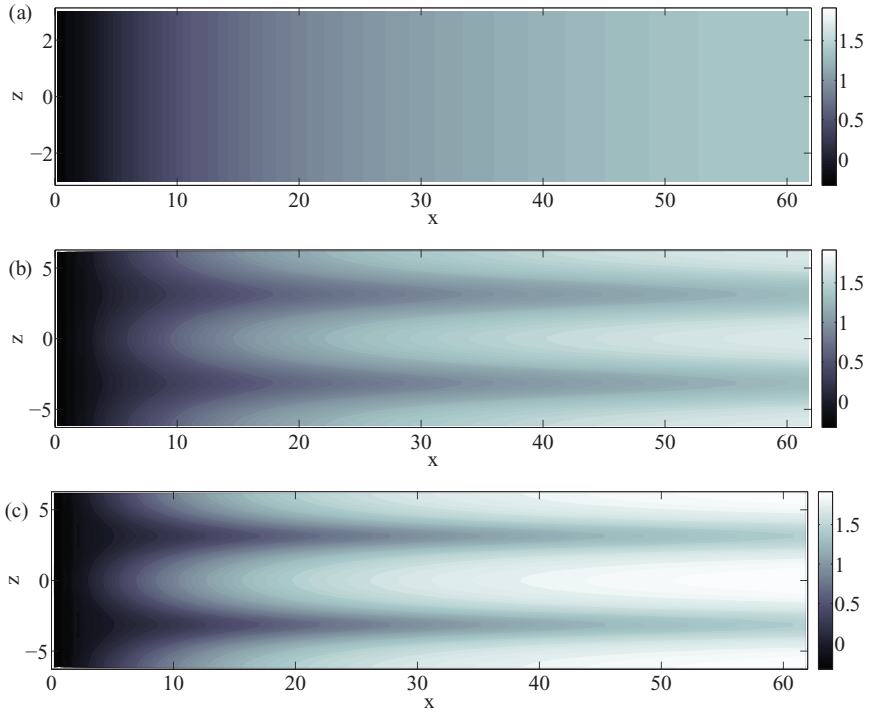

FIG. 7. Streaky basic flows. Distribution of the streamwise velocity $u(x, y = 0, z)$ in the $y = 0$ symmetry plane. The reference 2D case A is reported in panel (a), while cased C and E, obtained by increasing the amplitude A_0 of the inflow optimal perturbations, are reported in panels (b) and (c), respectively.

This article is copyrighted as indicated in the article. Reuse of AIP content is subject to the terms at: http://scitation.aip.org/termsconditions. Downloaded to IP: 195.83.231.74 On: Thu, 03 Jul 2014 08:13:51

the dominant absolute mode is subharmonic, i.e., its spanwise wavelength is twice that of the basic flow streaks. This is taken in due consideration by integrating the linearized equations in a domain including two basic flow streaks wavelengths ($L_z = 2\lambda_z$). Noisy initial conditions on $\mathbf{u}'$ are given for the reference 2D wake (case A). The unstable global mode emerging for large times in the reference 2D wake is then used, upon normalization of its amplitude, as initial condition on $\mathbf{u}'$ in simulations with the increasingly streaky basic flows B,...,E.

The temporal evolution of the global perturbation kinetic energy

$$E' = \frac{1}{2\delta L_x L_z} \int_0^{L_x} \int_{-L_y/2}^{L_y/2} \int_0^{L_z} \mathbf{u}' \cdot \mathbf{u}' \, dx \, dy \, dz$$

is reported in Fig. 6(b). After an initial transient extending to $t \approx 70$, the dependence of E' on time is exponential (a straight line in the lin-log scales used in the figure), where the rate of growth or of decay is twice the growth rate of the global mode.

As anticipated (see, e.g., Fig. 1(b)) the reference 2D wake (case A) is strongly linearly unstable at $Re = 50$. The forcing of 3D linearly optimal perturbations of increasing amplitude has a stabilizing effect on the global instability. The growth rate first reduced for low amplitude streaks (cases B and C) is then rendered quasi-neutral (case D) and finally completely stable for sufficiently large streak amplitudes (case E).

In the neutral and stable case the streaks amplitudes $A_s(x = 2.7)$, measured in the middle of the absolute instability region of the reference 2D wake, are respectively of $\approx$5% and $\approx$7%. These values are not far from the $\approx$8% value at which the absolute instability was completely quenched in our previous local stability analysis.[12] Also remark that, in the present non-parallel case A_s is given in terms of the entrance reference maximum $\Delta U_{2D}(x = 0)$, but if it was based on the local value of $\Delta U_{2D}(x)$ which is decreased with x, this would result in even larger downstream values of A_s. The stabilization of the global mode therefore appears to be associated to a strong reduction of the pocket of absolute instability that drives the global mode oscillations in the 2D reference case. A local stability analysis of the basic flow profiles extracted at $x = 2.7$ (not shown) indeed confirms that the local absolute growth rate is reduced with increasing streak amplitudes and that it is completely quenched by streak E.

C. Sensitivity of the global growth rate to the amplitude of 3D optimal structures

1. The first order sensitivity of the global growth rate to streaks is zero

In previous studies based on local stability analyses,[10,11] it was shown that the sensitivity of the absolute growth rate to 3D spanwise periodic modifications of the basic flow is zero. The argument developed in the local absolute instability analysis is easily extended to the global stability analysis of the nonparallel wake and proceeds as follows. Denote by $\mathbf{L}_{2D}$ the Navier-Stokes operator linearized near the 2D basic flow $\mathbf{U}_{2D}$. For small values of the inflow amplitude of optimal perturbations, the basic flow is modified by a small amount $\delta\mathbf{U} = \mathbf{U}_{3D} - \mathbf{U}_{2D}$ that induces a small change $\delta\mathbf{L}$ in the linear operator. At first order, the change of the leading eigenvalue induced by this small variation is[20,21] $\delta s = \langle \mathbf{w}_{2D}^\dagger, \delta\mathbf{L}\mathbf{w}_{2D} \rangle / \langle \mathbf{w}_{2D}^\dagger, \mathbf{w}_{2D} \rangle$, where $\mathbf{w}_{2D}$, s_{2D}, $\mathbf{w}_{2D}^\dagger$ are, respectively, the leading global mode, eigenvalue, and adjoint global mode associated to $\mathbf{U}_{2D}$, and the standard inner product is defined as $\langle \mathbf{a}, \mathbf{b} \rangle = \int_0^{L_x} \int_{-L_y/2}^{L_y/2} \int_0^{L_z} \mathbf{a} \cdot \mathbf{b} \, dx \, dy \, dz$. From Eq. (2) it is seen that the variation $\delta\mathbf{L}$ induced by $\delta\mathbf{U}$ consists only in spanwise periodic terms as $\delta\mathbf{U}$ is itself spanwise periodic. As $\mathbf{w}_{2D}$ and $\mathbf{w}_{2D}^\dagger$ do not depend on z, it follows[22] that $\langle \mathbf{w}^\dagger, \delta\mathbf{L}\mathbf{w} \rangle = 0$ and therefore that $\delta s = 0$. This is not the case for 2D (spanwise uniform) perturbations of $\mathbf{U}$ for which the variation of the leading eigenvalue is, in general, non-zero.

2. Effective sensitivity of global growth rate to spanwise periodic basic flow modifications and comparison with 2D modifications

We now consider the observed dependence of the most unstable global mode on the control amplitude. Such a control amplitude is unequivocally defined in terms of inflow optimal perturbation

This article is copyrighted as indicated in the article. Reuse of AIP content is subject to the terms at: http://scitation.aip.org/termsconditions. Downloaded to IP: 195.83.231.74 On: Thu, 03 Jul 2014 08:13:51

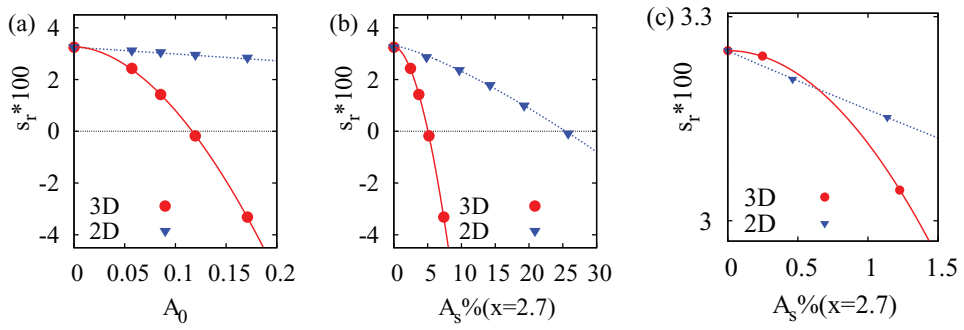

FIG. 8. Dependence of the growth rate of the global eigenvalue s_r on the inflow optimal perturbation amplitude A_0 (panel (a)) and on the streak amplitude $A_s(x = 2.7)$ measured in the centre of the absolute region of the reference 2D wake (panels (b) and (c) for a zoomed plot). A spanwise uniform perturbation (2D) has been also considered for comparison. Symbols denote data points, while lines are best fits to the data points.

amplitudes A_0. The dependence of the global growth rate s_r on the inflow optimal perturbation amplitude A_0 is displayed in Fig. 8(a). If this dependence is also to be reported in term of streaks amplitudes, for the considered streaks with $\beta = 1$, it makes no sense to report it in terms of $A_{s,max}$ because this value is attained far downstream, in the convectively unstable region. We instead take as an indicator of the "useful" streak amplitude the amplitude of the streaks in the middle of the absolute region of the unperturbed flow $A_s(x = 2.7)$. The dependence of s_r on this amplitude is reported in Fig. 8 (panels (b) and (c) for a zoom).

In the same figures the variation of the growth rate s_r induced by a 2D perturbation of the basic flow is also reported for comparison. The 2D perturbation has the same y shape as the optimal streak shape in the middle of the absolute region ($x = 2.7$) but is uniform instead of periodic in the spanwise direction. For this 2D perturbation, A_0 is unambiguously defined and A_s is defined as the maximum associated ΔU taken at $x = 2.7$.

From the figures it is clearly seen how the first order sensitivities ds_r/dA_0 and ds_r/dA_s computed for $A_0 = A_s = 0$ are zero for the 3D perturbations and non-zero for the 2D perturbations as predicted by the first order sensitivity analysis. According to a first-order sensitivity analysis one would expect the 2D perturbations to be more effective than 3D ones in quenching the global instability, but exactly the opposite is observed. Indeed, 2D perturbations are more effective than 3D ones in reducing s_r only for very small perturbation amplitudes, while the opposite is observed for larger amplitudes where the higher order dependence of s_r on A_0 and A_s induces more important reductions of s_r. We indeed find that 3D perturbations stabilize the global mode at a value of $A_s(x = 2.7)$ more than five times smaller, and more than ten times smaller in terms of A_0. A higher efficiency of 3D perturbations was expected for results expressed in terms of A_0, due to the gain associated with the lift-up of the 3D optimal perturbations. However, such a result was somehow unexpected when expressing the growth rate reductions in terms of A_s.

D. Nonlinear simulations

Non-linear simulations of the full Navier-Stokes equations have finally been performed to assess the effect of the inflow forcing of 3D optimal perturbations in the nonlinear regime. The same grid used in linear simulations has been used in the nonlinear ones. In a first simulation, the permanent harmonic self-sustained state supported by the reference 2D wake is allowed to develop. This 2D (spanwise uniform) self-sustained state is then given as an initial condition to simulations in the presence of the optimal perturbations (streaky wakes) of increasing amplitude. As expected from the linear analysis, the global perturbation kinetic energy E' associated to the self-sustained oscillations in the wake is reduced when the amplitude of the enforced optimal perturbations is increased (see Fig. 9). A stable steady streaky wake is found for case E, where the oscillations are completely suppressed.

This article is copyrighted as indicated in the article. Reuse of AIP content is subject to the terms at: http://scitation.aip.org/termsconditions. Downloaded to IP: 195.83.231.74 On: Thu, 03 Jul 2014 08:13:51

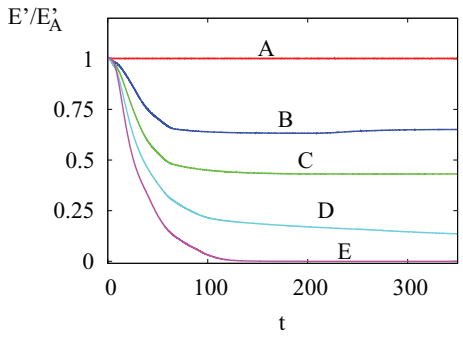

FIG. 9. Temporal evolution $E'(t)$ of the total perturbation kinetic energy, integrated over the whole computational box, supported by the streaky wakes, normalized to the E'_A of the reference 2D wake. The results are issued from nonlinear simulations where the permanent periodic state supported by the reference 2D wake is given as initial condition. In the presence of optimal perturbations of increasing amplitude, the amplitude of self-sustained oscillations is initially reduced (cases B, C, D), up to their complete suppression (case E).

Snapshots of the perturbation streamwise velocity in the $y = 0$ plane are reported in Fig. 10 for all the considered cases. For the reference 2D wake (case A), the self-sustained state is spanwise uniform (2D) with structures corresponding to standard von Kármán vortices. These vortical structures become increasingly modulated in the spanwise direction for increasing amplitudes A_0 of the forcing. Unsteady structures are completely suppressed for case E, where the basic flow streamwise streaks remain the only visible structures in the wake.

VI. SUMMARY AND DISCUSSION

In this study the optimal amplifications supported by an "artificial" non-parallel unstable 2D wake have been computed and their influence on the stability of the wake have been investigated by a global stability analysis. The main results can be summarized as follows:

- The energy of steady, symmetric spanwise periodic streamwise vortices forced at the inflow boundary can be significantly amplified downstream leading to large amplitude varicose streamwise streaks.
- An increase of the spanwise wavelength λ_z of the perturbations leads to larger energy amplification and to taller (in y) optimal structures.
- The used optimization technique, based on the simulation of the responses to a set of linearly independent inflow forcings, has proved very flexible. Only 16 simulations of independent forcings were needed to obtain accuracies higher than 1% on the optimal energy growths.
- The unstable global mode of the reference 2D wake at $Re = 50$ is completely stabilized when optimal inflow perturbations (vortices) are forced with sufficiently large amplitude.
- The results of first order local sensitivity analyses[10,11] are easily extended to the non-parallel case to show that the sensitivity of the 2D global mode eigenvalue to 3D spanwise periodic modifications of the basic flow is zero, while it is in general non-zero for 2D modifications.
- 3D optimal perturbations require smaller amplitudes than a reference 2D forcing to quench the global instability, and this both in terms of *rms*-amplitude of the inflow forcing and in terms of the basic flow distortion amplitude measured in the centre of the absolute instability region of the reference 2D wake. This is in contrast with the prediction of the sensitivity analysis.

The trends observed for the optimal energy amplification and the associated optimal perturbations in the non-parallel case are in qualitative agreement with those found in the local stability analysis.[12] In particular, the shapes of the optimal inputs (streamwise vortices) and those of the optimal outputs (streamwise streaks) are very similar for both analyses. When comparing the results, care must however be exerted in, e.g., selecting the appropriate spanwise wavenumbers to compare, as the local dimensionless wavenumber keeps increasing while going downstream in the non-parallel wake. Using the wavenumber made dimensionless with respect to the inflow reference length, the

This article is copyrighted as indicated in the article. Reuse of AIP content is subject to the terms at: http://scitation.aip.org/termsconditions. Downloaded to IP: 195.83.231.74 On: Thu, 03 Jul 2014 08:13:51

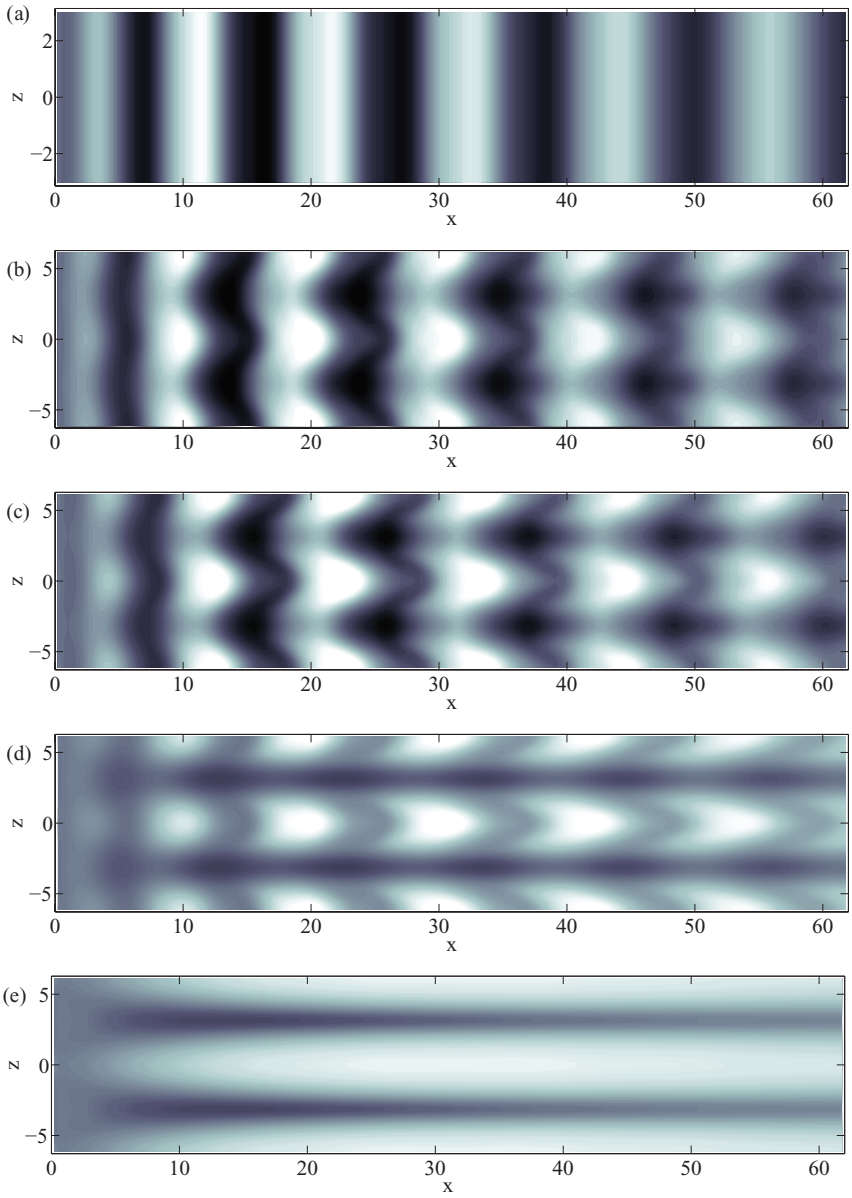

FIG. 10. Snapshots from fully nonlinear simulations. Streamwise perturbation velocity $u'(x, y = 0, z) = u(x, y = 0, z) - U_{2D}(x, y)$ in the $y = 0$ symmetry plane in the permanent regime ($t = 250$). The reference 2D case A is reported in panel (a), while cases B, C, D, and E, obtained by increasing the amplitude A_0 of the inflow optimal perturbations, are reported in panels (b) to (e) (top to bottom). Case A displays self-sustained periodic oscillations of 2D structures in the wake. These structures become increasingly 3D and of smaller *rms* value for increasing values of the enforced A_0 (cases B to D). The oscillations are completely suppressed in case E where the stable streaky basic flow is observed after transients are extinguished.

growths in the non-parallel wake appear smaller than the ones that would be predicted by keeping the wake frozen and parallel.

The fact that the linear global instability can be suppressed by optimal spanwise perturbations is in agreement with the idea that these 3D perturbations efficiently reduce the local absolute growth in the wave-maker region of the flow.[10,12] It also extends to flows with an "oscillator" dynamics[3,21] the control strategy based on the forcing of optimally amplified streaks that has been successfully used to stabilize convectively unstable waves in non-parallel boundary layers.[23–26] In this type of control strategy, optimal vortices are forced which then efficiently generate the streaks leading *in fine* to

This article is copyrighted as indicated in the article. Reuse of AIP content is subject to the terms at: http://scitation.aip.org/termsconditions. Downloaded to IP: 195.83.231.74 On: Thu, 03 Jul 2014 08:13:51

the stabilization. This control technique is much more efficient than directly forcing the stabilizing streaks because the lift-up effect is used as an amplifier of the control action. Otherwise, much larger forcing amplitudes would be required to directly force the streaks.

The conclusions concerning the sensitivity analysis are, we believe, probably the most relevant of this study. According to a first order sensitivity analysis, the 3D spanwise periodic forcing or modification of the basic flow with amplitude A is less effective than a 2D one with the same amplitude because the sensitivity of 3D perturbations is zero (growth rate reductions $\sim A^2$, with zero derivative in $A = 0$), while the 2D sensitivity is not zero (growth rate reductions $\sim A$). While these conclusions are correct for very small amplitudes A of the basic flow modifications, they are not correct for larger amplitudes where the parabola-shaped growth rate reductions (3D control) have grown larger than the straight line ones (2D control). In our specific case this cross-over happens at very small amplitudes of the forcing, of the order of 1/10 of the amplitude required for stabilization by 3D modifications and of the order of 1/100 of the one required by 2D modifications. Considering that these results have been obtained at a Reynolds number only 20% above the critical value for global instability, this means that except in very weakly unstable situations, where small control amplitudes suffice to stabilize the perturbations, a first order sensitivity leads to misleading conclusions when the stabilizing efficiency of 3D and 2D perturbations is compared.

An important question, left for future study, is how to force optimal perturbations in the presence of the bluff body. As already mentioned, many ways to modulate wakes in the spanwise direction have been already implemented, among which, the sinusoidal indentation of the leading and/or the trailing edge of the body,[4–7] and the spanwise periodic blowing and suction at the wall surface.[8] The achieved wake modulations are strikingly similar to the streaky wakes investigated in the present study, suggesting that, just like in boundary layers, the optimal streaks represent a sort of "attractor" of the spanwise modulated solutions. However, it is not clear which of these strategies, if any, predominantly uses vortices to force the streaks instead of directly forcing the streaks. It would also be interesting to investigate the optimal amplification and the control efficiency of periodic inflow perturbations. Additional work is granted on these issues.

ACKNOWLEDGMENTS

G.D.G. acknowledges the support of ANRT via the convention CIFRE 742/2011.

APPENDIX: NUMERICAL SIMULATIONS

The Navier-Stokes equations (nonlinear and linearized) have been numerically integrated using *OpenFoam*, an open-source finite volumes code (see http://www.openfoam.org). The flow is solved inside the domain $[0, L_x] \times [-L_y/2, L_y/2] \times [0, L_z]$ that is discretized using a grid with N_x and N_z equally spaced points in the streamwise and spanwise directions, respectively. N_y points are used in the y direction using stretching to densify points in the region where the basic flow shear is not negligible. The fractional step, pressure correction PISO (Pressure Implicit with Splitting of Operators) scheme is used to advance the solutions in time.

TABLE II. Numerical grids used for the computation of optimal perturbations. As a y-symmetry is enforced the equations are solved only in the $[0, L_y/2]$ half-domain.

β	L_z	Nz	$Ly/2$	Ny	Lx	Nx
0.5	12.57	48	20	120	124	300
0.75	8.38	48	20	120	124	300
1	6.28	24	10	80	124	300
1.25	5.03	24	10	80	124	300
1.5	4.20	12	10	80	124	300
1.75	3.60	12	10	80	124	300

This article is copyrighted as indicated in the article. Reuse of AIP content is subject to the terms at: http://scitation.aip.org/termsconditions. Downloaded to IP: 195.83.231.74 On: Thu, 03 Jul 2014 08:13:51

Different grids have been used to compute optimal linear perturbations of different spanwise wavenumbers, as reported in Table II.

Nonlinear streaky basic flows for $\beta = 1$ have been computed using the same grid used for the computation of the linear optimals at the same β. For the linear and nonlinear simulations of the perturbations to the 3D streaky basic flows, however, the domain is doubled in the y direction ($[-L_y/2, L_y/2]$ instead of $[0, L_y/2]$) as the y symmetry is no more enforced. Te box is also doubled in the spanwise direction ($L_z = 2\lambda_z$) in order to include subharmonic perturbations. The corresponding N_y and N_z are also doubled leading to a grid with $L_x = 124$, $L_y/2 = 10$, $L_z = 4\pi$, $N_x = 300$, $N_y = 160$, $N_z = 48$ with $\Delta x = 0.4$, $\Delta z = 0.26$ and a minimum $\Delta y = 0.01$ on the symmetry axis and a maximum $\Delta y = 0.1$ near the freestream boundary.

[1] J. M. Chomaz, P. Huerre, and L. G. Redekopp, "Bifurcations to local and global modes in spatially developing flows," Phys. Rev. Lett. **60**, 25–28 (1988).
[2] P. Monkewitz, "The absolute and convective nature of instability in two-dimensional wakes at low Reynolds numbers," Phys. Fluids **31**, 999–1006 (1988).
[3] P. Huerre and P. A. Monkewitz, "Local and global instabilities in spatially developing flows," Annu. Rev. Fluid Mech. **22**, 473–537 (1990).
[4] M. Tanner, "A method of reducing the base drag of wings with blunt trailing edges," Aeronaut. Q. **23**, 15–23 (1972).
[5] N. Tombazis and P. Bearman, "A study of three-dimensional aspects of vortex shedding from a bluff body with a mild geometric disturbance," J. Fluid Mech. **330**, 85–112 (1997).
[6] P. Bearman and J. Owen, "Reduction of bluff-body drag and suppression of vortex shedding by the introduction of wavy separation lines," J. Fluids Struct. **12**, 123–130 (1998).
[7] R. M. Darekar and S. J. Sherwin, "Flow past a square-section cylinder with a wavy stagnation face," J. Fluid Mech. **426**, 263–295 (2001).
[8] J. Kim and H. Choi, "Distributed forcing of flow over a circular cylinder," Phys. Fluids **17**, 033103 (2005).
[9] H. Choi, W. Jeon, and J. Kim, "Control of flow over a bluff body," Annu. Rev. Fluid Mech. **40**, 113–139 (2008).
[10] Y. Hwang, J. Kim, and H. Choi, "Stabilization of absolute instability in spanwise wavy two-dimensional wakes," J. Fluid Mech. **727**, 346–378 (2013).
[11] Y. Hwang and H. Choi, "Control of absolute instability by basic-flow modification in a parallel wake at low Reynolds number," J. Fluid Mech. **560**, 465 (2006).
[12] G. del Guercio, C. Cossu, and G. Pujals, "Stabilizing effect of optimally amplified streaks in parallel wakes," J. Fluid Mech. **739**, 37–56 (2014).
[13] T. Ellingsen and E. Palm, "Stability of linear flow," Phys. Fluids **18**, 487 (1975).
[14] M. T. Landahl, "A note on an algebraic instability of inviscid parallel shear flows," J. Fluid Mech. **98**, 243–251 (1980).
[15] N. Abdessemed, A. Sharma, S. Sherwin, and V. Theofilis, "Transient growth analysis of the flow past a circular cylinder," Phys. Fluids **21**, 044103 (2009).
[16] X. Mao, H. Blackburn, and S. Sherwin, "Optimal inflow boundary condition perturbations in steady stenotic flow," J. Fluid Mech. **705**, 306–321 (2012).
[17] P. Andersson, M. Berggren, and D. Henningson, "Optimal disturbances and bypass transition in boundary layers," Phys. Fluids **11**, 134–150 (1999).
[18] P. Luchini, "Reynolds-number independent instability of the boundary layer over a flat surface. Part 2: Optimal perturbations," J. Fluid Mech. **404**, 289–309 (2000).
[19] P. Andersson, L. Brandt, A. Bottaro, and D. Henningson, "On the breakdown of boundary layers streaks," J. Fluid Mech. **428**, 29–60 (2001).
[20] A. Bottaro, P. Corbett, and P. Luchini, "The effect of base flow variation on flow stability," J. Fluid Mech. **476**, 293–302 (2003).
[21] J. M. Chomaz, "Global instabilities in spatially developing flows: Nonnormality and nonlinearity," Annu. Rev. Fluid Mech. **37**, 357–392 (2005).
[22] This is a simple consequence of the integration in z of the product of spanwise sinusoidal and of a spanwise uniform function, which is itself spanwise sinusoidal and whose spanwise integral is therefore zero.
[23] C. Cossu and L. Brandt, "Stabilization of Tollmien-Schlichting waves by finite amplitude optimal streaks in the Blasius boundary layer," Phys. Fluids **14**, L57–L60 (2002).
[24] C. Cossu and L. Brandt, "On Tollmien–Schlichting waves in streaky boundary layers," Eur. J. Mech. B **23**, 815–833 (2004).
[25] J. Fransson, L. Brandt, A. Talamelli, and C. Cossu, "Experimental study of the stabilisation of Tollmien-Schlichting waves by finite amplitude streaks," Phys. Fluids **17**, 054110 (2005).
[26] J. Fransson, A. Talamelli, L. Brandt, and C. Cossu, "Delaying transition to turbulence by a passive mechanism," Phys. Rev. Lett. **96**, 064501 (2006).

This article is copyrighted as indicated in the article. Reuse of AIP content is subject to the terms at: http://scitation.aip.org/termsconditions. Downloaded to IP: 195.83.231.74 On: Thu, 03 Jul 2014 08:13:51

3

Article 3

Published in Journal of Fluid Mechanics ***752*** *pp572-588, 2014*

J. Fluid Mech. (2014), *vol.* 752, *pp.* 572–588. © Cambridge University Press 2014
doi:10.1017/jfm.2014.347

Optimal streaks in the circular cylinder wake and suppression of the global instability

Gerardo Del Guercio[1,2], Carlo Cossu[1,†] and Gregory Pujals[2]

[1]CNRS – Institut de Mécanique des Fluides de Toulouse (IMFT), Allée du Pr. Camille Soula, F-31400 Toulouse, France

[2]PSA Peugeot Citroën, Centre Technique de Velizy, 2 Route de Gisy, 78943 Vélizy-Villacoublay CEDEX, France

(Received 12 February 2014; revised 25 April 2014; accepted 14 June 2014)

The steady, spanwise-periodic, symmetric (varicose) optimal blowing and suction that maximizes energy amplification in the circular cylinder wake is computed at Reynolds numbers ranging from 50 to 100. It is found that the cylinder wake can sustain large energy amplifications that are associated with the generation by the optimal blowing and suction of streamwise vortices near the cylinder, which then induce the transient spatial growth of high-energy streamwise streaks further downstream. The most amplified perturbations have spanwise wavelengths ranging from five to seven times the cylinder diameter at the Reynolds numbers considered, with the corresponding optimal streaks reaching their maximum amplitude in the near wake, inside the pocket of absolute instability which sustains the global instability. The optimal blowing and suction is shown to stabilize the global linear instability. The most stabilizing spanwise wavelengths are in good agreement with previous findings. The amplitude of optimal blowing and suction required to suppress the global instability decreases when the Reynolds number Re is increased from 75 to 100. This trend reveals the key role played by the non-normal amplification of the streaks in the stabilization process, which is able to overcome the increase of the uncontrolled global growth rate with Re. Finally, it is shown that the global instability can be suppressed with control amplitudes smaller than those required by 2-D (spanwise-uniform) control. This result is not what would be expected from first-order sensitivity analyses, which predict a zero sensitivity of the global instability to spanwise-periodic control and, in general, a non-zero sensitivity to spanwise-uniform control.

Key words: absolute/convective instability, instability control, wakes/jets

1. Introduction

There is continuing interest in the control of self-sustained oscillations in bluff-body wakes, the archetype of which is the circular cylinder wake. The steady flow around a circular cylinder undergoes a Hopf bifurcation at Reynolds number $Re \approx 48$, leading to robust periodic self-sustained oscillations in the wake associated with the shedding

† Email address for correspondence: carlo.cossu@imft.fr

of two-dimensional (spanwise-uniform) von Kármán vortices. The Hopf bifurcation occurs in correspondence to a linear global instability driven by a pocket of local absolute instability in the near wake (Chomaz, Huerre & Redekopp 1988; Monkewitz 1988). Different approaches to suppressing these self-sustained oscillations have been studied, which can be classified into 2-D (spanwise-uniform) and 3-D (typically spanwise-periodic) control (Choi, Jeon & Kim 2008). Examples of 3-D control were given by Tanner (1972), Tombazis & Bearman (1997), Bearman & Owen (1998) and Darekar & Sherwin (2001), among others, who have shown that suitable spanwise-periodic modulations of the bluff-body geometry weaken and can even suppress the vortex shedding in the wake. Kim & Choi (2005) obtained similar results using spanwise-periodic blowing and suction (the reader is referred to the article by Choi *et al.* 2008 for a complete review of these results).

In addition to early interpretations of the stabilizing effect of 3-D control on 2-D wakes in terms of vortex dynamics, arguments based on general linear stability concepts have been advanced recently. In particular, it has been shown by Hwang, Kim & Choi (2013) that the local absolute growth rate of standard wake profiles can be reduced with suitable spanwise-periodic modulations of the streamwise velocity. This stabilizing effect is observed for shapes and spanwise wavelengths which are in agreement with previous observations.

A mathematically similar, but physically different, application of 3-D control is encountered in boundary layers where the 3-D spanwise-periodic modulations of the streamwise velocity are called 'streamwise streaks'. Kachanov & Tararykin (1987) found that streamwise streaks have a stabilizing effect on the primary 2-D instability of the flat-plate boundary layer. In the context of wall-bounded shear flows, it is well known that a very efficient way to generate streamwise streaks is to force low-energy streamwise vortices that fuel the growth of the streamwise streaks through the lift-up effect (see Moffatt 1967; Ellingsen & Palm 1975; Landahl 1990). In this process the energy of the vortices can be amplified by a factor proportional to Re^2 to give high-energy streaks (Gustavsson 1991). The precise shape of optimal vortices leading to optimally amplified streaks can be computed using standard optimization techniques and is associated with very large energy amplifications. Cossu & Brandt (2002, 2004) proposed using optimal vortices to force the stabilizing streaks, and showed that the primary 2-D instability of flat-plate boundary layers can be strongly stabilized in this way. The experiments of Fransson *et al.* (2006) show that transition to turbulence can be delayed by using this 3-D control technique.

Seeking to extend the approach used for boundary layers to bluff-body wakes, we recently computed the optimal streamwise uniform perturbations sustained by parallel absolutely unstable wakes (Del Guercio, Cossu & Pujals 2014*a*) and showed that, also in wakes, the optimal input consists of streamwise vortices and the optimal output consists of greatly amplified streamwise streaks. These optimally amplified streaks were shown to reduce the absolute growth rate and for sufficiently large amplitudes to completely suppress it, suggesting that global instabilities could be suppressed by quenching the wave-maker region in the near wake. To confirm this intuition, non-parallel model wakes with a finite region of absolute instability have been considered in a follow-up study (Del Guercio, Cossu & Pujals 2014*b*). Optimal downstream energy amplifications of steady perturbations were computed for these model wakes. It was found that inlet steady vortices (the control) can give rise to greatly amplified streaks downstream and that these streaks have a stabilizing effect on the global instability, leading to its suppression with sufficiently large control amplitudes.

By considering idealized non-parallel model wakes (as done in Del Guercio *et al.* 2014*b*), it is possible to analyse the streak generation and the global instability control

independently of the specific body generating the wake. However, this approach does not address the issue of how optimal steady vortices can be forced in practical applications. Some interesting questions therefore remain unanswered. Can large spatial energy amplifications be obtained by using a control device placed on the cylinder surface at low Reynolds numbers, e.g. ranging from 50 to 100? How do these optimal amplifications relate to those obtained for the idealized non-parallel wake? Does an optimally amplified finite spanwise wavelength exist in this case? If so, what is its value and how does this value compare to spanwise wavelengths that minimize the control energy? What is the minimum energy required to stabilize the global instability at Reynolds numbers ranging from, e.g., 50 to 100? How does the distribution of optimal blowing and suction compare with distributions used in previous investigations? How much can the control energy be reduced by using optimal forcing?

Another issue which has been addressed only partially by previous investigations is the comparative efficiency of spanwise-uniform (2-D) and spanwise-periodic (3-D) control for stabilization of the global instability. Hwang *et al.* (2013) had shown that the sensitivity of the absolute growth rate of parallel wakes to 3-D modulations of the basic flow is zero, whereas it is in general not zero for 2-D modulations. They therefore suggested that the higher efficiency of 3-D control, as observed by Kim & Choi (2005), for example, should be attributed to the higher efficiency of the forcing of 3-D perturbations as compared to 2-D ones. Del Guercio *et al.* (2014*b*) extended these sensitivity analysis results to global instabilities, showing that the first-order sensitivity of the global growth rate to 3-D modulations of the basic flow is also zero. They found that, despite this prediction, optimal 3-D perturbations are more efficient than 2-D ones in reducing the global growth rate in terms of both control energy and streak amplitude. It is currently unknown whether these conclusions can be extended to 'real' highly non-parallel wakes where the streaks would be forced by perturbations applied to the bluff-body surface.

The present study aims to answer the questions discussed above. To this end, we compute the optimal spanwise-periodic distributions of steady blowing and suction applied to the cylinder surface which maximize the perturbation energy at selected downstream stations. This approach is different from those where optimal initial or inflow conditions leading to the optimal temporal energy amplification are sought (see, e.g., Abdessemed *et al.* 2009 for the specific case of the circular cylinder). As detailed in § 2.1, the 3-D optimal blowing and suction and the associated optimal streaks are computed using a subspace reduction technique based on a set of independent simulations of the linearized Navier–Stokes equations. The results of the optimization, as well as their dependence on the spanwise wavelength and the Reynolds number, are discussed in § 3. The effect of finite-amplitude optimal blowing and suction on the growth rate of the unstable global mode is analysed in § 4. To this end, streaky wake basic flows are first computed by using finite-amplitude optimal forcing in nonlinear simulations; then, their linear stability is assessed by integration of the Navier–Stokes equations linearized near these streaky basic flows. The control sensitivity and efficiency are also discussed in § 4. Finally, nonlinear simulations are performed to validate the results of the linear stability analysis, as reported in § 4.6. The results and their implications are discussed in § 5.

2. Problem formulation

2.1. *Mathematical formulation*

We consider the flow of an incompressible viscous fluid of density ρ and kinematic viscosity ν past a circular cylinder of diameter D whose z axis is orthogonal to the

free-stream velocity $U_\infty \boldsymbol{e}_x$ (where $\boldsymbol{e}_x$ is the unit vector oriented parallel to the x axis). The Navier–Stokes equations governing the flow read as follows:

$$\boldsymbol{\nabla} \cdot \boldsymbol{u} = 0, \tag{2.1}$$

$$\frac{\partial \boldsymbol{u}}{\partial t} + \boldsymbol{u} \cdot \boldsymbol{\nabla} \boldsymbol{u} = -\boldsymbol{\nabla} p + \frac{1}{Re} \nabla^2 \boldsymbol{u}, \tag{2.2}$$

where $\boldsymbol{u}$ and p and the dimensionless velocity and pressure fields and $Re = U_\infty D/\nu$ is the Reynolds number. The velocity, pressure, lengths and times have been made dimensionless with U_∞, ρU_∞^2, D and D/U_∞, respectively. On the cylinder surface we enforce a radial velocity distribution $\boldsymbol{u}_w = \boldsymbol{u}(r = 1/2, \theta, z) = u_w(\theta, z)\boldsymbol{e}_r$, where $\boldsymbol{e}_r$ is the radial unit vector.

The reference basic flow $\boldsymbol{U}_{2D}(x, y)$ is obtained as a steady solution of the Navier–Stokes equations (2.1) and (2.2) in the case where no velocity is forced on the cylinder surface ($\boldsymbol{u}_w = \boldsymbol{0}$); $\boldsymbol{U}_{2D} = U(x, y)\boldsymbol{e}_x + V(x, y)\boldsymbol{e}_y$ is invariant with respect to translations and reflections in the spanwise coordinate z and is therefore two-dimensional (2-D).

In the first part of our study, which deals with linear optimal spatial perturbations of $\boldsymbol{U}_{2D}$, we consider steady perturbations $\boldsymbol{u}'$ of $\boldsymbol{U}_{2D}$ obtained by forcing a steady small radial velocity distribution $u'_w(\theta, z)\boldsymbol{e}_r$ on the cylinder surface. These perturbations satisfy the Navier–Stokes equations rewritten in perturbation form, i.e.

$$\boldsymbol{\nabla} \cdot \boldsymbol{u}' = 0, \tag{2.3}$$

$$\frac{\partial \boldsymbol{u}'}{\partial t} + \boldsymbol{u}' \cdot \boldsymbol{\nabla} \boldsymbol{U} + \boldsymbol{U} \cdot \boldsymbol{\nabla} \boldsymbol{u}' + \boldsymbol{u}' \cdot \boldsymbol{\nabla} \boldsymbol{u}' = -\boldsymbol{\nabla} p' + \frac{1}{Re} \nabla^2 \boldsymbol{u}', \tag{2.4}$$

using $\boldsymbol{U} = \boldsymbol{U}_{2D}$ as the basic flow and neglecting the nonlinear term $\boldsymbol{u}' \cdot \boldsymbol{\nabla} \boldsymbol{u}'$, which makes the perturbation equations linear. In the following, we will consider steady, spanwise-periodic perturbations of wavelength λ_z, which are of particular interest in open-loop flow control applications.

The (input) kinetic energy density per spanwise wavelength of the radial flow forced at the cylinder boundary is, in dimensionless form,

$$e'_w = \frac{1}{2\pi\lambda_z} \int_0^{\lambda_z} \int_0^{2\pi} (u'_w)^2 \, \mathrm{d}\theta \, \mathrm{d}z, \tag{2.5}$$

while the (output) local perturbation kinetic energy density at the station is

$$e'(x) = \frac{1}{\pi\lambda_z} \int_{-\infty}^{\infty} \int_0^{\lambda_z} \boldsymbol{u}' \cdot \boldsymbol{u}' \, \mathrm{d}y \, \mathrm{d}z. \tag{2.6}$$

The optimal spatial energy amplification of wall-control forcing is

$$G(x) = \max_{u_w} \frac{e'(x)}{e'_w}. \tag{2.7}$$

To compute $G(x)$ and the associated optimal wall perturbation, we follow an approach similar to the one recently applied to synthetic non-parallel wakes (Del Guercio *et al.* 2014*b*), which is summarized below. The control radial velocity enforced at the cylinder surface $u'_w(\theta, z)$ is decomposed using a set of linearly independent functions $b_w^{(m)}$, in practice limited to M terms, as

$$u'_w(\theta, z) = \sum_{m=1}^{M} q_m b_w^{(m)}(\theta, z). \tag{2.8}$$

If the perturbation velocity field obtained using $b_w^{(m)}(\theta, z)$ as the input perturbation is denoted by $\boldsymbol{b}^{(m)}(x, y, z)$, from linearity it follows that

$$\boldsymbol{u}'(x, y, z) = \sum_{m=1}^{M} q_m \boldsymbol{b}^{(m)}(x, y, z), \tag{2.9}$$

where the coefficients q_m are the same ones as in (2.8). The optimal energy growth, defined in (2.7), can therefore be approximated by

$$G(x) = \max_{\boldsymbol{q}} \frac{\boldsymbol{q}^{\mathrm{T}} \boldsymbol{H}(x) \boldsymbol{q}}{\boldsymbol{q}^{\mathrm{T}} \boldsymbol{H}_w \boldsymbol{q}}, \tag{2.10}$$

where $\boldsymbol{q}$ is the M-dimensional control vector and the components of the symmetric matrices $\boldsymbol{H}(x)$ and $\boldsymbol{H}_w$ are

$$H_{mn}(x) = \frac{1}{\pi \lambda_z} \int_{-\infty}^{\infty} \int_{0}^{\lambda_z} \boldsymbol{b}^{(m)}(x, y, z) \cdot \boldsymbol{b}^{(n)}(x, y, z) \, \mathrm{d}y \, \mathrm{d}z, \tag{2.11}$$

$$H_{w,mn} = \frac{1}{2\pi \lambda_z} \int_{0}^{\lambda_z} \int_{0}^{2\pi} b_w^{(m)}(\theta, z) \, b_w^{(n)}(\theta, z) \, \mathrm{d}\theta \, \mathrm{d}z. \tag{2.12}$$

The $G(x)$ in (2.10) is easily found as the largest eigenvalue μ_{max} of the generalized $M \times M$ eigenvalue problem $\mu \boldsymbol{H}_w \boldsymbol{w} = \boldsymbol{H} \boldsymbol{w}$. The corresponding eigenvector $\boldsymbol{q}^{(opt)}$ is the set of optimal coefficients maximizing the kinetic energy amplification at the selected streamwise station x, and the corresponding optimal blowing and suction is given by $u_w'^{(opt)}(\theta, z) = \sum_{m=1}^{M} q_m^{(opt)} b_w^{(m)}(\theta, z)$. The maximum growth is then defined as $G_{max} = \max_x G(x)$.

In the second part of the study, the effect of forcing three-dimensional finite-amplitude optimal perturbations on the global stability is investigated. To this end, first a set of increasingly three-dimensional basic flows $\boldsymbol{U}_{3D}(x, y, z; A_w)$ is obtained by computing steady solutions of the nonlinear Navier–Stokes equations with boundary conditions $\boldsymbol{u}_w = A_w u_w'^{(opt)}(\theta, z) \, \boldsymbol{e}_r$ (where $u_w'^{(opt)}$ is normalized to unit energy so that $e_w' = A_w^2$). The global linear stability of the $\boldsymbol{U}_{3D}$ basic flows is then analysed by integrating in time the linearized form of the Navier–Stokes equations (2.3) and (2.4) with $\boldsymbol{U} = \boldsymbol{U}_{3D}$ and enforcing $\boldsymbol{u}_w' = \boldsymbol{0}$. For sufficiently large times, the leading global mode emerges, inducing an exponential growth or decay of the solution. In this regime, the global growth rate is deduced from the slope of the global energy amplification curve.

2.2. *Numerical methods*

Numerical simulations of both the nonlinear and the linearized Navier–Stokes equations were performed using OpenFoam, an open-source finite volume code (see http://www.openfoam.org). The flow is solved in a C-type domain centred on the cylinder with L_x streamwise, L_y transverse and L_z spanwise extensions (see figure 1). Several preliminary tests guided us to the choices $L_x = 70$ and $L_y = 80$, with $L_z = \lambda_z$ for the computation of optimal perturbations and nonlinear streaky wakes and $L_z = 2\lambda_z$ for the global stability analyses and nonlinear direct numerical simulations used to confirm that the control is effective. The grid density is increased in the x–y plane in regions of high shear. We used $N_x = 300$ and $N_y = 200$ points in the streamwise and transverse directions, respectively, with $\Delta x_{min} = 0.01$, $\Delta x_{max} = 0.2$, $\Delta y_{min} = 0.01$ and $\Delta y_{max} = 0.2$ in the internal mesh blocks. A uniform grid spacing was used in the spanwise direction, always with $\Delta z \approx 0.25$, and the number of points used with each L_z is summarized in table 1. The PISO (Pressure Implicit with Splitting of

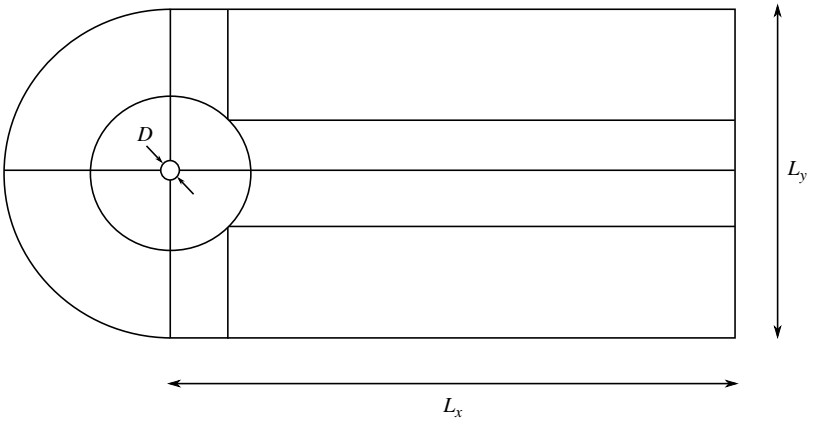

FIGURE 1. Numerical solution domain. For clarity, only the boundaries of the mesh blocks are shown.

L_z	12.57	8.37	6.28	5.03	4.20	3.60	3.14
N_z	48	34	24	20	16	14	12

TABLE 1. Spanwise extension L_z of the solution domain and the number of points N_z used in the spanwise direction for computation of the basic flows and optimal perturbations; L_z and N_z are doubled for the global stability analysis and for the nonlinear simulations.

Operators) algorithm is used to advance the solution in time. We have verified that with the chosen mesh, the length of the recirculation region of steady symmetric solutions and the drag coefficient both match, within 1 % accuracy, those found by Kim & Choi (2005) and Giannetti & Luchini (2007) in the 2-D case for the range of Reynolds numbers considered. Extending the domain size in the streamwise direction to $L_x = 100$ or in the transverse direction to $L_y = 100$ does not significantly improve the precision of these results. For 3-D simulations we have verified, in a few selected cases with active blowing and suction, that the perturbation energy (from which global growth rates are computed) does not change by more than 1 % when the number of grid points is doubled in the spanwise direction.

3. Optimal spatial energy amplifications sustained by the 2-D wake

The 2-D cylinder wake steady solution $\boldsymbol{U}_{2D}$ is the usual one computed in a number of previous studies (see, e.g., Dennis & Chang 1970; Fornberg 1980). It is found that $\boldsymbol{U}_{2D}$ is stable for $Re < Re_c \approx 48$. Here, $\boldsymbol{U}_{2D}$ is computed in the linearly unstable regime, for $Re = 50$, 75 and 100, by enforcing the y-symmetry of the solutions in direct temporal integrations of the Navier–Stokes equations. We have verified that the length of the recirculation bubble and the value of the separation angle are in good agreement with those found in previous studies.

Distributions of optimal blowing and suction $u_w(\theta, z)$ which maximize the spatial amplification of perturbation energy are computed following the procedure described in § 2.1. As the basic flow $\boldsymbol{U}_{2D}$ is spanwise invariant and the equations are linear, single-harmonic spanwise-periodic perturbations can be considered without loss of generality, i.e. $u'_w(\theta, z) = f(\theta)\sin(2\pi z/\lambda_z)$. A number of previous studies have shown

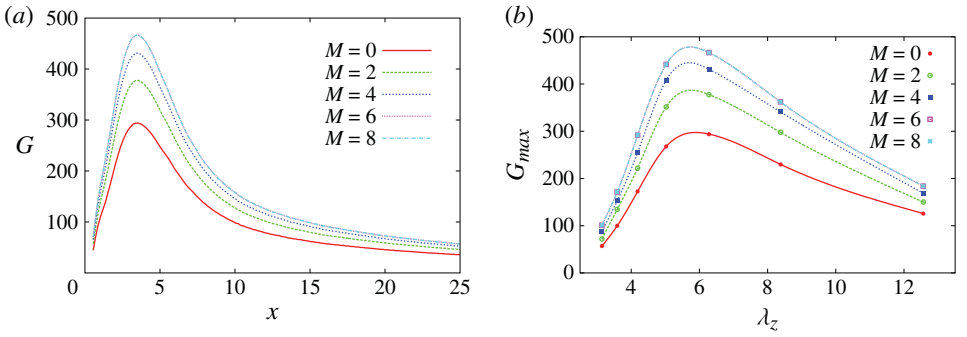

FIGURE 2. (Colour online) Convergence at $Re = 75$ of (a) the optimal energy growth $G(x)$ for $\lambda_z = 2\pi$ and (b) $G_{max}(\lambda_z)$, as the number M of linearly independent distributions of wall blowing and suction is increased. Well-converged results are obtained with $M = 6$.

that varicose perturbations (which are mirror-symmetric with respect to the $y = 0$ plane) are the most efficient for control (see, e.g., Darekar & Sherwin 2001; Kim & Choi 2005; Choi *et al.* 2008; Hwang *et al.* 2013; Del Guercio *et al.* 2014*a*,*b*), even if they are slightly less amplified than sinuous ones (Del Guercio *et al.* 2014*a*). We therefore enforce $f(-\theta) = f(\theta)$, which leads to varicose streaks. A standard cosine series expansion in θ is used, leading to the choice $b_w^{(m)}(\theta, z) = \cos(m\theta)\sin(2\pi z/\lambda_z)$ $(m = 0, \ldots, M)$ for the set of linearly independent inflow conditions used in (2.8). Optimal energy growths have been computed by increasing M until a precision of 1 % or better on G_{max} was achieved for a set of spanwise wavelengths λ_z. Typical $G(x)$ and $G_{max}(\lambda_z)$ obtained for $Re = 75$, along with their convergence histories, are reported in figure 2. From the figure one can see that the optimal growths have converged with better than 1 % precision with only $M = 6$ terms.

The computations have been repeated at $Re = 50$ and 100. The convergence of the results with increasing M is similar to that in the $Re = 75$ case. As shown in figure 3, the main effect of an increase in Re is to increase both the maximum amplification G_{max} and the position x_{max} at which this maximum is attained. The large amplifications found are consistent with those found in our previous investigations (Del Guercio *et al.* 2014*a*,*b*) and with those of Abdessemed *et al.* (2009), who found optimal temporal energy amplifications of the order of 10–10^2 for initial perturbations with $4 \lesssim \lambda_z \lesssim 8$ at $Re = 45$. From figure 3(b) it is also seen that x_{max} is an increasing function of λ_z. The most amplified wavelengths are found to be $\lambda_z = 6.5$ for $Re = 50$, $\lambda_z = 5.7$ for $Re = 75$ and $\lambda_z = 6.1$ for $Re = 100$, with corresponding optimal streamwise stations $x_{max} = 3.4$, $x_{max} = 3.5$ and $x_{max} = 3.6$.

The radial distributions $\widetilde{u}_w^{(opt)}(\theta)$ of the optimal blowing and suction $\widetilde{u}_w^{(opt)}(\theta) \times \sin(2\pi z/\lambda_z)$ are shown in figure 4. They correspond to spanwise-periodic blowing and suction with a maximum near $\theta \approx \pm 90°$ and minima at the bow and the stern of the cylinder. The variations of $\widetilde{u}_w^{(opt)}(\theta)$ with λ_z and Re are small and may be neglected in a first approximation. As shown in figure 5, this spanwise-periodic optimal blowing and suction induces counter-rotating streamwise vortices which decay downstream while forcing the growth of varicose streamwise streaks. Also in this relatively complicated flow, therefore, the main mechanism at play seems to be the lift-up effect. The facts that $\widetilde{u}_w^{(opt)}(\theta)$ is maximal at $\theta \approx \pm 90°$ (and not at, e.g., $\theta = 0$ and $\theta = 180°$) and that the local (in z) net mass flux is not zero (the $M = 0$ harmonic has an important contribution) suggest that the main effect of the optimal

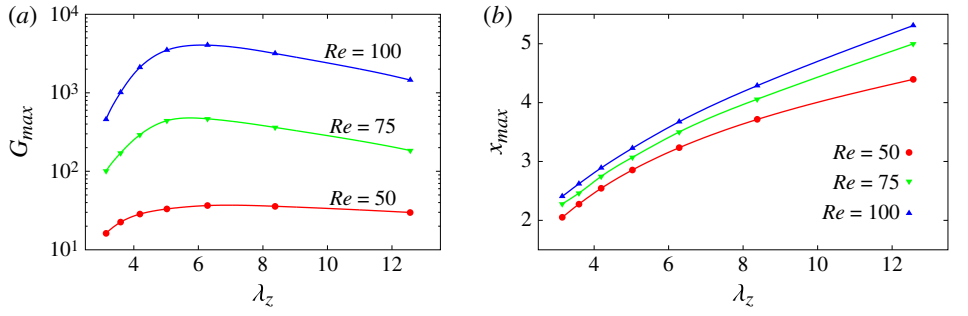

FIGURE 3. (Colour online) Dependence on the spanwise wavelength λ_z of (*a*) the maximum transient energy growth G_{max} and (*b*) the streamwise station x_{max} at which the maximum is attained, for selected Reynolds numbers $Re = 50$, 75 and 100.

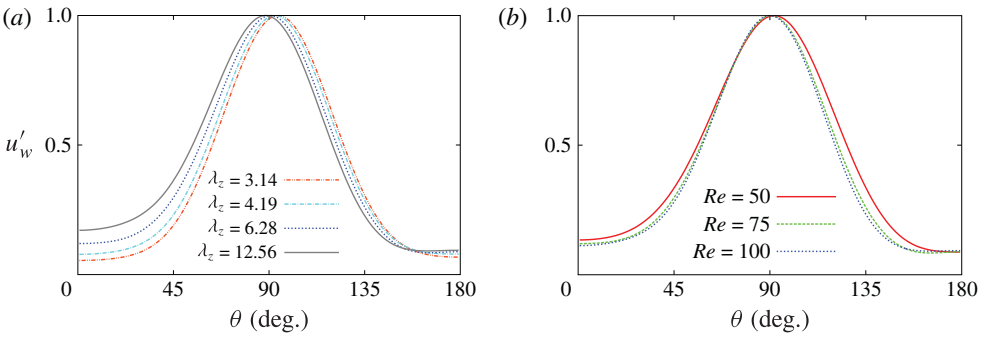

FIGURE 4. (Colour online) Azimuthal distributions $\widetilde{u}_w^{(opt)}(\theta)$ of the optimal blowing and suction normalized by their maximum value: (*a*) results obtained for a set of spanwise wavelengths λ_z at $Re = 75$; (*b*) distributions pertaining to the most amplified λ_z at each considered Reynolds number.

blowing and suction is to force the streamwise vortices that will best exploit the lift-up effect.

The existence of a finite optimal value of λ_z is probably the most important difference from our previous results pertaining to parallel and non-parallel synthetic wakes, where G_{max} was a monotonic increasing function of λ_z (Del Guercio *et al.* 2014*a*,*b*). This difference is due to the fact that in those previous investigations the optimal perturbations could assume any admissible shape in y, and indeed their y-extension increased with λ_z. In the present case, because the velocity forcing is localized on the cylinder surface, only a finite effective extension in y can be efficiently attained, and therefore a maximum value of G_{max} is attained in correspondence to the λ_z values for which the effective maximum y-extension of the forced functions is reached.

Finally, it is instructive to compare the effects of the optimal distribution of blowing and suction here and the θ-localized one used by Kim & Choi (2005). Simulations of the linearized Navier–Stokes equations show that the maximum energy gain attained with localized blowing and suction located at $\theta = 90°$ is 75 times smaller than the maximum energy gain obtained by using optimal blowing and suction. The two gain curves are, however, nearly indistinguishable if renormalized by the maximum gain

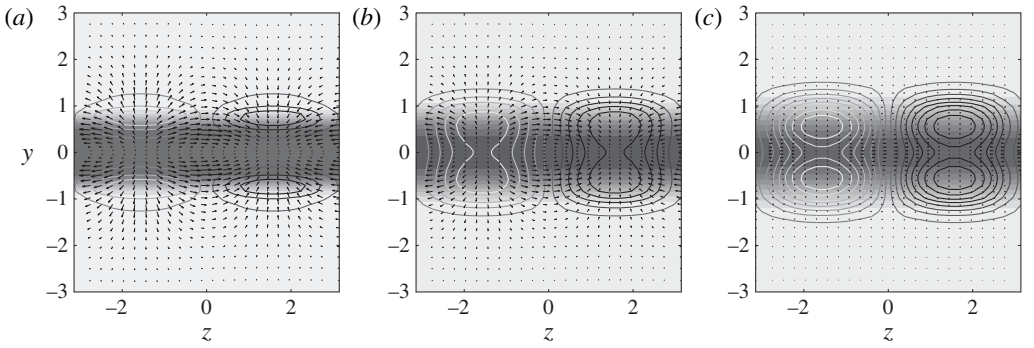

FIGURE 5. Cross-stream (y–z) view of the velocity perturbations forced by the optimal blowing and suction at $Re = 75$ with $\lambda_z = 2\pi$ at three selected streamwise stations: (a) $x = 1/2$ (cylinder stern); (b) $x = x_{max}/2$ (midway to the position of maximum streak amplitude); (c) $x = x_{max}$ (position of maximum streak amplitude). The scale used to plot the streamwise u' (streamwise streaks, contour lines) and the cross-stream v'–w' components (streamwise vortices, arrows) is the same in all panels. The reference 2-D basic flow streamwise velocity $U_{2D}(y)$ is represented in grey-scale with light grey corresponding to the freestream velocity and dark grey corresponding to the minimum velocity (wake centreline).

(not shown), meaning that streaks with essentially the same shape are forced. The main effect of using optimal perturbations is therefore to reduce the input energy for forcing these streaks.

4. Stabilizing effect of finite-amplitude optimal streaks

4.1. *A family of steady nonlinear streaky wake basic flows*

Non-parallel streaky (3-D) wake basic flows $\boldsymbol{U}_{3D}(x, y, z; A_w)$ are computed by enforcing at the wall the boundary condition $U_w(\theta, z) = A_w u_w'^{(opt)}(\theta, z)$ and then computing the corresponding steady solution of the nonlinear Navier–Stokes equations, as explained in § 2.1. Symmetry with respect to the $y = 0$ plane is enforced to compute steady solutions which may be unstable. A few cases with increasing A_w are selected and listed in table 2. We consider the intermediate Reynolds number $Re = 75$ and the spanwise wavelength $\lambda_z = 2\pi$, which is chosen slightly ($\approx 10\,\%$) larger than its optimal value 5.7 so as to approach the value that minimizes the control energy, as discussed below.

The reference two-dimensional wake profile $\boldsymbol{U}_{2D}$ is called case A, and cases B, C and D correspond to increasingly streaky wakes, as shown in figure 6. The local streak amplitude is measured with the standard formula of Andersson *et al.* (2001),

$$A_s(x) = \frac{\max_{y,z}(U_{3D} - U_{2D}) - \min_{y,z}(U_{3D} - U_{2D})}{2U_\infty}. \tag{4.1}$$

The evolutions $A_s(x)$ associated with the velocity fields $\boldsymbol{U}_{3D}$ corresponding to the four cases are plotted in figure 7(a), and the corresponding maximum streak amplitudes $A_{s,max}$ are listed in table 2. It is interesting that the maximum streak amplitudes are naturally reached inside the region of absolute instability of the reference 2-D wake, which almost coincides with the recirculation region ($x \lesssim 5$ at $Re = 75$). This is good news. Indeed, the global instability has been shown to be sustained by the region

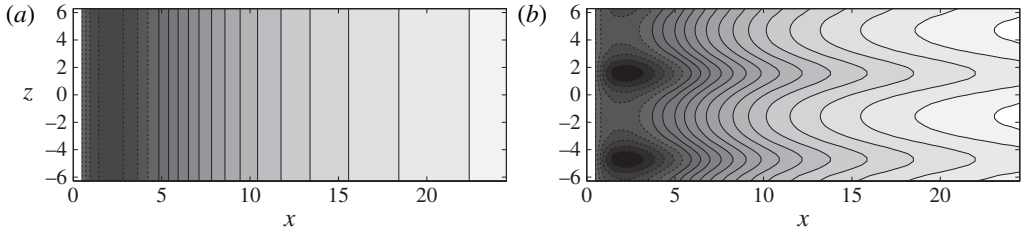

FIGURE 6. Distribution of the streamwise velocity $U_{3D}(x, y=0, z)$ in the $y=0$ symmetry plane of two selected basic flows: (*a*) the reference 2-D case, i.e. case A; (*b*) the streaky wake of case C. Contour levels are spaced by $u_\infty/20$, with low (high) velocities represented by dark (light) grey.

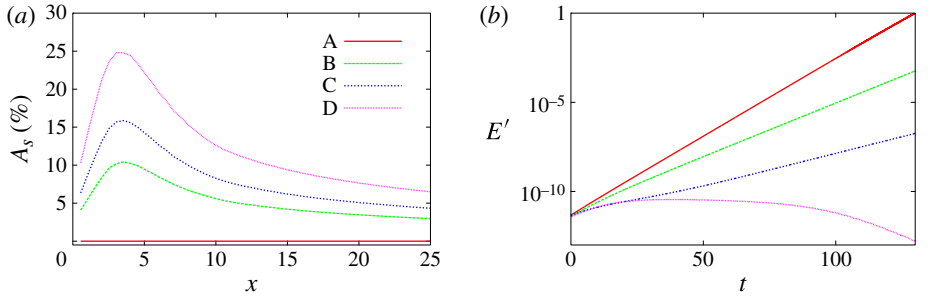

FIGURE 7. (Colour online) Plots for increasing amplitudes A_w of the optimal blowing and suction: (*a*) spatial evolution of the nonlinear streak amplitude $A_s(x)$; (*b*) temporal evolution of the global kinetic energy density $E'(t)$ of secondary perturbations to the nonlinear basic flows under consideration. The results were obtained for $Re = 75$ and $\lambda_z = 2\pi$.

Case	A	B	C	D
A_w	0	0.0031	0.0048	0.0080
$u_{w,max}$ (%)	0	0.75	1.2	2.1
$A_{s,max}$ (%)	0	10.45	16.16	25.44

TABLE 2. Nonlinear streaky wakes considered in this study: A_w is the finite amplitude of the optimal blowing and suction corresponding to the root-mean-square (r.m.s.) value of the blowing or suction velocity; $u_{w,max}$ is the maximum absolute value of the blowing or suction velocity; $A_{s,max}$ is the maximum streak amplitude reached in the wake. Values of $A_{s,max}$ and $u_{w,max}$ are given as percentages of U_∞. Case A corresponds to the reference 2-D wake, while cases B, C and D are for increasing values of A_w and correspond to increasingly streaky wakes. All the data refer to the parameter settings $Re = 75$ and $\lambda_z = 2\pi$.

of absolute instability, which acts as a wave-maker (see, e.g., Huerre & Monkewitz 1990); this is therefore the region where it is useful to reduce the absolute growth rate. As this reduction is proportional to the square of the streak amplitude, as shown by Hwang *et al.* (2013) and Del Guercio *et al.* (2014*a*), having large-amplitude streaks in the wave-maker region is therefore expected to induce a high control efficiency.

4.2. *Global linear stability of the streaky wakes*

The global linear stability of the nonlinear streaky basic flows is examined by integrating with respect to time the Navier–Stokes equations (2.3) and (2.4), linearized with respect to the $\boldsymbol{U}_{3D}$ considered. The linearized equations are integrated over a domain including two basic flow streak spanwise wavelengths ($L_z = 2\lambda_z$) to take into account the potential subharmonic nature of the dominant absolute mode (see Hwang *et al.* 2013; Del Guercio *et al.* 2014*a*,*b*). For the reference 2-D wake (case A), a random solenoidal perturbation velocity field $\boldsymbol{u}'$ is chosen as initial condition and the integration is continued in time until the emergence of the unstable global mode. This global mode is then renormalized to a small amplitude and used as the initial condition for all the cases under consideration. We then monitor the evolution of the global perturbation kinetic energy density $E' = (1/\mathscr{V}) \int_{\mathscr{V}} \boldsymbol{u}' \cdot \boldsymbol{u}' \, \mathrm{d}x \, \mathrm{d}y \, \mathrm{d}z$, where $\mathscr{V}$ is the fluid control volume. As shown in figure 7(*b*), $E'(t)$ grows exponentially in time, after the extinction of the initial transient. In this regime, the exponential growth rate of E' is twice that of the most unstable global mode. At the Reynolds number considered, $Re = 75$, it is already well known that the reference 2-D wake (case A) is linearly unstable. In the presence of increasing amplitudes of optimal blowing and suction and, therefore, increasing amplitudes of the streaks, the growth rate of the global mode is initially reduced (cases B and C), becoming negative for case D. These results confirm for a 'real wake' the scenario already observed in non-parallel model wakes (Del Guercio *et al.* 2014*b*) and associated with the weakening or complete suppression of the pocket of absolute instability, in accordance with the conclusions of Hwang *et al.* (2013) and Del Guercio *et al.* (2014*a*).

4.3. *Sensitivity of the global growth rate to the 3-D control amplitude*

Let us now examine the dependence of the growth rate s_r on the control amplitude at $Re = 75$, shown in figure 8 for a selected set of spanwise wavelengths. The amplitude of the control is reported in terms of both the optimal blowing and suction amplitude A_w and the maximum streak amplitude $A_{s,max}$. In all the computed cases, the data $s_r(A)$ are well approximated by the quadratic fit $s_r(Re, \lambda_z, A) = s_{r,2D}(Re) - C(Re, \lambda_z) A^2$, where $s_{r,2D}$ is the growth rate of the uncontrolled 2-D reference wake, A is the amplitude and C is a constant. Such a quadratic dependence is expected from first-order sensitivity analyses, which predict that for spanwise-periodic basic flow modulations, $\mathrm{d}s_r/\mathrm{d}A|_{A=0} = 0$ (see, e.g., Del Guercio *et al.* 2014*b* for the global mode sensitivity analysis). That the first-order sensitivity is zero could also have been inferred by observing that changing the sign of A in a spanwise-sinusoidal basic flow modification simply corresponds to a spanwise shift of $\lambda_z/2$ in physical space, and therefore we must have $s_r(A) = s_r(-A)$, implying a zero first-order derivative at the origin.

4.4. *Comparison of the control efficiency of 3-D and 2-D perturbations*

Since for 2-D modulations of the basic flow the first-order sensitivity is in general not zero (see, e.g., Bottaro, Corbett & Luchini 2003; Chomaz 2005), it might be

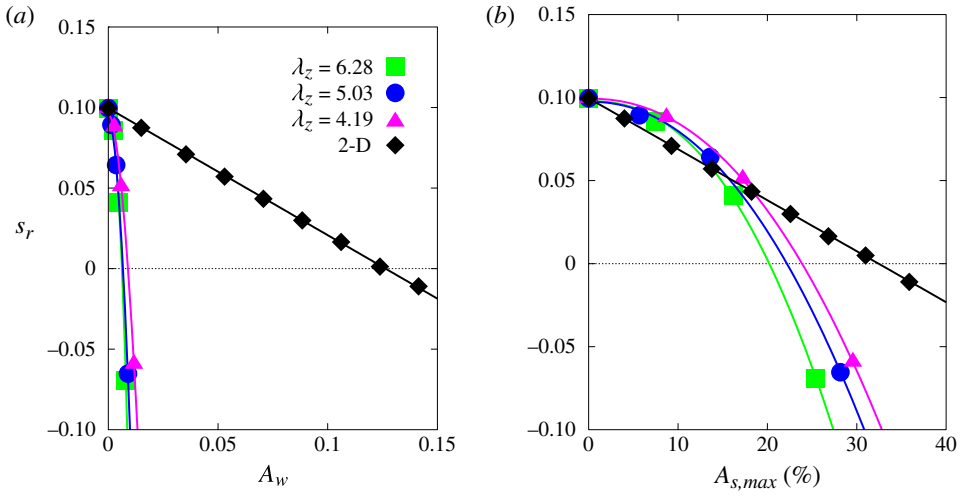

FIGURE 8. (Colour online) Dependence of the global mode growth rate s_r on (*a*) the optimal blowing and suction amplitude A_w and (*b*) the maximum streak amplitude $A_{s,max}$. A spanwise-uniform (2-D) perturbation has also been considered for comparison. The symbols represent data points, while the lines are best fits to the data points using quadratic interpolation for the 3-D data and linear interpolation for the 2-D data.

expected that 2-D perturbations are more effective than 3-D ones in quenching the global instability. To check whether this is actually the case, we computed the growth rate variations induced at $Re = 75$ by spanwise-uniform (2-D) wall blowing and suction with $m = 1$ azimuthal dependence $U_w = A_{2D}\cos(\theta)$, which has zero net mass flux and is associated with bleeding in the wake, and is known to efficiently reduce the absolute growth rate (Monkewitz 1988). The $s_{r,2D}(A_{2D})$ curves pertaining to the 2-D control are also plotted in figure 8 for comparison with the 3-D control. The analogue of the streak amplitude is defined for the 2-D perturbation as the maximum of the basic flow streamwise velocity variation induced by the 2-D suction.

As expected, the $s_{r,2D}(A_{2D})$ curve has non-zero slope at $A_{2D} = 0$ and is well approximated by a straight line. The 2-D perturbations considered are more stabilizing than the optimal 3-D ones only for $A_{s,max} \lesssim 14\,\%$, corresponding to the negligible $A_w \approx 0.005$. As already observed by Del Guercio *et al.* (2014*b*), a higher efficiency of 3-D perturbations is expected in terms of A_w, because such perturbations can exploit the energy gain associated with the lift-up effect, which is a 3-D mechanism. The fact that these 3-D perturbations are also more efficient in terms of basic flow deformation is not *a priori* obvious. We have verified that qualitatively similar results are obtained for a few other shapes of the 2-D forcing.

4.5. *Optimal spanwise wavelengths and amplitudes required for suppression of the global instability*

The dependence on the spanwise wavelength λ_z of the critical amplitudes A_c for which the global instability is suppressed is illustrated in figure 9 in terms of both A_w and $A_{s,max}$. At $Re = 75$, the spanwise wavelength minimizing the control amplitude necessary for the stabilization of the global instability is $\lambda_z \approx 6$. The value minimizing A_w ($\lambda_z = 6.2$) is slightly larger than that minimizing $A_{s,max}$ ($\lambda_z = 5.9$). When the

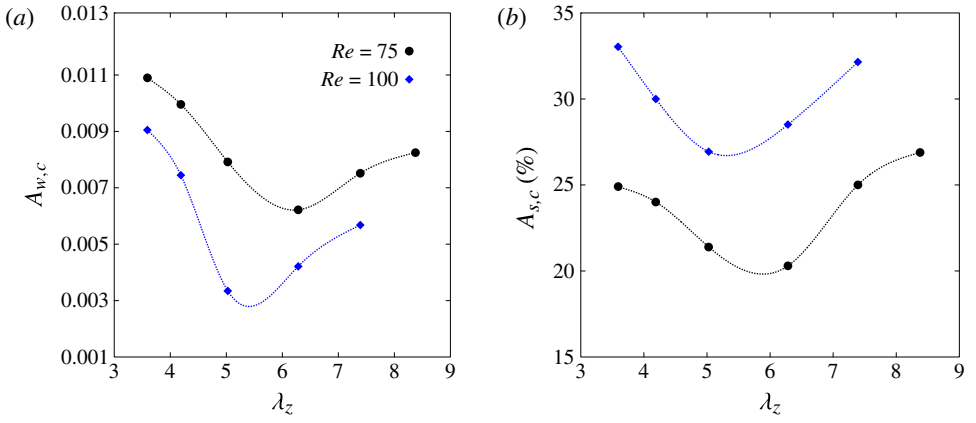

FIGURE 9. (Colour online) Dependence on the spanwise wavelength of (*a*) the critical amplitude of the forcing, $A_{w,c}$, and (*b*) the critical amplitude of the streaks, $A_{s,c}$, for which the global instability is suppressed. The data pertains to the Reynolds numbers $Re = 75$ and $Re = 100$.

Reynolds number is increased to $Re = 100$, the spanwise wavelength minimizing the control amplitude is reduced to $\lambda_z \approx 5.3$, with the value minimizing A_w ($\lambda_z = 5.4$) being very slightly larger than the one minimizing $A_{s,max}$ ($\lambda_z = 5.3$). These results are in very good agreement with those of Kim & Choi (2005), who found that the minimum drag is achieved for $\lambda_z = 5$–6 (but at the fastest rate for $\lambda_z = 6$) at $Re = 80$, and for $\lambda_z = 4$–5 (but at the fastest rate for $\lambda_z = 5$) at $Re = 100$. Less energy is required to suppress the global instability when using optimal blowing and suction instead of localized blowing and suction (0.62 % instead of 8 % of U_∞ in terms of maximum blowing/suction velocity, and 5.6×10^{-5} instead of 1.2×10^{-3} in terms of the momentum coefficient of forcing $C_\mu = 2\pi A_w^2$ at $Re = 100$), which is also confirmed by nonlinear simulations (not shown). This is not surprising given the observed large differences in energy gains obtained using these different distributions of blowing and suction. Despite its higher efficiency, however, the optimal distribution of blowing and suction may be more difficult to realize experimentally than localized blowing and suction.

For all the spanwise wavenumbers considered, larger streak amplitudes are required to stabilize the global instability at $Re = 100$ than at $Re = 75$. This is to be expected, because at $Re = 100$ the global mode is more unstable than at $Re = 50$, and hence larger streak amplitudes are needed to quench it. However, the amplitudes of the optimal blowing and suction required to stabilize the global instability are smaller at $Re = 100$ than at $Re = 75$, for all the λ_z considered. The increase in energy amplification of the control due to the lift-up associated with an increase in Reynolds number (see figure 3*a*) therefore overcomes the larger control action necessary to quench the more unstable global mode. In other words, the results reported in figure 9(*a*) confirm the essential role played by the non-normal amplification of streaks in stabilization of the global instability.

4.6. *Nonlinear simulations*

Finally, the stabilizing effect of optimal blowing and suction 3-D optimal perturbations is assessed in the fully nonlinear regime. The same cases examined with linear

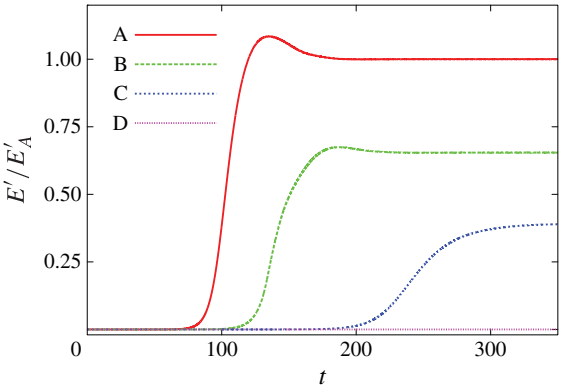

FIGURE 10. (Colour online) Temporal evolution of the normalized total perturbation kinetic energy density, $E'(t)/E'_A$, for increasing control amplitudes. The global perturbation kinetic energy $E'(t)$ is normalized with respect to the permanent regime value E'_A of the reference 2-D wake of case A. The results were obtained from fully nonlinear simulations at $Re = 75$ with $\lambda_z = 2\pi$.

simulations (see § 4.2) are re-examined by switching on the nonlinear terms in the numerical simulations and integrating the equations until a permanent regime develops. In all the cases considered, the permanent regime is periodic in time, except for sufficiently large amplitudes of the optimal blowing and suction, where, as expected from the linear analysis, self-sustained oscillations are quenched. Figure 10 shows that for increasing A_w, the mean value of the global perturbation kinetic energy E' in the permanent regime is reduced (cases B and C) and is eventually driven to zero for case D. The increasingly three-dimensional nature of the controlled wakes in the permanent regime can be appreciated from figure 11.

5. Summary and conclusions

In the first part of this study, a subspace reduction method was introduced for the computation of steady, spanwise-periodic, symmetric (varicose) optimal blowing and suction that maximizes the energy amplification at selected streamwise stations in the circular cylinder wake. It has been shown that the energy of the optimal blowing and suction can be greatly amplified in the wake and that the maximum energy amplification and the position at which it is reached are both increasing functions of the Reynolds number.

The azimuthal distribution of the optimal blowing and suction displays a maximum near $\theta = 90°$, in accordance with the results of Kim & Choi (2005), who found that the optimal position of θ-localized spanwise-periodic blowing and suction is near $\theta = 90°$. The optimal blowing and suction induces streamwise vortices, which in turn induce the transient spatial growth of highly amplified streamwise streaks. The most amplified spanwise wavelengths λ_z range from $5D$ to $7D$ at the Reynolds numbers considered, with the corresponding optimal streaks reaching their maximum amplitude at approximately $\lambda_z/2$ downstream in the wake, well inside the pocket of absolute instability sustaining the global instability. The existence of a finite optimal spanwise wavelength is one of the most notable differences between our results and the case of synthetic wakes studied by Del Guercio *et al.* (2014*b*), where the generation mechanism of the optimal vortices by actuation on the body surface was not taken into account.

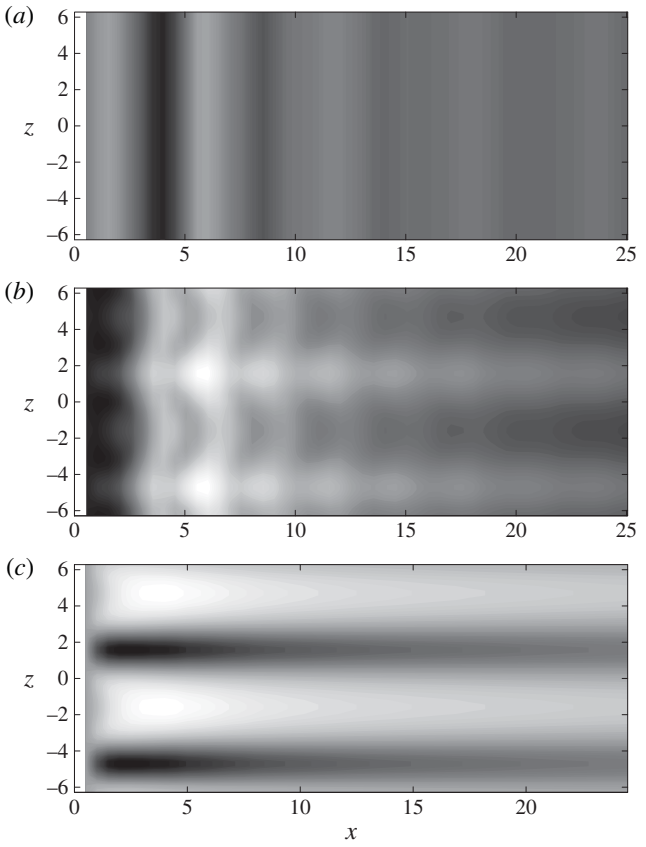

FIGURE 11. Streamwise perturbation velocity $u'(x, y=0, z) = u(x, y=0, z) - U_{2D}(x, y=0)$ in the $y=0$ symmetry plane in the permanent regime ($t=450$) of the fully nonlinear simulations at $Re=75$ for $\lambda_z = 2\pi$. (*a*) The reference 2-D case (case A) displays the usual self-sustained periodic oscillations of 2-D structures in the wake. (*b*) In the presence of moderate-amplitude 3-D perturbations (case C), the self-sustained periodic oscillations acquire a typical 3-D nature while reducing their r.m.s. amplitude. (*c*) For sufficiently large 3-D perturbations (case D), the periodic oscillations are completely suppressed and only the forced stable streaks are visible in the wake.

We then investigated the effect on the global linear instability of forcing optimal blowing and suction with finite amplitudes. First, nonlinear simulations were used to compute nonlinear streaky wake basic flows with increasing finite-amplitude optimal blowing and suction. Then, the global stability of these nonlinear streaky wakes was investigated using the linearized equations.

The global mode growth rate is shown to be reduced proportionally to the square of the optimal blowing and suction amplitude and to the square of the maximum amplitude of the associated streaks. Complete stabilization of the global mode is achieved with blowing and suction amplitudes much smaller than those required by 2-D (spanwise-uniform) blowing and suction. This result is not expected from first-order sensitivity analyses, which predict the opposite. Predictions based on first-order sensitivity analyses are therefore to be treated with extreme caution when considering spanwise-periodic controls and, more generally, when far from the

instability threshold. Indeed, higher-order terms are likely to become more important than linear terms when moderate control amplitudes are considered.

We also show that the optimal blowing and suction amplitude A_w required to suppress the global instability decreases when the Reynolds number is increased from 75 to 100, despite the fact that the global instability is stronger at $Re = 100$ than at $Re = 75$. This reveals the essential role played by the lift-up effect, which amplifies the control energy with an efficiency that increases with Re; this efficiency increase probably explains why 3-D control of 2-D wakes remains effective far from the critical Reynolds number, and even in the turbulent regime. The spanwise wavelength for which the stabilization is obtained with minimum amplitude is found to decrease from $\lambda_z \approx 6$ to $\lambda_z \approx 5$ as Re is increased from 75 to 100, in good agreement with the results of Kim & Choi (2005).

The present study also pinpoints the relevance of the role played by streamwise vortices in the very near wake. Indeed, although the analyses of Hwang *et al.* (2013) show that a key stabilizing role is played by the streaks, here and in our related previous investigations of parallel and non-parallel model wakes (Del Guercio *et al.* 2014*a*,*b*), we show that forcing optimal vortices instead of directly forcing the streaks is much more efficient and that the energy amplification associated with this process plays a key role in the stabilization. In this sense, the present results extend to 2-D wakes the rationale already implemented in boundary layers, where optimal or nearly optimal streamwise vortices were forced to induce streaks able to delay the 2-D Tollmien–Schlichting instability and delay transition to turbulence (Cossu & Brandt 2002, 2004; Fransson *et al.* 2005, 2006). Current effort is directed at extending the present approach to the control of turbulent wakes, in the same spirit as Cossu, Pujals & Depardon (2009), Pujals, Cossu & Depardon (2010*a*) and Pujals, Depardon & Cossu (2010*b*).

Acknowledgement

G.D.G. acknowledges the support of ANRT via the convention CIFRE 742/2011.

REFERENCES

ABDESSEMED, N., SHARMA, A. S., SHERWIN, S. J. & THEOFILIS, V. 2009 Transient growth analysis of the flow past a circular cylinder. *Phys. Fluids* **21**, 044103.

ANDERSSON, P., BRANDT, L., BOTTARO, A. & HENNINGSON, D. 2001 On the breakdown of boundary layer streaks. *J. Fluid Mech.* **428**, 29–60.

BEARMAN, P. W. & OWEN, J. C. 1998 Reduction of bluff-body drag and suppression of vortex shedding by the introduction of wavy separation lines. *J. Fluids Struct.* **12** (1), 123–130.

BOTTARO, A., CORBETT, P. & LUCHINI, P. 2003 The effect of base flow variation on flow stability. *J. Fluid Mech.* **476**, 293–302.

CHOI, H., JEON, W. P. & KIM, J. 2008 Control of flow over a bluff body. *Annu. Rev. Fluid Mech.* **40**, 113–139.

CHOMAZ, J. M. 2005 Global instabilities in spatially developing flows: nonnormality and nonlinearity. *Annu. Rev. Fluid Mech.* **37**, 357–392.

CHOMAZ, J. M., HUERRE, P. & REDEKOPP, L. G. 1988 Bifurcations to local and global modes in spatially developing flows. *Phys. Rev. Lett.* **60**, 25–28.

COSSU, C. & BRANDT, L. 2002 Stabilization of Tollmien–Schlichting waves by finite amplitude optimal streaks in the Blasius boundary layer. *Phys. Fluids* **14**, L57–L60.

COSSU, C. & BRANDT, L. 2004 On Tollmien–Schlichting waves in streaky boundary layers. *Eur. J. Mech. (B/Fluids)* **23**, 815–833.

COSSU, C., PUJALS, G. & DEPARDON, S. 2009 Optimal transient growth and very large scale structures in turbulent boundary layers. *J. Fluid Mech.* **619**, 79–94.

DAREKAR, R. M. & SHERWIN, S. J. 2001 Flow past a square-section cylinder with a wavy stagnation face. *J. Fluid Mech.* **426** (1), 263–295.

DENNIS, S. C. R. & CHANG, G. Z. 1970 Numerical solutions for steady flow past a circular cylinder at Reynolds numbers up to 100. *J. Fluid Mech.* **42**, 471–489.

ELLINGSEN, T. & PALM, E. 1975 Stability of linear flow. *Phys. Fluids* **18**, 487–488.

FORNBERG, B. 1980 A numerical study of steady viscous flow past a circular cylinder. *J. Fluid Mech.* **98**, 819–855.

FRANSSON, J., BRANDT, L., TALAMELLI, A. & COSSU, C. 2005 Experimental study of the stabilisation of Tollmien–Schlichting waves by finite amplitude streaks. *Phys. Fluids* **17**, 054110.

FRANSSON, J., TALAMELLI, A., BRANDT, L. & COSSU, C. 2006 Delaying transition to turbulence by a passive mechanism. *Phys. Rev. Lett.* **96**, 064501.

GIANNETTI, F. & LUCHINI, P. 2007 Structural sensitivity of the first instability of the cylinder wake. *J. Fluid Mech.* **581**, 167–197.

DEL GUERCIO, G., COSSU, C. & PUJALS, G. 2014*a* Stabilizing effect of optimally amplified streaks in parallel wakes. *J. Fluid Mech.* **739**, 37–56.

DEL GUERCIO, G., COSSU, C. & PUJALS, G. 2014*b* Optimal perturbations of non-parallel wakes and their stabilizing effect on the global instability. *Phys. Fluids* **26**, 024110.

GUSTAVSSON, L. H. 1991 Energy growth of three-dimensional disturbances in plane Poiseuille flow. *J. Fluid Mech.* **224**, 241–260.

HUERRE, P. & MONKEWITZ, P. A. 1990 Local and global instabilities in spatially developing flows. *Annu. Rev. Fluid Mech.* **22**, 473–537.

HWANG, Y., KIM, J. & CHOI, H. 2013 Stabilization of absolute instability in spanwise wavy two-dimensional wakes. *J. Fluid Mech.* **727**, 346–378.

KACHANOV, Y. S. & TARARYKIN, O. I. 1987 Experimental investigation of a relaxing boundary layer. *Izv. Sib. Otd. An. Tech.* **18**, 9–19.

KIM, J. & CHOI, H. 2005 Distributed forcing of flow over a circular cylinder. *Phys. Fluids* **17**, 033103.

LANDAHL, M. T. 1990 On sublayer streaks. *J. Fluid Mech.* **212**, 593–614.

MOFFATT, H. K. 1967 The interaction of turbulence with strong wind shear. In *Proceedings of the URSI-IUGG International Colloquium on Atmospheric Turbulence and Radio Wave Propagation* (ed. A. M. Yaglom & V. I. Tatarsky), pp. 139–154. Nauka.

MONKEWITZ, P. A. 1988 The absolute and convective nature of instability in two-dimensional wakes at low Reynolds numbers. *Phys. Fluids* **31**, 999–1006.

PUJALS, G., COSSU, C. & DEPARDON, S. 2010*a* Forcing large-scale coherent streaks in a zero pressure gradient turbulent boundary layer. *J. Turbul.* **11** (25), 1–13.

PUJALS, G., DEPARDON, S. & COSSU, C. 2010*b* Drag reduction of a 3-D bluff body using coherent streamwise streaks. *Exp. Fluids* **49** (5), 1085–1094.

TANNER, M. 1972 A method of reducing the base drag of wings with blunt trailing edges. *Aeronaut. Q.* **23**, 15–23.

TOMBAZIS, N. & BEARMAN, P. W. 1997 A study of three-dimensional aspects of vortex shedding from a bluff body with a mild geometric disturbance. *J. Fluid Mech.* **330**, 85–112.